International Journal of Electrochemistry

Electrochemical Sensors and Biosensors

Guest Editors: Farnoush Faridbod, Vinod Kumar Gupta, and Hassan Ali Zamani

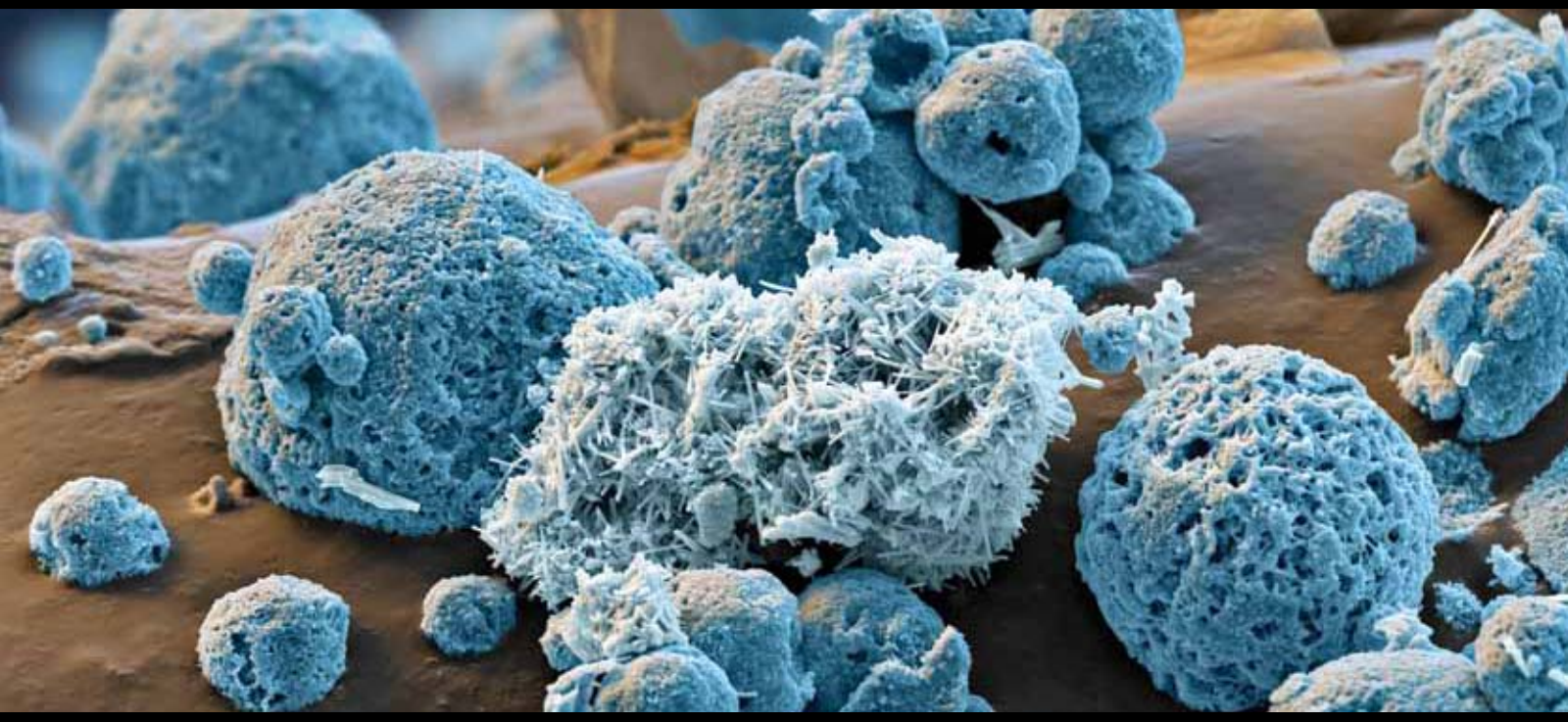

Electrochemical Sensors and Biosensors

International Journal of Electrochemistry

Electrochemical Sensors and Biosensors

Guest Editors: Farnoush Faridbod, Vinod Kumar Gupta, and Hassan Ali Zamani

Copyright © 2011 SAGE-Hindawi Access to Research. All rights reserved.

This is a special issue published in "International Journal of Electrochemistry." All articles are open access articles distributed under the Creative Commons Attribution License, which permits unrestricted use, distribution, and reproduction in any medium, provided the original work is properly cited.

Editorial Board

Maria Carmen Arévalo, Spain
Shen-Ming Chen, Taiwan
Abel César Chialvo, Argentina
Jean-Paul Chopart, France
Adalgisa R. de Andrade, Brazil
Sergio Ferro, Italy
Gerd-Uwe Flechsig, Germany
Rubin Gulaboski, Germany
Shengshui Hu, China
Mehran Javanbakht, Iran
Jiye Jin, Japan
Emilia Kirowa-Eisner, Israel
Boniface Kokoh, France
Emmanuel Maisonhaute, France
Grzegorz Milczarek, Poland
Valentin Mirceski, Macedonia
Mohamed Mohamedi, Canada
Angela Molina, Spain
Davood Nematollahi, Iran
K. I. Ozoemena, South Africa
María Isabel Pividori, Spain
Miloslav Pravda, Ireland
Manfred Rudolph, Germany
B. R. Scharifker, Venezuela
Auro Atsushi Tanaka, Brazil
Germano Tremiliosi-Filho, Brazil
Hamilton Varela, Brazil
Jay D. Wadhawan, UK
Jose H. Zagal, Chile
Sheng S. Zhang, USA
Jiujun Zhang, Canada
Xueji Zhang, USA

Contents

SAGE-Hindawi Access to Research
International Journal of Electrochemistry
Volume 2011, Article ID 352546, 2 pages
doi:10.4061/2011/352546

Editorial

Electrochemical Sensors and Biosensors

Farnoush Faridbod,[1] Vinod Kumar Gupta,[2,3] and Hassan Ali Zamani[4]

[1] *Endocrinology and Metabolism Research Center, Tehran University of Medical Sciences, Tehran 1411413137, Iran*
[2] *Department of Chemistry, Indian Institute of Technology Roorkee, Roorkee 247 667, India*
[3] *Chemistry Department, King Fahd University of Petroleum and Minerals, Dhahran 31261, Saudi Arabia*
[4] *Department of Applied Chemistry, Mashhad Branch, Islamic Azad University, Mashhad, Iran*

Correspondence should be addressed to Farnoush Faridbod, faridbodf@tums.ac.ir

Received 19 December 2011; Accepted 20 December 2011

Copyright © 2011 Farnoush Faridbod et al. This is an open access article distributed under the Creative Commons Attribution License, which permits unrestricted use, distribution, and reproduction in any medium, provided the original work is properly cited.

Electrochemical sensors and biosensors have recently found extensive applications in diverse industries. Nowadays, many analytical instruments used in environmental, food, pharmaceutical, or clinical laboratories and also most of the commercial point-of-care devices work using chemical sensors or biosensors, as a whole or a basic part. Glucose biosensors used widely in glucometers and pH electrodes are the important and known examples of the electrochemical sensors. Day by day, the numbers of sensors or biosensors coming from the bench of research laboratories to the shelf of the commercial markets are increasing. Due to the high demand of the world market and human interest for having a device to check the concentration of species in different samples, simple and fast, in recent years, a hard competition on design and construct of new sensors and biosensors has occurred among the researchers.

Because of such an importance and to show various applications of this kind of devices, the topic of this special issue was devoted to electrochemical sensors and biosensors. Electrochemical sensors and biosensors can offer advantages of low detection limits, a wide linear response range, and good stability and reproducibility.

An electrochemical sensor is a device that transforms electrochemical information into an analytically useful signal. Electrochemical sensors usually composed of two basic components, a chemical (molecular) recognition system which is the most important part of a sensor and a physicochemical transducer which is a device that converts the chemical response into a signal that can be detected by modern electrical instrumentations. These two parts form a working (or sensing) electrode. A reference electrode and sometimes a counter electrode are also used in electrical measurements. Biosensors are chemical sensors in which the recognition system utilizes a biochemical mechanism.

Transduction of a biological or chemical signal into an electrical signal can be done by amperometry, voltammetry, potentiometry, or conductometry.

Next generation of sensor or biosensors will require considerable improvements in sensitivity, selectivity, and accuracy to meet the future needs in diversity of fields. Today, application of different nanoparticles in construction of sensors and biosensors as a modifier causes to approach to this purpose. The nanoparticles have different effects on response of the sensor or biosensor besides improving their thermal, electrical, and mechanical properties.

The papers selected for this special issue represent different kind of electrochemical sensing, different sensing materials, and also various nanoparticles used in determination various species. Although the papers are not an exhaustive representation of all area of electrochemical sensing or biosensing, the papers can give the readers an idea how to make a sensor or biosensor for different applications using electrochemical methods.

This special issue contains 15 papers, where 8 papers reported new design biosensors for different biological molecules. In one of them recent advances in electrochemical aptamer-based biosensors have been discussed.

Most of the papers have used nanoparticles in construction of their sensors or biosensors.

Three of sensors have applied voltammetric method for transduction of the sensor signal, and three ones have reported new designed potentiometric sensors.

One paper has used a chemically modified electrochemiluminescence sensor for determination of atropine sulfate in capillary electrophoresis system.

At last, we would like to thank the authors for their admirable contributions and patience in publishing this special issue. Also, the fundamental works of all reviewers on these papers are sincerely acknowledged.

Farnoush Faridbod
Vinod Kumar Gupta
Hassan Ali Zamani

SAGE-Hindawi Access to Research
International Journal of Electrochemistry
Volume 2011, Article ID 930203, 8 pages
doi:10.4061/2011/930203

Research Article

Potentiometric Polymeric Film Sensors Based on 5,10,15-tris(4-aminophenyl) Porphyrinates of Co(II) and Cu(II) for Analysis of Biological Liquids

Larisa Lvova,[1] Roberto Paolesse,[1] Corrado Di Natale,[2] Arnaldo D'Amico,[2] and Alberto Bergamini[3]

[1] *Department of Chemical Science and Technologies, University of Rome "Tor Vergata", 00173 Rome, Italy*
[2] *Department of Electronic Engineering, University of Rome "Tor Vergata", 00173 Rome, Italy*
[3] *Department of Public Health and Cellular Biology, University of Rome "Tor Vergata", 00173 Rome, Italy*

Correspondence should be addressed to Larisa Lvova, llvova@hotmail.com

Received 15 May 2011; Revised 7 September 2011; Accepted 11 September 2011

Academic Editor: Farnoush Faridbod

Copyright © 2011 Larisa Lvova et al. This is an open access article distributed under the Creative Commons Attribution License, which permits unrestricted use, distribution, and reproduction in any medium, provided the original work is properly cited.

Novel carbonate-selective potentiometric sensors based on 5,10,15-tris(4-aminophenyl)-20-phenyl porphyrinates of Cu(II) and Co(II) have been developed. Ionophore functioning mechanism and possible source of carbonate sensitivity have been evolved. Potentiometric properties of Co(II)- and Cu(II)TATPP-based sensors were compared with common carbonate-ISEs containing trifluoroacetophenone derivatives. The analytical utility of newly developed sensors has been demonstrated by measuring the bicarbonate content in human blood plasma.

1. Introduction

An accurate detection of hydrophilic anions, carbonate in particular, in physiological fluids, seawater, industrial, and environmental samples is still a big challenge. Ion-selective potentiometric sensors represent a useful approach to this task [1]. After pioneering work of Herman and Rechnitz in 1974 [2], several studies on trifluoroacetophenone (TFAP) derivatives as ionophores for carbonate-selective solvent polymeric membrane sensors development have been reported [3–6]. The effect of acceptor substituents incorporation in para- [7, 8] and meta- [9, 10] positions of phenyl ring of TFAP, as far as the influence of lipophilic cationic sites addition [3, 11, 12] on selectivity properties of such sensors have been studied. Various constructive and strategic modifications such as incorporation of TFAP ionophore in photocurable polyurethane [13] and cellulose acetate membranes [14] have been applied in order to diminish the influence of lipophilic anions on carbonate ion response. The other types of ionophores are such as tweezer-type derivatives of cholic acid [15], urea-functionalized calix[4], arenes [11], and hydrogen bonding diamide receptors [16] and metallocorroles [17]. Unfortunately, many of reported membranes were still exhibiting much higher selectivity for several lipophilic anions, like salicylate, over carbonate, which is a serious drawback for their application, for example, in clinical analysis (e.g., human serum) [8, 12].

In this contribution we report a development of novel carbonate-selective potentiometric sensors based on 5,10,15-tris(4-aminophenyl)-20-phenyl porphyrinates of Co(II) and Cu(II) (Co(II)TATPP and Cu(II)TATPP correspondingly). PVC solvent polymeric membranes doped with Co(II)TATPP alone and containing lipophilic cationic additive (TDACl), and films of poly-Co(II)TATPP and poly-Cu(II)TATPP electropolymerized on Pt working electrodes (WE) from various organic solvents (acetonitrile, dimethylformamide, pyridine) have been studied with the aim to evolve the origin of sensitivity towards carbonate ion. Potentiometric properties of Co(II)- and Cu(II)TATPP-containing sensors were compared with those based on TFAP (carbonate ionophore I, ETH-6010, and carbonate ionophore IV), Scheme 1. The analytical utility of

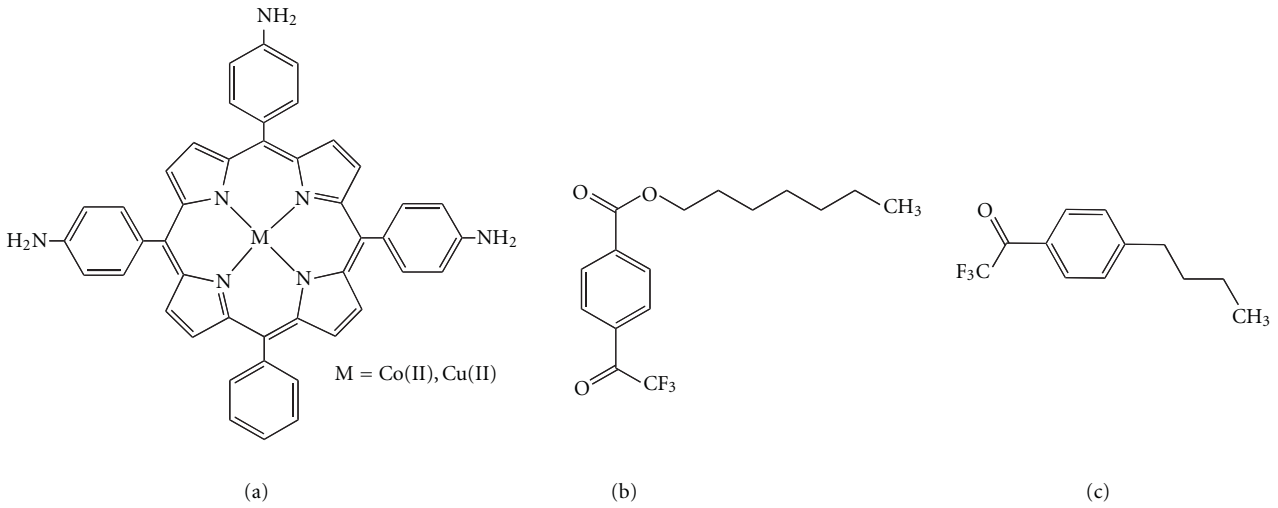

(a) (b) (c)

Scheme 1: Molecular structures of studied ionophores: (a) 5,10,15-tris(4-aminophenyl)-20-phenyl porphyrinate of Cu(II) and Co(II), (b) heptyl-4-trifluoroacetylbenzoate (carbonate ionophore I), and (c) 4-butyl-α,α,α-trifluroacetophenone (carbonate ionophore IV).

newly developed electrodes has been demonstrated by measuring the bicarbonate content in human blood plasma.

2. Experimental

2.1. Reagents. Poly(vinyl chloride) (PVC) high molecular weight; plasticizer bis(2-ethylhexyl) sebacate (DOS), heptyl-4-trifluoroacetylbenzoate (Carbonate Ionophore I), 4-butyl-α,α,α-trifluroacetophenone (Carbonate Ionophore IV), tetradodecyl ammonium chloride (TDACL), potassium tetra-*p*-chlorophenylborate (TpClPBK), tetrabutylammonium perchlorate ($TBAClO_4$), 2-amino-2-(hydroxymethyl)-1,3-propanediol (TRIS), tetrahydrofuran (THF), acetonitrile (ACN), dimethylformamide (DMF), pyridine, and aniline were purchased from Sigma-Aldrich. 5,10,15-tris(4-aminophenyl)-20-phenyl porphyrinates of Cu(II) and Co(II) were synthesized according to the literature methods [6–19] and fully characterized by NMR and UV-visible spectroscopy. All other chemicals were of analytical grade and were used without further purification. All solutions were prepared by using distilled water.

2.2. Sensors' Preparation and Evaluation. PVC membranes were prepared according to a common procedure. Membrane of 100 mg weight contained 1.5–3.5 wt% of ionophore and/or 1–6 wt% of lipophilic additive distributed in PVC/DOS (1 : 2) polymeric matrix, Table 1. Membrane components were dissolved in 1 mL of THF with addition of 7 wt% of pyridine to membranes III, IV in order to improve an ionophore solubility. Membrane cocktails were then cast out on flat GC electrode surface (3 mm in diameter) previously buffed with alumina slurries, cleaned in ultrasonic bath, rinsed with methanol, and dried on air. THF was allowed to evaporate overnight. Porphyrin electropolymers (EP) were deposited by means of cyclic voltammetry on Pt WE (3 mm surface diameter) from 1.0 mM/L Co(II)TATPP or Cu(II)TATPP and 0.1 M/L $TBAClO_4$ solutions in (a) acetonitrile, (b) DMF, (c) pyridine, and (d) DMF: 0.5 M aniline in 1 M/L H_2SO_4 = 1 : 1. Solutions were deoxygenated by bubbling N_2 for 10 min before the experiment. The potential of WE was cycled in the range from −0.2 to 0.8–1.4 V versus SCE with a scan rate of 50 mV/sec by AMEL 7050 potentiostat (AMEL, Italy). Pt 0.5 mm wire was used as counterelectrode.

Table 1: Membrane compositions and deposition details.

	Ionophore, wt%	Additive, wt%	Film/solvent
I.a-d	Co(II)TATPP	—	EP/(a-d)[a]
II	Cu(II)TATPP	—	EP/(d)
III	Co(II)TATPP, 1.5%	TDACl, 1%	PVC/DOS
IV	Co(II)TATPP, 1.5%	—	PVC/DOS
V	Carb.Ion I, 2.7%	TDACl, 2%	PVC/DOS
VI	Carb.Ion IV, 3.5%	TDACl, 2%	PVC/DOS
VII	—	TDACl, 6%	PVC/DOS
VII	PANI	—	EP[b]

[a] See experimental section for details.
[b] Deposition from 0.5 M/L aniline solution in 1 M/L H_2SO_4.

Freshly prepared EP and solvent polymeric membrane sensors were soaked in 0.1 M/L $NaHCO_3$ at least for 24 hours before first measurement. The potentiometric responses of sensors have been studied in solutions of several salts in a range 10^{-7}–10^{-1} M/L. The known volumes of standard salts solutions were added to 0.1 M Tris-H_2SO_4 buffer pH 8.6 or distilled water (with simultaneous pH control). Three replica electrodes were studied with each membrane formulation. Sensor potentials were measured versus double-junction SCE reference electrode (AMEL, Italy) and recorded using high-impedance 8-channel potentiometer LiquiLab (Ecosens, Italy). Selectivity coefficients were calculated by the separate solution method (SSM) using EMF values measured in 0.01 M salt solutions and theoretical slope values [1].

2.3. Optical Measurements. UV-visible spectroscopic data were acquired with a Cary-50 Scan spectrophotometer.

The quartz and methacrylate cells 45 × 10 × 10 mm with a path length of 10 mm were used. 15 μL of the same membrane cocktails as used in the potentiometric measurements were deposited on glass slides (20 × 6 × 1 mm). After THF evaporation, a thin polymer film was left adhered to the glass slide. Absorption spectra of dry polymer films and those exposures for 10 min period in aqueous solutions of several salts of varied concentration were registered. In order to evaluate the absorption spectra of Co(II)- and Cu(II)TATPP electropolymers, they were electrochemically deposited over transparent the 15 × 7 × 1 mm indium tin oxide-modified glass slides (ITO, Aldrich) with a nominal resistance of 30–60 Ω/cm^2.

2.4. Plasma Measurements. Arterial blood samples were taken from 5 male subjects (3 healthy persons and 2 with respiratory acidosis, samples A, C). Blood plasma was isolated by centrifugation of fresh samples and following removal of suspended blood cells. Samples were analyzed few hours after collection. At least tree replicas were performed for each plasma sample during the same day. If not analyzed immediately, samples were stored at −20°C. Standard addition method was applied to detect bicarbonate ion content in samples [20]. For this 50 μL of plasma, sample has been dissolved in 50 mL of 1 mM/L NaCl ($E1$), and two consecutive 150 μL injections ($E2$, $E3$) of 0.01 M $NaHCO^3$ were performed. The concentrations of CO_3^{2-} and HCO_3^- ions were then evaluated on the base of $R = \Delta E3/\Delta E2$ ratio, solution pH, and dissociation constants of carbonic acid ($pK_1 = 6.4$, $pK_2 = 10.3$). For comparison, the amount bicarbonate in plasma samples was analyzed with GEM Premier 3000 blood analyzer (Instrumentation Laboratory, USA).

Sensor array was composed of 5 carbonate-selective electrodes and pH glass electrode. Prior to measurements in real plasma samples, array was calibrated in 25 model solutions mimicking human plasma composition. Each solution contained 4 salts; the salt concentration was similar to those in plasma and varied in the following range: 70–100 mM/L NaCl, 20–60 mM/L $NaHCO_3$, 1–8 mM/L Na_3PO_4, 1 mM/L NaSal; solutions pH was fixed in a range 7.2–7.4 by addition of 0.1 M/L HCl.

2.5. Data Analysis. Partial Least Square regression (PLS) method was applied to train multisensory array in artificial solutions mimicking human blood plasma samples and to correlate bicarbonate content determined commercial blood analyzer with multisensory array response. The autoscaling procedure was applied to the data. Since the number of measurements composing the dataset was not big enough to divide the dataset in a training and test set, a leave-one-out validation was applied. The Unscrambler v.9.1 (2004, CAMO PROSESS AS, Norway) was used for data treatment.

3. Results and Discussion

3.1. Electropolymerized Films of Co(II)- and Cu(II)TATPP. Porphyrin electropolymers based on polyaniline (PANI) are well studied. The electropolymerisation of mono-, bis-, tris- and tetra-2- or 4-aminophenyl substituted porphyrinates of various metals on Pt or GC WE has been previously reported by several authors [21–24]. Bettelheim et al. have found that the electropolymerisation of aminophenyl-substituted porphyrins occurs oxidatively via the *meso*-aniline rings in a head-to-tail fashion, the same way as aniline itself. The resulting material is in practice a polyaniline chain with bridged porphyrin units. Anion-selective electrodes, based on such a films, were reported to possess selectivity different from the Hofmeister selectivity series [25, 26]. Moreover, an inherent advantage of these electrodes is their stability and a prolonged lifetime due to the retention of the ionophore in the polymer film.

In the present study we have focused on the development and investigation of the potentiometric behavior of sensors based on Co(II)- and Cu(II)-tris-4-aminophenyl porphyrinates due to their known sensitivity towards hydrophilic anions [27]. First, an optimization of electropolymerisation conditions for deposition of poly-Co(II)TATPP films from four various solvents (see Section 2 for details) has been performed. No film formation on the Pt WE surface has occurred from acetonitrile, insulating yellow-colored poly-Co(II)TATPP films have formed from DMF and pyridine, while a conductive film growth has been detected from DMF/aniline solution (membrane I.d), Figure 1. In the latter case, a dominating PANI film formation process was accompanied by a partial Co(II)TATPP embedding in PANI film during the first 5 cycles. The cyclic voltammograms after first, fifth, and tenth potential scan during the electrodeposition of membrane I.d in the range from −0.2 to 1.5 V are shown in Figure 2. The oxidative wave at about 0.2 V may be attributed to the PANI emeraldine form formation; with growth of scan number this wave shifts to the more positive potential and covers the reversible peak at about 0.4 V corresponding to the reversible Co(II)/Co(III) one-electron redox process. The sharp anodic peaks at 0.65, 0.85, and 1.35 V evident during the first five scans are typical for oxidation of both aryl-substituted porphyrins and aniline [23]. A high capacitive background anodic current which appears in the range 0.3–1.1 V is probably caused by an incorporation to the PANI film either free SO_4^{2-} ions or negatively charged Co(II)TATPP/SO_4^{2-} complexes [28].

The incorporation of Co-TATPP in PANI backbone formed on the ITO glass electrodes was confirmed by the presence of Soret's band ($\lambda = 454$ nm), a typical signature of porphyrin aromatic ring, on UV-visible absorption spectra of membrane I.d, Figure 3. The broadening of Soret's band indicates a multilayer film formation, while the bathochromic shift of the peak maximum in polymeric film in the comparison to the fresh monomer solution in CH_2Cl_2 may be attributed to the axial coordination of porphyrin aminophenyl fragments (which in part remain nonoxidized during the electropolymerisation) on the central Co ions of the neighboring porphyrin units.

Potentiometric responses of poly-Co(II)TATPP electropolymerized membranes I.b–I.d deposited from DMF, pyridine, and DMF/aniline towards several anions have been studied. Membranes I.b and I.c did not show any

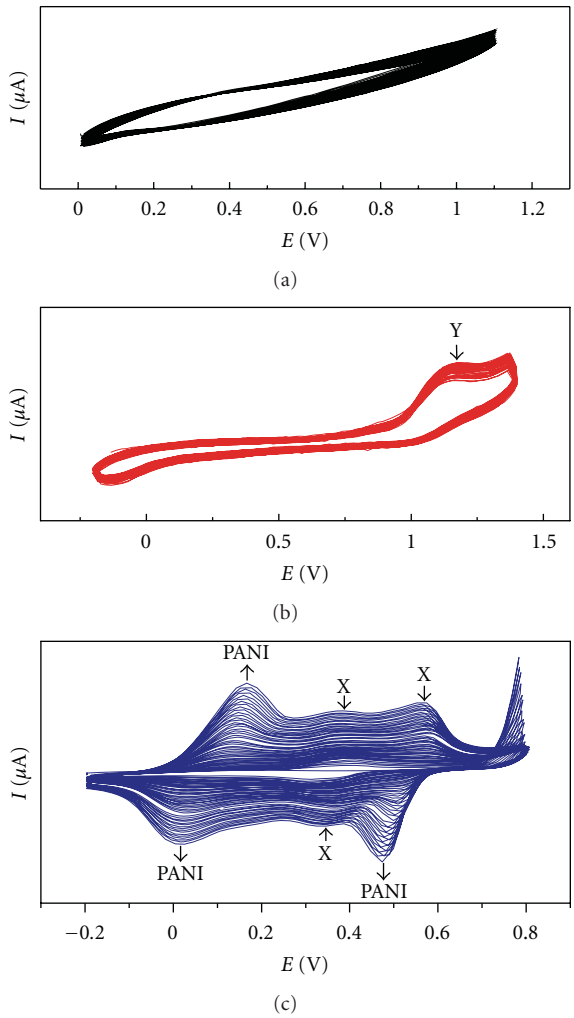

Figure 1: Cyclic voltammograms of PANI-Co(II)TATPP film electrodeposition on Pt WE from (a) acetonitrile; (b) DMF; (c) DMF: 0.5/L M aniline in 1 M/L H_2SO_4 = 1 : 1. The working and counterelectrodes were platinum, and the scan rate was 0.1 V/s. On figure X corresponds to incorporation of Co(II)TATPP in film; Y indicates the decrease of current and insulating film formation.

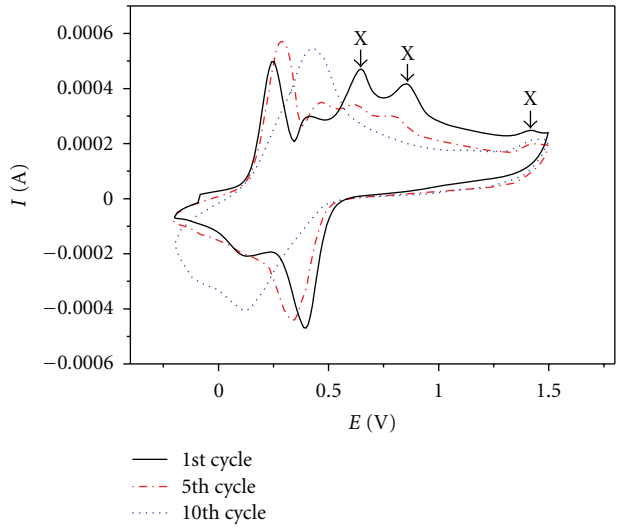

Figure 2: The details of PANI-Co(II)TATPP membrane I.d electropolymerisation from DMF/aniline solution. Peaks indicated as X show an incorporation of Co(II)TATPP in PANI film during first 5 cycles.

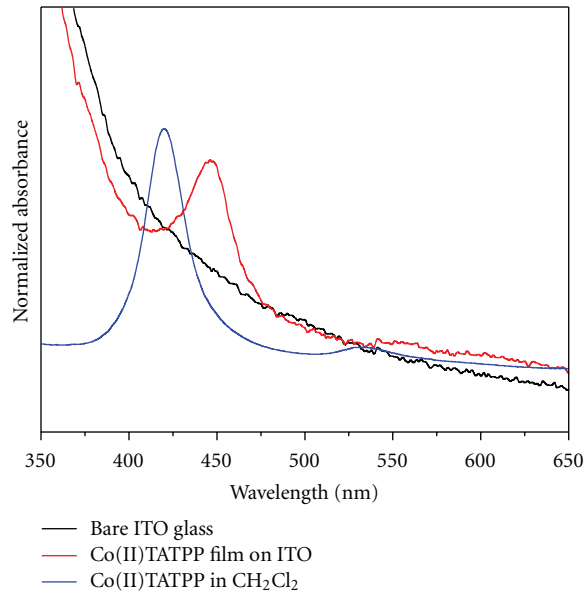

Figure 3: UV-visible absorption spectra of PANI-Co(II)TATPP electropolymer (membrane I.d) deposited on ITO glass slide. The spectra of Co(II)TATPP in CH_2Cl_2 and bare ITO glass are given for comparison.

significant response to all the tested anions probably due to the prevalence of insulating EP formation. Selectivity patterns significantly different from the Hofmeister series were detected for membrane I.d, as far for membrane II based on Cu(II)TATPP-doped PANI film, Figure 4. For both membranes, the highest response with a slope close to theoretical Nernstian was found towards CO_3^{2-} ions (27 and 28 mV/dec correspondingly). Strong interference influence of I^- and SCN^- ions (slopes of 56 and 59 mV/dec correspondingly) was also detected. Membrane VII (PANI) did not show any specific response to all studied anions and was strongly influenced by solution pH. In fact, the pH sensitivity of PANI films is well known, and several sensors for pH detection based on polyaniline have been previously reported [30, 31].

A high sensitivity of membranes I.d and II towards $NaHCO_3$ concentration change could be explained either by PH influence on Co(II)TATPP- and Cu(II)TATPP-doped PANI films or by selective complexation of bicarbonate/carbonate ions by metalloporphyrins. In fact, the growth of $NaHCO_3$ concentration increase the solution pH, and; hence, the correct determination of various forms of CO_2 (i.e., CO_2, H_2CO_3, HCO_3^-, CO_3^{2-}) existing in analyzed sample requires either simultaneous pH control or the application of an appropriate buffer background [14].

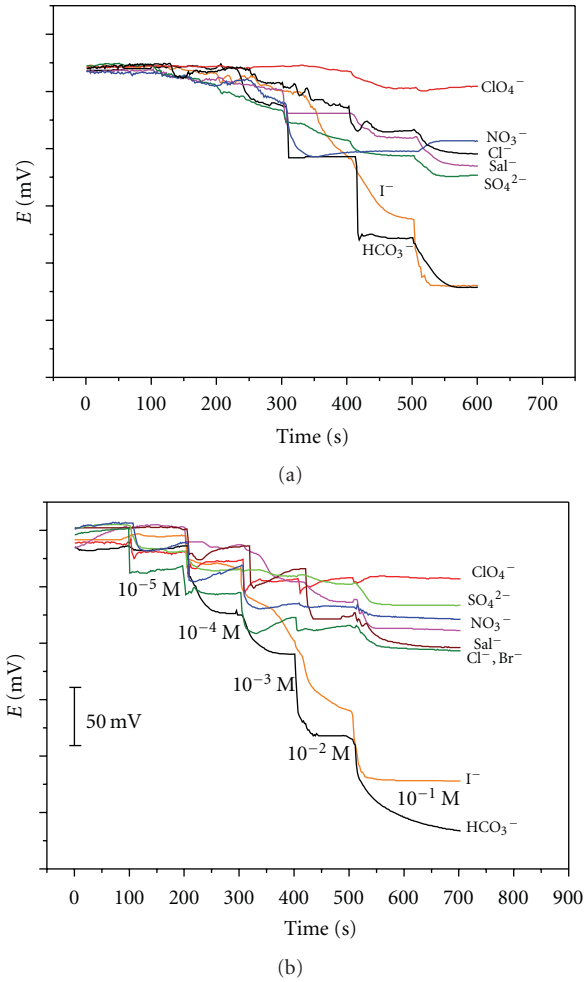

Figure 4: Potentiometric dynamic response of EP films towards several anions: (a) membrane I .d based on Co(II)TATPP and (b) membrane II based on Co(II)TATPP.

The pH response of membranes I.b–I.d, II, and VIII has been, hence, studied by stepwise addition of 1 M/L NaOH to the universal buffer (11.4 mM/L boric acid, 6.17 mM/L citric acid, 10 mM/L NaH_2PO_4, pH 2.75) and achieving the final solution pH 10. A relatively little effect of pH on electrodes with membranes I.b–I.d and II have been detected in a pH range from 6 to 10 (−9.1, −2.9, and −14.0 mV/pH correspondingly), while PANI membrane VIII has shown a significant pH response in the all examined range with a slope −41.2 mV/decade (data not shown). It can hence be assumed that Co(II)- and Cu(II)-5,10,15-tris(4-aminophenyl)-20-phenyl porphyrinates may selectively coordinate carbonate ions and are promising candidates as ionophores for carbonate-selective sensor development.

3.2. Potentiometric and Optical Study of Co(II)TATPP Ionophore Functioning Mechanism. In order to evolve the source of high sensitivity towards carbonate as far as elucidating the ionophore functioning mechanism, potentiometric and optical properties of solvent polymeric PVC/DOS membranes III and IV doped with Co(II)TATPP (see Table 1) have been studied and compared with membranes V and VI based on commercially available TFAP derivatives (carbonate ionophores I and IV) and membrane VII based on anion exchanger TDACl. During the sensors' preparation, we have faced the problem of a low Co(II)TATPP solubility in THF-dissolved PVC membrane cocktails. Such a low solubility can be attributed to the partial monomer self-aggregation occurring via axial coordination of porphyrin phenylamine substituents on the metallic centers of neighboring molecules. An addition of 7 wt% of pyridine to the membrane cocktail resulted in aggregate breakage and improved the ionophore solubility due to the prevalent axial coordination of pyridine. Membrane IV doped with 1.5 wt% of Co(II)TATPP ionophore without any lipophilic additive showed a partial anionic response towards several anions, while an addition of 1 wt% of anionic $TpClPB^-$ sites (data not shown) resulted in a cationic response with slopes 40–45 mV/decade towards all studied aqueous salt solutions. Such a behavior indicates the neutral carrier functioning mechanism of Co(II)TATPP ionophore. As well known, to stabilize potentiometric properties of neutral carrier-based membrane, an addition of cationic lipophilic sites is often required [1]. Moreover, basing on the amount of incorporated cationic sites, an assumption on possible stoichiometry of forming ionophore/primary ion complexes can be made [4]. It has been found that the ratio Co(II)TATPP/TDACl = 1.5 in membrane III gives the best performance and selectivity towards carbonate ions close to selectivity of TFAP-derivative-based membranes, Figure 5. A potentiometric response towards CO_3^{2-}-ions with a slope of 30.3 mV/decade close to a theoretical Nernstian has been found for membrane III in a range 3×10^{-6}–10^{-3} M/L at the distilled water background and 28.7 mV/decade in a range 3×10^{-5}–10^{-1} M for 0.1 M/L Tris-H_2SO_4 buffer pH 8.6. The fact of higher carbonate selectivity of EP membrane I.d should be noticed and will be discussed later.

The formation both of 1 : 1 and 2 : 1 adducts between metalloporphyrin and CO_3^{2-} ions in membrane phase may be supposed. UV-visible spectroscopy of thin films of membrane III deposited on glass slides and measured dry and in solutions of $NaHCO_3$ in 10^{-6}–10^{-2} M/L concentration range showed that three concurrent processes occur in a membrane phase, Figure 6. First, the decrease of absorbance intensity at 444 nm and the growth of 420 nm absorbance peak indicate a partial substitution of pyridine initially coordinated on metal center [32] by primary anion (red shifted 444 nm peak) followed then by the liberation of Co(II)TATPP monomers in membrane phase (formation of 420 nm peak) and finally by formation of hydroxide-/or carbonate ion-bridged dimers (appearance and growth of blue shifted 367 nm peak) [33]. The comparison of selectivity patterns observed by the optical transduction in solutions of $NaHCO_3$, NaCl, $NaNO_3$, and NaSCN and those obtained potentiometrically showed the high ability of carbonate ions to shift the dimer-monomeric equilibrium within the membrane phase. Thus, it has been found that carbonate ions in higher degree than

Table 2: Results of developed sensors application for bicarbonate detection in plasma*.

	HCO_3^- content, mM/L			
	Co(II)TATPP		Carbonate ionophore I, membrane VI	Blood analyzer
	Membrane I.d	Membrane III		
A	48.4 ± 3.7	52.4 ± 4.2	48.3 ± 2.2	51.4
B	31.9 ± 2.3	—	29.7 ± 1.7	31.8
C	—	—	42.1 ± 1.5	42.8
D	—	20.8 ± 2.2	—	21.2
E	30.7 ± 4.6	25.2 ± 4.4	30.3 ± 2.2	28.9

* Data reprinted from [29] with the author's permission.

other studied anions are responsible for a fast breakage of Co(II)TATPP-pyridine complexes and following partial formation of ionophore dimers in membrane phase.

On the contrary to PVC/DOS solvent polymeric membranes, no ionophore dimerization occurs in electropolymerized membrane I.d due to the rigid fixation of Co(II)TATPP inside PANI matrix. The only process that takes place in EP film is an axial coordination of target primary ion on metal center of porphyrin ionophore. This fact may explain the higher carbonate selectivity of EP membranes I.d and II over the solvent polymeric PVC membrane III.

3.3. An Application of Developed Co(II)- and Cu(II)TATPP-Based Sensors for Human Plasma Analysis. Due to the fact of elevated CO_3^{2-} selectivity, an attempt to apply Co(II)TATPP-based sensors with membranes I.d and III for detection of carbonate ions and following evaluation of HCO_3^- content in human blood plasma have been performed. The results of the bicarbonate content determination in 5 human plasma samples are given in Table 2. A good correlation between bicarbonate content evaluated with Co(II)TATPP-based membranes I.d and III, TFAP derivative-based membrane VI, and commercial blood analyzer has been achieved.

The effectiveness of single sensor application for bicarbonate content analysis in human plasma has been compared to the multisensory approach. For this purpose sensor array composed of 5 carbonate-selective sensors with membranes I.d, II, III, VI, and VIII, and pH electrode has been utilized. Before application in plasma, array was calibrated in artificial solutions mimicking human plasma composition (see Section 2 for details). The potential of each sensor was measured in every calibration solution at least in 3 replicates, so the final dataset was composed of $6*25*3 = 450$ readings. A good PLS correlation between the array response and real amount of HCO_3^- ions detected with blood analyzer (slopes of $S_{cal} = 0.949$ and $S_{val} = 0.941$ and correlation coefficients $R_{cal} = 0.974$ and $R_{val} = 0.969$ for calibration and full cross-validation correspondingly) was received, while no influence of salicylate and phosphates presence on sensors response was detected, Figure 7.

From PLS1 model the concentration of HCO_3^- was then evaluated as 50.2 ± 1.5 mM/L and 30.2 ± 1.1 mM/L for plasma samples A and E correspondingly. Hence, the application of

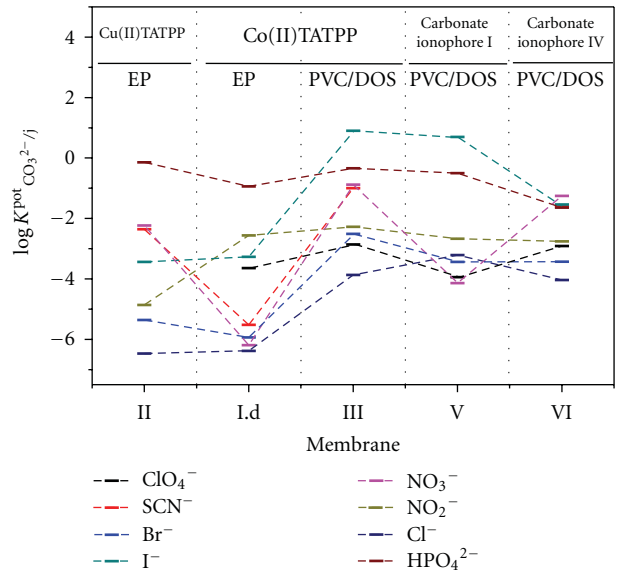

Figure 5: The comparison of the selectivity coefficients of electropolymerized (EP) and solvent polymeric membranes (PVC/DOS) containing Co(II)- and Cu(II)TATPP and TFAP derivatives (commercially available carbonate ionophore I and IV). Selectivity coefficients were evaluated by SSM method, the theoretical Nernstian slope of 29 mV/pCO_3 was used in calculations.

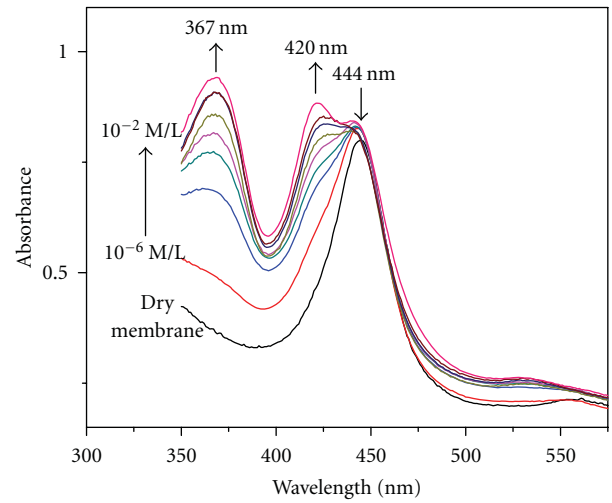

Figure 6: UV-visible spectra of dry membrane III and soaked in 10^{-6}–10^{-2} M/L solutions of $NaHCO_3$.

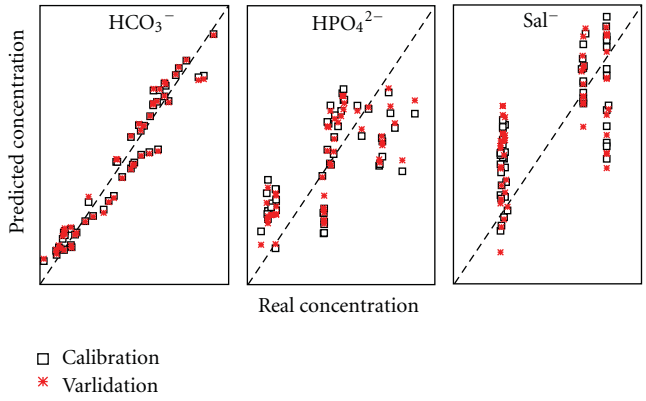

Figure 7: The results of PLS model calibration and validation in multicomponent solutions mimicking plasma for bicarbonate, hydrophosphate, and salicylate ion content detection.

sensor array has permitted to decrease the relative error of HCO_3^- content evaluation in human plasma in comparison to the single ISEs.

4. Conclusions

Newly developed sensors prepared by formation of electropolymerized PANI film doped with 5,10,15-tris(4-aminophenyl)-20-phenyl porphyrinates of Co(II) and Cu(II) have showed a high capability to detect CO_3^{2-} and HCO_3^- ion content and were effective for physiological sample analysis. An inherent advantage of these electrodes is a prolonged lifetime due to the retention of ionophore in the polymeric film and a possibility of an easy miniaturization, which is fundamental when the small sample volume is available or *in vivo* measurements are required.

Acknowledgments

The authors would like to acknowledge Dr. F. Mandoj and Dr. G. Pomarico from the Department of Chemical Science, and Technologies, University of Rome "Tor Vergata", Rome, Italy, for porphyrin ionophores synthesis and G. Romeo and C. Andreozzi for the technical assistance.

References

[1] P. Buhlmann, E. Pretsch, and E. Bakker, "Carrier-based ion-selective electrodes and bulk optodes. 2. Ionophores for potentiometric and optical sensors," *Chemical Reviews*, vol. 98, no. 4, pp. 1593–1687, 1998.

[2] H. B. Herman and G. A. Rechnitz, "Carbonate ion-selective membrane electrode," *Science*, vol. 184, no. 4141, pp. 1074–1075, 1974.

[3] J. A. Greenberg and M. E. Meyerhoff, "Response properties, applications and limitations of carbonate-selective polymer membrane electrodes," *Analytica Chimica Acta*, vol. 141, no. C, pp. 57–64, 1982.

[4] M. E. Meyerhoff, E. Pretsch, D. H. Welti, and W. Simon, "Role of trifluoroacetophenone solvents and quaternary ammonium salts in carbonate-selective liquid membrane electrodes," *Analytical Chemistry*, vol. 59, no. 1, pp. 144–150, 1987.

[5] H. J. Lee, I. J. Yoon, C. L. Yoo, H. J. Puyn, G. S. Cha, and H. Nam, "Potentiometric evaluation of solvent polymeric carbonate-selective membranes based on molecular tweezer-type neutral carriers," *Analytical Chemistry*, vol. 72, no. 19, pp. 4694–4699, 2000.

[6] A. Smirnova, "Membranes for chemical sensors selective to doubly charged anions," *Fresenius' Journal of Analytical Chemistry*, vol. 361, no. 3, pp. 296–300, 1998.

[7] T. Sokalski, D. Paradowski, J. Ostaszewska et al., "Observations on the behaviour of some trifluoroacetophenone derivatives as neutral carriers for carbonate ion-selective electrodes," *Analyst*, vol. 121, no. 2, pp. 133–138, 1996.

[8] M. Maj-Zurawska, T. Sokalski, J. Ostaszewska et al., "Carbonate ion selective electrodes with trifluoroacetophenone derivatives in potentiometric clinical analyser," *Talanta*, vol. 44, no. 9, pp. 1641–1647, 1997.

[9] S. Makarychev-Mikhailov, O. Goryacheva, J. Mortensen, A. Legin, S. Levitchev, and Y. Vlasov, "Carbonate sensors based on 4-hexyltrifluoroacetophenone modified by acceptor substituents in phenyl ring," *Electroanalysis*, vol. 15, no. 15-16, pp. 1291–1296, 2003.

[10] S. Makarychev-Mikhailov, A. Legin, J. Mortensen, S. Levitchev, and Y. Vlasov, "Potentiometric and theoretical studies of the carbonate sensors based on 3-bromo-4-hexyl-5-nitrotrifluoroacetophenone," *Analyst*, vol. 129, no. 3, pp. 213–218, 2004.

[11] H. K. Lee, H. Oh, K. C. Nam, and S. Jeon, "Urea-functionalized calix[4]arenes as carriers for carbonate-selective electrodes," *Sensors and Actuators, B*, vol. 106, no. 1, pp. 207–211, 2005.

[12] Y. K. Hong, W. J. Yoon, H. J. Oh et al., "Effect of varying quaternary ammonium salt concentration on the potentiometric properties of some trifluoroacetophenone derivative-based solvent-polymeric membranes," *Electroanalysis*, vol. 9, no. 11, pp. 865–868, 1997.

[13] S. S. Levitchev, A. L. Smirnova, V. L. Khitrova, L. B. Lvova, A. V. Bratov, and Y. G. Vlasov, "Photocurable carbonate-selective membranes for chemical sensors containing lipophilic additives," *Sensors and Actuators, B*, vol. 44, no. 1–3, pp. 397–401, 1997.

[14] K. S. Lee, G. H. Shin, S. H. Han, G. S. Cha, D. S. Shin, and H. D. Kim, "Asymmetric carbonate ion-selective cellulose acetate membrane electrodes with reduced salicylate interference," *Analytical Chemistry*, vol. 65, no. 21, pp. 3151–3155, 1993.

[15] Y. S. Choi, L. Lvova, J. H. Shin et al., "Determination of oceanic carbon dioxide using a carbonate-selective electrode," *Analytical Chemistry*, vol. 74, no. 10, pp. 2435–2440, 2002.

[16] A. K. Jain, V. K. Gupta, and J. R. Raisoni, "Anion recognition using newly synthesized hydrogen bonding diamide receptors: PVC based sensors for carbonate," *Electrochimica Acta*, vol. 52, no. 3, pp. 951–957, 2006.

[17] L. Lvova, C. Di Natale, A. D'Amico, and R. Paolesse, "Corrole-based ion-selective electrodes," *Journal of Porphyrins and Phthalocyanines*, vol. 13, no. 11, pp. 1168–1178, 2009.

[18] A. D. Adler, F. R. Longo, J. D. Finarelli, J. Goldmacher, J. Assour, and L. Korsakoff, "A simplified synthesis for meso-tetraphenylporphin," *Journal of Organic Chemistry*, vol. 31, no. 2, p. 476, 1967.

[19] R. Luguya, L. Jaquinod, F. R. Fronczek, M. G. H. Vicente, and K. M. Smith, "Synthesis and reactions of meso-(p-nitrophenyl)porphyrins," *Tetrahedron*, vol. 60, no. 12, pp. 2757–2763, 2004.

[20] D. Harvey, *Modern Analytical Chemistry*, McGraw-Hill, New York, NY, USA, 1st edition, 2000.

[21] K. A. Macor and T. G. Spiro, "Porphyrin electrode films prepared by electrooxidation of metalloprotoporphyrins," *Journal of the American Chemical Society*, vol. 105, no. 17, pp. 5601–5607, 1983.

[22] A. Bettelheim, B. A. White, S. A. Raybuck, and R. W. Murray, "Electrochemical polymerization of amino-, pyrrole-, and hydroxy-substituted tetraphenylporphyrins," *Inorganic Chemistry*, vol. 26, no. 7, pp. 1009–1017, 1987.

[23] F. Bedioui, J. Devynck, and C. Bied-Charreton, "Immobilization of metalloporphyrins in electropolymerized films: design and applications," *Accounts of Chemical Research*, vol. 28, no. 1, pp. 30–36, 1995.

[24] J. R. Fish, E. Kubaszewski, A. Peat et al., "Synthesis and electrochemistry of conductive copolymeric porphyrins," *Chemistry of Materials*, vol. 4, no. 4, pp. 795–803, 1992.

[25] S. Daunert, S. Wallace, A. Florido, and L. G. Bachas, "Anion-selective electrodes based on electropolymerized porphyrin films," *Analytical Chemistry*, vol. 63, no. 17, pp. 1676–1679, 1991.

[26] T. L. Blair, J. R. Allen, S. Daunert, and L. G. Bachas, "Potentiometric and fiber optic sensors for ph based on an electropolymerized cobalt porphyrin," *Analytical Chemistry*, vol. 65, no. 15, pp. 2155–2158, 1993.

[27] R. Volf, T. V. Shishkanova, P. Matejka, M. Hamplova, and V. Kral, "Potentiometric anion response of poly(5,15-bis(2-aminophenyl)porphyrin) electropolymerized electrodes," *Analytica Chimica Acta*, vol. 381, no. 2-3, pp. 197–205, 1999.

[28] A. Watanabe, K. Mori, Y. Iwasaki, Y. Nakamura, and S. Niizuma, "Electrochromism of polyaniline film prepared by electrochemical polymerization," *Macromolecules*, vol. 20, no. 8, pp. 1793–1796, 1987.

[29] R. Paolesse, L. Lvova, S. Nardis, C. Di Natale, A. D'Amico, and F. Lo Castro, "Chemical images by porphyrin arrays of sensors," *Microchimica Acta*, vol. 163, no. 1-2, pp. 103–112, 2008.

[30] B. Adhikari and S. Majumdar, "Polymers in sensor applications," *Progress in Polymer Science*, vol. 29, no. 7, pp. 699–766, 2004.

[31] M. Kaempgen and S. Roth, "Transparent and flexible carbon nanotube/polyaniline pH sensors," *Journal of Electroanalytical Chemistry*, vol. 586, no. 1, pp. 72–76, 2006.

[32] B. A. White and R. W. Murray, "Kinetics of electron self-exchange reactions between metalloporphyrin sites in sub-micrometer polymeric films on electrodes," *Journal of the American Chemical Society*, vol. 109, no. 9, pp. 2576–2581, 1987.

[33] E. D. Steinle, S. Amemiya, P. Buhlmann, and M. E. Meyerhoff, "Origin of non-Nernstian anion response slopes of metalloporphyrin-based liquid/polymer membrane electrodes," *Analytical Chemistry*, vol. 72, no. 23, pp. 5766–5773, 2000.

SAGE-Hindawi Access to Research
International Journal of Electrochemistry
Volume 2011, Article ID 958647, 7 pages
doi:10.4061/2011/958647

Research Article

Ion-Selective Electrode for Anionic Surfactants Using Hexadecyl Trimethyl Ammonium Bromide-Sodium Dodecylsulfate as an Active Ionophore

Junwei Wang, Zhiping Du, Wanxu Wang, and Wei Xue

Key Laboratory of Surfactant and Interfaces, China Research Institute of Daily Chemical Industry, Shanxi Province, Taiyuan 030001, China

Correspondence should be addressed to Wanxu Wang, wanxuwang@163.com

Received 9 May 2011; Revised 2 September 2011; Accepted 5 September 2011

Academic Editor: Hassan Ali Zamani

Copyright © 2011 Junwei Wang et al. This is an open access article distributed under the Creative Commons Attribution License, which permits unrestricted use, distribution, and reproduction in any medium, provided the original work is properly cited.

The construction and characteristic performance of PVC membrane electrode responsive to sodium dodecylsulfate (SDS) are described in this paper. The electrode is based on hexadecyl trimethyl ammonium bromide-Sodium dodecylsulfate (CTA^+DS^-) ion pair as ionophore in PVC membrane, which displays a Nernstian slope of -58 ± 0.9 mV/decade in a 5.0×10^{-6} to 2.5×10^{-3} mol L^{-1} concentration range and a limit of detection of 2.9×10^{-6} mol L^{-1}. The electrode can be used for 3 months without showing significant changes in the value of slope or working range. Also the electrode has wide pH range of application and short response time. The electrode shows a selective response to SDS and a poor response to common inorganic anions. The selective sequence found was SDS > HCO_3^- > CH_3COO^- > Cl^- > I^- > NO_3^- ≈ Br^- > F^- > CO_3^{2-} > $C_6H_5O_7^{3-}$ > $C_2O_4^{2-}$ > SO_4^{2-} > $C_4H_4O_6^{2-}$ > SO_3^{2-} > PO_4^{3-}. The potentiometric selectivity coefficients determined are indicating that common anions would not interfere in the SDS determination. The electrode has been utilized as an end point indicator electrode for potentiometric titration involving hyamine as titrant.

1. Introduction

Anionic surfactants are widely used in the industrial and domestic field, for example, in washing agents, household detergents, and personal care products. Traditional analysis methods of anionic surfactant concentration require tedious procedures (such as liquid and gas chromatography), or the use of large amounts of undesired solvents (such as chloroform in the spectrophotometric "Methylene Blue" method) [1–4]. An alternative to these methods is the use of electrodes (such as ion-selective electrodes [5–10] or ion-selective field-effect transistors [11–15]). Potentiometric methods using ion-selective electrodes have found wide applications in diverse fields of analysis for being of low cost, sensitive, and applicable over a wide range of experimental conditions [16].

Surfactant titrations are based on so-called antagonist reaction, where an ionic surfactant reacts with an oppositely charged ion forming a water insoluble salt (ion pair) [17–20]; when the oppositely charged ion surfactants react with each other at equal mol, the potential of the electrode has greatly changed; then the end point can be detected by the electrode.

The use of surfactant selective electrodes for the potentiometric determination of anionic surfactants concentration has been described in several papers. The surfactant selective electrode based on single-walled carbon nanotubes constructed by Najafi et al. [21] was used to determine the concentration of CTA^+ and DS^-. Juan Soto and coworkers [1, 22] constructed an ion-selective electrode for anionic surfactants using a new aza-oxa-cycloalkane and cyclam derivative as active ionophore in PVC membrane.

The present work investigates the feasibility of the preparation of stable, long life, high selectivity, and fast response anionic surfactant ion-selective electrode. The PVC membrane electrode is based on hexadecyl trimethyl ammonium bromide-sodium dodecylsulfate (CTA^+DS^-) ion pair as ionophore and di-n-octyl-phthalate (DOP) as plasticizer. The sensitivity and stability offered by this electrode configuration are high enough to allow accurate determination of

low levels of anionic surfactant by direct potentiometry and potentiometric titration.

2. Experimental

2.1. Reagents. Sodium dodecylsulfate (SDS), hexadecyl trimethyl ammonium bromide (CTAB), hyamine and poly (vinyl chloride) of high molecular weight were from Aldrich (analytical grade). Di-n-octyl-phthalate (DOP) and tetrahydrofuran (THF) are both from Tianjin kermel Chemical Reagent Company. All other reagents used for the preparation of electrode were of analytical grade. Distilled water was used for the preparation of the solutions and for the cleaning of all glassware and apparatus in the experiments.

2.2. Apparatus. The potentiometric measurements were performed with a pH^s 3C pH/mV meter and a saturated calomel electrode (SCE) was used as external reference electrode. pH^s 3C pH/mV meter and saturated calomel electrode were purchased from Shanghai Precision and Scientific Instrument Co., Ltd. The indicating electrode was self-made anionic surfactant selective electrode. Potentiometric titrations were conducted with the help of an automatic burette and a titroprocessor (Beijing Xianquweifeng Technology Development Company) using a 25.0 ± 0.1°C water-thermostated vessel and an automatic burette.

2.3. Preparation of Electrode. The surfactant ion-selective electrode was made according to the classical method described in the literature [23] and the preparation could be formulated as follows.

2.3.1. Preparation of the Ion Pair. The ion pair CTA^+DS^- was prepared by pouring together equimolar amounts of sodium dodecyl sulfate (SDS) and hexadecyl trimethyl ammonium bromide (CTAB) in hot aqueous solution. The ion pair CTA^+DS^- is formed as a white precipitate, which was filtered off, washed with distilled water, and recrystallized twice from hot acetone.

2.3.2. Preparation of the Membrane. The best membranes, obtained with PVC : DOP 2 : 3, contained 10^{-3} mol CTA^+DS^- ion pair per kilogram of PVC and DOP mixture. PVC, DOP, and CTA^+DS^- ion pair were dissolved in tetrahydrofuran, poured on a flat-bottomed glass dish. Tetrahydrofuran evaporated from the solution at room temperature for 48 h, and then the requisite membrane was obtained.

2.3.3. Construction of the Electrode. A disk of 1.0 cm in diameter was cut from the obtained membrane and attached to the end of a PVC tube using the solution of PVC dissolved in tetrahydrofuran (THF) as adhesive. The Ag/AgCl electrode was used as inner reference electrode. 1.0×10^{-3} mol L^{-1} SDS and 1.0×10^{-3} mol L^{-1} KCl mixture solution was used as inner solution. Respectively, to fabricate an electrode, the electrode was preconditioned in 10^{-3} mol L^{-1} SDS solution for 24 h.

2.4. Theory. A rapid and reliable potentiometric analysis method with surfactant ion-selective electrode has been developed for the determination of surfactants; surfactant concentration and potential comply with Nernstian equation written as

$$E = E^\circ + 2.303\frac{RT}{zF}\log a_{\mathrm{DS}^-}, \quad (1)$$

where E stands for the equilibrium electrode potential, E° is the standard electrode formal potential, R is the gas constant, T is the temperature, z is the transfer electron number of electrode reaction, F is the Faradays constant, and a_{DS^-} is the activity of the SDS solution. Therefore, the surfactant concentration can be acquired from the potentiometry measured using surfactant ion-selective electrode.

2.5. Emf Measurements and Titration Procedure. The external reference electrode was a saturated calomel electrode and self-made electrode was used for all EMF measurements. Potentiometric measurements were carried out by using the following cell assembly: external reference electrode, Saturated KCl solution, sample solution, PVC membrane, inner solution, and Ag/AgCl. All potential measurements were carried out on a pH^s 3C pH/mV meter. Potentiometric selectivity coefficients were determined according to the fixed interference method using 2.5×10^{-2} mol L^{-1} solution of interfering ion. Calibration curves were constructed by plotting the potential, E, versus the logarithm of the sodium dodecyl sulfate (SDS) concentration.

The electrode has been calibrated with standard solutions of SDS in the range of 1.0×10^{-7} to 5.0×10^{-2} mol L^{-1}. The volume of tested solution used for titration was 25.0 mL. The titrant dosage rate was 0.1 mL s^{-1}. The concentration of titrant hyamine was 4.043×10^{-3} mol L^{-1}. All the measurements and titration were performed at 25.0 ± 0.1°C.

3. Results and Discussion

3.1. Influence of Membrane Composition. The ion pair CTA^+DS^- was synthesized and tested as ionophore in PVC membrane. As it has been reported, the response of ion-selective electrodes in terms of selectivity and sensitivity depends not only on the ionophore but also on the final composition of the membrane ingredients. Therefore, in a first step several compositions of the membrane ingredients ionophore, plasticizer, and PVC were tested. All the membranes prepared were studied against SDS. The three electrodes (1–3) prepared with different membrane compositions were shown in Table 1. The membrane of electrodes 1, 2, and 3 had a similar composition, and the only difference was the content of ion pair. A comparison of the response characteristics of electrodes 1–3 against SDS is shown in Figure 1 and Table 1. It can be found that Electrode 2 with the composition (wt%) of DOP (60%), PVC (33%), and ion pair (2%) showed a better performance than electrodes 1 and 3. On one hand it had the lowest detection limit and the best linear correlation coefficient, on the other hand the slope value is the nearest to theory

Table 1: Response characteristics of the anionic surfactant-selective electrode based on PVC membrane to SDS with different composition.

Membrane[a]	Slope (mV/decade)	Linear range (mol L^{-1})	Detection limit (mol L^{-1})	Correlation coefficient (r)
1	-50.7 ± 1.2	7.5×10^{-6} to 2.5×10^{-3}	4.6×10^{-6}	0.9972 ± 0.0004
2	-58.0 ± 0.9	5.0×10^{-6} to 2.5×10^{-3}	2.9×10^{-6}	0.9987 ± 0.0003
3	-65.5 ± 2.4	7.5×10^{-6} to 2.5×10^{-3}	5.9×10^{-6}	0.9935 ± 0.0007

[a] Ingredients of membrane (wt%): (1) DOP (60%), PVC (34%), ion pair (1%), (2) DOP (60%), PVC (33%), ion pair (2%), (3) DOP (60%), PVC (32%), ion pair (3%).

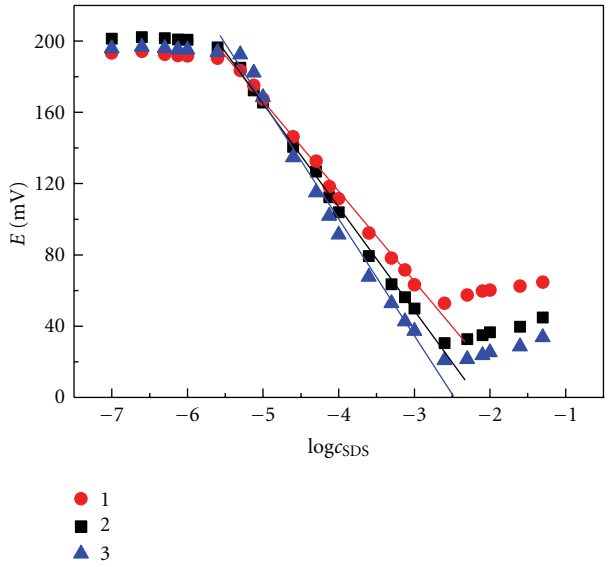

Figure 1: Potential response of the surfactant-selective electrode with different composition to SDS. Ingredients (wt%): ●: DOP (60%), PVC (34%), ion pair (1%), ■: DOP (60%), PVC (33%), ion pair (2%), ▲: DOP (60%), PVC (32%), ion pair (3%).

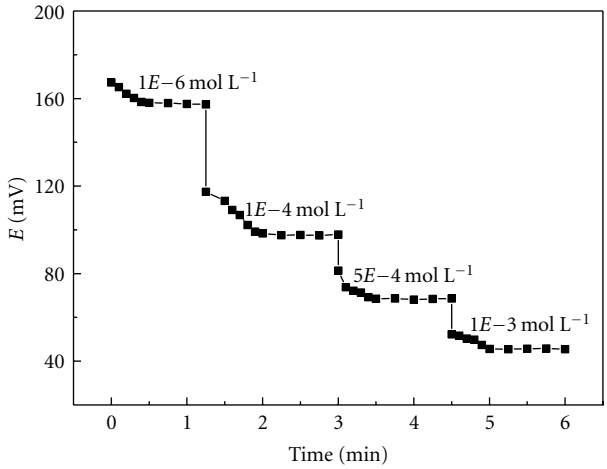

Figure 2: Response time of anionic surfactant selective electrode for step changes in different concentration of SDS solution.

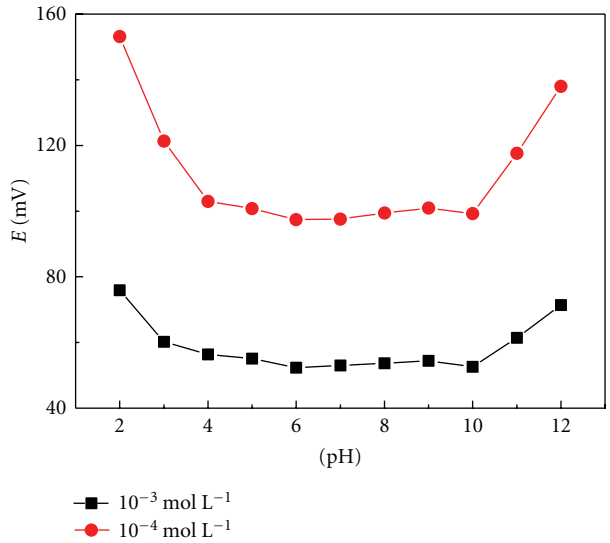

Figure 3: Effect of pH on the potentials of anionic surfactant selective electrode in 1×10^{-4} and 1×10^{-3} mol L^{-1} SDS solution.

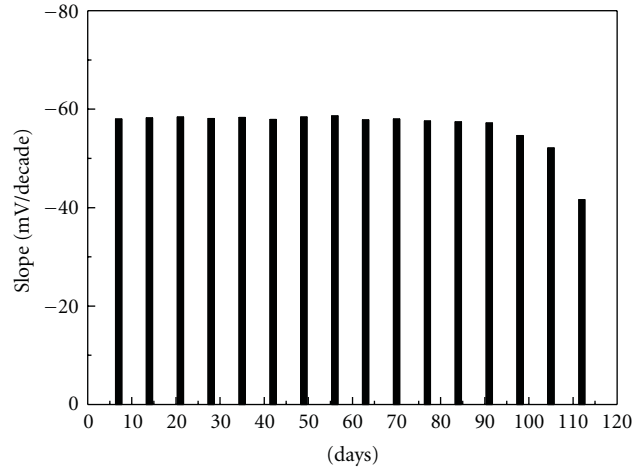

Figure 4: Plot of the slope of anionic surfactant selective electrode in the presence of SDS versus time (days).

value 59.2 mV/decade. So we chose the composition as the ingredients of electrode membrane for the following studies.

3.2. Response Behavior of the Electrode. Electromotive force of the membrane electrode 2 assembly dipped in the solution of anionic surfactant SDS investigated was given by Nernstian equation. The response characteristics of anion surfactant selective electrode in solutions of sodium dodecylsulfate (SDS) were shown in Figure 1 (curve 2). Statistical evaluation of the electrode characteristics was given in Table 1 (membrane 2). The slope value and correlation coefficients were calculated from the linear region

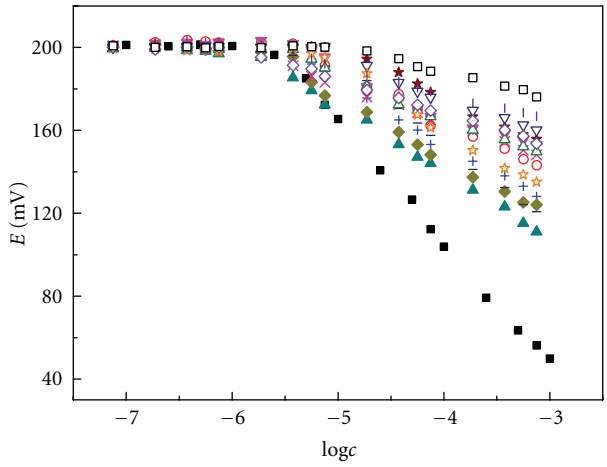

Figure 5: Response of anionic surfactant selective electrode in the presence of certain anions: (■)SDS; (◯) F^-; (+) Cl^-; (▲) Br^-; (▼) I^-; (♦) NO_3^-; (−) SO_4^{2-}; (★) PO_4^{3-} (×) SO_3^{2-}; (△) CO_3^{2-}; (▽) HCO_3^-; (☆) CH_3COO^-; (|) $C_2O_4^{2-}$; (⋄) $C_4H_4O_6^{2-}$; (□) $C_6H_5O_7^{3-}$.

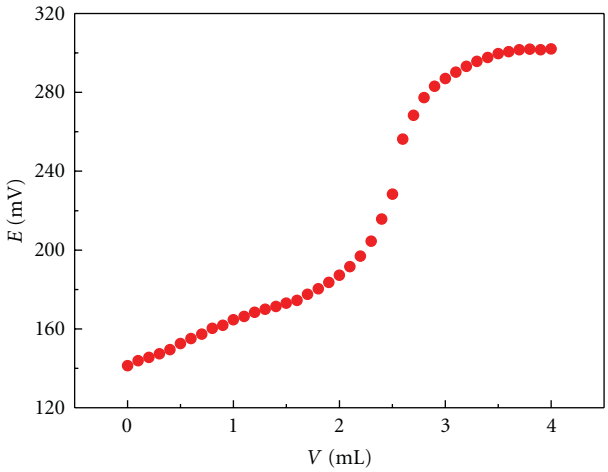

Figure 6: Potentiometric titration curve of 25.0 mL tested SDS solution with 4.043×10^{-3} mol L^{-1} hyamine as titrant in water, using the electrode as an indicator electrode.

of the calibration graph of the measurements using linear regression analysis.

Detection limit is defined as the concentration of SDS corresponding to the intersection of the extrapolated linear segments of the calibration graph [24] which was 2.9×10^{-6} mol L^{-1}. The electrode investigated showed Nernstian response (−58.0 ± 0.9 mV/decade) between 5.0×10^{-6} and 2.5×10^{-3} mol L^{-1} for SDS. It can be seen that the electrode exhibits linear response for SDS.

3.3. Response Time. The static response time of the electrode was measured after successive immersion of the electrode in a series of SDS solutions, from 1.0×10^{-5} to 1.0×10^{-3} mol L^{-1}. The response time of electrode was evaluated by measuring the time required to achieve a steady-state potential [25, 26]. As shown in Figure 2, a response time of 40 s was found as the time required for the electrode to reach a potential within ±1 mV of the final equilibrium. The standard deviation of the response time calculated from four measurements was ±5 s; the response time of the electrode was 40 ± 5 s.

Table 2: The life time study of the anionic surfactant selective electrode.

Period (weeks)	Slope (mV/decade)	Linear range (mol L^{-1})	Detection limit (mol L^{-1})
1	−58.0	5.0×10^{-6} to 2.5×10^{-3}	2.9×10^{-6}
2	−58.2	4.6×10^{-6} to 2.5×10^{-3}	2.9×10^{-6}
3	−58.4	4.7×10^{-6} to 2.5×10^{-3}	3.0×10^{-6}
4	−58.1	5.2×10^{-6} to 2.5×10^{-3}	3.0×10^{-6}
5	−58.3	5.5×10^{-6} to 2.7×10^{-3}	3.4×10^{-6}
6	−57.9	5.9×10^{-6} to 1.9×10^{-3}	2.2×10^{-6}
7	−58.4	6.4×10^{-6} to 2.2×10^{-3}	3.9×10^{-6}
8	−58.6	5.4×10^{-6} to 1.8×10^{-3}	2.6×10^{-6}
9	−57.8	7.1×10^{-6} to 1.5×10^{-3}	4.9×10^{-6}
10	−58.0	6.7×10^{-6} to 2.8×10^{-3}	3.5×10^{-6}
11	−57.6	8.1×10^{-6} to 2.4×10^{-3}	4.3×10^{-6}
12	−57.4	7.8×10^{-6} to 3.1×10^{-3}	4.1×10^{-6}
13	−57.2	8.2×10^{-6} to 3.4×10^{-3}	5.0×10^{-6}
14	−54.6	9.1×10^{-6} to 3.5×10^{-3}	6.1×10^{-6}
15	−52.1	1.1×10^{-5} to 2.9×10^{-3}	7.6×10^{-6}
16	−41.6	2.4×10^{-5} to 3.1×10^{-3}	1.6×10^{-5}

3.4. Effect of pH. The influence of pH on the potential response of the electrode was studied at a fixed concentration of SDS of 1×10^{-4} mol L^{-1} and 1×10^{-3} mol L^{-1} over the pH range of 2–12. CTA^+DS^- ion pair mainly response to DS^-. DS^- can combine with H^+ at low pH, and then DSH formed. At low pH $[H^+] > [DS^-]$, the concentration of DS^- was decreased in the solution which is probably related to the increasing of DSH concentration. The pH values higher than 10 also affected the potential response of electrode. Potential increases most likely due to a membrane response to the OH^- anion, that is because in such medium OH^- ions compete with DS^- ions. So out of the pH range 4 and 10, the potential was not the same as in the pH range 4–10. As illustrated in Figure 3, potentials remained constant between pH 4–10, which was chosen as the pH range for the studies [1].

3.5. Life Time of the Electrode. The electrode characteristics obtained at various time intervals were illustrated in Table 2 and Figure 4. The electrode exhibited good reproducibility in slope, linear concentration range, and detection limit for 13 weeks, but slight drifts in its slope and detection limit were observed after 14 weeks. The life time of the electrode was more than 3 months [1].

3.6. Determination of Potentiometric Selectivity Coefficients. We carried several studies with the electrode in relation to its response in the presence of SDS. As can be seen in Figure 5, the electrode displayed a remarkable selective response to SDS and a very poor change of the potential in the presence of the anions F^-, Cl^-, Br^-, I^-, NO_3^-, SO_4^{2-}, PO_4^{3-},

Table 3: Potentiometric selective coefficients for anionic surfactant selective electrode.

Interfering ion	$k^{pot}_{DS^-, X^-}$ (log)	Interfering ion	$k^{pot}_{DS^-, X^-}$ (log)
F^-	−4.34	SO_3^{2-}	−5.02
Cl^-	−3.94	CO_3^{2-}	−4.55
Br^-	−4.27	HCO_3^-	−3.46
I^-	−4.22	CH_3COO^-	−3.55
NO_3^-	−4.26	$C_2O_4^{2-}$	−4.85
SO_4^{2-}	−4.89	$(C_4H_4O_6^{2-})$[a]	−4.97
PO_4^{3-}	−5.13	$(C_6H_5O_7^{3-})$[b]	−4.59

[a]tartrate, [b]citrate.

Table 4: Results of determining the concentration of SDS by potentiometric titration using anionic surfactant selective electrode compared with the two-phase titration in sample solutions.

Number	V_{SDS} (mL)	Potentiometric titration		Two-phase titration	
		$V_{Hyamine}$ (mL)	c_{SDS} (mol L^{-1})	$V_{Hyamine}$ (mL)	c_{SDS} (mol L^{-1})
1	25.0	2.53	4.09×10^{-4}	2.51	4.06×10^{-4}
2	25.0	2.54	4.11×10^{-4}	2.52	4.08×10^{-4}
3	25.0	2.54	4.11×10^{-4}	2.53	4.09×10^{-4}
Average	25.0	2.54	4.11×10^{-4}	2.52	4.08×10^{-4}
RSD (%)[a]			1.41		1.58

[a]Relative standard deviation of potentiometric titration and two-phase titration method for triplicate measurements.

Table 5: Comparison of the results obtained by the potentiometric and two-phase titration of commercial detergents.

Sample	SDS (wt%)	
	Potentiometric titration	Two-phase titration
1[a]	14.37	14.23
2[a]	14.34	14.20
3[a]	14.39	14.26
RSD (%)[b]	2.05	2.45

[a]Number 1, 2, 3: washing liquid (SDS, glycerine, sodium chloride, diethanolamid, and additives).
[b]Relative standard deviation of potentiometric method for triplicate measurements.

SO_3^{2-}, CO_3^{2-}, HCO_3^-, CH_3COO^-, $C_2O_4^{2-}$, $C_4H_4O_6^{2-}$, and $C_6H_5O_7^{3-}$. As it can be seen that the electrode displays negligible response to these anions when compared with that found for SDS.

In order to quantify the selective behavior found for the electrode towards SDS, we have carried out studies to determine potentiometric selectivity coefficients. Selectivity is one of the most important characteristics of electrodes that gives an idea of the preference of the electrode for the primary ion with respect to potentially interfering species and display the ability to distinguish this ion from a complex mixture. The potentiometric selectivity coefficients ($k^{pot}_{DS^-, X^-}$) of the electrode were calculated by means of the fixed interference method considering SDS as the principal anion and using concentration of 2.5×10^{-2} mol L^{-1} for interfering anions. $k^{pot}_{DS^-, X^-}$ was calculated with the following equation [27]

$$K^{pot}_{ij} = \frac{a_{DS^-}}{(a_{X^-})^{z_{DS^-}/z_{X^-}}}, \quad (2)$$

where a_{DS^-} is the activity of the primary ion of DS^-, a_{X^-} is the activity of the corresponding interfering ion, and z_{DS^-} and z_{X^-} are the corresponding charge of the primary ion and the interfering ion, respectively. The calculated potentiometric selectivity coefficients were listed in Table 3. The selectivity sequence for the electrode was SDS > HCO_3^- > CH_3COO^- > Cl^- > I^- > NO_3^- ≈ Br^- > F^- > CO_3^{2-} > $C_6H_5O_7^{3-}$ > $C_2O_4^{2-}$ > SO_4^{2-} > $C_4H_4O_6^{2-}$ > SO_3^{2-} > PO_4^{3-}. As can be seen in Table 3, the logarithm of the potentiometric selectivity coefficients determined for the electrode are generally lower than −3.0 indicating that most of the anions would not significantly disturb the determination of SDS in real samples.

3.7. Analytical Applications. Our investigations showed that the electrode can not only be used for direct determination of SDS, but also was found useful as a sensor in titration of SDS with precipitating reagent (hyamine). As an example, it was applied in the titration of an SDS solution with hyamine. The amount of SDS in solution can be accurately determined by the electrode. In order to determine the concentration of SDS in model solutions, the electrode has been used for the determination of SDS in water by potentiometric titration in conjunction with SCE (saturated calomel electrode) as reference electrode and the results have been compared with those obtained using the reference standard technique the two-phase titration [28]. A typical sigmoid shape titration curve obtained from the titration of SDS was shown in Figure 6. The titration volume was estimated at the inflection point of the titration curve. As shown in Table 4, the results recorded by potentiometric titration are in good accordance with those given by the two-phase titration. Relative standard

Table 6: Comparison table with previously similar reported works.

Ionophore	Slope (mV/decade)	Linear range (mol L^{-1})	Detection limit (mol L^{-1})	pH range
New cyclic aza-oxa-cycloalkane[a]	−57.7 ± 0.2	3.3×10^{-6} to 6.7×10^{-3}	2.9×10^{-6}	4.5–8
Cyclam derivative [b]	−60.0 ± 0.9	7.9×10^{-6} to 2.0×10^{-3}	4.0×10^{-6}	5–8.5
Single walled carbon nanotubes[c]	−59.5	9.0×10^{-5} to 5.0×10^{-3}	5.2×10^{-6}	Without mention
CTA^+DS^- ion pair [d]	−58.0 ± 0.9	5.0×10^{-6} to 2.5×10^{-3}	2.9×10^{-6}	4–10

[a]Reference [22], [b]Reference [1], [c]Reference [21], [d]Textual content.

deviation of potentiometric titration and two-phase titration method for triplicate measurements are less than 1.6%.

For the determination of SDS in commercial detergents, 15–30 mg sample was dissolved in 2 mL methanol and diluted to 100 mL with water and 20 mL portion applied to the determination of SDS in samples by the electrode. The results of the potentiometric titration using the electrode were compared with those obtained using the two-phase titration. As shown in Table 5, the results recorded by the potentiometric titration are in good accordance with those given by two-phase titration.

4. Conclusion

Comparison with previously similar reported works was shown in Table 6. It can be found that the response slope to SDS of those electrodes was similar. The membrane containing new cyclic aza-oxa-cycloalkane as ionophore had the widest linear range and the lowest detection limit. The membrane containing CTA^+DS^- ion pair as ionophore had the widest pH usage range and also had the lowest detection limit. An anionic surfactant selective electrode based on CTA^+DS^- ion pair as an active ionophore provided advantages of easy preparation, simplicity, fast, and clean method of analysis of anion surfactant. This electrode displayed a Nernstian slope of −58.0 ± 0.9 mV/decade over the 5.0×10^{-6} to 2.5×10^{-3} mol L^{-1} concentration range and shows a limit of detection of 2.9×10^{-6} mol L^{-1}. The electrode can be applied in a pH range of 4–10. Response time is 40 ± 5 s in average and can be used more than 3 months without showing significant changes in the value of slope. The electrode showed a clear anionic response to SDS. The selective sequence found for the electrode was $SDS > HCO_3^- > CH_3COO^- > Cl^- > I^- > NO_3^- \approx Br^- > F^- > CO_3^{2-} > C_6H_5O_7^{3-} > C_2O_4^{2-} > SO_4^{2-} > C_4H_4O_6^{2-} > SO_3^{2-} > PO_4^{3-}$. Furthermore, the potentiometric selectivity coefficients determined were relatively low, indicating that common anions would not interfere in the SDS determination. Also it can be used for the determination of SDS in water samples by titration procedures.

Acknowledgments

This work was supported by Natural Fund of Shanxi Province (2010011017), Natural Science Fund of China (21073234, 21103228), and Shanxi Province Science Fund for Youths (2011021010-2).

References

[1] J. L. Lizondo-Sabater, R. M. Máñez, F. Sancenón, M. J. Seguí, and J. Soto, "Ion-selective electrodes for anionic surfactants using a cyclam derivative as ionophore," *Talanta*, vol. 75, no. 1, pp. 317–325, 2008.

[2] A. Shaheen, I. Kaur, and R. K. Mahajan, "Potentiometric studies of micellization behavior of cationic surfactants in the presence of glycol additives and triblock polymer (Pluronic F68), using surfactant-selective sensors based on neutral ion-pair complexes," *Industrial & Engineering Chemistry Research*, vol. 46, no. 13, pp. 4706–4709, 2007.

[3] K. Vytras, J. Kalous, and J. Jezkova, "Automated potentiometry as an ecologic alternative to two-phase titrations of surfactants," *Egypt Journal of Analytical Chemistry*, vol. 6, no. 1, pp. 107–123, 1997.

[4] C. Vogt and K. Heinig, "Trace analysis of surfactants using chromatographic and electrophoretic techniques," *Fresenius' Journal of Analytical Chemistry*, vol. 363, no. 7, pp. 612–618, 1999.

[5] Q. He and H. Chen, "Flow injection spectrophotometric determination of anionic surfactants using methyl orange as chromogenic reagent," *Fresenius' Journal of Analytical Chemistry*, vol. 367, no. 3, pp. 270–274, 2000.

[6] T. Fujinaga, S. Okazaki, and H. Freiser, "Ion selective electrodes responsive to anionic detergents," *Analytical Chemistry*, vol. 46, no. 12, pp. 1842–1844, 1974.

[7] M. Gerlache, Z. Sentürk, J. C. Viré, and J. M. Kauffmann, "Potentiometric analysis of ionic surfactants by a new type of ion-selective electrode," *Analytica Chimica Acta*, vol. 349, no. 1–3, pp. 59–65, 1997.

[8] B. Kovács, B. Csóka, G. Nagy, and A. Ivaska, "All-solid-state surfactant sensing electrode using conductive polymer as internal electric contact," *Analytica Chimica Acta*, vol. 437, no. 1, pp. 67–76, 2001.

[9] N. Alizadeh and H. K. Tazekendi, "Linear alkylbenzenesulfonate (LAS) ion-selective electrode based on electrochemically prepared polypyrrole and PVC," *Sensors and Actuators B*, vol. 75, no. 1-2, pp. 5–10, 2001.

[10] J. Sànchez and M. Del Valle, "A new potentiometric photocurable membrane selective to anionic surfactants," *Electroanalysis*, vol. 13, no. 6, pp. 471–476, 2001.

[11] R. K. Mahajan and A. Shaheen, "Effect of various additives on the performance of a newly developed PVC based potentiometric sensor for anionic surfactants," *Journal of Colloid and Interface Science*, vol. 326, no. 1, pp. 191–195, 2008.

[12] L. Campanella, M. Battilotti, A. Borraccino, C. Colapicchioni, M. Tomassetti, and G. Visco, "A new ISFET device repsonsive to anionic detergents," *Sensors and Actuators B*, vol. 19, no. 1–3, pp. 321–328, 1994.

[13] J. Sànchez, A. Beltran, J. Alonso, C. Jiménez, and M. D. Valle, "Development of a new ion-selective field-effect transistor

sensor for anionic surfactants: application to potentiometric titrations," *Analytica Chimica Acta*, vol. 382, no. 1-2, pp. 157–164, 1999.

[14] J. Sànchez and M. D. Valle, "Photocurable ISFET for anionic surfactants. Monitoring of photodegradation processes," *Talanta*, vol. 54, no. 5, pp. 893–902, 2001.

[15] W. H. Chan, A. W. M. Lee, and J. Z. Lu, "Optode for the specific determination of anionic surfactants," *Analytica Chimica Acta*, vol. 361, no. 1-2, pp. 55–61, 1998.

[16] J. Sánchez and M. del Valle, "Determination of anionic surfactants employing potentiometric sensors—a review," *Critical Reviews in Analytical Chemistry*, vol. 35, no. 1, pp. 15–29, 2005.

[17] M. M. Hassanien, K. S. Abou-El-Sherbini, and G. A. E. Mostafa, "A novel tetrachlorothallate (III)-PVC membrane sensor for the potentiometric determination of thallium (III)," *Talanta*, vol. 59, no. 2, pp. 383–392, 2003.

[18] R. W. Cattrall and H. Freiser, "Coated wire ion selective electrodes," *Analytical Chemistry*, vol. 43, no. 13, pp. 1905–1906, 1971.

[19] H. James, G. Carmack, and H. Freiser, "Coated wire ion selective electrodes," *Analytical Chemistry*, vol. 44, no. 4, pp. 856–857, 1972.

[20] T. Fujinaga, S. Okazaki, and H. Freiser, "Ion selective electrodes responsive to anionic detergents," *Analytical Chemistry*, vol. 46, no. 12, pp. 1842–1844, 1974.

[21] M. Najafia, L. Maleki, and A. A. Rafati, "Novel surfactant selective electrochemical sensors based on single walled carbon nanotubes," *Journal of Molecular Liquids*, vol. 159, pp. 226–229, 2011.

[22] M. J. Seguí, J. L. Sabater, R. M. Máñez, T. Pardo, F. Sancenón, and J. Soto, "Ion-selective electrodes for anionic surfactants using a new aza-oxa-cycloalkane as active ionophore," *Analytica Chimica Acta*, vol. 525, no. 1, pp. 83–90, 2004.

[23] D. O. Hummel, *Handbook of Surfactant Analysis*, Wiley, New York, NY, USA, 1999.

[24] G. A. E. Mostafa, "s-Benzylthiuronium PVC matrix membrane sensor for potentiometric determination of cationic surfactants in some pharmaceutical formulation," *Journal of Pharmaceutical and Biomedical Analysis*, vol. 41, no. 4, pp. 1110–1115, 2006.

[25] R. P. Buck and E. Lindner, "Recommendation for nomenclature of ion-selective electrodes," *Pure and Applied Chemistry*, vol. 66, no. 12, pp. 2527–2536, 1994.

[26] C. Maccà, "Response time of ion-selective electrodes: current usage versus IUPAC recommendations," *Analytica Chimica Acta*, vol. 512, no. 2, pp. 183–190, 2004.

[27] IUPAC, "Recommendations for nomenclature of ion-selective electrodes," *Pure and Applied Chemistry*, vol. 48, no. 1, pp. 127–132, 1976.

[28] APHA-AWWA-SPCF, "Standard methods for examination of water and waste-water," in *Proceedings of the 16th American Public Health Association*, p. 512A, Washington, DC, USA, 1985.

SAGE-Hindawi Access to Research
International Journal of Electrochemistry
Volume 2011, Article ID 823734, 6 pages
doi:10.4061/2011/823734

Research Article

A Novel ZnO-Methylene Blue Nanocomposite Matrix for Biosensing Application

Shibu Saha,[1] S. K. Arya,[2] S. P. Singh,[3] and Vinay Gupta[1]

[1] *Department of Physics & Astrophysics, University of Delhi, Delhi 110007, India*
[2] *Bio-MEMS and Microsystem Lab, Department of Electrical Engineering, University of South Florida, Tampa, FL 33620, USA*
[3] *Department of Engineering Sciences and Materials, University of Puerto Rico, Mayaguez, PR 00680, USA*

Correspondence should be addressed to Vinay Gupta, drvin_gupta@rediffmail.com

Received 14 April 2011; Accepted 17 August 2011

Academic Editor: Hassan Ali Zamani

Copyright © 2011 Shibu Saha et al. This is an open access article distributed under the Creative Commons Attribution License, which permits unrestricted use, distribution, and reproduction in any medium, provided the original work is properly cited.

A novel hybrid matrix of zinc oxide-methylene blue (ZnO-MB) has been successfully developed for biosensing application. The introduction of methylene blue into the ZnO thin film leads to reduction in the charge transfer resistance and suggests an increase in the electron transfer capacity of the composite. Glucose oxidase (GOx) was chosen as the model enzyme and effectively immobilized on the surface of hybrid ZnO-MB nanocomposite matrix. Electrochemical measurements were employed to study biosensing response of the GOx/ZnO-MB/ITO bioelectrode as a function of glucose concentration. The low oxidation potential (-0.23 V) of the hybrid bioelectrode, in a mediatorless electrolyte, makes it resistant against interference from other bio-molecules. The low value of Michaelis-Menten constant (2.65 mM) indicates that immobilized GOx retains its enzymatic activity significantly on the surface of nanocomposite hybrid matrix that results in an enhanced affinity towards its substrate (glucose). The ZnO-MB nanocomposite hybrid matrix, exhibiting enhanced sensing response ($0.2\,\mu\text{AmM}^{-1}\text{cm}^{-2}$) with long shelf-life (>10 weeks), has potential for the realization of an integrated biosensing device.

1. Introduction

Though the last decade has witnessed a fast growth in the research, development, and marketing of biosensors still no clear unanimity has been made in favor of specific biomatrix [1–7]. The modern day's biosensors combine the natural sensitivity and specificity of complimentary bio-molecules with the advantages of microelectronics, through a suitable biomatrix, for realization of lab-on-chip device [1]. Zinc oxide (ZnO), a wide band-gap semiconductor, is recently grabbing attention of the scientific community for its application in the field of biosensors due to its novel properties like high isoelectric point (IEP) and biocompatibility. Owing to its high IEP the surface of ZnO matrix can adsorb the biocatalysts having low IEP (~4.2 for glucose oxidase) via electrostatic interaction. The possibility of growing large-area thin films of ZnO nanostructures on variety of materials at a relatively low cost led to a good progress in development of ZnO-based biosensor [8–12]. Recently, we have confirmed that ZnO provides direct charge transfer to immobilized enzymes and they retain their bio-activity on its surface [10]. However, due to the absence of a redox couple in ZnO, the amperometric biosensors have to depend on detecting the oxidation of H_2O_2 produced during the reactions. It is important to note that the oxidation potential of H_2O_2 is high enough to cause interference in the electrical signal, from other bio-molecules present in blood serum and thereby hinder the miniaturization of biosensor. Moreover, the ZnO-based sensors require an electron transfer reagent (mediator) in the electrolyte. Therefore, a novel biomatrix is essentially required for lab-on-chip device that can be utilized for effective detection of bio-molecules.

The excellent redox properties of methylene blue (MB), a cationic dye, and its low formal potential ($E^\circ = 0.08$–-0.25 V in solution with pH 2–8) is good enough a reason for its exploitation, as a mediator, in biosensors. Therefore the synthesis of a hybrid matrix exploiting the excellent properties of ZnO along with the redox species may lead to development of an interference-free biosensor. Few biosensors have been developed, where biomolecules are

immobilized along with the mediators, on the surface of the matrix [13–15]. However, due to the low molecular weight and good solubility in water the mediators have a tendency to leach out and thereby destabilizing the bio-electrode [16]. This could be overcome by a composite matrix having the mediator embedded in it. In the present study, we have developed a nanocomposite biomatrix of ZnO with methylene blue (ZnO-MB) and successfully demonstrated the interference-free and effective glucose sensing. The low value of Michaelis Menten Constant (K_m^{app}) and a fairly interferenceless system has indicated the importance of the prepared matrix in the field of amperometric biosensors.

2. Experimental

2.1. Materials. GOx (200 U/mg), horseradish peroxidase (HRP, 200 U/mg), *o*-dianisidine, and glucose were purchased from Sigma-Aldrich. Sodium phosphate monobasic anhydrous and sodium phosphate dibasic dihydrate were obtained from Sisco chemical, India. Lithium hydroxide monohydrate and zinc acetate monohydrate were procured from Thomas Baker, India. MB was acquired from Merck & Co. Inc. All chemicals were used without further purification. Deionized water was used in the preparation of aqueous solutions.

2.2. Preparation of Solutions. Phosphate buffer saline (PBS) 50 mM of pH 7.0 (0.9% NaCl) solution was prepared by adjusting the proportion of monobasic sodium phosphate solution and dibasic sodium phosphate solution and then adding 0.9% NaCl to the solution. GOx (1 mg/mL) solution and HRP solution (1 mg/mL) were freshly prepared in PBS buffer of pH 7.0. Different concentrations of glucose solution and solution of *o*-dianisidine (1%) were freshly prepared in deionized water.

2.3. Preparation of ZnO-MB Film and Immobilization of GOx. The ZnO nanoparticles were first prepared by a wet chemical route, as reported by Yadav et al. [17]. The obtained ZnO nanoparticles are redispersed in ethanol. To obtain ZnO-MB sol, 0.1 mL of the MB solution (10 mg/mL in ethanol) is added to 1 mL of redispersed ZnO sol. The ZnO-MB/ITO electrodes were prepared by spin-coating on ITO-coated glass plates with the ZnO-MB sol.

Immobilization of GOx onto the ZnO-MB matrix was achieved via electrostatic interaction of positively charged ZnO and negatively charged GOx enzyme at 7.0 pH. For GOx immobilization, 30 μL of the freshly prepared GOx solution was dropped on the surface of ZnO-MB composite thin film and was kept at 4°C overnight followed by extensive washing with buffer to remove any unbound GOx. The bioelectrodes were dried under dry nitrogen flow and kept at 4°C when not in use.

2.4. Measurement and Apparatus. The ZnO-MB/ITO electrode was characterized by UV-visible, fourier transform infrared (FTIR), and electrochemical impedance spectroscopy techniques. FTIR studies were further carried out on the GOx/ZnO-MB/ITO bio-electrode to confirm the immobilization of GOx enzyme. The sensing response studies of the bio-electrode were carried out using cyclic voltametry (CV) techniques. The apparent enzyme activity was studied by enzymatic photometric assay. CV measurements were carried out on a Potentiostat/Galvanostat (Gamry Instruments Inc.) using a three-electrode cell configuration with Ag/AgCl electrode as a reference electrode and platinum foil as a counter electrode in 10 mL of phosphate buffer saline (PBS) solution (50 mM, pH 7.0, 0.9% NaCl). Electrochemical impedance spectroscopy (EIS) studies were made in PBS solution (pH 7.0) containing 5 mM $Fe(CN)_6^{3-/4-}$. The apparent enzyme activity of bioelectrode was studied using UV-visible spectrophotometer (Perkin Elmer lambda 35). For the photometric assay bioelectrode was dipped in the 3 mL PBS solution containing 20 μL of dye (*o*-dianisidine, 1% in H_2O), 50 μL of HRP and 100 μL of substrate (glucose). After 1 minute of incubation of bio-electrode the absorbance corresponding to the oxidation of *o*-dianisidine was noted at 500 nm for monitoring the enzyme kinetics.

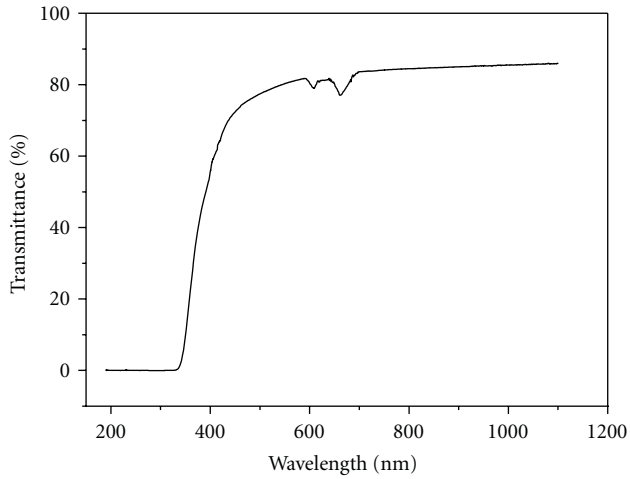

Figure 1: UV-visible spectrum of the ZnO-MB matrix.

3. Results and Discussion

3.1. UV-Visible Studies. ZnO-MB film was deposited on a fused quartz slide for optical characterization. UV-Visible spectra (Figure 1) confirms the deposition of a thin film having high transmission (>80%) in the visible region. The band gap estimated from the fundamental absorption edge (using Tauc plot) was found to be 3.61 eV. The estimated value of the bandgap is much higher than the corresponding value (~3.3 eV) reported for bulk ZnO [18] and may be attributed to the quantum confinement effect which comes into the picture due to the small size of the synthesized ZnO nanoparticles (~4 nm). It is important to point out that two small dips in the transmittance spectra are seen at 610 nm and 660 nm and are attributed to the presence of methylene blue in the prepared composite matrix [16].

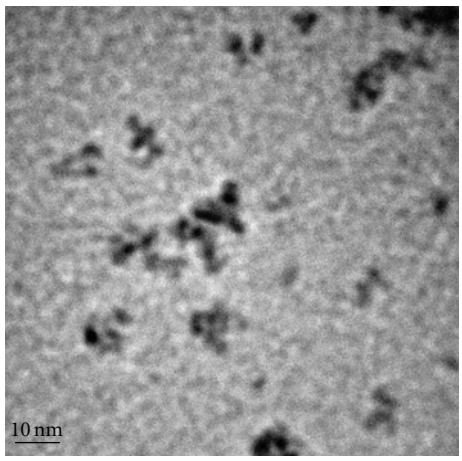

Figure 2: TEM image of the ZnO-MB nanoparticles.

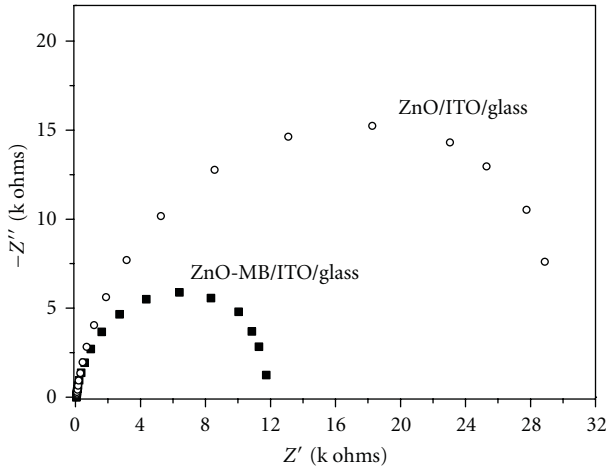

Figure 3: Impedance spectra of the pure ZnO and composite ZnO-MB thin films.

3.2. TEM Analysis of the ZnO-MB Sol. The transmission electron microscope (TEM) image (Figure 2) of the ZnO-MB nanoparticles shows the synthesis of spherical shape and monodispersed nanoparticles with average size of about 4 nm. MB can be seen congregated on the ZnO nanoparticles.

3.3. Electrochemical Impedance Studies. Electrochemical impedance spectroscopy (EIS) study was carried out, on both ZnO-MB thin film and ZnO thin film, to have an insight into the effect of methylene blue on the charge transfer behavior of ZnO in nanocomposite biomatrix. Figure 3 shows the impedance spectra of ZnO/ITO/glass and ZnO-MB/ITO/glass electrodes. The impedance plots are semicircular in shape for both the electrodes. The diameter of the semicircle was found to reduce with incorporation of MB in the ZnO matrix. The plot can be modeled by an equivalent electrical circuit consisting of a resistance (R_S) in series with parallel combination of a capacitance (C_p) and a resistance (R_{CT}) [19]. The value of R_{CT} for ZnO/ITO electrode was found to be 30.6 kΩ which decreased to 12.1 kΩ for the composite ZnO-MB/ITO electrode. The reduction in the value of R_{CT} clearly indicates that the presence of mediator (MB) in the ZnO matrix plays an important role in increasing the charge transfer capacity of the ZnO biomatrix.

3.4. FTIR Studies. The FTIR studies on the ZnO-MB film (Figure 4(a)) confirm the formation of a hybrid composite matrix. In Figure 4(a) the absorption peak observed at 452 cm^{-1} corresponds to the E2 mode of wurtzite ZnO [20]. The appearance of absorption bands at 1574 cm^{-1}, 1413 cm^{-1}, and 1340 cm^{-1} are due to the presence of MB in matrix [16]. The presence of modes corresponding to both the ZnO and MB, in the FTIR spectra, clearly shows that the MB has formed a composite with ZnO without disturbing its lattice structure. FTIR of the GOx/ZnO-MB bio-electrode (Figure 4(b)) shows additional absorption mode corresponding to the characteristic band of protein at 1655 cm^{-1}, assigned to amide II, confirming the immobilization of GOx on the surface of composite (ZnO-MB) matrix [21].

3.5. CV Studies. Cyclic voltammograms of the ZnO-MB electrode at different scan rates (0.01 V/s to 0.08 V/s) are shown in Figure 5(a). A well-defined redox peak was obtained in reagentless phosphate buffer saline (PBS) solution using ZnO-MB/ITO electrode. The oxidation peak is seen at −0.23 V and can be attributed to the oxidation of MB in the nanocomposite biomatrix. However the peak is slightly shifted to negative potential as compared to the oxidation potential of MB (−0.20 V) suggesting good catalytic behavior of the system [9]. The CVs remained essentially unchanged on consecutive scanning thereby ruling out the possibility of any leaching effect of mediator (MB) from the composite (ZnO-MB) matrix as reported previously by other workers [16]. The anodic ($I_p{}^a$) and the cathodic ($I_p{}^c$) peak current are found to vary linearly with potential scan rate (inset of Figure 5(a)) indicating improved electrocatalytic behavior of the prepared system and demonstrating that the hybrid composite matrix is suitable for biosensing applications.

Immobilization of GOx enzyme onto the ZnO-MB/ITO electrode resulted in the decrease of oxidation current in CV (inset of Figure 5(b)) and is attributed to the effective binding of GOx, which is a protein having macromolecular structure of nonconducting nature. Brown-Anson model (1) has been used to calculate the value of surface concentration of redox species for ZnO-MB/ITO and GOx/ZnO-MB/ITO electrodes

$$I_p = \frac{n^2F^2I^*Av}{4RT}. \quad (1)$$

I_p is the peak current, n is the number of electrons transferred, F is the faraday constant, I^* is the surface concentration, A is the surface area of the electrode, v is the scan rate, R is the gas constant, and T is the absolute temperature [22]. The surface concentration of redox species in the GOx/ZnO-MB/ITO bio-electrode (3.46×10^{-11} mol/cm^2) was found to be higher than the corresponding value obtained for ZnO-MB/ITO electrode (2.93×10^{-11} mol/cm^2). An increment

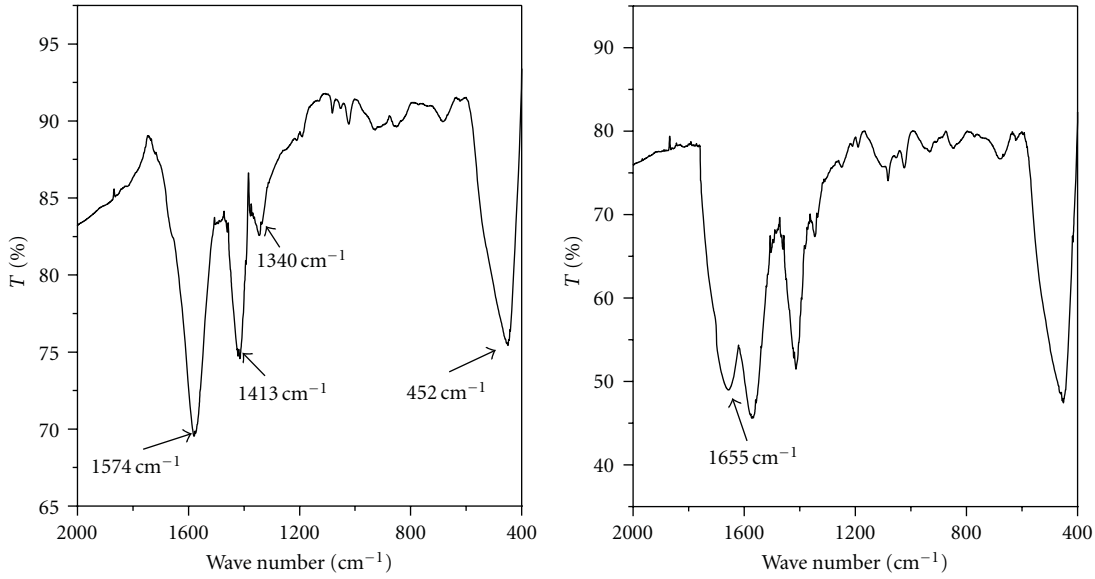

Figure 4: FTIR spectra of (a) ZnO-MB film and (b) GOx/ZnO-MB electrode.

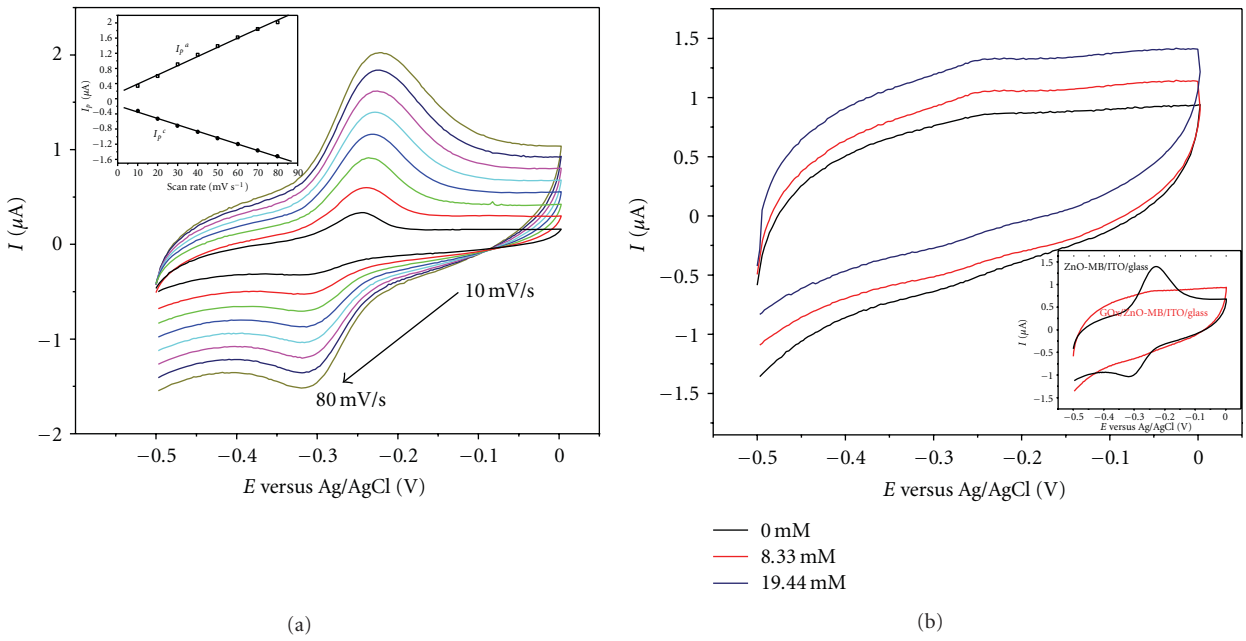

Figure 5: (a) Cyclic voltammograms of ZnO-MB/ITO film at different scan rate (inset shows the variation of anodic and cathodic peak current with potential scan rate) (b) CV of GOx/ZnO-MB/ITO bio-electrode with different glucose concentration (Inset shows CV of ZnO-MB/ITO and GOx/ZnO-MB/ITO electrodes).

in the number of redox species indicates the activation of the redox centers present in the enzyme being immobilized on the composite hybrid matrix. The oxidation current was found to increase continuously, in the CV, with an increase in the glucose concentration (Figure 5(b)). The GOx oxidizes the glucose in the solution and in the process it gets reduced. The reduced GOx donates the excess electron to the ZnO-MB nanocomposite matrix to reduce the redox species. The MB reoxidizes by transferring the electron to the external circuit due to efficient electron transfer and good redox property of prepared nanocomposite biomatrix (Scheme 1). The increase in current with increasing concentration of glucose is attributed to the increase in the number of released electrons during oxidation of glucose.

Figure 6(a) shows the variation of the current measured for the GOx/ZnO-MB/ITO bio-electrode at a fixed potential of −0.23 V as a function of glucose concentration. The observed linear response upto 16.67 mM indicates that

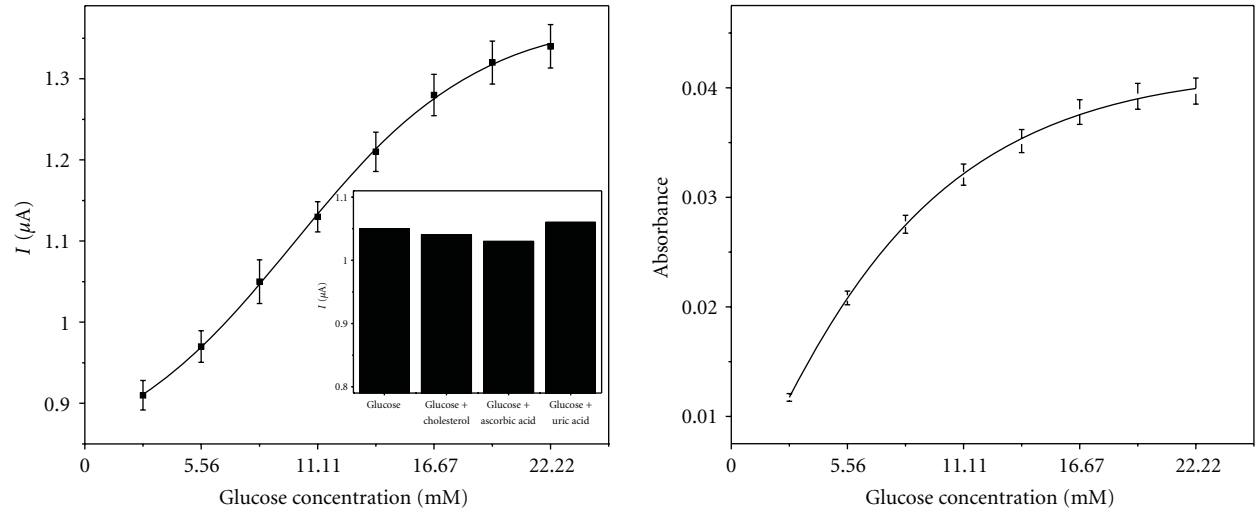

(a) (b)

Figure 6: (a) Response curve: variation of current at a fixed potential of −0.23 V for GOx/ZnO-MB/ITO bio-electrode with glucose concentration (inset shows the effect of various interferants on the response of the biosensor), (b) Photometric assay of GOx/ZnO-MB bio-electrode.

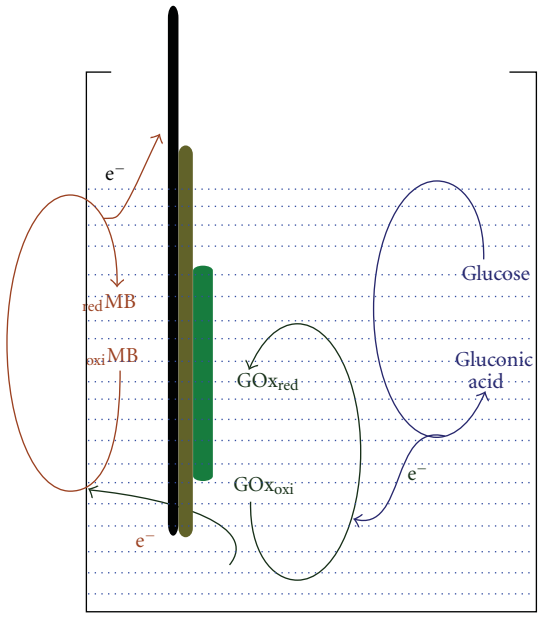

Scheme 1: The electron transfer process of the matrix.

the prepared bio-electrode can be efficiently used for glucose sensing. The sensitivity estimated from the linearity curve is found to be 0.2 μAmM^{-1}cm^{-2}. The results of triplicate sets indicated by error bars reveal the reproducibility of measurements within ±2% and show the higher reliability of prepared bio-electrode based on ZnO-MB nanocomposite matrix for glucose detection.

3.6. Estimation of Michaelis-Menten Kinetic Parameters (K_m^{app}). Hanes plot, that is, a graph between (substrate concentration) and (substrate concentration/current), has been employed to estimate the Michaelis-Menten kinetic parameter (K_m^{app}) of enzymatic reaction [3]. The value of K_m^{app} is found to be 2.65 mM for the GOx immobilized on the nanocomposite matrix. The low K_m^{app} value, as compared to free GOx (27 mM), indicates that the immobilized GOx attains favourable conformation for enzymatic reaction on the ZnO-MB/ITO nanocomposite biomatrix that result in enhanced affinity of GOx towards glucose.

3.7. Interference Study. Upon addition of similar concentration of interferants such as cholesterol, ascorbic acid, and uric acid with glucose (8.33 mM) in PBS, the value of the currents at the peak potential varies insignificantly within the error limits only as is shown in the bar graph (inset of Figure 6(a)). The low working potential of the prepared hybrid biomatrix prevents the effect of interferants on the sensing response characteristics and thereby result in an interference-free biosensor.

3.8. Photometric Assay. The photometric assay was carried out to estimate the apparent enzyme activity (Figure 6(b)) and has been calculated using the equation a_{app}^{enz} (Units cm^{-2}) = $AV/\varepsilon ts$, where a_{app}^{enz} is the apparent enzyme activity, A is the difference in absorbance before and after incubation, V is the total volume (3.17 cm^3), ε is the millimolar extinction coefficient (7.5 for o-dianisidine at 500 nm), t is the reaction time (min), and s is the surface area (cm^2) of the electrode [3]. The estimated value of apparent enzyme activity of the prepared hybrid biomatrix was about 1.65 × 10^{-2} U cm^{-2}. The photometric assay was further used to carry out the shelf life studies, at regular interval for 10 weeks with 8.33 mM glucose concentration (data not shown). The study indicates that the prepared bioelectrode retain more than 80% of activity even after 10 weeks.

4. Conclusion

The present study shows that the ZnO thin film matrix incorporated with methylene blue is a promising nanocomposite hybrid matrix for biosensor application. The ZnO nanoparticles offer a suitable microenvironment for enzyme immobilization and enhanced electron transfer between the enzyme's active site and the electrode. Due to low oxidation potential (−0.23 V), the hybrid composite matrix is practically immune from interferants in the biological system. Glucose oxidase enzyme has been successfully immobilized on the ZnO-MB nanocomposite films deposited onto ITO coated glass. The CV studies of the prepared bioelectrode (GOx/MB-ZnO/ITO) shows linearity up to 16.67 mM indicating the potential of nanocomposite biomatrix for realization of a interference-free biosensor. The GOx immobilized on the ZnO-MB/ITO electrode displays excellent catalytic property towards glucose which is confirmed by the relatively low value of Michaelis-Menten constant (2.65 mM). The shelf life of the prepared bioelectrode is more than 10 weeks suggesting that the hybrid composite matrix provides an attractive option for fabrication of a stable lab-on-chip biosensing device.

Acknowledgments

The support by DST and UGC, Government of India are gratefully acknowledged for sponsored research projects. One author (S. Saha) acknowledges UGC for fellowship and University of Delhi for teaching assistantship.

References

[1] A. Härtl, E. Schmich, J. A. Garrido et al., "Protein-modified nanocrystalline diamond thin films for biosensor applications," *Nature Materials*, vol. 3, no. 10, pp. 736–742, 2004.

[2] J. Lee, P. Hernandez, J. Lee, A. O. Govorov, and N. A. Kotov, "Exciton-plasmon interactions in molecular spring assemblies of nanowires and wavelength-based protein detection," *Nature Materials*, vol. 6, no. 4, pp. 291–295, 2007.

[3] S. Saha, S. K. Arya, S. P. Singh, K. Sreenivas, B. D. Malhotra, and V. Gupta, "Nanoporous cerium oxide thin film for glucose biosensor," *Biosensors and Bioelectronics*, vol. 24, no. 7, pp. 2040–2045, 2009.

[4] M. Viticoli, A. Curulli, A. Cusma et al., "Third-generation biosensors based on TiO_2 nanostructured films," *Materials Science and Engineering C*, vol. 26, no. 5–7, pp. 947–951, 2006.

[5] P. Pandey, S. P. Singh, S. K. Arya et al., "Application of thiolated gold nanoparticles for the enhancement of glucose oxidase activity," *Langmuir*, vol. 23, no. 6, pp. 3333–3337, 2007.

[6] G. Liu and Y. Lin, "Amperometric glucose biosensor based on self-assembling glucose oxidase on carbon nanotubes," *Electrochemistry Communications*, vol. 8, no. 2, pp. 251–256, 2006.

[7] Z. Matharu, G. Sumana, S. K. Arya, S. P. Singh, V. Gupta, and B. D. Malhotra, "Polyaniline Langmuir—blodgett film based cholesterol biosensor," *Langmuir*, vol. 23, no. 26, pp. 13188–13192, 2007.

[8] C. D. Corso, A. Dickherber, and W. D. Hunt, "An investigation of antibody immobilization methods employing organosilanes on planar ZnO surfaces for biosensor applications," *Biosensors and Bioelectronics*, vol. 24, no. 4, pp. 805–811, 2008.

[9] Z. W. Zhao, X. J. Chen, B. K. Tay, J. S. Chen, Z. J. Han, and K. A. Khor, "A novel amperometric biosensor based on ZnO:Co nanoclusters for biosensing glucose," *Biosensors and Bioelectronics*, vol. 23, no. 1, pp. 135–139, 2007.

[10] S. P. Singh, S. K. Arya, P. Pandey et al., "Cholesterol biosensor based on rf sputtered zinc oxide nanoporous thin film," *Applied Physics Letters*, vol. 91, no. 6, Article ID 063901, 2007.

[11] J. X. Wang, X. W. Sun, A. Wei et al., "Zinc oxide nanocomb biosensor for glucose detection," *Applied Physics Letters*, vol. 88, no. 23, Article ID 233106, 2006.

[12] A. Wei, X. W. Sun, J. X. Wang et al., "Enzymatic glucose biosensor based on ZnO nanorod array grown by hydrothermal decomposition," *Applied Physics Letters*, vol. 89, no. 12, Article ID 123902, 2006.

[13] G. Li, J. M. Liao, G. Q. Hu, N. Z. Ma, and P. J. Wu, "Study of carbon nanotube modified biosensor for monitoring total cholesterol in blood," *Biosensors and Bioelectronics*, vol. 20, no. 10, pp. 2140–2144, 2005.

[14] S. Han, M. Zhu, Z. Yuan, and X. Li, "A methylene blue-mediated enzyme electrode for the determination of trace mercury(II), mercury(I), methylmercury, and mercury-glutathione complex," *Biosensors and Bioelectronics*, vol. 16, no. 1-2, pp. 9–16, 2001.

[15] D. Chen, B. Liu, Z. Liu, and J. Kong, "An amperometric biosensor for hydrogen peroxidase based on the co-immobilization of catalase and methylene blue in an Al_2O_3 sol-gel modified electrode," *Analytical Letters*, vol. 34, no. 5, pp. 687–699, 2001.

[16] H. Yao, N. Li, S. Xu, J. Z. Xu, J. J. Zhu, and H. Y. Chen, "Electrochemical study of a new methylene blue/silicon oxide nanocomposition mediator and its application for stable biosensor of hydrogen peroxide," *Biosensors and Bioelectronics*, vol. 21, no. 2, pp. 372–377, 2005.

[17] H. K. Yadav, K. Sreenivas, V. Gupta, S. P. Singh, and R. S. Katiyar, "Effect of surface defects on the visible emission from ZnO nanoparticles," *Journal of Materials Research*, vol. 22, no. 9, pp. 2404–2409, 2007.

[18] H. K. Yadav, K. Sreenivas, and V. Gupta, "Enhanced response from metal/ZnO bilayer ultraviolet photodetector," *Applied Physics Letters*, vol. 90, no. 17, Article ID 172113, 2007.

[19] S. Saha, S. K. Arya, S. P. Singh, K. Sreenivas, B. D. Malhotra, and V. Gupta, "Zinc oxide-potassium ferricyanide composite thin film matrix for biosensing applications," *Analytica Chimica Acta*, vol. 653, no. 2, pp. 212–216, 2009.

[20] G. Xiong, U. Pal, J. G. Serrano, K. B. Ucer, and R. T. Williams, "Photoluminescence and FTIR study of ZnO nanoparticles: the impurity and defect perspective," *Physica Status Solidi (C)*, vol. 3, no. 10, pp. 3577–3581, 2006.

[21] M. M. Huković and S. Omanović, "Electrocatalytic oxidation of preadsorbed monolayer of CO on polycrystalline Pt_{60}-Ru_{40} electrocatalyst: nucleation and growth of oxygen-containing species," *Journal of Molecular Catalysis A*, vol. 136, no. 1, pp. 75–84, 1998.

[22] A. J. Bard and L. R. Faulkner, *Electrochemical Methods: Fundamentals and Applications*, John Wiley & Sons, New York, NY, USA, 2nd edition, 2000.

SAGE-Hindawi Access to Research
International Journal of Electrochemistry
Volume 2011, Article ID 460850, 16 pages
doi:10.4061/2011/460850

Review Article

Label-Free Biosensors for Cell Biology

Ye Fang

Biochemical Technologies, Science and Technology Division, Corning Inc., Corning, NY 14831, USA

Correspondence should be addressed to Ye Fang, fangy2@corning.com

Received 23 May 2011; Revised 5 July 2011; Accepted 6 July 2011

Academic Editor: Vinod Kumar Gupta

Copyright © 2011 Ye Fang. This is an open access article distributed under the Creative Commons Attribution License, which permits unrestricted use, distribution, and reproduction in any medium, provided the original work is properly cited.

Label-free biosensors for studying cell biology have finally come of age. Recent developments have advanced the biosensors from low throughput and high maintenance research tools to high throughput and low maintenance screening platforms. In parallel, the biosensors have evolved from an analytical tool solely for molecular interaction analysis to powerful platforms for studying cell biology at the whole cell level. This paper presents historical development, detection principles, and applications in cell biology of label-free biosensors. Future perspectives are also discussed.

1. Introduction

The cell is the functional basic unit of life. The ability of examining living cells is crucial to cell biology. In the past several decades, advances in molecular biology have made it a routine laboratory practice to manipulate a cellular target in living cells. Gene expression can be used to increase the amount of a specific protein in cells, while interference RNA can be used to suppress or eliminate a specific protein, and mutagenesis to alter the structure and functions of a particular protein, so that the functional consequences of the target protein can be studied [1, 2]. In parallel, analytical techniques have also been advanced to meet the increasing demands in characterizing molecules in living cells with high temporal and spatial resolutions, as well as with high throughput [3, 4]. Although these molecular assays only measure independent molecules one at a time, they have made it possible to identify various activators, effectors, enzymes, and substrates for many important cellular processes including signaling [5]. Thus, these assays have been dominating cell biology studies nowadays. However, since signaling proteins mostly operate through a large and complex network to direct the propagation of signals within a cell and ultimately to determine how the cell responds to environmental cues [6, 7], there are increasing demands in technologies that not only allow one to investigate cellular responses at the whole cell and cell systems level, but also enable mechanistic delineation. Label-free biosensors fulfill these needs by measuring integrated and phenotypic responses of whole cells with high temporal resolutions [8, 9]. Further, these biosensors enable noninvasive and highly sensitive measurements of many different cellular responses, ranging from cell adhesion to cell barrier functions, signaling, infection, migration, proliferation and death, and differentiation (Figure 1), part of which are topics of this paper.

2. Label-Free Biosensors

Label-free biosensors generally use a transducer to convert a stimulus-induced cellular response into a quantifiable signal (i.e., biosensor signal) [9]. Depending on the nature of transducers, label-free biosensors used for whole cell sensing are mostly divided into optical- and electric-based (Figure 2). It is worth noting that there are many other types of biosensors currently under development. These include atomic force microscopy for measuring biomechanics of cells [10, 11], Raman imaging for measuring the production and organization of unsaturated fatty molecules in cells [12, 13], and whispering-gallery-mode biosensors [14] and resonant mirrors [15] for biosensing. Since these biosensors have limited throughput for whole cell sensing at the present time, they are excluded in this paper.

Optical biosensors include surface plasmon resonance (SPR) and resonant waveguide grating (RWG), both of which use a surface bound evanescent wave to characterize alterations in local refractive index at the sensor surface. SPR

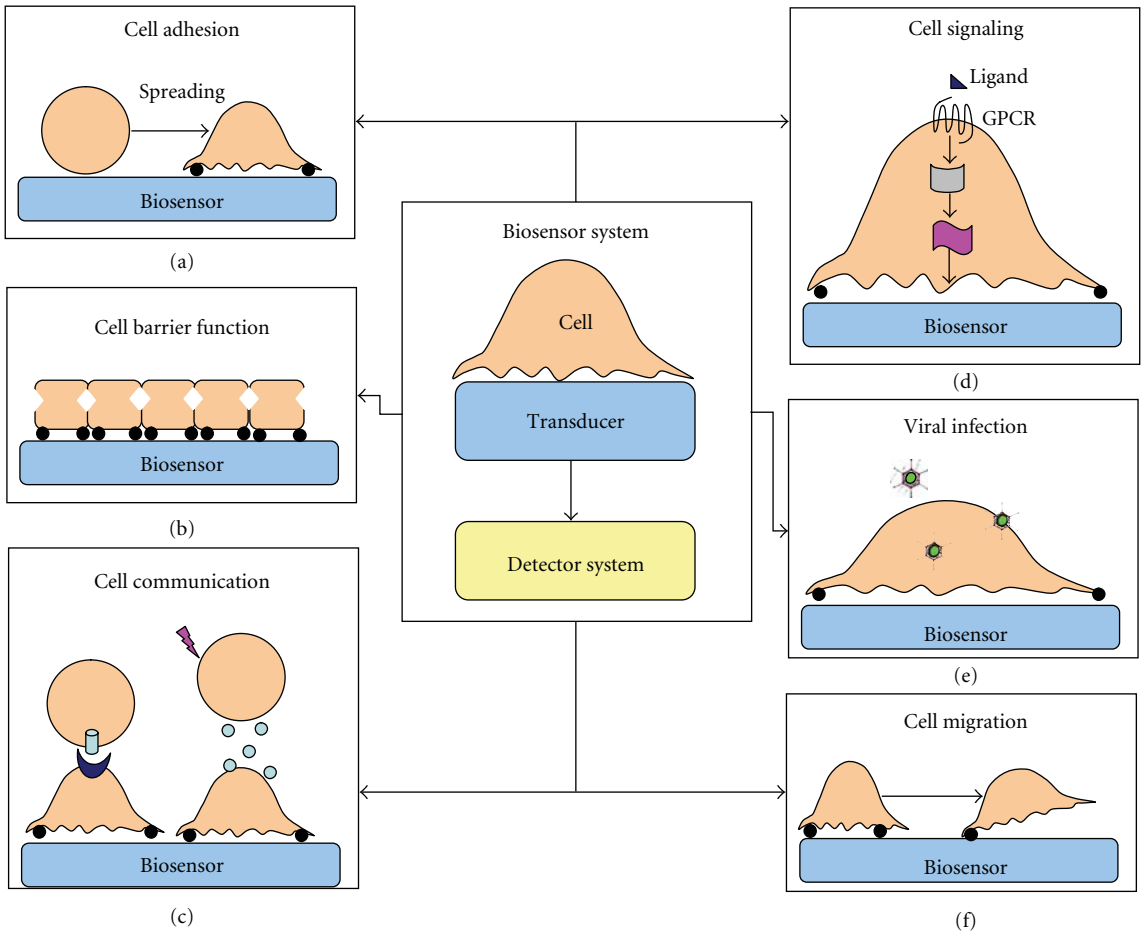

Figure 1: Label-free biosensor and its uses for cell biology. (a) Cell adhesion to a surface; (b) cell barrier functions and regulation; (c) cell-to-cell communication via direct interactions or chemical communication; (d) cell signaling via the receptor activation by an agonist; (e) viral infection; and (f) cell migration.

employs light excited surface plasmon polaritons (SPPs) to detect the adsorption of biomolecules onto a metallic surface (typically gold or silver) [16] (Figure 2(a)). The SPP is a surface-bound electromagnetic wave arising from the interaction of light with mobile surface chargers in a metal [17, 18]. The waves propagate along the interface between materials with negative and positive permittivities (e.g., the metal/dielectric interface), leading to an electromagnetic field that is primarily present in and decays evanescently into the dielectric medium due to increased damping in the metal [19]. Biacore (now GE Healthcare) first introduced a SPR instrument for biomolecular interaction analysis to the market in 1990 [20]. Because of its ability to measure the binding affinity and kinetics of an interaction, SPR is often referred to affinity-based biosensors. Recently SPR imaging has become a reality [21], and localized SPR also has started gaining attractions [22]. However, SPR is still limited to low throughput in processing different samples today. Commercial products include SPR series from GE Healthcare and SPR imager from GWC instruments and others (Figure 2(a)).

RWG uses a leaky mode nanograting waveguide structure to couple light into the waveguide thin film via diffraction, so an evanescent wave is generated (Figure 2(b)). RWG is also named grating coupler, or photonic crystal biosensor. Resonant anomalies in periodic structures were first reported in 1902 [23, 24]. Only until 1980s, a surface bound and waveguide guided mode resonance was achieved using grating couplers and used for chemical sensing by Teifenthaler and Lukosz [25, 26]. Similar to SPR, RWG also employs an evanescent wave for detection, and thus, was initially developed for biomolecular interaction analysis [27, 28]. In recent years, large-scale fabrication, together with new biosensor and instrument designs as well as advanced assay protocols, has made RWG system the first commercial platform for high throughput biochemical and cell-based assays [9, 29–38]. Commercial products include Epic system from Corning Inc., EnSpire multimodal reader containing Epic technology from PerkinElmer, and BIND system from SRU BioSystems (Figure 2(b)).

Electric biosensors use a low electrolyte impedance interface to detect the impedance of a cell layer under electric fields generated with sinusoidal voltages [38, 39]. Under the electric fields the cellular plasma membrane acts as an insulating barrier directing the current to flow between or beneath the cells, leading to extracellular and transcellular

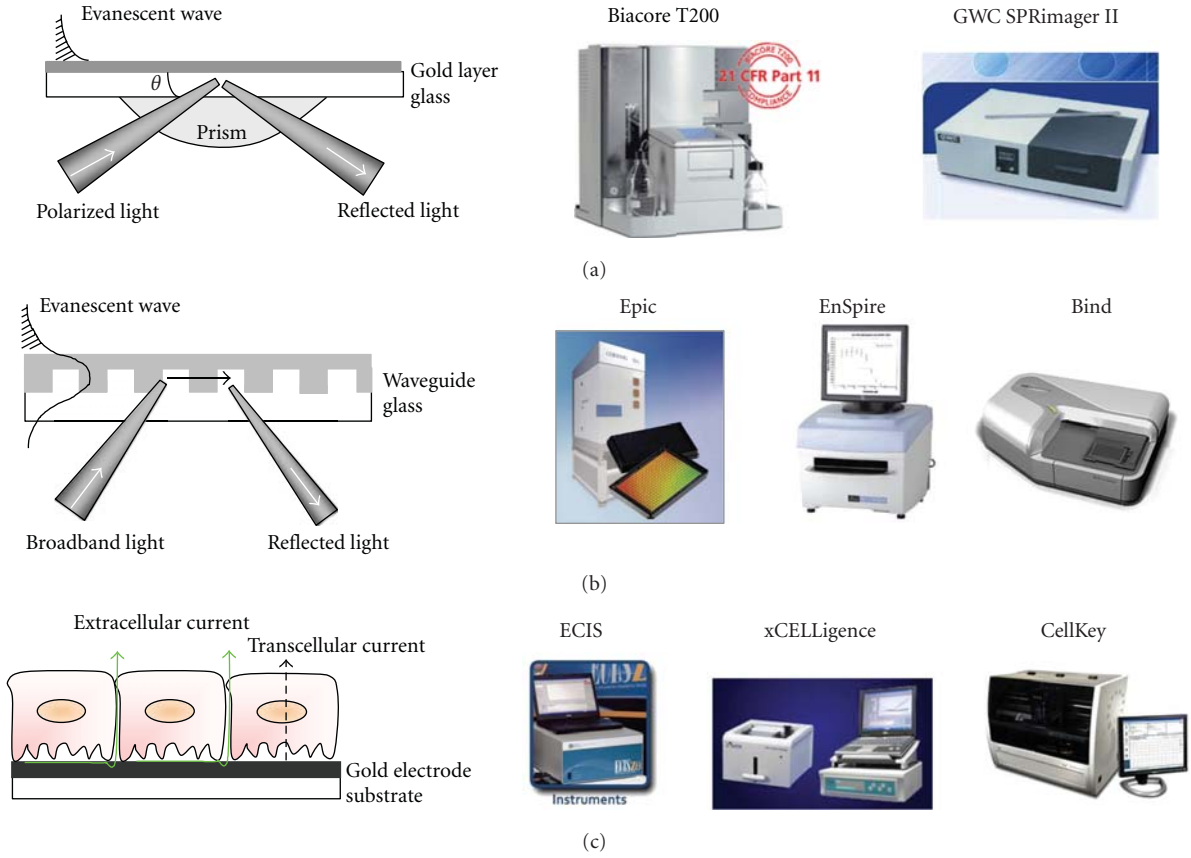

Figure 2: Principles and commercial instruments of three distinct types of label-free biosensors. (a) Surface plasmon resonance, which uses light excited surface plasmon polaritons to sense whole cells. Biacore SPR T200 and GWC SPRImagerII are two examples of commercial products. (b) Resonant waveguide grating, which uses leaky mode nanograting waveguide structure to generate an evanescent wave to sensor whole cell responses. Epic, EnSpire, and BIND are three commercially available products. (c) Electric biosensor, which uses a low electrolyte impedance interface to sense whole cell responses. ECIS, xCELLigence, and CellKey are three commercial products.

currents, respectively (Figure 2(c)). The extracellular current is mostly due to the intercellular conduction, while the transcellular current is a result of the control of cell-membrane capacitance. The extracellular current can be separated from the transcellular current using sophisticated algorithms and is more robust than the transcellular current. ECIS (Electric cell-substrate impedance sensing) instruments from Applied BioPhysics were the first commercial impedance systems for cell-based assays [40, 41]. Newer systems use sophisticated algorithms to record and process impedance signals, leading to improved signal to noise ratios [42]. Commercial products include ECIS systems from Applied BioPhysics, xCELLigence (Real Time Cell Electric Sensing; RT-CES) from Roche/Acea Biosciences and Cellkey (Cellular Dielectric Spectroscopy; CDS) from Molecular Devices (Figure 2(c)).

The first generation biosensor systems can only measure a few samples at a time. SPR was limited up to 4 individual channels for parallel measurements and also required microfluidics for sample delivery. The first ECIS system measured the impedance of living cells cultured on small electrodes up to 16-well plate [41]. The current generation systems are targeting moderate to high throughput screening (HTS), which requires highly reproducible data collection and straightforward data analysis. The user experience is the top priority of these products; thus, innovative instrument designs, assay protocols, and data analysis software have made these systems low maintenance screening platforms [9, 32].

The current biosensor systems differ greatly in measurements. For optical biosensors, the cellular responses are often referred to dynamic mass redistribution (DMR) [8, 9]. This is because the local refractive index is mostly proportional to the mass density at the sensor surface; thus, a change in local refractive index (i.e., the detected signal) reflects the redistribution of cellular matter within the sensing volume of the biosensor. Due to the relatively short penetration depth (~200 nm) of the evanescent waves, both SPR and RWG measure the DMR originated from the bottom portion of cells. However, for electric biosensors, the cellular responses are often referred to impedance signal, which is sensitive to ionic movement and cell morphological changes [9, 41].

The current biosensor systems differ greatly in instrument configurations. All biosensor systems are standalone readers, except for EnSpire which is a benchtop multimodal microtiter plate reader containing Epic label-free technology in addition to label technologies. All biosensor systems are benchtop instruments targeting low to moderate screening

markets, except for Epic system which is specifically designed for HTS laboratories. Although there are somewhat differences in spatial and temporal resolutions, all biosensor systems provide an averaged response of a population of cells. It is worth noting that due to relatively low volume in manufacturing as well as being in early phase of development and adoption of these technologies, all label-free biosensors are considered to be moderate or high in cost.

3. Cell Adhesion

Cell adhesion refers to the binding of a cell to a surface, extracellular matrix (ECM) or another cell. Almost all of the early works related to label-free whole cell sensing are centered on cell adhesion (Figure 1(a)). This is no surprise partly because cell adhesion often leads to great alterations of local environment at the sensor surface, and partly because cell adhesion is important to the survival and functions of tissue cells.

In a landmark paper of the ECIS, Giaever and Keese [40] investigated the behavior of two fibroblast cell lines on gold electrodes under an alternating electric field at 4000 Hz. Results showed that the adhesion and spreading of these cells had a marked effect on the impedance of the biosensor system. Further, the impedance after cell adhesion fluctuated with time and was sensitive to the presence of an actin inhibitor, cytochalasin B. Later, they found that electric biosensor can detect cell micromotions down to the nanometer level [43]. Thus, they concluded that electronic biosensor is a morphological biosensor for living cells [41].

The ECM onto which cells are harbored is part of environmental cues for regulating the dynamic behaviors of cells. Focal adhesion complex and podosome are commonly formed during the adhesion of cells to a surface and ECM. The focal adhesion complex is a specific attachment site where the cell attaches to the underlying ECM or to cell-surface molecules on neighboring cells via the interaction with integrin receptors in the plasma membrane. The podosome is a cell-matrix adhesion complex that functions in the cell adhesion events associated with cell motility and cell spreading. Label-free biosensors have been used to investigate the adhesion and spreading of distinct types of cells on various surfaces including distinct ECM proteins [44–48] and self-assembled monolayers (SAMs) presenting ligands for integrins [49, 50].

Cell adhesion mechanisms are dependent on the types of cells and ECM. Wegener et al. [45] applied the ECIS to study the adhesion and spreading of Madin Darby Canine kidney (MDCK) epithelial cells and found that distinct mechanisms regulate the cell adhesion on different ECM coatings-cell adhesion on laminin was primarily mediated by the binding of a glycolipid, Forssman antigen, while cell adhesion on fibronectin was mostly due to the interaction with integrin receptors. Luong et al. [48] found that the adhesion of a human rhabdomyosarcoma cell line RDX2C2 to collagen- or laminin-coated gold electrodes increased in the cells transfected with $\alpha 2\beta 1$ integrin. However, on fibronectin the cell adhesion appears to be optimal; the expression of $\alpha 2\beta 1$ integrin had little impact on the cell adhesion degree, but the deletion of its $\alpha 2$ cytoplasmic domain resulted in marked decrease in cell adhesion. This $\alpha 2\beta 1$ mutant was believed to lead to dysregulated recruitment to focal adhesion complexes that mediate the binding of the cells to fibronectin.

Since ECM proteins are macromolecules with multiple binding sites for cell surface integrins, it is highly possible that multiple mechanisms are involved in cell adhesion process. Thus, SAMs presenting a specific integrin binding motif would be advantageous to study cell adhesion. Roberts et al. [49] applied SPR to study the adhesion of bovine capillary endothelial cells on SAMs of alkanethiolates on gold. The SAMs obtained contain a mixture of arginine-glycine-aspartate (RGD) and oligo(ethylene glycol) moieties. RGD is a tripeptide that promotes cell adhesion by binding to cell surface integrin receptors, and oligo(ethylene glycol) moieties resist nonbiospecific adsorption of cells. The attachment and subsequent soluble GRGDSP-induced detachment of cells suggest that RGD alone is sufficient for adhesion and survival of the cells over 24 h.

Cell adhesion to substrates is an active and dynamic process. Characteristics of cell adhesion can be studied in details using label-free biosensors because they allow noninvasive and real-time quantitation of entire cell adhesion process [51–53]. In the first paper describing the use of RWG biosensor for studying cell adhesion, Ramsden et al. found that cell adhesion follows a biphasic process: an initial passive sedimentation followed by active spreading [51]. Using infrared SPR (IR-SPR) which provides an extended penetration depth, Yashunsky et al. found that MDCK epithelial cells underwent a multiphase cell adhesion and proliferation process, starting from initial contact with the substrate to cell spreading, to formation of intercellular contacts, to cell clustering, and finally to the formation of a continuous cell monolayer [52].

An important feature of cell adhesion is the cell-substrate separation distance. Lo et al. applied the ECIS to measure changes in averaged cell-substrate separation in response to an upward magnetic force [53]. The magnetic force was controlled by the position and the number of permanent magnets, applying an average 320 or 560 pN per cell after collagen-coated ferric oxide beads attached to integrin receptors in the dorsal surfaces of osteoblast-like ROS 17/2.8 cells. The average distance between the basal cell surface and substrate was found to be sensitive to temperature; the distance was estimated to be about 84, 45, and 38 nm at temperatures of 4°, 22°, and 37°C, respectively. The cell-substrate distance was also sensitive to external magnetic force; an increased force led to an increased separation distance; and at 22°C the force-induced changes were 11 and 21 nm for 320 and 560 pN, respectively. The authors further estimated that the spring constant of individual adhesion bonds is from about 10^{-3} to 10^{-1} pN nm^{-1}.

The ability of cells to recognize, interact, and respond to environmental signals, including ECM components, is central to many biological processes including inflammation and organogenesis. Thus, it is no surprise to see that various effectors influencing cell adhesion and spreading process have been extensively investigated using label-free biosensors. These effectors include biosensor surface chemistry

[44–51], temperature [53], biosensor surface roughness [54], cell numbers [55], cell types [56], and expression of specific proteins such as integrins [48], cyclooxygenase and lipoxygenase [57], and small molecules that modulate cellular targets important to cell adhesion [8, 58]. Using high throughput RWG we examined the ability of small molecules to modulate cell adhesion process. Using human skin cancerous cell line A431 as a model, RWG measurements showed that vincristine, a plant alkaloid that inhibits microtubule assembly by binding to tubulin proteins, significantly reduced the cell adhesion degree and the kinetics of cell spreading. This study opens possibility for HT screening of cell adhesion-modulating small molecules.

The adhesion of cells to the ECM is a complex and dynamic process involving biological signaling processes. The cell surface integrins often bind to ligands in the ECM substratum and transduce signals through their intracellular domains, thus regulating diverse functions of cells. Label-free biosensors may offer insights about the cell signaling during the cell adhesion process. Using a reverse waveguide configuration that allows multidepth sensing, Horvath et al. showed that the adhesion of fibroblast cells results in inhomogeneity in refractive index within the distinct layers of the cells perpendicular to the biosensor surface [58], possibly due to the consequence of cell signaling during the adhesion process.

Interactions with the ECM shape the signaling and functions of many types of cells and receptors. Further, distinct ECM coatings have been used in a wide array of substrates for characterizing receptor biology, and for assaying and screening drug molecules. Thus, elucidating the impacts of surface chemistry on receptor biology and ligand pharmacology is important to improve the quality of screening assays and hits identified. Recently, we applied RWG to systematically study the influence of distinct ECM coatings on the signaling of endogenous purinergic P2Y receptors in human embryonic kidney HEK293 cells [59]. Purinergic 2Y (P2Y) receptors are a family of G protein-coupled receptors (GPCRs) whose natural agonists are nucleotides including ATP, ADP, UTP, UDP, and UDP-glucose. The label-free receptor assays showed that the potency and efficacy of P2Y agonists were sensitive to ECM coatings. Compared to those on the tissue culture treated surfaces, fibronectin coating increased the potency of all agonists, while gelatin had little impact. Further, fibronectin, collagen IV and gelatin all generally increased the biosensor signal amplitudes of all P2Y agonists.

4. Cell Barrier Functions

Label-free biosensors have found applications in characterizing cell barrier functions including blood-brain barrier (BBB) and epithelial cell barriers (Figure 1(b)). The BBB is the regulated interface between peripheral circulation and central nervous system (CNS) [60]. Endothelial cells line cerebral microvessels and form the BBB. The BBB controls the exchange of molecules between blood and CNS, thus maintaining the homeostasis of the brain microenvironment that is crucial to neuronal signaling. The BBB works together with astrocytes, pericytes, neurons, and the ECM to form a neurovascular unit that is essential for the health and function of the CNS. Further, the BBB often limits *in vivo* efficacy of many drug candidate molecules that are designed to target diseases associated with the CNS such as malignant primary or metastatic brain tumors [61].

A hallmark of the BBB is its intrinsic and high electrical resistance because the BBB consists of capillary endothelial cells that are connected together with continuous tight junctions [62]. The permeability of the BBB is tightly regulated via a vital and complex process involving intracellular signaling and rearrangement of tight junction proteins. Upon stimulation with exogenous signals and substances, the BBB undergoes remodeling, leading to a change in transendothelial permeability. Thus, measuring the permeability of the BBB can offer insights about its integrity and regulation mechanisms. To date, transepithelial electrical resistance (TEER or TER) is the most popular technique to measure the functions of the BBB *in vitro* [63]. Electric biosensors are also suited to measure the functions of *in vitro* endothelia cell model systems, due to their sensitivity to ionic movement and ability to separate extracellular resistance from transcellular resistance [9, 39].

Thrombin is a potent stimulus for endothelium-dependent vasodilatation and is a natural agonist to thrombin receptor (protease-activated receptor-1; PAR1). Thrombin cleaves the amino terminus of the PAR1 to unmask a tethered ligand, which, in turn, binds intramolecularly to and activates the receptor. Thrombin was found to cause the formation of the intercellular gap, leading to decrease in impendence via a protein kinase C inhibitor-sensitive manner when both bovine pulmonary microvessel endothelial cells and bovine pulmonary artery endothelial cells were tested with the ECIS [64].

PAR1 is known to mediate signaling via multiple pathways. Thus, it is possible that multiple pathways govern the thrombin-induced permeability of endothelia cells [65–67]. McLaughlin et al. compared the functional consequences of the PAR1 activation induced by thrombin and PAR activating peptides [65]. Results showed that the potency (EC_{50}: 0.1 nM) for thrombin to cause the increased endothelial monolayer permeability obtained using the ECIS was higher than that to cause mobilization of intracellular calcium (EC_{50}: 1.7 nM). However, the opposite order of activation was observed for the agonist peptides (SFLLRN-$CONH_2$ or TFLLRNKPDK). Further, only PAR1 activation affected barrier function, which is mostly via $G_{\alpha 12/13}$-mediated signaling, instead of $G_{\alpha q}$-mediated signaling. However, for human umbilical vein endothelial cells (HUVECs), Wang et al. [66] found that Ca^{2+}/calmodulin-dependent protein kinase II (CaMKII) is a mediator of thrombin-stimulated increases in permeability of the cell monolayer. CaMKIIδ6 isoform is the predominant CaMKII isoform expressed in the HUVEC. Thrombin potently and maximally increased CaMKIIδ6 activation, which, in turn, activates RhoA. siRNA targeting endogenous CaMKIIδ suppressed expression of the kinase by >80% and significantly inhibited 2.5 nM thrombin-induced increases in monolayer permeability assessed by the ECIS. Further, Rho kinase inhibition strongly suppressed

thrombin-induced HUVEC hyperpermeability, but inhibiting ERK1/2 activation had no effect. Interestingly, the relative contribution of the CaMKIIδ6/RhoA pathway(s) diminished with increasing thrombin doses, indicating recruitment of alternative signaling pathways that regulate the endothelial barrier dysfunction.

The measurement of cell barrier functions with the ECIS is complicated by the presence of multiple types of resistance including cell-cell, cell-matrix, and transcellular resistances [68–70]. Generally, cell-to-cell gaps mainly affect the total resistance value, while cell-to-substrate gaps mainly affect total capacitance value. Effectors that modulate the components of resistance of endothelial cells include cell types and confluency [68, 71], endogenous and exogenous extracellular matrices [71], the presence of exogenous molecules [68, 72, 73], and the substrate [74, 75]. For confluent cultured HUVEC cells, an ECIS measurement suggests that histamine led to a rapid decrease in transendothelial resistance mostly via decreases in cell-cell resistance, and the restoration of resistance was initiated by first increase in cell-matrix resistance, followed by increase in cell-cell resistance [66]. However, histamine led to increased resistance in subconfluent HUVECs in which there was limited or no cell-cell contact. Together, these results suggest that it is possible to deconvolute the molecular mechanisms that regulate the cell barrier functions.

For investigating cell barrier functions, distinct biosensors can offer complementary insights how cell barrier functions are regulated. Because of the short penetration depth or sensing volume, optical biosensors can directly resolve cell-matrix interactions, but cannot directly resolve cell-cell interactions. In contrast, electrical biosensors provide an aggregated measurement that integrates cell-cell and cell-matrix interactions, which can be separated using mathematical modeling [69, 70].

5. Cell-to-Cell Communication

Label-free biosensors are flexible in assay conditions and formats [9]. Together with real-time kinetics, label-free biosensors offer an alternative means to study cell communication (Figure 1(c)). Cell-to-cell communication is essential for multicellular organisms. Cells that are connected through gap junctions can communicate rapidly with each other by passing electrical current or through the diffusion of small second messengers such as cyclic AMP and inositol 1-, 4-, 5-trisphosphate (InsP3). Sriram et al. [76] used the ECIS to study the effect of ovarian cancer cells on the permeability of a confluent pleural mesothelial cell (PMC) monolayer. Results showed that ovarian cancer cells adhered to the PMC monolayer, which, in turn, induced a localized dysfunction of the PMC barrier.

In the case of chemical communication, one cell upon activation releases a stimulus, which diffuses to a target cell that has receptors for the stimulus. The binding of the stimulus activates the receptor, leading to cell signaling in the target cells. Treeratanapiboon et al. [77] applied the ECIS to study the effect of membrane-associated malarin antigen-activated human peripheral blood mononuclear cells (PBMCs) on the integrity of porcine brain capillary endothelial cells (PBCEC). Results showed that the antigens obtained from lysed Plasmodium falciparum schizont-infected erythrocytes caused the PBMC to secrete tumor necrosis factor alpha, which, in turn, led to the breakdown of the endothelia PBCEC monolayer, possibly via disruption of tight junction complexes.

The human immune system enables the destruction of dangerous microbes with great precision via specific targeting of immune cells to sites of infection. Central to the defense mechanism is the interaction of cells with adhesion molecules involved in migration and invasion. Kataoka et al. [78] used the ECIS to study the interaction of monocytes with endothelial cells. By combining AFM with the ECIS, they found that the interaction of monocytic THP-1 cells with the interlukin-1β-stimulated HUVEC monolayer caused a decrease in adhesion to the substrate and an increase in deformability of the endothelial cells. A recent RT-CES study showed that adhesion of human monoblastic cell line U937 cells to endothelial cells was sensitive the presence of lipopolysaccharide [79].

Critical to human immune defense mechanisms is the effector-cell-mediated killing of target cells [80]. For example, natural killer (NK) cell-mediated cytotoxicity requires cell-to-cell contact, which is mediated by the pairwise recognition between multiple receptors present on the surfaces of effector and target cells. The NK cells are considered the major cytotoxic effector cells for innate immunity that can recognize and kill malignantly transformed and infected cells. Glamann and Hansen [81] utilized real-time cell electrical sensing (RT-CES) to detect the interactions between natural killer (NK) cells in suspension and adherent breast cancer cells MCF7 cultured on the electrode biosensor surface. Results showed that NK cells caused apoptosis of MCF7 cells, depending on the NK cell-to-target cell ratio.

6. Cell Signaling

Cell signaling is a tightly regulated process to direct the information flow and ultimately control cellular responses once the cell receives exogenous signals (Figure 1(d)). Signaling by membrane receptors begins with the activation of receptors, followed by generation of intracellular messengers. These messengers then engage various effectors to activate diverse cellular responses including microfilament remodeling, protein trafficking, and alterations in cell adhesion and gene expression. Molecular assays have led to identification of many protein components of various signaling pathways, and high-resolution imaging have resolved many cellular events downstream the activation of a receptor. However, the use of label-free biosensors for studying cell signaling was sparse in the literature before 2004 [64]. Since 2004, two important developments had made label-free a versatile technology for cell signaling study. First, high throughput label-free systems became a reality [29, 42, 82–87], so it became possible to study receptor signaling in native cells without any labels at an unprecedented scale. Second, it

was finally realized that a biosensor signal arising from the activation of a receptor is an integrated response that faithfully reflects the signaling pathways downstream the receptor activation [8, 83, 85, 86]. This led to subsequent adoption of chemical biology for pathway deconvolution of receptor signaling [85, 86]. These developments have turned label-free a morphological biosensor into a systems cell biology biosensor [9, 29].

6.1. G Protein-Coupled Receptors. GPCRs are the largest gene families in the human genome and are the leading molecular target class against which the drugs are designed. GPCRs transmit an enormous number and variety of exogenous signals including light, odorants, neurotransmitters, hormones, and proteases. These exogenous ligands bind to a receptor, and induce a conformational change in the receptor that is then transmitted through the membrane to activate the heterotrimeric GTP-binding proteins (G proteins). The G proteins function as the transducers to relay information to different signaling pathways such as the cyclic AMP and InsP3/diacylglycerol signaling pathways. Since 2005, label-free cellular assays have attracted much attention in molecular delineation of receptor biology and ligand pharmacology for many GPCRs [8, 42, 59, 62, 65, 85–120]. Many GPCRs in distinct cell backgrounds have been examined using label-free cellular assays (Tables 1 and 2). These receptors are either endogenously expressed in native cells including primary cells, or stably or transitly expressed in various cell lines.

Label-free profiling of endogenous receptors in native cells had led to discover "signatures" of distinct classes of GPCRs, depending on the G protein with which the receptor is coupled [9, 42, 86, 88, 92]. Although it holds great promise in a given cell background and for receptors which lead to a single G protein-mediated pathway, the concept of "signature" quickly yielded to "phenotypic response" or "systems cell biology readout" [9, 29, 99, 115, 121]. This is because label-free signals often reflect the cellular background-dependent and receptor-specific complexity in receptor signaling.

Label-free characterization of many GPCRs in various cell backgrounds has led to discovery of novel pathways downstream a receptor [9, 86, 96, 101, 105, 115], and also led to high-resolution classification of distinct ligands acting on a specific receptor [9, 65, 96, 100, 101, 108, 109, 119, 120]. These receptors include bradykinin B2 receptor, protease activated receptor-1 (PAR1) and -2 (PAR2), lysophosphatidic acid (LPA) receptors, histamine H1 receptor, adenosine A2B receptor, β2-adrenergic receptor, purinergic P2Y receptors P2Y1, P2Y2, P2Y4, and P2Y11, sphingosine-1 phosphate (S1P) receptors, vasoactive intestinal peptide (VIP) receptor VPAC1, vasopressin V1a receptor, serotonin 5HT1A receptor, dopamine D1, D2, D3, and D5 receptors, muscarinic M1, M2, M3, and M4 receptors, cannabinoid CB1 and CB2 receptors,, pituitary adenylate cyclase-activating polypeptide receptor (PACAP1), chemokine CXCR2 receptor, free fatty acid receptor-1, 2 and 3 (GPR40, GPR43, and GPR41, respectively), metabotropic glutamate receptor 1 (mGluR1) and 7 (mGluR7), prostaglandin EP2 and EP4 receptors, GPR55, chemoattractant receptor-homologous molecule expressed on Th2 cells (CRTH2), corticotropin releasing hormone receptor 1 (CRF), melanocortin receptor-4 (MC4R), mu and delta opioid receptors, and GPR35.

6.2. Receptor Tyrosine Kinases. Receptor tyrosine kinases (RTKs) are a family of cell surface growth factor receptors with an intrinsic, ligand-regulated tyrosine-kinase activity. Epidermal growth factor receptor (EGFR) is one of the most well-studied RTKs. EGFR is a single membrane-spanning protein with an N-terminal extracellular ligand-binding domain and a C-terminal region that has a kinase domain and numerous tyrosine docking sites participating signaling. EGF binds to the receptor and stimulates its intrinsic protein-tyrosine kinase activity, initiating signal transduction that principally involves multiple pathways, including MAPK, STAT, and the PLCγ pathways. RWG was the first label-free biosensor used to characterize and deconvolute the pathways of EGFR in native A431 cells [39, 83, 85]. This study was based on chemical intervention of the EGF-induced DMR signal to map out the pathways downstream the EGFR activation (Figure 3). This study had led to a hypothesis that label-free signals arising from the activation of a receptor is an integrative readout of systems cell biology. Follow-up studies of EGFR signaling with different label-free technologies [122–127] confirmed such a hypothesis.

6.3. Ion Channels. Ion channels control the electrical properties of neurons and other excitable cells by selectively allowing ions to flow through the plasma membrane. These receptors transduce the information into channel opening, leading to marked amplification of the signal via conducting large amounts of charge. Such an amplification makes these receptors effective transducers of sensory information. Ion channels are often modified by signaling proteins and molecules to regulate neuronal excitability and other cell functions. Label-free cellular assays hold promise to follow in real-time the pathways downstream the open and close of ion channels. Such an ability overcomes the poor resolution of traditional assays to examine the interaction between channels and regulatory proteins in living cells. Using DMR assays enabled by RWG biosensor, Fleming and Kaczmarek found that the activation of endogenous Gq-coupled receptors in HEK-293 cells was significantly modified by the presence of a sodium-activated potassium channel, Slack-B [110]. Recently, Pänke et al. also showed that electric biosensor is also feasible to characterize transient receptor potential (TRP) ion channels including TRP1 [128]. TRP channels are nonselective ion channels permeable to cations including Na^+, Ca^{2+}, and Mg^{2+}. The TRP channels are involved in many Ca^{2+}-mediated cell functions and implicated in inflammation.

6.4. Immunoreceptors. Immunoglobulin E (IgE) is one of immunoglobulins produced by the immune system, and the one most associated with allergies. Allergic individuals exposed to minute quantities of allergen often experience an immediate response, which is due to the permanent sensitization of mucosal mast cells by allergen-specific IgE antibodies bound to their high-affinity receptor (FcεRI). The IgE-mediated mast cell activation includes two important

Table 1: Receptors, cell lines, and technologies and key points of the studies related to the use of label-free cellular assays for GPCRs.

Receptors	Cells	Biosensors	Key findings	Ref
PAR2 Bradykinin B2	A431	DMR	Biosensor signal is originated from DMR	[8]
Adenosine A2B Bradykinin B2 β2-adrenergic	A431	DMR	Similarity analysis segregates ligands into clusters	[38]
EP4 H1 LPA receptors P2Y1			DMR signatures of distinct classes of GPCRs	[92]
PAR1 PAR2 S1P receptors VPAC1			Integrative roles of adenylyl cyclases in GPCRs	[93]
P2Y1/2/11	HEK293	DMR	ECM coatings impact receptor signaling	[59]
LPA receptors	Porcine brain endothelial cells	ECIS	LPA increases tight junction permeability	[62]
PAR1	Primary endothelial cells	ECIS	Thrombin promotes the formation of intercellular gaps	[64]
PAR1	HMEC-1	ECIS	Functional selectivity of PAR1 agonists	[65]
Bradykinin B2	A431	DMR	Systems cell biology of B2 receptor	[86]
PAR1	A431	DMR	HTS compatibility test	[87]
Endogenous receptors	HeLa U-937 U2OS TE671	CDS	Receptor panning	[88] [89]
LPA receptors S1P receptors	Rabit corneal epithelial cell Rabit corneal endothelial cells	ECIS	The role of Gi signaling in cell monolayer permeability	[90]
Histamine H1 Vasopressin V1a 5-HT1A D1	CHO-H1 1321-N1-V1a CHO-5HT1A CHO-D1	RT-CES	Impedance signals were correlated with morphological changes	[91]
PAR1 PAR2	A431	DMR	Receptor cross-desensitization	[94]
Dopamine D2S Muscarinic M4 Dopamine D5	CHO-D2S CHO-M4 CHO-D5	CDS	Ligand pharmacology characterization	[95]
Muscarinic M1 Melanocortin MC4 Cannabinoid CB1 Cannabinoid CB2	CHO-M1 CHO-MC4 HEK-MC4 CHO-CB1 CHO-CB2	CDS	Ligand-directed functional selectivity GPCR pleiotropic signaling	[96]
Histamine H1 β2-AR	A431	DMR	Duplexed receptor assays for HT screening	[97]

events: cell sensitization resulting from IgE binding to the FcεRI receptor and cell activation triggered by allergen-mediated oligomerization of membrane-bound IgE. Abassi et al. used the RT-CES to characterize IgE-mediated activation of RBL-2H3 mast and found that the impedance results were correlated with morphological dynamics and mediator release [129].

Hide and his colleagues reported a series of papers related to the use of SPR for characterizing the activation of RBL-2H3 mast cell and found that SPR detects the downstream events of active PKCβ in antigen-stimulated mast cells [130–133]. The RBL-2H3 mast cells overexpressing dominant-negative spleen tyrosine kinase or src-like adaptor protein led to a suppressed SPR signal arising from the mast cell activation. Likewise, expression of dominant-negative linker for activation of T cells and Grb2-related adaptor protein led to almost complete suppression of the antigen-induced SPR signal. Overexpression of protein kinase C

Table 2: Receptors, cell lines, and technologies and key points of the studies related to the use of label-free cellular assays for GPCRs.

Receptors	Cells	Biosensor	Key findings	Ref
Dopamine D3 Muscarinic M1	CHO-D3 CHO-M1	DMR	Ligand pharmacology characterization	[98]
β2-AR	A431	DMR	Systems cell biology of the β2AR Ligand-directed functional selectivity Ligand-directed desensitization	[99] [100] [101]
PACAP1	TM3	RT-CES	PACAP agonists suppress the proliferation of immature mouse Leydig cell line TM3	[102]
CXCR2	NIH-3T3-CXCR2	ECIS	The role of CXCR2 in cell transformation	[103]
Muscarinic M2	CHO-M2	DMR	Novel dualsteric M2 agonists	[104] [105]
Muscarinic M1	CHO-M1	DMR	HT screening identified novel M1 ligands	[106]
GPR40/FFA1 GPR41/FFA3 GPR43/FFA2	1321N1-GPR40 HEK-GPR43 HEK-GPR41 HEK-GPR40	DMR	Discovery of potent and selective agonists for FFA receptors	[107] [108] [109]
Endogenous muscarinic receptor	HEK-293	DMR	GPCR activation modulates Slack ion channel activity	[110]
Cannabinoid CB2 mGluR1	CHO-CB2 CHO-mGluR1	RT- CES	Ligand pharmacology characterization	[111]
Prostaglandin EP2	C6G-EP2 HCT15-EP2	DMR	Compound nanoparticles act as allosteric potentiators	[112]
mGluR7	HEK-mGluR7	DMR	Negative allosteric modulators	[113]
GPR55	HEK-GPR55	DMR	GPR55 pleiotropic signaling	[114]
Muscarinic M2 β2-AR Muscarinic M3 GPR55 CRTH2 EP2/3 GPR40 EP receptors EP receptors	CHO-M2 CHO-β2AR CHO-M3 HEK-GPR55 HEK-CRTH2 HEK-EP2/3 HEK-GPR40 HaCaT Keratinocytes	DMR	Pathway deconvolution GPCR pleiotropic signaling Novel pathways for M3	[115]
Muscarinic M1 Muscarinic M2 CRF MC4R	CHO-M1 CHO-M2 CHO-CRF CHO-MC4R	CDS BIND DMR	Label-free reader comparison	[116]
CRTH2	HEK-CRTH2	DMR	Novel function of CRTH2 C-terminal	[117]
Mu opioid Cannabinoid CB1 Cannabinoid CB2 Delta opioid	CHO-MOR CHO-CB1 CHO-CB2 CHO-DOR	DMR	Pathway deconvolution	[118]
PAR1	A549	DMR	Ligand-directed functional selectivity on receptor trafficking	[119]
GPR35	HT29	DMR	Discovery of tyrphostins as GPR35 agonists	[120]

(PKCs), apart from PKCβ, showed a reduced SPR signal in response to antigen stimulation, while knockdown PKCβ with interference RNA suppressed the antigen-induced signal. These results indicate that the activation of multiple kinases in the PKC pathway is determinative in the antigen-induced SPR signal of mast cells.

7. Viral Infection

Viral infections provoke an immune response that normally leads to elimination of the infecting virus. However, certain viruses including those causing AIDS evade human immune responses and result in chronic infections. Cytopathic effect

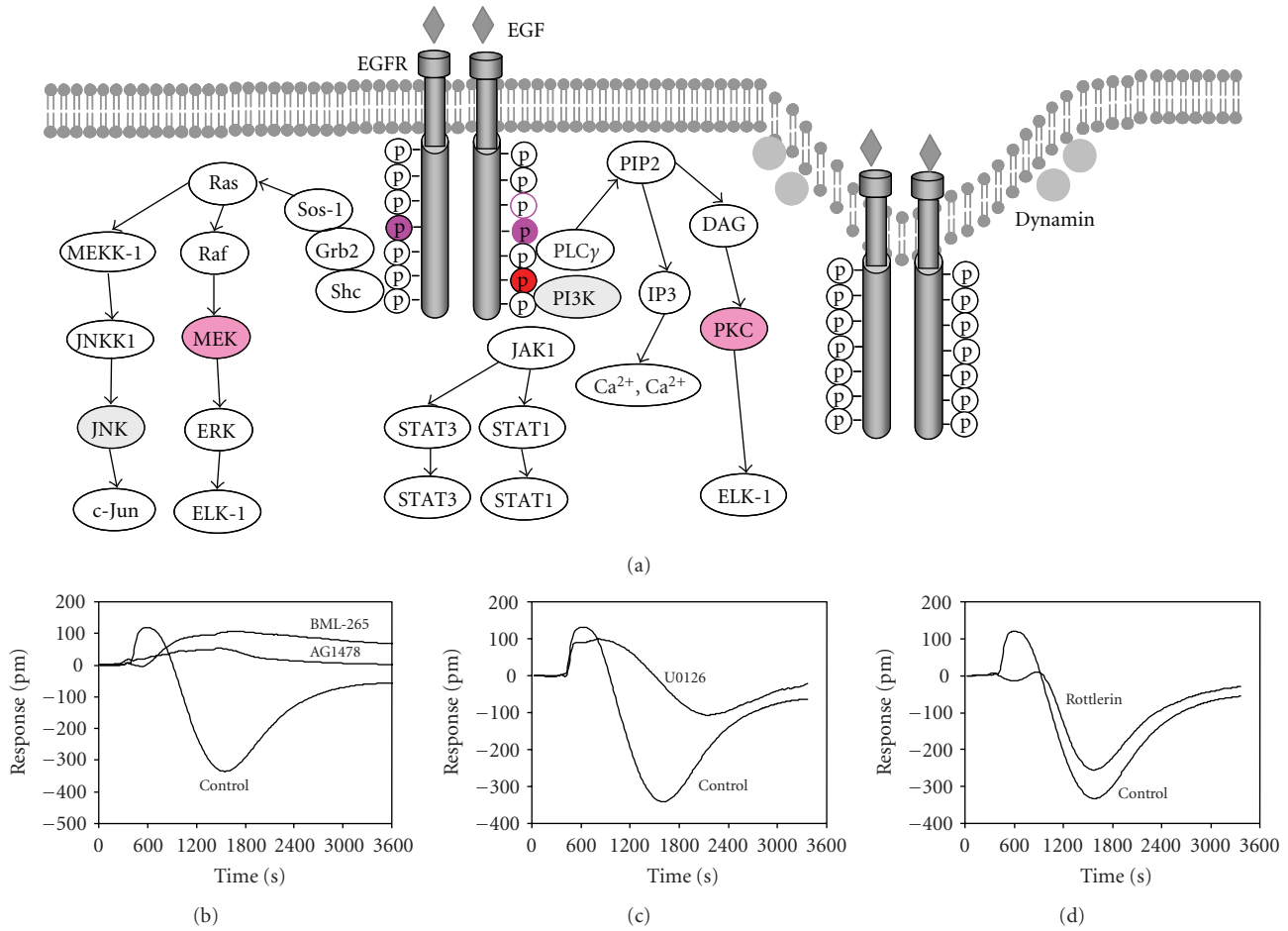

Figure 3: The DMR signal arising from epidermal growth factor (EGF) activated EGFR in native A431 cells is a systems cell biology readout of the EGFR. (a) Schematic drawing of EGFR signaling. (b, c, d) The sensitivity of the EGF DMR signal to different modulators, the two EGFR tyrosine kinase inhibitors AG1478 and BML-265 (b), the MEK1/2 inhibitor U0126 (c) and the PKC kinase inhibitor rottlerin (d). The control is the EGF response of cells pretreated with the assay vehicle only. In all experiments, EGF was at 32 nM, whereas the rest compounds used to pretreat the cells were at 10 μM.

(CPE) due to virus infection in cell culture has been used as *in vitro* model systems to study viral infection and screen molecules that inhibit the viral infection. However, the CPE has long been difficult to quantify. The ability to work with native cells makes label-free an attractive means to real-time-monitor the viral infection process (Figure 1(e)). The ECIS has been explored to monitor the progression of CPE due to influenza A virus infection [134]. Recently, Owens et al. used the DMR assays to monitor the infection process of HeLa cells with two different human rhinovirus strains, HRV14 and HRV16 [135]. Results showed that both virus strains triggered a virus titer-dependent DMR signal, which is correlated with multiple phases of viral infection, starting from early signaling mediated by viral entry to viral replication, and finally cell apoptosis. This study also showed that it is possible to screen inhibitors that modulate distinct processes of viral infection. Jia et al. also showed that DMR assays with Epic system enabled high throughput screening of inhibitors that block the cytopathic effect induced by influenza virus (A/Udorn/72, H3N2) [136].

Cocaine is a suspected cofactor in human-immunodeficiency-virus- (HIV-) associated dementia. However, it is unknown how cocaine influences HIV infection. Fiala et al. used the ECIS to study the mechanism by which cocaine increases HIV-1 invasion through brain microvascular endothelial cells (BMVECs) [137]. Results showed that cocaine treatment of BMVECs disrupts intercellular junctions and induces cell ruffling, and also alters the location patterns of virus once entered the cells. This study suggests that the toxicity of cocaine for the blood-brain barrier may lead to increased virus neuroinvasion and neurovascular complications of cocaine abuse.

Recombinant viral vectors are widely used in genetic manipulation of living cells. However, the impact of these vectors on cell biology is largely unknown. Using the ECIS, Müller et al. found that adenoviral transfection vector (Ad5-derivate) dose dependently caused the apoptosis of porcine ileal epithelial cell line IPI-2I [138]. This study suggests that label-free is an attractive alterative to determine minimal nontoxic doses for viral vector-based transfection study.

8. Label-Free versus Label-Based Cellular Assays

The quest to discover the full complement of cell signaling components has made label-based cellular assays the mainstream technology in cell biology. Label technologies can provide high spatial resolutions to resolve the location, trafficking, and organization of single signaling molecules within a specific pathway. Multicolor molecular assays can further investigate the interactions among distinct signaling molecules and the functional consequences of the invention of a cellular target with a molecule. However, the molecular assays often give rise to low temporal resolution, are weak in resolving cell-surface biology, and provide a linear measure of cell signaling.

Label-free cellular assays are complementary to label-based technologies. First, in contrast to label technologies which are biased towards a single pathway and/or a single molecule, label-free offers integrated and systems cell biology readouts of cell signaling. This allows one to study the integration of cell signaling in native cells, to map out signaling pathways downstream receptor activation with wide pathway coverage, and to greatly differentiate the on-target pharmacology of drug molecules acting on a single target receptor [139]. Second, in comparison with the relatively poor dynamic resolution of label technologies, label-free provides a real-time kinetic measurement of cell signaling with high temporal resolutions and high sensitivity. This allows one to track the entire process of diverse cell signaling and cellular processes in native cells. Third, in contrast to label technologies that often require modifications or even destruction of live cells, label-free is noninvasive without the need of any cellular manipulations. This allows one to design distinct assay formats, as well as to integrate label-free with other technologies, so different aspects of receptor signaling and drug pharmacology can be studied. For example, adoption of microfluidics enables one to control the duration of receptor activation, so that comparison of label-free signals under sustained stimulation conditions with those under pulse stimulation conditions can differentiate the routes of signal propagation after receptor activation, as well as the long acting agonism or antagonism of drug molecules [9, 101, 119, 140, 141]. However, unlike label technologies, label-free lacks intracellular spatial resolution to resolve many important cellular processes, including the location and organization of signaling molecules, intracellular trafficking, metabolism, and cytoskeletal remodeling. Thus, it is important to know what the hypotheses is being tested so the appropriate technologies can be used.

9. Conclusion Remarks

Advances in label-free biosensors, particularly high throughput screening platforms and adoption of chemical biology tools in label-free cellular assays, have made them indispensable platforms in cell biology studies. Today, label-free biosensors have found applications in a wide array of cellular processes ranging from cell adhesion to cell barrier functions, receptor signaling, and viral infection. The ever increasing use of label-free cellular assays for studying various targets including GPCRs, RTKs, ion channels, and immunoreceptors have been witnessed in the increased numbers of published literature in recent years. Novel insights about the integration of cell signaling, the complexity of receptor signaling pathways, and the modes of action of drug molecules have been obtained. New generation label-free currently under development will have better spatial resolutions, so that cell signaling can be studied at the single cell level [142–145]. Development of novel methodologies for data analysis [9, 38, 146] will further advance label-free to become a *de facto* technology in cell biology.

References

[1] B. R. Stockwell, "Chemical genetics: ligand-based discovery of gene function," *Nature Reviews Genetics*, vol. 1, no. 2, pp. 116–125, 2000.

[2] G. J. Hannon, "RNA interference," *Nature*, vol. 418, no. 6894, pp. 244–251, 2002.

[3] J. Inglese, R. L. Johnson, A. Simeonov et al., "High-throughput screening assays for the identification of chemical probes," *Nature Chemical Biology*, vol. 3, no. 8, pp. 466–479, 2007.

[4] T. P. Kenakin, "Cellular assays as portals to seven-transmembrane receptor-based drug discovery," *Nature Reviews Drug Discovery*, vol. 8, no. 8, pp. 617–626, 2009.

[5] K. Oda, Y. Matsuoka, A. Funahashi, and H. Kitano, "A comprehensive pathway map of epidermal growth factor receptor signaling," *Molecular Systems Biology*, vol. 1, article 2005.0010, 2005.

[6] J. D. Jordan, E. M. Landau, and R. Iyengar, "Signaling networks: the origins of cellular multitasking," *Cell*, vol. 103, no. 2, pp. 193–200, 2000.

[7] B. N. Kholodenko, "Four-dimensional organization of protein kinase signaling cascades: the roles of diffusion, endocytosis and molecular motors," *Journal of Experimental Biology*, vol. 206, no. 12, pp. 2073–2082, 2003.

[8] Y. Fang, A. M. Ferrie, N. H. Fontaine, J. Mauro, and J. Balakrishnan, "Resonant waveguide grating biosensor for living cell sensing," *Biophysical Journal*, vol. 91, no. 5, pp. 1925–1940, 2006.

[9] Y. Fang, "Label-free receptor assays," *Drug Discovery Today Technologies*, vol. 7, no. 1, pp. e5–e11, 2010.

[10] E. A-Hassan, W. F. Heinz, M. D. Antonik et al., "Relative microelastic mapping of living cells by atomic force microscopy," *Biophysical Journal*, vol. 74, no. 3, pp. 1564–1578, 1998.

[11] A. Ehrlicher and J. H. Hartwig, "Cell mechanics: contracting to stiffness," *Nature Materials*, vol. 10, no. 1, pp. 12–13, 2011.

[12] J. X. Cheng and X. S. Xie, "Coherent anti-Stokes Raman scattering microscopy: instrumentation, theory, and applications," *Journal of Physical Chemistry B*, vol. 108, no. 3, pp. 827–840, 2004.

[13] M. C. Wang, W. Min, C. W. Freudiger, G. Ruvkun, and X. S. Xie, "RNAi screening for fat regulatory genes with SRS microscopy," *Nature Methods*, vol. 8, no. 2, pp. 135–138, 2011.

[14] F. Vollmer and S. Arnold, "Whispering-gallery-mode biosensing: label-free detection down to single molecules," *Nature Methods*, vol. 5, no. 7, pp. 591–596, 2008.

[15] M. Zourob, S. Elwary, X. Fan, S. Mohr, and N. J. Goddard, "Label-free detection with the resonant mirror biosensor," *Methods in Molecular Biology*, vol. 503, pp. 89–138, 2009.

[16] B. Liedberg, C. Nylander, and I. Lundstrom, "Biosensing with surface plasmon resonance—how it all started," *Biosensors and Bioelectronics*, vol. 10, no. 8, pp. 1–9, 1995.

[17] R. H. Ritchie, "Plasma losses by fast electrons in thin films," *Physical Review*, vol. 106, no. 5, pp. 874–881, 1957.

[18] A. Otto, "Excitation of nonradiative surface plasma waves in silver by the method of frustrated total reflection," *Zeitschrift für Physik A Hadrons and Nuclei*, vol. 216, no. 4, pp. 398–410, 1968.

[19] H. N. Daghestani and B. W. Day, "Theory and applications of surface plasmon resonance, resonant mirror, resonant waveguide grating, and dual polarization interferometry biosensors," *Sensors*, vol. 10, no. 11, pp. 9630–9646, 2010.

[20] R. L. Rich and D. G. Myszka, "Advances in surface plasmon resonance biosensor analysis," *Current Opinion in Biotechnology*, vol. 11, no. 1, pp. 54–61, 2000.

[21] C. E. Jordan, A. G. Frutos, A. J. Thiel, and R. M. Corn, "Surface plasmon resonance imaging measurements of DNA hybridization adsorption and streptavidin/DNA multilayer formation at chemically modified gold surfaces," *Analytical Chemistry*, vol. 69, no. 24, pp. 4939–4947, 1997.

[22] A. Dahlin, M. Zäch, T. Rindzevicius, M. Käll, D. S. Sutherland, and F. Höök, "Localised surface plasmon resonance sensing of lipid-membrane-mediated biorecognition events," *Journal of the American Chemical Society*, vol. 127, no. 14, pp. 5043–5048, 2005.

[23] R. W. Wood, "Remarkable spectrum from a diffraction grating," *Philosophical Magazine*, vol. 4, no. 40, pp. 396–402, 1902.

[24] A. Hessel and A. A. Oliner, "A new theory of Wood's anomalies on optical gratings," *Applied Optics*, vol. 4, no. 10, pp. 1275–1297, 1965.

[25] K. Tiefenthaler and W. Lukosz, "Grating couplers as integrated optical humidity and gas sensors," *Thin Solid Films*, vol. 126, no. 3-4, pp. 205–211, 1985.

[26] K. Teifenthaler and W. Lukosz, "Sensitivity of grating couplers as integrated-optical chemical sensors," *Journal of the Optics Society of America*, vol. 6, no. 2, pp. 209–220, 1989.

[27] B. Cunningham, P. Li, B. Lin, and J. Pepper, "Colorimetric resonant reflection as a direct biochemical assay technique," *Sensors and Actuators B*, vol. 81, no. 2-3, pp. 316–328, 2002.

[28] M. Wu, B. Coblitz, S. Shikano et al., "Phospho-specific recognition by 14-3-3 proteins and antibodies monitored by a high throughput label-free optical biosensor," *FEBS Letters*, vol. 580, no. 24, pp. 5681–5689, 2006.

[29] Y. Fang, "Label-free cell-based assays with optical biosensors in drug discovery," *Assay and Drug Development Technologies*, vol. 4, no. 5, pp. 583–595, 2006.

[30] M. A. Cooper, "Optical biosensors: where next and how soon?" *Drug Discovery Today*, vol. 11, no. 23-24, pp. 1061–1067, 2006.

[31] R. L. Rich and D. G. Myszka, "Survey of the year 2005 commercial optical biosensor literature," *Journal of Molecular Recognition*, vol. 19, no. 6, pp. 478–534, 2006.

[32] Y. Fang, "Non-invasive optical biosensor for probing cell signaling," *Sensors*, vol. 7, no. 10, pp. 2316–2329, 2007.

[33] A. K. Shiau, M. E. Massari, and C. C. Ozbal, "Back to basics: label-free technologies for small molecule screening," *Combinatorial Chemistry and High Throughput Screening*, vol. 11, no. 3, pp. 231–237, 2008.

[34] P. H. Lee, "Label-free optical biosensor: a tool for G protein-coupled receptors pharmacology profiling and inverse agonists identification," *Journal of Receptors and Signal Transduction*, vol. 29, no. 3-4, pp. 146–153, 2009.

[35] J. J. Ramsden and R. Horvath, "Optical biosensors for cell adhesion," *Journal of Receptors and Signal Transduction*, vol. 29, no. 3-4, pp. 211–223, 2009.

[36] M. A. Cooper, "Signal transduction profiling using label-free biosensors," *Journal of Receptors and Signal Transduction*, vol. 29, no. 3-4, pp. 224–233, 2009.

[37] M. Rocheville and J. C. Jerman, "7TM pharmacology measured by label-free: a holistic approach to cell signalling," *Current Opinion in Pharmacology*, vol. 9, no. 5, pp. 643–649, 2009.

[38] Y. Fang, "Probing cancer signaling with resonant waveguide grating biosensors," *Expert Opinion on Drug Discovery*, vol. 5, no. 12, pp. 1237–1248, 2010.

[39] R. McGuinness, "Impedance-based cellular assay technologies: recent advances, future promise," *Current Opinion in Pharmacology*, vol. 7, no. 5, pp. 535–540, 2007.

[40] I. Giaever and C. R. Keese, "Monitoring fibroblast behavior in tissue culture with an applied electric field," *Proceedings of the National Academy of Sciences of the United States of America*, vol. 81, no. 12, pp. 3761–3764, 1984.

[41] I. Giaever and C. R. Keese, "A morphological biosensor for mammalian cells," *Nature*, vol. 366, no. 6455, pp. 591–592, 1993.

[42] G. J. Ciambrone, V. F. Liu, D. C. Lin, R. P. McGuinness, G. K. Leung, and S. Pitchford, "Cellular dielectric spectroscopy: a powerful new approach to label-free cellular analysis," *Journal of Biomolecular Screening*, vol. 9, no. 6, pp. 467–480, 2004.

[43] I. Giaever and C. R. Keese, "Micromotion of mammalian cells measured electrically," *Proceedings of the National Academy of Sciences of the United States of America*, vol. 88, no. 17, pp. 7896–7900, 1991.

[44] M. Kowolenko, C. R. Keese, D. A. Lawrence, and I. Giaever, "Measurement of macrophage adherence and spreading with weak electric fields," *Journal of Immunological Methods*, vol. 127, no. 1, pp. 71–77, 1990.

[45] J. Wegener, C. R. Keese, and I. Giaever, "Electric cell-substrate impedance sensing (ECIS) as a noninvasive means to monitor the kinetics of cell spreading to artificial surfaces," *Experimental Cell Research*, vol. 259, no. 1, pp. 158–166, 2000.

[46] C. Xiao, B. Lachance, G. Sunahara, and J. H. T. Luong, "An in-depth analysis of electric cell-substrate impedance sensing to study the attachment and spreading of mammalian cells," *Analytical Chemistry*, vol. 74, no. 6, pp. 1333–1339, 2002.

[47] Y. Chen, J. Zhang, Y. Wang et al., "Real-time monitoring approach: assessment of effects of antibodies on the adhesion of NCI-H460 cancer cells to the extracellular matrix," *Biosensors and Bioelectronics*, vol. 23, no. 9, pp. 1390–1396, 2008.

[48] J. H. T. Luong, C. Xiao, B. Lachance et al., "Extended applications of electric cell-substrate impedance sensing for assessment of the structure-function of $\alpha 2\beta 1$ integrin," *Analytica Chimica Acta*, vol. 501, no. 1, pp. 61–69, 2004.

[49] C. Roberts, C. S. Chen, M. Mrksich, V. Martichonok, D. E. Ingber, and G. M. Whitesides, "Using mixed self-assembled monolayers presenting RGD and $(EG)_3OH$ groups to characterize long-term attachment of bovine capillary endothelial cells to surfaces," *Journal of the American Chemical Society*, vol. 120, no. 26, pp. 6548–6555, 1998.

[50] C. H. Chang, J. D. Liao, J. J. J. Chen, M. S. Ju, and C. C. K. Lin, "Cell adhesion and related phenomena on the surface-modified Au-deposited nerve microelectrode examined by

total impedance measurement and cell detachment tests," *Nanotechnology*, vol. 17, no. 10, pp. 2449–2457, 2006.

[51] J. J. Ramsden, S. Y. Li, J. E. Prenosil, and E. Heinzle, "Kinetics of adhesion and spreading of animal cells," *Biotechnology and Bioengineering*, vol. 43, no. 10, pp. 939–945, 1994.

[52] V. Yashunsky, V. Lirtsman, M. Golosovsky, D. Davidov, and B. Aroeti, "Real-time monitoring of epithelial cell-cell and cell-substrate interactions by infrared surface plasmon spectroscopy," *Biophysical Journal*, vol. 99, no. 12, pp. 4028–4036, 2010.

[53] C. M. Lo, M. Glogauer, M. Rossi, and J. Ferrier, "Cell-substrate separation: effect of applied force and temperature," *European Biophysics Journal*, vol. 27, no. 1, pp. 9–17, 1998.

[54] R. Lange, F. Lüthen, U. Beck, J. Rychly, A. Baumann, and B. Nebe, "Cell-extracellular matrix interaction and physicochemical characteristics of titanium surfaces depend on the roughness of the material," *Biomolecular Engineering*, vol. 19, no. 2-6, pp. 255–261, 2002.

[55] C. Xiao, B. Lachance, G. Sunahara, and J. H. T. Luong, "An in-depth analysis of electric cell-substrate impedance sensing to study the attachment and spreading of mammalian cells," *Analytical Chemistry*, vol. 74, no. 6, pp. 1333–1339, 2002.

[56] I. H. Heijink, S. M. Brandenburg, J. A. Noordhoek, D. S. Postma, D. J. Slebos, and A. J. M. Van Oosterhout, "Characterisation of cell adhesion in airway epithelial cell types using electric cell-substrate impedance sensing," *European Respiratory Journal*, vol. 35, no. 4, pp. 894–903, 2010.

[57] C. K. Choi, M. Sukhthankar, C. H. Kim et al., "Cell adhesion property affected by cyclooxygenase and lipoxygenase: opto-electric approach," *Biochemical and Biophysical Research Communications*, vol. 391, no. 3, pp. 1385–1389, 2010.

[58] R. Horvath, K. Cottier, H. C. Pedersen, and J. J. Ramsden, "Multidepth screening of living cells using optical waveguides," *Biosensors and Bioelectronics*, vol. 24, no. 4, pp. 799–804, 2008.

[59] E. Tran, H. Sun, and Y. Fang, "Dynamic mass redistribution assays decode surface influence on signaling of endogenous purinergic P2Y receptors," *Assay and Drug Development Technologies*. In press.

[60] B. T. Hawkins and T. P. Davis, "The blood-brain barrier/neurovascular unit in health and disease," *Pharmacological Reviews*, vol. 57, no. 2, pp. 173–185, 2005.

[61] P. R. Lockman, R. K. Mittapalli, K. S. Taskar et al., "Heterogeneous blood-tumor barrier permeability determines drug efficacy in experimental brain metastases of breast cancer," *Clinical Cancer Research*, vol. 16, no. 23, pp. 5664–5678, 2010.

[62] C. Schulze, C. Smales, L. L. Rubin, and J. M. Staddon, "Lysophosphatidic acid increases tight junction permeability in cultured brain endothelial cells," *Journal of Neurochemistry*, vol. 68, no. 3, pp. 991–1000, 1997.

[63] M. Gumbleton and K. L. Audus, "Progress and limitations in the use of in vitro cell cultures to serve as a permeability screen for the blood-brain barrier," *Journal of Pharmaceutical Sciences*, vol. 90, no. 11, pp. 1681–1698, 2001.

[64] C. Tiruppathi, A. B. Malik, P. J. Del Vecchio, C. R. Keese, and I. Giaever, "Electrical method for detection of endothelial cell shape change in real time: assessment of endothelial barrier function," *Proceedings of the National Academy of Sciences of the United States of America*, vol. 89, no. 17, pp. 7919–7923, 1992.

[65] J. N. McLaughlin, L. Shen, M. Holinstat, J. D. Brooks, E. DiBenedetto, and H. E. Hamm, "Functional selectivity of G protein signaling by agonist peptides and thrombin for the protease-activated receptor-1," *Journal of Biological Chemistry*, vol. 280, no. 26, pp. 25048–25059, 2005.

[66] Z. Wang, R. Ginnan, I. F. Abdullaev, M. Trebak, P. A. Vincent, and H. A. Singer, "Calcium/calmodulin-dependent protein kinase II delta 6 (CaMKIIδ 6) and RhoA involvement in thrombin-induced endothelial barrier dysfunction," *Journal of Biological Chemistry*, vol. 285, no. 28, pp. 21303–21312, 2010.

[67] A. K. Fordjour and E. O. Harrington, "PKCδ influences p190 phosphorylation and activity: events independent of PKCδ-mediated regulation of endothelial cell stress fiber and focal adhesion formation and barrier function," *Biochimica et Biophysica Acta*, vol. 1790, no. 10, pp. 1179–1190, 2009.

[68] A. B. Moy, M. Winter, A. Kamath et al., "Histamine alters endothelial barrier function at cell-cell and cell- matrix sites," *American Journal of Physiology*, vol. 278, no. 5, pp. L888–L898, 2000.

[69] J. E. Bodmer, A. English, M. Brady et al., "Modeling error and stability of endothelial cytoskeletal membrane parameters based on modeling transendothelial impedance as resistor and capacitor in series," *American Journal of Physiology*, vol. 289, no. 3, pp. C735–C747, 2005.

[70] A. E. English, A. B. Moy, K. L. Kruse, R. C. Ward, S. S. Kirkpatrick, and M. H. Goldman, "Instrumental noise estimates stabilize and quantify endothelial cell micro-impedance barrier function parameter estimates," *Biomedical Signal Processing and Control*, vol. 4, no. 2, pp. 86–93, 2009.

[71] C. Hartmann, A. Zozulya, J. Wegener, and H. J. Galla, "The impact of glia-derived extracellular matrices on the barrier function of cerebral endothelial cells: an in vitro study," *Experimental Cell Research*, vol. 313, no. 7, pp. 1318–1325, 2007.

[72] C. Betzen, R. White, C. M. Zehendner et al., "Oxidative stress upregulates the NMDA receptor on cerebrovascular endothelium," *Free Radical Biology and Medicine*, vol. 47, no. 8, pp. 1212–1220, 2009.

[73] P. Anastasiadis and J. S. Allen, "Ultrasound-mediated endothelial cell permeability changes with targeted contrast agents," in *Proceedings of the IEEE International Ultrasonics Symposium (IUS '09)*, Rome, Italy, September 2009.

[74] C. M. Lo, C. R. Keese, and I. Giaever, "Cell-substrate contact: another factor may influence transepithelial electrical resistance of cell layers cultured on permeable filters," *Experimental Cell Research*, vol. 250, no. 2, pp. 576–580, 1999.

[75] T. Sun, E. J. Swindle, J. E. Collins, J. A. Holloway, D. E. Davies, and H. Morgan, "On-chip epithelial barrier function assays using electrical impedance spectroscopy," *Lab on a Chip*, vol. 10, no. 12, pp. 1611–1617, 2010.

[76] P. S. Sriram, K. A. Mohammed, N. Nasreen et al., "Adherence of ovarian cancer cells induces pleural mesothelial cell (PMC) permeability," *Oncology Research*, vol. 13, no. 2, pp. 79–85, 2002.

[77] L. Treeratanapiboon, K. Psathaki, J. Wegener, S. Looareesuwan, H. J. Galla, and R. Udomsangpetch, "In vitro study of malaria parasite induced disruption of blood-brain barrier," *Biochemical and Biophysical Research Communications*, vol. 335, no. 3, pp. 810–818, 2005.

[78] N. Kataoka, K. Iwaki, K. Hashimoto et al., "Measurements of endothelial cell-to-cell and cell-to-substrate gaps and micromechanical properties of endothelial cells during monocyte adhesion," *Proceedings of the National Academy of Sciences of the United States of America*, vol. 99, no. 24, pp. 15638–15643, 2002.

[79] Y. Ge, T. Deng, and X. Zheng, "Dynamic monitoring of changes in endothelial cell-substrate adhesiveness during leukocyte adhesion by microelectrical impedance assay," *Acta Biochimica et Biophysica Sinica*, vol. 41, no. 3, pp. 256–262, 2009.

[80] J. Lieberman, "The ABCs of granule-mediated cytotoxicity: new weapons in the arsenal," *Nature Reviews Immunology*, vol. 3, no. 4, pp. 361–370, 2003.

[81] J. Glamann and A. J. Hansen, "Dynamic detection of natural killer cell-mediated cytotoxicity and cell adhesion by electrical impedance measurements," *Assay and Drug Development Technologies*, vol. 4, no. 5, pp. 555–563, 2006.

[82] B. T. Cunningham, P. Li, S. Schulz et al., "Label-free assays on the BIND system," *Journal of Biomolecular Screening*, vol. 9, no. 6, pp. 481–490, 2004.

[83] Y. Fang, A. M. Ferrie, N. H. Fontaine, and P. K. Yuen, "Optical biosensors for monitoring dynamic mass redistribution in living cells mediated by epidermal growth factor receptor activation," in *Proceedings of the 27th Annual International Conference of the Engineering in Medicine and Biology Society (EMBS '05)*, vol. 1, pp. 666–669, September 2005.

[84] Y. Fang, A. M. Ferrie, and G. Li, "Probing cytoskeleton modulation by optical biosensors," *FEBS Letters*, vol. 579, no. 19, pp. 4175–4180, 2005.

[85] Y. Fang, A. M. Ferrie, N. H. Fontaine, and P. K. Yuen, "Characteristics of dynamic mass redistribution of epidermal growth factor receptor signaling in living cells measured with label-free optical biosensors," *Analytical Chemistry*, vol. 77, no. 17, pp. 5720–5725, 2005.

[86] Y. Fang, G. Li, and J. Peng, "Optical biosensor provides insights for bradykinin B2 receptor signaling in A431 cells," *FEBS Letters*, vol. 579, no. 28, pp. 6365–6374, 2005.

[87] G. Li, A. M. Ferrie, and Y. Fang, "Label-free profiling of ligands for endogenous GPCRs using a cell-based high-throughput screening technology," *Journal of the Association for Laboratory Automation*, vol. 11, no. 4, pp. 181–187, 2006.

[88] G. Leung, H. R. Tang, R. McGuinness, E. Verdonk, J. M. Michelotti, and V. F. Liu, "Cellular dielectric spectroscopy: a label-free technology for drug discovery," *Journal of the Association for Laboratory Automation*, vol. 10, no. 4, pp. 258–269, 2005.

[89] E. Verdonk, K. Johnson, R. McGuiness et al., "Cellular dielectric spectroscopy: a label-free comprehensive platform for functional evaluation of endogenous receptors," *Assay and Drug Development Technologies*, vol. 4, no. 5, pp. 609–619, 2006.

[90] F. Yin and M. A. Watsky, "LPA and S1P increase corneal epithelial and endothelial cell transcellular resistance," *Investigative Ophthalmology and Visual Science*, vol. 46, no. 6, pp. 1927–1933, 2005.

[91] N. Yu, J. M. Atienza, J. Bernard et al., "Real-time monitoring of morphological changes in living cells by electronic cell sensor arrays: an approach to study G protein-coupled receptors," *Analytical Chemistry*, vol. 78, no. 1, pp. 35–43, 2006.

[92] Y. Fang, G. Li, and A. M. Ferrie, "Non-invasive optical biosensor for assaying endogenous G protein-coupled receptors in adherent cells," *Journal of Pharmacological and Toxicological Methods*, vol. 55, no. 3, pp. 314–322, 2007.

[93] E. Tran and Y. Fang, "Label-free optical biosensor for probing integrative role of adenylyl cyclase in G protein-coupled receptor signaling," *Journal of Receptors and Signal Transduction*, vol. 29, no. 3-4, pp. 154–162, 2009.

[94] Y. Fang and A. M. Ferrie, "Optical biosensor differentiates signaling of endogenous PAR1 and PAR2 in A431 cells," *BMC Cell Biology*, vol. 8, article 24, pp. 1–12, 2007.

[95] M. F. Peters, K. S. Knappenberger, D. Wilkins et al., "Evaluation of cellular dielectric spectroscopy, a whole-cell, label-free technology for drug discovery on Gi-coupled GPCRs," *Journal of Biomolecular Screening*, vol. 12, no. 3, pp. 312–319, 2007.

[96] M. F. Peters and C. W. Scott, "Evaluating cellular impedance assays for detection of GPCR pleiotropic signaling and functional selectivity," *Journal of Biomolecular Screening*, vol. 14, no. 3, pp. 246–255, 2009.

[97] E. Tran and Y. Fang, "Duplexed label-free G protein-coupled receptor assays for high-throughput screening," *Journal of Biomolecular Screening*, vol. 13, no. 10, pp. 975–985, 2008.

[98] P. H. Lee, A. Gao, C. Van Staden et al., "Evaluation of dynamic mass redistribution technology for pharmacological studies of recombinant and endogenously expressed G protein-coupled receptors," *Assay and Drug Development Technologies*, vol. 6, no. 1, pp. 83–94, 2008.

[99] Y. Fang, A. M. Ferrie, and G. Li, "Systems biology and pharmacology of β_2 adrenergic receptors in A431," in *Trends in Signal Transduction Research*, J. N. Meyers, Ed., pp. 145–171, Nova Science Publishers, New York, NY, USA, 2007.

[100] Y. Fang and A. M. Ferrie, "Label-free optical biosensor for ligand-directed functional selectivity acting on β2 adrenoceptor in living cells," *FEBS Letters*, vol. 582, no. 5, pp. 558–564, 2008.

[101] V. Goral, Y. Jin, H. Sun, A. M. Ferrie, Q. Wu, and Y. Fang, "Agonist-directed desensitization of theβ_2-adrenergic receptor," *PLoS ONE*, vol. 6, no. 4, article e19282, 2011.

[102] S. Matsumoto, Y. Arakawa, M. Ohishi, H. Yanaihara, T. Iwanaga, and N. Kurokawa, "Suppressive action of pituitary adenylate cyclase activating polypeptide (PACAP) on proliferation of immature mouse Leydig cell line TM3 cells," *Biomedical Research*, vol. 29, no. 6, pp. 321–330, 2008.

[103] G. Park, C. K. Choi, A. E. English, and T. E. Sparer, "Electrical impedance measurements predict cellular transformation," *Cell Biology International*, vol. 33, no. 3, pp. 429–433, 2009.

[104] A. Kebig, E. Kostenis, K. Mohr, and M. Mohr-Andr, "An optical dynamic mass redistribution assay reveals biased signaling of dualsteric GPCR activators," *Journal of Receptors and Signal Transduction*, vol. 29, no. 3-4, pp. 140–145, 2009.

[105] J. Antony, K. Kellershohn, M. Mohr-Andrä et al., "Dualsteric GPCR targeting: a novel route to binding and signaling pathway selectivity," *FASEB Journal*, vol. 23, no. 2, pp. 442–450, 2009.

[106] K. Dodgson, L. Gedge, D. C. Murray, and M. Coldwell, "A 100K well screen for a muscarinic receptor using the Epic® label-free system a reflection on the benefits of the label-free approach to screening seven-transmembrane receptors Label-free approach to screening seven-transmembrane receptors," *Journal of Receptors and Signal Transduction*, vol. 29, no. 3-4, pp. 163–172, 2009.

[107] E. Christiansen, C. Urban, N. Merten et al., "Discovery of potent and selective agonists for the free fatty acid receptor 1 (FFA1/GPR40), a potential target for the treatment of type II diabetes," *Journal of Medicinal Chemistry*, vol. 51, no. 22, pp. 7061–7064, 2008.

[108] J. Schmidt, K. Liebscher, N. Merten et al., "Conjugated linoleic acids mediate insulin release through islet G protein-coupled receptor FFA1/GPR40," *Journal of Biological Chemistry*, vol. 286, no. 14, pp. 11890–11894, 2011.

[109] J. Schmidt, N. J. Smith, E. Christiansen et al., "Selective orthosteric free fatty acid receptor 2 (FFA2) agonists: identification of the structural and chemical requirements for

selective activation of FFA2 versus FFA3," *Journal of Biological Chemistry*, vol. 286, no. 12, pp. 10628–10640, 2011.

[110] M. R. Fleming and L. K. Kaczmarek, "Use of optical biosensors to detect modulation of Slack potassium channels by G protein-coupled receptors," *Journal of Receptors and Signal Transduction*, vol. 29, no. 3-4, pp. 173–181, 2009.

[111] P. Scandroglio, R. Brusa, G. Lozza et al., "Evaluation of cannabinoid receptor 2 and metabotropic glutamate receptor 1 functional responses using a cell impedance-based technology," *Journal of Biomolecular Screening*, vol. 15, no. 10, pp. 1238–1247, 2010.

[112] J. Jiang, T. Ganesh, Y. Du et al., "Neuroprotection by selective allosteric potentiators of the EP2 prostaglandin receptor," *Proceedings of the National Academy of Sciences of the United States of America*, vol. 107, no. 5, pp. 2307–2312, 2010.

[113] C. M. Niswender, K. A. Johnson, N. R. Miller et al., "Context-dependent pharmacology exhibited by negative allosteric modulators of metabotropic glutamate receptor 7," *Molecular Pharmacology*, vol. 77, no. 3, pp. 459–468, 2010.

[114] C. M. Henstridge, N. A. Balenga, R. Schröder et al., "GPR55 ligands promote receptor coupling to multiple signalling pathways," *British Journal of Pharmacology*, vol. 160, no. 3, pp. 604–614, 2010.

[115] R. Schröder, N. Janssen, J. Schmidt et al., "Deconvolution of complex G protein-coupled receptor signaling in live cells using dynamic mass redistribution measurements," *Nature Biotechnology*, vol. 28, no. 9, pp. 943–949, 2010.

[116] M. F. Peters, F. Vaillancourt, M. Heroux, M. Valiquette, and C. W. Scott, "Comparing label-free biosensors for pharmacological screening with cell-based functional assays," *Assay and Drug Development Technologies*, vol. 8, no. 2, pp. 219–227, 2010.

[117] R. Schröder, N. Merten, J. M. Mathiesen et al., "The C-terminal tail of CRTH2 is a key molecular determinant that constrains Gαi and downstream signaling cascade activation," *Journal of Biological Chemistry*, vol. 284, no. 2, pp. 1324–1336, 2009.

[118] E. E. Codd, J. R. Mabus, B. S. Murray, S.-P. Zhang, and C. M. Floresm, "Dynamic mass redistribution as a means to measure and differentiate signaling via opioid and cannabinoid receptors," *Assay and Drug Development Technologies*, vol. 9, no. 4, pp. 362–372, 2011.

[119] V. Goral, Q. Wu, H. Sun, and Y. Fang, "Label-free optical biosensor with microfluidics for sensing ligand-directed functional selectivity on trafficking of thrombin receptor," *FEBS Letters*, vol. 585, no. 7, pp. 1054–1060, 2011.

[120] H. Deng, H. Hu, and Y. Fang, "Tyrphostin analogs are GPR35 agonists," *FEBS Letters*, vol. 585, no. 12, pp. 1957–1962, 2011.

[121] Y. Fang, A. G. Frutos, and R. Verklereen, "Label-free cell-based assays for GPCR screening," *Combinatorial Chemistry and High Throughput Screening*, vol. 11, no. 5, pp. 357–369, 2008.

[122] J. M. Atienza, N. Yu, X. Wang, X. Xu, and Y. Abassi, "Label-free and real-time cell-based kinase assay for screening selective and potent receptor tyrosine kinase inhibitors using microelectronic sensor array," *Journal of Biomolecular Screening*, vol. 11, no. 6, pp. 634–643, 2006.

[123] Y. Du, Z. Li, L. Li et al., "Distinct growth factor-induced dynamic mass redistribution (DMR) profiles for monitoring oncogenic signaling pathways in various cancer cells," *Journal of Receptor and Signal Transduction Research*, vol. 29, no. 3-4, pp. 182–194, 2009.

[124] F. Liu, J. Zhang, Y. Deng, D. Wang, Y. Lu, and X. Yu, "Detection of EGFR on living human gastric cancer BGC823 cells using surface plasmon resonance phase sensing," *Sensors and Actuators B*, vol. 153, no. 2, pp. 398–403, 2011.

[125] J. Y. Chen, M. Li, L. S. Penn, and J. Xi, "Real-time and label-free detection of cellular response to signaling mediated by distinct subclasses of epidermal growth factor receptors," *Analytical Chemistry*, vol. 83, no. 8, pp. 3141–3146, 2011.

[126] E. Kakiashvili, Q. Dan, M. Vandermeer et al., "The epidermal growth factor receptor mediates tumor necrosis factor-α-induced activation of the ERK/GEF-H1/RhoA pathway in tubular epithelium," *Journal of Biological Chemistry*, vol. 286, no. 11, pp. 9268–9279, 2011.

[127] Y. Fang, A. M. Ferrie, and G. Li, "Cellular functions of cholesterol probed with optical biosensors," *Biochimica et Biophysica Acta*, vol. 1763, no. 2, pp. 254–261, 2006.

[128] O. Pänke, W. Weigel, S. Schmidt, A. Steude, and A. A. Robitzki, "A cell-based impedance assay for monitoring transient receptor potential (TRP) ion channel activity," *Biosensors and Bioelectronics*, vol. 26, no. 5, pp. 2376–2382, 2011.

[129] Y. A. Abassi, J. A. Jackson, J. Zhu, J. Oconnell, X. Wang, and X. Xu, "Label-free, real-time monitoring of IgE-mediated mast cell activation on microelectronic cell sensor arrays," *Journal of Immunological Methods*, vol. 292, no. 1-2, pp. 195–205, 2004.

[130] M. Hide, T. Tsutsui, H. Sato et al., "Real-time analysis of ligand-induced cell surface and intracellular reactions of living mast cells using a surface plasmon resonance-based biosensor," *Analytical Biochemistry*, vol. 302, no. 1, pp. 28–37, 2002.

[131] Y. Yanase, H. Suzuki, T. Tsutsui, T. Hiragun, Y. Kameyoshi, and M. Hide, "The SPR signal in living cells reflects changes other than the area of adhesion and the formation of cell constructions," *Biosensors and Bioelectronics*, vol. 22, no. 6, pp. 1081–1086, 2007.

[132] H. Suzuki, Y. Yanase, T. Tsutsui, K. Ishii, T. Hiragun, and M. Hide, "Applying surface plasmon resonance to monitor the IgE-mediated activation of human basophils," *Allergology International*, vol. 57, no. 4, pp. 347–358, 2008.

[133] M. Tanaka, T. Hiragun, T. Tsutsui, Y. Yanase, H. Suzuki, and M. Hide, "Surface plasmon resonance biosensor detects the downstream events of active PKCβ in antigen-stimulated mast cells," *Biosensors and Bioelectronics*, vol. 23, no. 11, pp. 1652–1658, 2008.

[134] M. H. McCoy and E. Wang, "Use of electric cell-substrate impedance sensing as a tool for quantifying cytopathic effect in influenza a virus infected MDCK cells in real-time," *Journal of Virological Methods*, vol. 130, no. 1-2, pp. 157–161, 2005.

[135] R. M. Owens, C. Wang, J. A. You et al., "Real-time quantitation of viral replication and inhibitor potency using a label-free optical biosensor," *Journal of Receptors and Signal Transduction*, vol. 29, no. 3-4, pp. 195–201, 2009.

[136] F. Jia, C. Maddox, A. Gao et al., "A novel cell-based 384-well, label-free assay for discovery of inhibitors of influenza A virus," *International Journal of High Throughput Screening*, vol. 1, pp. 57–67, 2010.

[137] M. Fiala, A. J. Eshleman, J. Cashman et al., "Cocaine increases human immunodeficiency virus type 1 neuroinvasion through remodeling brain microvascular endothelial cells," *Journal of NeuroVirology*, vol. 11, no. 3, pp. 281–291, 2005.

[138] J. Müller, C. Thirion, and M. W. Pfaffl, "Electric cell-substrate impedance sensing (ECIS) based real-time measurement of titer dependent cytotoxicity induced by adenoviral vectors in an IPI-2I cell culture model," *Biosensors and Bioelectronics*, vol. 26, no. 5, pp. 2000–2005, 2011.

[139] A. M. Ferrie, H. Sun, and Y. Fang, "Label-free integrative pharmacology on-target of drugs at the β_2-adrenergic receptor," *Scientific Reports*, vol. 1, no. 33, 2011.

[140] N. Zaytseva, W. Miller, V. Goral, J. Hepburn, and Y. Fang, "Microfluidic resonant waveguide grating biosensor system for whole cell sensing," *Applied Physics Letters*, vol. 98, no. 16, Article ID 163703, 2011.

[141] T. Ona and J. Shibata, "Advanced dynamic monitoring of cellular status using label-free and non-invasive cell-based sensing technology for the prediction of anticancer drug efficacy," *Analytical and Bioanalytical Chemistry*, vol. 398, no. 6, pp. 2505–2533, 2010.

[142] A. M. Ferrie, Q. Wu, and Y. Fang, "Resonant waveguide grating imager for live cell sensing," *Applied Physics Letters*, vol. 97, no. 22, Article ID 223704, 2010.

[143] L. Ghenim, H. Kaji, Y. Hoshino et al., "Monitoring impedance changes associated with motility and mitosis of a single cell," *Lab on a Chip*, vol. 10, no. 19, pp. 2546–2550, 2010.

[144] W. Wang, K. Foley, X. Shan et al., "Single cells and intracellular processes studied by a plasmonic-based electrochemical impedance microscopy," *Nature Chemistry*, vol. 3, no. 3, pp. 251–257, 2011.

[145] T. Sandu, D. Vrinceanu, and E. Gheorghiu, "Linear dielectric response of clustered living cells," *Physical Review E*, vol. 81, no. 2, Article ID 021913, 2010.

[146] N. Ke, B. Xi, P. Ye et al., "Screening and identification of small molecule compounds perturbing mitosis using time-dependent cellular response profiles," *Analytical Chemistry*, vol. 82, no. 15, pp. 6495–6503, 2010.

SAGE-Hindawi Access to Research
International Journal of Electrochemistry
Volume 2011, Article ID 403691, 6 pages
doi:10.4061/2011/403691

Research Article

Determination of Atropine Sulfate in Human Urines by Capillary Electrophoresis Using Chemical Modified Electrode as Electrochemiluminescence Sensor

Min Zhou,[1] Juan Mi,[1] Yujie Li,[1] Huashan Zhang,[2] and Yanjun Fang[1,2]

[1] *Key Laboratory of Eco-Environment-Related Polymer Materials, Ministry of Education, Key Laboratory of Polymer Materials of Gansu Province, and College of Chemistry and Chemical Engineering, Northwest Normal University, Lanzhou 730070, China*
[2] *Institute of Hygienic and Environmental Medicinal Science, Key Laboratory of Risk Assessment and Control for Environment & Food Safety, Tianjin 300050, China*

Correspondence should be addressed to Yanjun Fang, yanjunfang1973@163.com

Received 10 April 2011; Revised 13 July 2011; Accepted 13 July 2011

Academic Editor: Farnoush Faridbod

Copyright © 2011 Min Zhou et al. This is an open access article distributed under the Creative Commons Attribution License, which permits unrestricted use, distribution, and reproduction in any medium, provided the original work is properly cited.

A $Ru(bpy)_3^{2+}$-based electrochemiluminescence (ECL) detection coupled with capillary electrophoresis (CE) was developed for the determination of atropine sulfate on the basis of an Eu-PB modified platinum electrode as the working electrode. The analyte was injected to separation capillary of 50 cm length (25 μm i.d., 360 μm o.d.) by electrokinetic injection for 10 s at 10 kV. Parameters related to the separation and detection were discussed and optimized. It was proved that 10 mM phosphate buffer at pH 8.0 could achieve the most favorable resolution, and the high sensitivity of detection was obtained by using the detection potential at 1.15 V and 5 mM $Ru(bpy)_3^{2+}$ in 80 mM phosphate buffer at pH 8.0 in the detection reservoir. Under the optimized conditions, the ECL peak area was in proportion to atropine sulfate concentration in the range from 0.08 to 20 $\mu g \cdot mL^{-1}$ with a detection limit of 50 $ng \cdot mL^{-1}$ (3σ). The relative standard derivations of migration time and peak area were 0.81 and 3.19%, respectively. The developed method was successfully applied to determine the levels of atropine sulfate in urine samples of patients with recoveries between 90.9 and 98.6%.

1. Introduction

Atropine ((±)-hyoscyamine) is an active tropine alkaloid from solanaceous plants (as one of a traditional Chinese crude herb), and its chemical structure is shown in Figure 1. Atropine sulfate has been utilized clinically for many years as anticholinergic agent in premedication of anesthesia. However, a high dosage of atropine sulfate can stimulate the central nerve system and disrupt the human renal function leading to toxic reaction [1]. Therefore, it is necessary to establish sensitive and effective methods for the quantitation of atropine sulfate in the field of clinical medicine.

Up to date, different chromatographic methods including liquid chromatography (LC) [2], high-performance liquid chromatography (HPLC) [3, 4], thin-layer chromatography (TLC) [5], and gas chromatography (GC) [6] have been reported for the analysis of atropine. However, a drawback of chromatography appears to be time consuming due to necessary extraction, concentration, and/or derivatization prior to the analysis. In addition, a bulk acoustic wave sensor has recently been fabricated and utilized for the determination of atropine sulfate in serum and urine [7]. Of the applied field of spectroscopic analysis, the atomic absorption method (AAS) [8], chemiluminescence method (CL) [9], and the electrochemiluminescence method (ECL) [10] have also been developed for atropine detection. However, these methods often encounter poor selectivity in the assay of complicated samples when coupled with no other separated techniques.

Capillary electrophoresis (CE) represents an interesting alternative as a powerful separation tool and has been applied for atropine analysis already. However, the present CE methods for atropine are usually coupled with UV-V detector, resulting in the restricted detection limits [11]. In recent years, the marriage of CE to $Ru(bpy)_3^{2+}$-based ECL detection has proved to be a promising and efficient

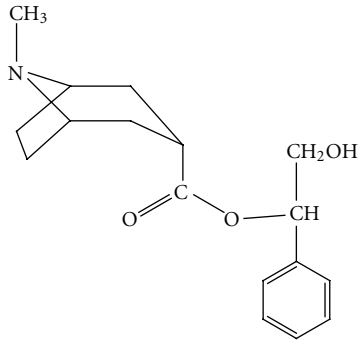

Figure 1: Structure of atropine.

analytical technique in the field of biochemical analysis with high sensitivity and excellent separation efficiency [12–15]. However, the utilization of a bare metal platinum electrode in CE-ECL detection can deteriorate stability and sensitivity because of the poisoning effect of complicated matrices in real biological fluids [10].

In recent years, chemical modified electrodes have been widely used for the detection of trace amounts of real biological fluids since the poisoning effect of complex matrixes on the bare platinum electrode could deteriorate the stability and sensitivity [16]. Especially, Prussian Blue (PB), its analogue and related composite film modified electrodes have received more attention in wide range of electrochemistry because of inherent stability, highly reversible nature of the electrode reactions, ease of preparation, and low cost [17]. Unfortunately, the application of a PB analogue modified electrode with rare earth ions in CE-ECL systems has not been reported by other workers although some modified electrodes have also been used as solid-state ECL detectors in CE-ECL detection [16, 18]. It was proved in our previous works [19, 20] that only europium (III)-doped Prussian blue analogue film (Eu-PB) modified platinum microelectrode had good catalytic activity to the electrochemiluminescence of $Ru(bpy)_3^{2+}$-based system. Given this, a platinum electrode modified by Eu-PB is prepared and applied as a working electrode and a $Ru(bpy)_3^{2+}$-based CE-ECL method is developed for the direct determination of atropine sulfate in urine samples of patients in this paper. By this alternative, a wider linear range and significantly improved sensitivity for atropine sulfate has been obtained since the possible electrode fouling can be avoided.

2. Experimental

2.1. Reagents and Chemicals. Atropine sulfate was from Sigma (St. Louis, MO, USA) and freshly prepared by serial dilution with doubly deionized water just before use. Tris (2,2′-bipyridyl) ruthenium (II) chloride hexahydrate (98%) was from Aldrich (Milwaukee, Wis, USA). Sodium phosphate (pH 8.0, G. R.) was used as the buffer solution. All chemicals and reagents were of analytical grade except specific statements. Doubly deionized water was used throughout, and all solutions were filtered through a 0.22 μm pore-size membrane before use.

2.2. Apparatus. MPI-A multiparameter chemiluminescence capillary electrophoresis analysis system with self-compiled CE-ECL software (Xi'an Remax Electronic and Technological Co., China) was employed. Uncoated fused silica capillary (50 cm × 25 μm i.d.) was obtained from Yongnian Optical Fiber Factory (Hebei, China). The end-column ECL detection was installed with a three-electrode configuration, which was made up of a Eu-PB modified platinum disk (Φ = 0.5 mm) as a working electrode, an Ag/AgCl filled with saturated KCl as a reference electrode and a platinum wire as an auxiliary electrode.

A CHI832 electrochemical analyzer (Shanghai Chenhua Apparatus Corporation, China) was used for both modification of the working electrode and measurement of the differential pulse voltammograms (D.P.V.s).

2.3. Procedure. The schematic diagram of the CE-ECL detection system was the same as reported in the previous work [19]. A solution of 5 mM $Ru(bpy)_3^{2+}$ in 80 mM phosphate buffer (pH 8.0) was directly injected into the reaction reservoir. Running buffer solution was 10 mM phosphate buffer (pH 8.0). Samples were injected in an electrokinetic mode at 10 kV for 10 s. The separation voltage was 17 kV. The photomultiplier tube (PMT) was biased at −850 V. The capillary-to-working electrode distance was adjusted to about 150 μm. Fresh $Ru(bpy)_3^{2+}$ was replaced every 3 h in order to obtain good reproducibility. Capillary was rinsed with the running buffer between two sample injections until the baseline was stable. The sample concentrations were quantified by ECL peak area.

2.4. Preparation of Eu-PB Modified Platinum Electrode. The modified composite film was prepared on a smooth and cleaning surface of a platinum electrode. A solution of 10.0 mL $FeCl_3$, 10.0 mL $K_3Fe(CN)_6$, 6.5 mL HCl, 5.0 mL $EuCl_3$, and 5.0 mL potassium hydrogen phthalate (all concentration were 0.01 M) was directly added into the electrochemical cell. The Eu-PB film was gradually electrodeposited when cell potential was cyclically scanned from 0 to 1.3 V at a rate of 20 mV/s for twenty segments round (versus SCE reference electrode).

2.5. The Urine Sample Preparation. Fresh urine samples of patients were obtained from Lanzhou University Second Hospital and collected from two male patients after 3 h and 8 h when 0.5 mg atropine sulfate were injected, respectively. The urine samples were centrifugated at 2000 rpm for 10 min. Then the top layer was separated and diluted 20-fold with deionized water, followed by passing through a 0.22 μm membrane and being directly injected into the CE-ECL system and analyzed.

3. Results and Discussions

3.1. Effect of the Eu-PB Modified Platinum Working Electrode

3.1.1. Effect on Electrooxidation Characterization of $Ru(bpy)_3^{2+}$. The electrooxidation characterization of $Ru(bpy)_3^{2+}$ was tested before and after modification of

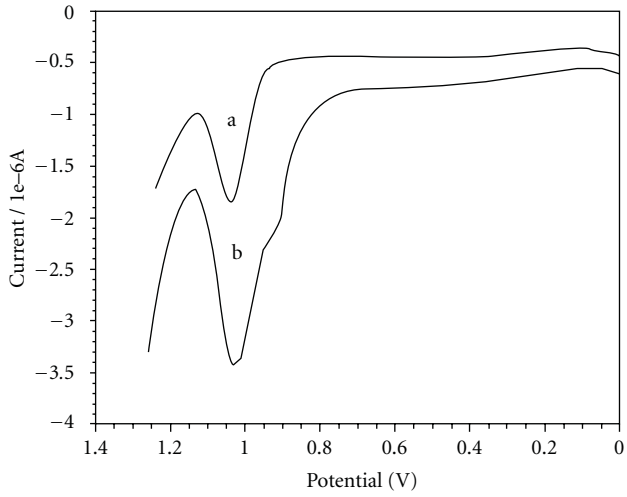

Figure 2: Differential pulse voltammograms of $Ru(bpy)_3^{2+}$ in phosphate buffer (pH 8.0): (a) at bare Pt electrode; (b) at Eu-PB modified Pt electrode. Amplitude: 0.05 V; pulse width: 0.05 s; pulse period: 0.2 s. Concentrations: $Ru(bpy)_3^{2+}$, 5 mM; phosphate buffer, 80 mM.

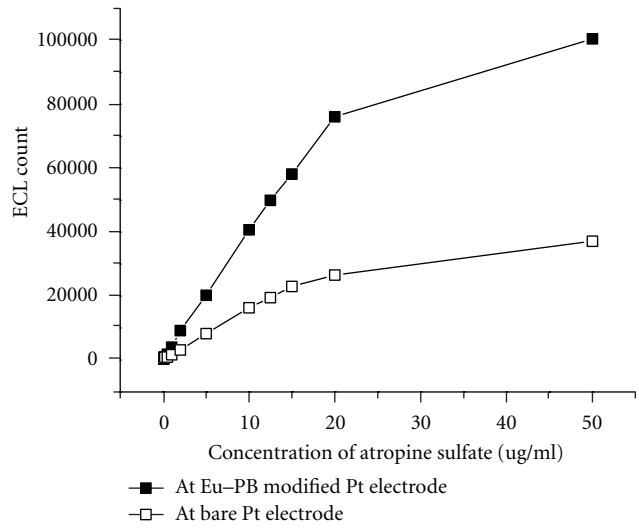

Figure 3: Luminescence response of atropine sulfate at bare Pt electrode and at Eu-PB modified electrode: separation capillary: 25 μm, i.d., 45 cm length; sample injection: 10 s at 10 kV; separation voltage: 17 kV; running buffer: 10 mM sodium phosphate, concentration in detection cell: 80 mM, all at pH 8.0.

working electrode by differential pulse voltammetry. As shown in Figure 2, the peak current from the electrooxidation of $Ru(bpy)_3^{2+}$ was enhanced significantly at the modified electrode, and the oxidation peak of $Ru(bpy)_3^{2+}$ was observed at ca. 1.05 V (versus Ag/AgCl), with slight negative shift ca. 20 mV with respect to that obtained on the unmodified electrode. Consequently, ECL efficiency of $Ru(bpy)_3^{2+}$ could be improved due to catalytic oxidation of $Ru(bpy)_3^{2+}$ and therefore more production of excited state of $Ru(bpy)_3^{2+}$ in the prepared electrode.

3.1.2. Effect on the ECL Response of Atropine. Luminescence response of atropine was investigated in the prepared electrode as illustrated in Figure 3. It was found that the ratio of the change of ECL signal versus the change of atropine sulfate concentration ($\Delta I/\Delta C$) was significantly increased by using the Eu-PB modified platinum electrode as ECL sensor, indicating that the change of ECL signal was more sensitive to the change of atropine sulfate concentration. Consequently, the slope of calibration curve would be enhanced. In addition, it was also indicated in Figure 3 that the linear range would be broadened when the Pt electrode was modified. Thus, the prepared electrode would benefit from the improved sensitivity and linearity for atropine sulfate.

3.1.3. Antipoisoning Effect of the Modified Electrode. In order to investigate the Antipoisoning effect of the modified electrode, atropine sulfate in real urine samples of patients were determined by the CE-ECL method using a platinum electrode and the prepared electrode as ECL sensor, respectively. It was found that the use of unmodified electrode led to peak broadening and a considerably unstable measurement due to poisoning effect of electrode, and therefore was unfit for the assay of real urine samples. While it was found that uric acid, other matrices, and atropine metabolites in urine samples had little interference to the detection by use of the prepared electrode, and consequently the enhanced ECL signal, lower noise, better peak shape, and improved reproducibility were obtained. It was proved as well that the prepared electrode was stable enough for repetitive use in the detection system over one month with no need for electrode replacement. In a word, the modified electrode shows advantage of excellent Antipoisoning effect for real urine samples.

3.2. Conditions Optimization

3.2.1. Effect of $Ru(bpy)_3^{2+}$ Concentration. Concentration of $Ru(bpy)_3^{2+}$ had great effect on the ECL signal. The results showed that the ECL intensity increased markedly with increasing $Ru(bpy)_3^{2+}$ concentration from 0.2 to 5.0 mM due to the acceleration of reaction rate. In this work, 5 mM $Ru(bpy)_3^{2+}$ in 80 mM phosphate buffer was adopted due to concerned oversensitivity and economy in use of reagent.

3.2.2. Effect of Running Buffer. Determination of atropine was studied in different buffer systems including phosphate, acetate, Tris-HCl, citric acid-sodium citrate, and borate buffers. Finally, phosphate was chosen in terms of the stable baseline, lower noise, shorter analysis time, and better peak shape.

Further, pH effect of phosphate on the detection was investigated in a wide pH range of 4.5–10.0 at intervals of 0.5 pH units. As indicated in Figure 4, the ECL intensity increased with increase in pH value in the pH range 4.5–7.5 and reached a plateau at pH 7.5–8.5, above which it decreased a little. The possible reason was considered as

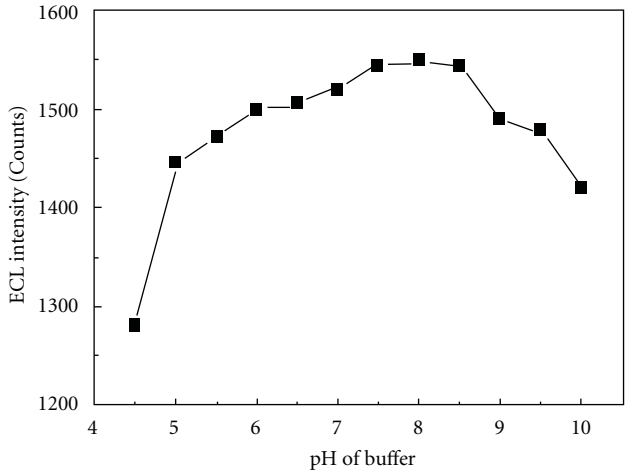

Figure 4: pH effect of running buffer on ECL intensity: other conditions, the same as in Figure 3.

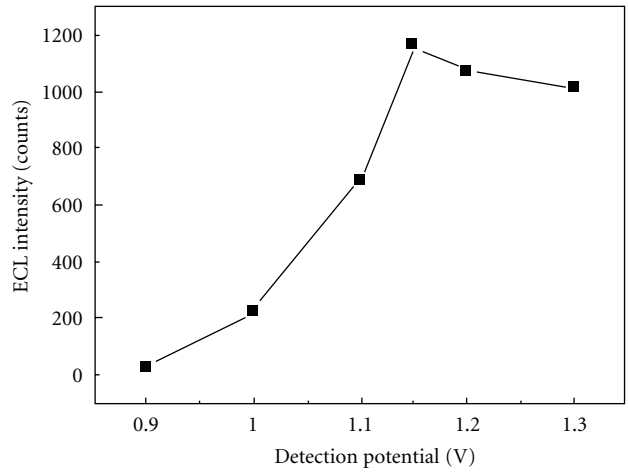

Figure 5: Effect of detection potential on ECL intensity: other conditions, the same as in Figure 3.

the competitive reaction between $Ru(bpy)_3^{2+}$ and OH^- ions produced at high pH value [21]. So pH 8.0 was selected for all the following work.

With fixed pH value at 8.0, the concentration of running buffer was changed from 5 to 20 mM. It was found that working at high buffer concentration allowed improved sensitivity and resolution. However, high buffer concentration would induce excessive heating caused by Joule effect, resulting in an unstable measurement. Hence, 10 mM phosphate at pH 8.0 was used as the running buffer.

3.2.3. Effect of Detection Potential. The ECL intensity depends on the efficiency of electroproduced $Ru(bpy)_3^{3+}$ and substantially depends on the oxidation potential applied to the electrode. As seen in Figure 5, the increased production of $Ru(bpy)_3^{3+}$ with a rise of potential resulted in an increased response and the highest value was obtained at 1.15 V. Above which, the response slightly diminished, implying that the efficiency of electroproduced $Ru(bpy)_3^{3+}$ decreased as competitive reactions involving the buffer dominate. Thus, the optimal potential was 1.15 V.

3.2.4. Effect of Separation Voltage. Separation voltage simultaneously impacted on the ECL intensity and migration time. More analyte arrived in the diffusion layer of working electrode within a given time with the increasing separation voltage, leading to higher ECL signal. Also, increasing separation voltage shortened the migration time because of the increase of EOF. However, the inability of the system to remove excess Joule heat generated at high voltages resulted in peak broadening and a decrease in reproducibility. Finally, the best choice for separation voltage was 17 kV.

3.2.5. Effect of Injection Voltage and Injection Time. The effects of injection voltage and injection time were studied as well. The results demonstrated that it was difficult to obtain a favorable ECL intensity though a high column efficiency could be achieved when the injection time was shortened and the injection voltage was diminished. Also, the reproducibility became worse when an excessive sample volume was introduced. Finally, the injection parameters of 10 s at 10 kV were recommended.

3.3. Calibration and Detection. Under the optimum conditions, the calibration graph of atropine sulfate concentration versus ECL peak area was linear in the range from 0.08 to 20 $\mu g \cdot mL^{-1}$, which was wider than that obtained at a bare platinum electrode [22]. The regression equation could be expressed as: $\Delta S = 566.26 + 2256.75C/\mu g\,mL^{-1}$ with a correlation coefficient of 0.9994 ($n = 8$). The detection limit, defined as three times the S.D. for the reagent blank signal, was 50 $ng \cdot mL^{-1}$.

The precision of the proposed method was determined by reduplicate injections ($n = 6$) of 5.0 $\mu g \cdot mL^{-1}$ atropine sulfate standard solution. The relative standard deviations (R.S.D.) of migration time and ECL peak area were 0.81 and 3.19%, respectively.

3.4. Applications. In order to examine the application for clinic analysis, the levels of atropine sulfate in real urine samples of two patients were determined by the proposed method. The electropherogram in Figure 6 showed that uric acid, other matrices, and atropine metabolites in urine samples had little interference to the detection by use of the prepared electrode. As seen in Figure 6, the peak at 267 s was identified to be from atropine sulfate by spiking the standards to the sample solution. The quantitative recovery was 98.6% ($n = 5$), and about 22.4% atropine sulfate was excreted from urine with unchanged form. In the measurement process, another peak at 375 s was always detected, which was estimated to be from a normal metabolite in human urine. Similarly, another urinary sample was analyzed as well and the recovery of 90.9% ($n = 5$) was obtained. The results were listed in Table 1.

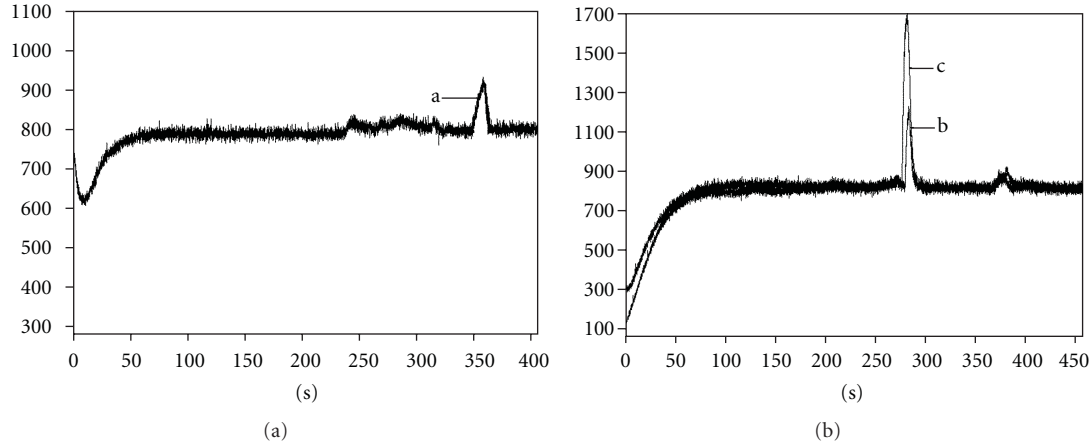

Figure 6: Electropherograms of (a) the diluted urinary sample of a healthy male; (b) the diluted urinary sample of a male patient; (c) the diluted urinary sample of the male patient spiked with 5.0 $\mu g \cdot mL^{-1}$ atropine sulfate standard solution; other conditions are the same as in Figure 3.

Table 1: The determination of atropine sulfate in patient urines ($n = 5$).

Sample	Found ($mg \cdot mL^{-1}$)	R.S.D. (%) for peak area	Added ($mg \cdot mL^{-1}$)	Recovered ($mg \cdot mL^{-1}$)	Recovery (%)
1	0.112	1.52	0.100	0.0986	98.6
2	0.0782	2.19	0.100	0.0909	90.9

Conditions were the same as Table 1. Sample 1 was from the patient who was operated for the polyp excision after ca. 3 h when atropine sulfate was injected; sample 2 was from the patient who was operated for uremia after ca. 8 h when atropine sulfate was injected.

4. Conclusion

This paper described a $Ru(bpy)_3^{2+}$-based ECL method coupling to CE technique for the determination of atropine sulfate. An Eu-PB modified platinum electrode was prepared and used as ECL sensor to replace the traditional bare Pt electrode since the adsorption and direct oxidation of electroactive species in real urine samples of patients on the surface of working electrode could be avoided as much as possible. Consequently, the stability and reproducibility in signals, the linear range, and the ratio of ECL signal to atropine sulfate concentration were all significantly improved. To sum up, the proposed method showed an excellent performance with respect to selectivity, sensitivity, linearity, and stability, and further it holds great promise for the determination of tropane alkaloids in body fluids.

Acknowledgments

The authors are grateful to Natural Foundation (no. 1010RJZA017) of Gansu Province and the Natural Foundation of the National (no. 20707039) for supporting the research.

References

[1] K. Dost and G. Davidson, "Development of a packed-column supercritical fluid chromatography/atmospheric pressure chemical-ionisation mass spectrometric technique for the analysis of atropine," *Journal of Biochemical and Biophysical Methods*, vol. 43, no. 1–3, pp. 125–134, 2000.

[2] O. Rbeida, B. Christiaens, P. Hubert et al., "Integrated on-line sample clean-up using cation exchange restricted access sorbent for the LC determination of atropine in human plasma coupled to UV detection," *Journal of Pharmaceutical and Biomedical Analysis*, vol. 36, no. 5, pp. 947–954, 2005.

[3] M. Nakamura, M. Ono, T. Nakajima, Y. Ito, T. Aketo, and J. Haginaka, "Uniformly sized molecularly imprinted polymer for atropine and its application to the determination of atropine and scopolamine in pharmaceutical preparations containing Scopolia extract," *Journal of Pharmaceutical and Biomedical Analysis*, vol. 37, no. 2, pp. 231–237, 2005.

[4] R. Sharma, P. K. Gupta, A. Mazumder, D. K. Dubey, K. Ganesan, and R. Vijayaraghavan, "A quantitative NMR protocol for the simultaneous analysis of atropine and obidoxime in parenteral injection devices," *Journal of Pharmaceutical and Biomedical Analysis*, vol. 49, no. 4, pp. 1092–1096, 2009.

[5] A. P. Gupta, M. M. Gupta, and S. Kumar, "High performance thin layer chromatography of asiaticoside in Centella asiatica," *Journal of the Indian Chemical Society*, vol. 76, no. 6, pp. 321–322, 1999.

[6] J. Pohjola and M. Harpf, "Determination of atropine and obidoxime in automatic injection devices used as antidotes against nerve agent intoxication," *Journal of Chromatography A*, vol. 686, no. 2, pp. 350–354, 1994.

[7] H. Peng, C. Liang, A. Zhou, Y. Zhang, Q. Xie, and S. Yao, "Development of a new atropine sulfate bulk acoustic wave sensor based on a molecularly imprinted electrosynthesized copolymer of aniline with o-phenylenediamine," *Analytica Chimica Acta*, vol. 423, no. 2, pp. 221–228, 2000.

[8] M. A. El Ries and S. Khalil, "Indirect atomic absorption determination of atropine, diphenhydramine, tolazoline, and levamisole based on formation of ion-associates with potassium tetraiodometrcurate," *Journal of Pharmaceutical and Biomedical Analysis*, vol. 25, no. 1, pp. 3–7, 2001.

[9] P. A. Greenwood, C. Merrin, T. McCreedy, and G. M. Greenway, "Chemiluminescence μTAS for the determination of atropine and pethidine," *Talanta*, vol. 56, no. 3, pp. 539–545, 2002.

[10] Q. Song, G. M. Greenway, and T. McCreedy, "Tris(2,2′-bipyridine)ruthenium(II) electrogenerated chemiluminescence of alkaloid type drugs with solid phase extraction sample preparation," *Analyst*, vol. 126, no. 1, pp. 37–40, 2001.

[11] Y. Bitar and U. Holzgrabe, "Impurity profiling of atropine sulfate by microemulsion electrokinetic chromatography," *Journal of Pharmaceutical and Biomedical Analysis*, vol. 44, no. 3, pp. 623–633, 2007.

[12] X.-B. Yin and E. Wang, "Capillary electrophoresis coupling with electrochemiluminescence detection: a review," *Analytica Chimica Acta*, vol. 533, no. 2, pp. 113–120, 2005.

[13] B. Yuan, C. Zheng, H. Teng, and T. You, "Simultaneous determination of atropine, anisodamine, and scopolamine in plant extract by nonaqueous capillary electrophoresis coupled with electrochemiluminescence and electrochemistry dual detection," *Journal of Chromatography A*, vol. 1217, no. 1, pp. 171–174, 2010.

[14] F. J. Lara, A. M. García-Campaña, and A. I. Velasco, "Advances and analytical applications in chemiluminescence coupled to capillary electrophoresis," *Electrophoresis*, vol. 31, no. 12, pp. 1998–2027, 2010.

[15] E. Aehle and B. Dräger, "Tropane alkaloid analysis by chromatographic and electrophoretic techniques: an update," *Journal of chromatography B*, vol. 878, no. 17-18, pp. 1391–1406, 2010.

[16] S.-N. Ding, J.-J. Xu, and H.-Y. Chen, "Tris(2,2′-bipyridyl)ruthenium(II)-zirconia-Nafion composite films applied as solid-state electrochemiluminescence detector for capillary electrophoresis," *Electrophoresis*, vol. 26, no. 9, pp. 1737–1744, 2005.

[17] M. H. Pournaghi-Azar and H. Dastangoo, "Palladized aluminum as a novel substrate for the non-electrolytic preparation of a Prussian Blue film modified electrode," *Journal of Electroanalytical Chemistry*, vol. 573, no. 2, pp. 355–364, 2004.

[18] W. Cao, J. Jia, X. Yang, S. Dong, and E. Wang, "Capillary electrophoresis with solid-state eletrochemiluminescence detector," *Electrophoresis*, vol. 23, no. 21, pp. 3692–3698, 2002.

[19] M. Zhou, Y.-J. Ma, X.-N. Ren, X.-Y. Zhou, L. Li, and H. Chen, "Determination of sinomenine in Sinomenium acutum by capillary electrophoresis with electrochemiluminescence detection," *Analytica Chimica Acta*, vol. 587, no. 1, pp. 104–109, 2007.

[20] X. Ren, Y. Ma, M. Zhou, S. Huo, J. Yao, and H. Chen, "Determination of tropane alkaloid components in Przewalskia tangutica Maxim, by capillary electrophoresis with electrochemiluminescence detection," *Chinese Journal of Chromatography*, vol. 26, no. 2, pp. 223–227, 2008.

[21] J. Liu, W. Cao, X. Yang, and E. Wang, "Determination of diphenhydramine by capillary electrophoresis with tris(2,2′-bipyridyl)ruthenium(II) electrochemiluminescence detection," *Talanta*, vol. 59, no. 3, pp. 453–459, 2003.

[22] Y. Gao, Y. Tian, and E. Wang, "Simultaneous determination of two active ingredients in Flos daturae by capillary electrophoresis with electrochemiluminescence detection," *Analytica Chimica Acta*, vol. 545, no. 2, pp. 137–141, 2005.

SAGE-Hindawi Access to Research
International Journal of Electrochemistry
Volume 2011, Article ID 213107, 6 pages
doi:10.4061/2011/213107

Research Article

Porous Materials to Support Bilayer Lipid Membranes for Ion Channel Biosensors

Thai Phung,[1] Yanli Zhang,[1] James Dunlop,[2] and Julie E. Dalziel[1]

[1] *AgResearch, Grasslands Research Centre, Tennent Drive, Private Bag 11008, Palmerston North 4442, New Zealand*
[2] *MacDiarmid Institute for Advanced Materials and Nanotechnology, Victoria University of Wellington, P.O. Box 600, Wellington 6140, New Zealand*

Correspondence should be addressed to Julie E. Dalziel, julie.dalziel@agresearch.co.nz

Received 31 March 2011; Accepted 6 July 2011

Academic Editor: Vinod Kumar Gupta

Copyright © 2011 Thai Phung et al. This is an open access article distributed under the Creative Commons Attribution License, which permits unrestricted use, distribution, and reproduction in any medium, provided the original work is properly cited.

To identify materials suitable as membrane supports for ion channel biosensors, six filter materials of varying hydrophobicity, tortuosity, and thickness were examined for their ability to support bilayer lipid membranes as determined by electrical impedance spectroscopy. Bilayers supported by hydrophobic materials (PTFE, polycarbonate, nylon, and silanised silver) had optimal resistance (14–19 GΩ) and capacitance (0.8–1.6 μF) values whereas those with low hydrophobicity did not form BLMs (PVDF) or were short-lived (unsilanised silver). The ability of ion channels to function in BLMs was assessed using a method recently reported to improve the efficiency of proteoliposome incorporation into PTFE-supported bilayers. Voltage-gated sodium channel activation by veratridine and inhibition by saxitoxin showed activity for PTFE, nylon, and silanised silver, but not polycarbonate. Bilayers on thicker, more tortuous, and hydrophobic materials produced higher current levels. Bilayers that self-assembled on PTFE filters were the longest lived and produced the most channel activity using this method.

1. Introduction

A biological bilayer lipid membrane (BLM) is approximately four nanometres thick consisting of two adjacent monolayer sheets, each composed of molecules with hydrophilic headgroups exposed to water and acyl chains buried into the hydrophobic membrane interior. Integral membrane proteins such as receptors and/or ion channels are responsible for a range of cellular functions that include recognition of pathogens, intracellular signalling, energy transduction, development of energy gradients, and the transport of nutrients and metabolites. Many membrane proteins therefore have potential for use as the sensing entity in biosensors. Two major barriers to the development of biosensors using ion channels are the fragility of biological membranes and their analogues, and the functional requirement of membrane proteins of having solution on both sides of the membrane. Methods that provide enhanced mechanical strength while retaining sensitive electrochemical properties of BLM are being sought to overcome these limitations.

BLM stability can be improved by reducing the area (typically 100–300 μm in diameter). Some researchers have addressed this by putting holes in a support structure to create many small BLMs. For example, in films of amorphous Teflon, where it was found that reducing the pore diameter to under 40 μm increased BLM stability [1]. Multiple BLMs increase the total BLM area which is important for efficient incorporation of membrane proteins. This has also been achieved by forming a BLM over a polymer matrix in which micro-BLMs are thought to form. Demonstration of BLM formation is determined from either a sufficient membrane capacitance or from functional reconstitution of membrane-spanning peptides or proteins that require the BLM to be 4-5 nm thick. Polymers of varying porosity and morphology have been found to provide support for BLMs, for example, commercially available filters of polytetrafluoroethylene (PTFE/Teflon, 5 and 10 μm pore diameter), polycarbonate (0.4–8 μm pore diameters), polyethylene (PETE), and poly(L-lactic acid) (PLLA) [2–4]. Polycarbonate filters have also been utilised as a support for mixed hybrid BLMs formed over 1 μm pore diameters rendered hydrophobic by a gold coating and octadecanethiol [5] in which a glutamate-gated chloride channel was functional [6]. Nylon microfiltration membranes in combination with

S-layers (crystalline bacterial cell surface layers) produced stable BLMs and functional pore-forming peptide activity [7]. Suspended BLMs supported on highly porous alumina and porous silicon (up to 1 μm pore diameter) coated with gold and rendered hydrophobic [3, 8] provided a functional environment for OmpF, a bacterial outer membrane protein [9]. BLM formation, determined from capacitance measurements, has also been shown to occur on hydrophobically silanised silicon nitride surface with 200 nm diameter pores [10].

We recently showed that the pore-forming peptide, gramicidin, and voltage-gated sodium ion channels are functional in BLMs formed on PTFE filters (5 μm pore diameter) [11]. By hydrating the PTFE filter with ionic solution and ion channel proteoliposomes prior to BLM formation, functional reconstitution was enhanced compared with addition of proteoliposomes to the bulk solution. Since this is a convenient means for efficient liposome-BLM fusion, we wanted to know whether other filter materials are suitable BLM supports and if preloading with liposomes enhances incorporation. In this study we examined the physical properties of commercially available membrane filters of polycarbonate, PTFE, nylon, silanised or unsilanised silver, and PVDF, and related this to their ability to support BLMs. The filters were hydrated and BLMs monitored for their stability and longevity by measuring their resistance and capacitance over several hours. The ability of ion channels to function in these BLMs was assessed in filters preloaded with voltage-gated sodium ion channel proteoliposomes. This allowed us to identify which porous materials are able to support BLMs in which ion channels can function, and are therefore of use in biosensor applications.

2. Materials and Methods

2.1. Filter Properties. Contact angles were determined from a photograph of a 2 μL water droplet placed on a filter [12]. Bubble point (values used were as specified by manufacturers) was used as a measure of the resistance to the flow of fluids through pores of filter materials [13]. The bubble point value is determined by observing when bubbles first begin to emerge on the permeate side or downstream side of a fully wetted membrane filter when pressurized with a gas on the feed (upstream) side of the membrane filter.

2.2. BLM-Support Assembly. Porous supports were constructed by heat-pressing a 3 mm diameter disc filter over a 1 mm diameter hole in a polystyrene semi-microcuvette (LP Italiana SPA, cat. no. LPI112117), as detailed in our recent publication using a Teflon filter [11]. The same system was assembled in conjunction with six different filter materials with 5 μm average pore diameters: polycarbonate (Osmonics Inc., cat. no. K50SH58050), polytetrafluoroethylene (PTFE, Teflon; Millipore, cat. no. LSWP01300), nylon (Osmonics Inc., cat. no. R50SH04700), polyvinylidene fluoride (Durapore PVDF; Millipore, cat. no. SVLP01300), and silanised and unsilanised metal silver (Sterlitech, cat. no. AG47SP6). Silanised samples of porous silver material were prepared by treating with dimethyldichlorosilane (BDH) at 170°C for 2 hours. The filter-cuvette assembly was hydrated with ionic solution and ion channel proteoliposomes by vacuum infiltration at −75 kPa for 2 hours, as previously described [11].

2.3. Bilayer Formation. The BLM-forming solution contained 5% (w/w) phosphatidylcholine (PC), extracted from egg yolk [14], and 2% (w/w) cholesterol (Ajax Finechem, Australia) dissolved in n-octane (Sigma Chemical Co., St Louis, MO, USA), centrifuged at 10,000 rpm for 1 minute and the supernatant collected. 10–20 μL was "painted" onto the outer surface of the filter (cis chamber) whereupon a BLM self-assembled.

2.4. Electrical Impedance Spectroscopy. Electrical impedance spectra were obtained using a three-electrode system comprising a platinum counter electrode (cis), a Ag/AgCl wire as a reference electrode (cis), and a Ag/AgCl measuring electrode (trans). Electrical impedance spectra (EIS) were obtained using PCI14/300 Potentiostat and FAS2 Femtostat manufactured by Gamry Instruments operating under Gamry Framework, Echem Analyst, and EIS300 analysis software (Gamry Instruments, Warminster, PA, USA). Absolute values of the impedance $[Z](f)$ and the phase angle $\psi(f)$ between voltage and current were recorded within a frequency range of 10^5–10^{-2} Hz optimising for speed with nine data points per decade equally spaced on a logarithmic scale. Data were obtained at zero offset potential applying a 10 mV sinusoidal AC voltage. A nonlinear least square fitting programme was used to fit an equivalent circuit model to the experimental data.

2.5. Ion Channels. Human voltage-gated sodium channel (VGSC) protein was produced using the insect-baculovirus expression system and the preparation enriched for the VGSC, and incorporated into liposomes as previously described [15]. The VGSC proteoliposomes were preloaded into the filter using vacuum infiltration, as detailed previously [11]. Both chambers contained 300 mM NaCl, 10 mM HEPES, pH 7.4. Water was purified by a Millipore Milli-Q system (Molsheim, France). Sodium channels were activated using 100 μM veratridine (VTD; Sigma) and inhibited using 200 nM tetrodotoxin (TTX; Alomone Labs, Jerusalem Israel). All electrophysiology experiments were carried out at room temperature. Voltage-clamp recordings of ion channel activity were made at a holding potential of −80 mV, 0 and +80 mV over a period of 15 minutes. A 15-minute control recording was taken prior to addition of the VGSC activator veratridine. Recording and reference Ag/AgCl electrodes connected the cell to the amplifier to record ionic currents. VGSC activity was recorded using HEKA EPC7 or EPC9 amplifiers with Pulse v.8.53 and PulseTools v8.8 (HEKA, Lambrecht/Pfalz Germany) and Bruxton Acquire 5.0.1 data acquisition software and analysed using TAC v.4.2.0.

3. Results and Discussion

The suitability of each material as a support for a biosensor BLM was determined as the ability to form BLM on

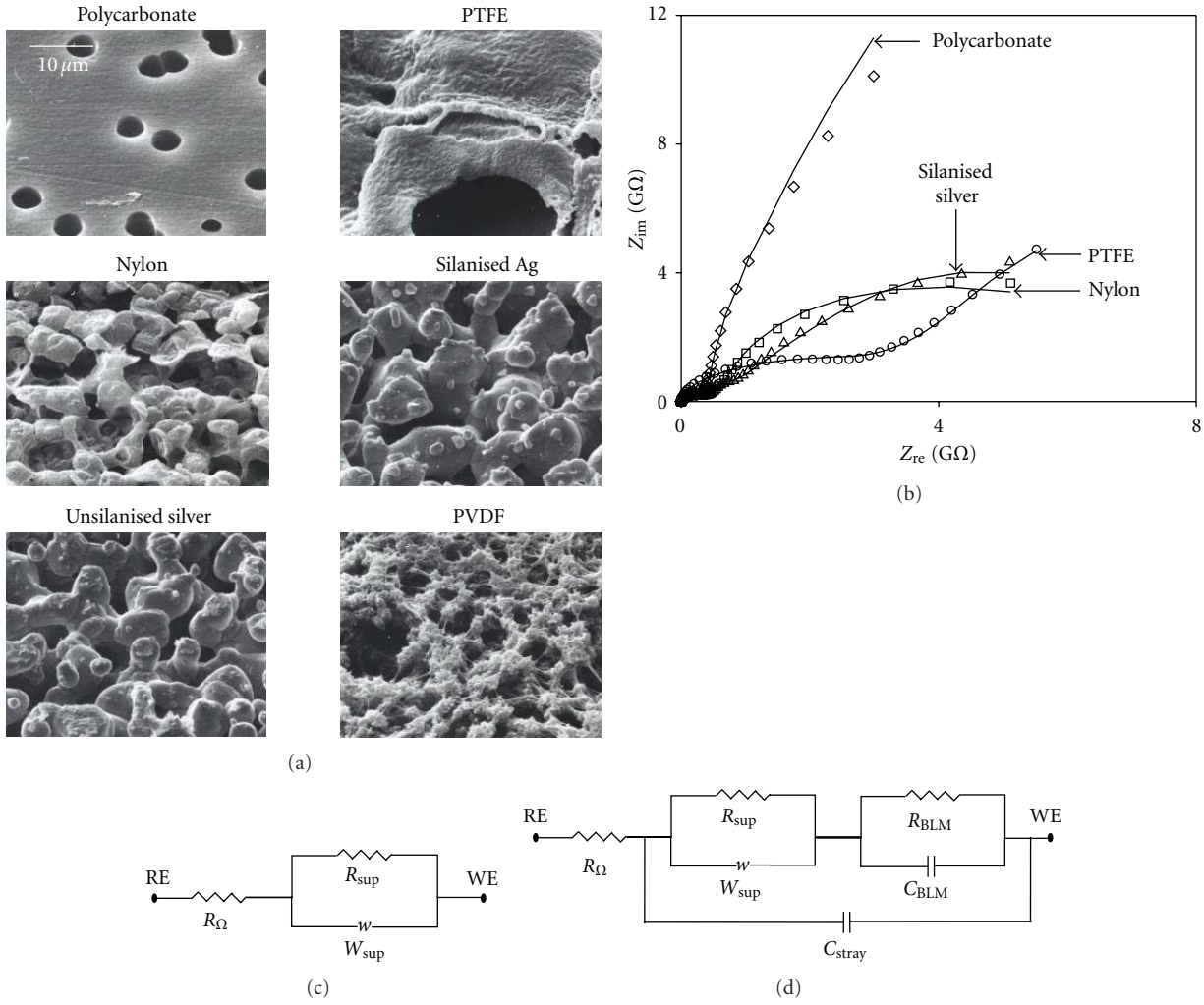

Figure 1: (a) Electron micrographs showing surfaces and structures of various porous materials (magnification ×2000). (b) Faradaic impedance spectra are presented in the form of Nyquist plots showing real (Z_{re}) versus imaginary (Z_{im}) components of BLMs formed on different porous support materials. Electrical circuit models for support (c) and supported BLM (d).

Table 1: Properties of filter materials as porous supports.

Filter material	Thickness (μm)[a]	Contact angle (degrees)	Bubble point[ab]	BLM formed % (n)	Longevity[c] min.(n)	Na^+ current[e] % (n)
PTFE	140	141	0.70	100 (15)	101 ± 7 (22)[d]	40 (10)
Nylon	65–125	135	0.21	71 (14)	18 ± 3 (9)	38 (8)
Silanised Ag	50	109	n/a	92 (12)	38 ± 5 (12)	13 (8)
Unsilanised Ag	50	60	0.14	30 (10)	< 5 (3)	—
Polycarbonate	10	70–90[a]	0.08	100 (13)	29 ± 5 (14)	0 (8)
PVDF	125	n/a	n/a	0 (10)	—	—

[a]Data from manufacturer in methods. [b]Alcohol bubble point (kg.cm^{-2}). [c]Mean ± S.E.M. [d]PTFE monitored for up to 2 h, 73% lasted > 2 h. [e]Number of experiments that gave Na^+ current increases in supported BLMs preloaded with VGSC liposomes after activation by veratridine and were inhibited by saxitoxin. n/a, data not available.

their surface and for the preloaded ion channel protein to reconstitute into the BLM and function.

3.1. Properties of Filter Supports. Polycarbonate filters consist of a uniform series of holes on a smooth surface. The pores approximate straight cylindrical holes from one surface to the other. In contrast, apertures of PTFE, nylon, silver, and PVDF filters, are irregular in shape and size (Figure 1(a)). There is no uniform orientation of pores in these filter materials, particularly for nylon and silver, and matrix void spaces vary in their degree of complexity or tortuousity. The thickness of filter materials also varies from 10 μm for

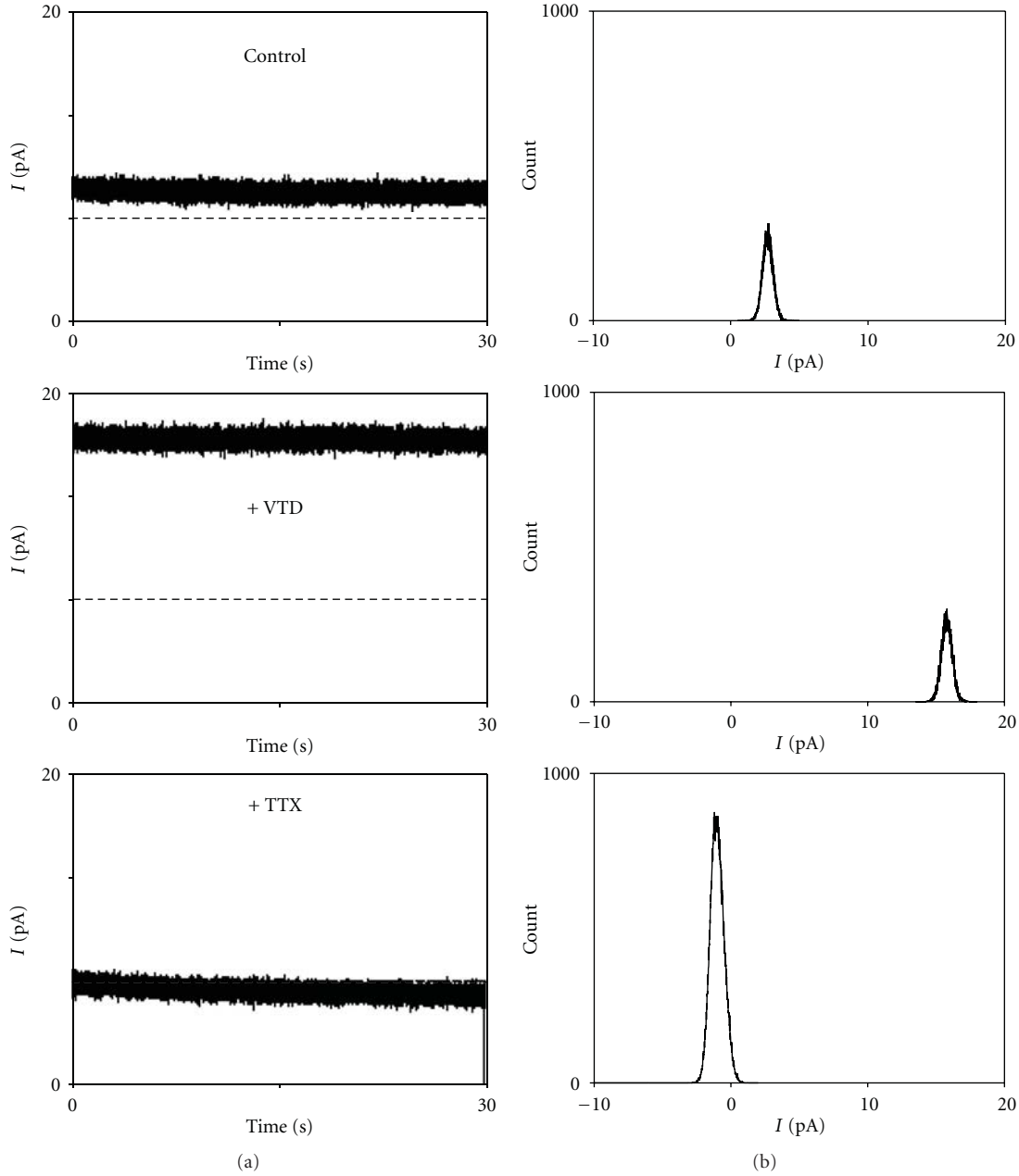

Figure 2: (a) Current recordings from a single experiment are shown for a PTFE filter preloaded with voltage-gated sodium channel (VGSC) liposomes. A BLM was formed on the PTFE filter and the control current level shown after 15 min at +80 mV. The current level is shown 15 min after addition of 100 μM veratridine (VTD) to both sides of the BLM, then 15 min after addition of 100 nM tetrodotoxin (TTX). (b) Corresponding histograms show the current amplitude distribution over the period of the recording.

Table 2: Resistances and capacitances of BLMs on porous supports.

Parameters	PTFE	Nylon	Polycarbonate	Silanised Ag
R_{BLM} (GΩ)	15.1 ± 1.6	18.9 ± 5.8	17.2 ± 3.3	13.8 ± 2.3
C_{BLM} (μF)	1.6 ± 0.1	1.1 ± 0.2	0.8 ± 0.1	0.9 ± 0.1
C_{Stray} (nF)	37.6 ± 0.3	38.5 ± 0.8	36.2 ± 0.4	36.5 ± 0.4
N	40	8	12	12

Values determined from fit of equivalent model circuit to the data. Data are mean ± S.E.M.
R_{BLM}: membrane resistance, C_{BLM}: capacitance of the BLM, C_{Stray}: stray capacitance.

polycarbonate to 140 μm for PTFE (Table 1). It is reasonable to assume that for higher degrees of tortuosity, resistance of fluid flow through the filters is also higher. Silanisation did not change the appearance and structure of silver metal filters (Figure 1(a)).

Contact angles determined from a water droplet were used as a relative measure of hydrophobicity [12] (Table 1). Hydrophobic materials would not allow the bath solution to permeate through the filter. It was therefore necessary to apply a negative pressure to remove all air trapped inside the filter before solution would fill the void space. As expected the hydrophobic materials had higher contact angles than hydrophilic materials. PTFE and nylon had the highest contact angles indicating that they are the most hydrophobic materials tested while unsilanised porous silver gave the lowest contact angle and is therefore the least hydrophobic. Silanisation resulted in a higher contact angle for the porous silver indicating an increased degree of hydrophobicity. The contact angle for the polycarbonate and PVDF filters could not be measured because a droplet could not be formed due to water permeation but was obtained from the manufacturer where possible.

Bubble point is a measure of the resistance to the flow of fluids through the filters caused by their thickness and the tortuosity of the void space [13] (Other factors such as uniformity, surface activity, and surface tension can affect bubble point). A high bubble point indicates a high resistance. PTFE and nylon have similar contact angles but the bubble point for the nylon filters was 70% lower than for PTFE filters (Table 1). Polycarbonate was the thinnest material tested and it had the lowest bubble point. The bubble point of the silanised silver filters was not determined but it would be similar to that of the unsilanised silver material because they have the same pore geometry.

3.2. Bilayer Lipid Membrane Formation. To ascertain whether BLMs were formed on microporous supports, we monitored the electrical properties expected for BLM coverage. Electrical impedance spectroscopy (EIS) provides comprehensive information about the electrical processes of a system under investigation. EIS are generally represented in an equivalent electrical circuit model consisting of parallel and serial elements such as resistance, capacitance, constant phase element, and different types of Warburg elements. The usefulness of EIS to provide quantitative evidence for the presence of BLMs have been demonstrated by many researchers including supported BLMs on PTFE [11], platinum [16], and porous alumina [8]. An electrical circuit model was constructed to fit data obtained from EIS of BLMs on various porous supports (Figures 1(b)–1(d), Table 2). Resistance R_Ω in serial combination represents the resistance of the solution between the working and reference electrodes. The resistance of support is R_{sup} while W_{sup} represents any diffusion of ion across the support. A BLM is in series with the support and comprises a resistor R_{BLM} and capacitor C_{BLM} in parallel. The equivalent circuit is extended to take into account capacitance C_s representing the stray capacitance of the measuring cuvette.

A total area of all micro BLMs assumedly formed over void space inside the support structure should be taken into account when calculating capacitances of BLMs. Apart from polycarbonate filter, other porous filters have an ill-defined structure, therefore this measure is unknown. Furthermore, when lipid is applied to a microporous filter, it will ideally form a single BLM, but could also form a series of BLMs in each pore, or a lipid-solvent plug, or a combination of these [4]. Values determined from curve fits for filter supports of PTFE, nylon, polycarbonate, and silanised silver were within ranges for BLM supports reported by other authors for capacitance [7, 17–21] and resistance [8, 19, 21–24].

BLMs self-assembled on most filters except for PVDF and were short lived on silanised silver filters. The data show that the most hydrophobic material (PTFE) produced the most stable BLMs and that they could not be supported by hydrophilic materials such as PVDF and unsilanised silver. Silanisation of silver filter appears to have rendered the surface hydrophobic for lipid interaction (Table 1). The shorter longevity of BLMs in those with lower hydrophobicity, this suggests that strong hydrophobicity of materials is an important factor for the self-assembly of BLMs.

3.3. Voltage-Gated Sodium Channel Activity. To determine whether filter materials besides PTFE could be preloaded with proteoliposomes and ion channels reconstituted into the BLM, their function was assessed in filters that formed robust BLMs, that is nylon, silanised silver, and polycarbonate, and compared with PTFE. Current responses of filters preloaded with voltage-gated sodium ion channel proteoliposomes were monitored before and after addition of the VGSC-activator veratridine, followed by addition of the VGSC-specific inhibitor tetrodotoxin.

Current responses were measured at a holding potential of −80 mV, 0, and +80 mV over a period of 15 minutes, and was averaged over a one minute recording. The current responses increased from 0 pA (control) to 15–50 pA (after addition of veratridine) over 10–15 min, reversed at 0 mV and were inhibited by tetrodotoxin (Figure 2). The number of filters which responded in this way for a given material were determined (Table 1). The results showed that when VGSC proteoliposomes are preloade into the filter matrices they are able to incorporate into the corresponding BLM in some materials but not others. Nylon and silanised silver filters showed sodium current responses but polycarbonate did not. The 5.6-fold higher BLM longevity for PTFE compared to nylon suggests that PTFE would be the filter material of choice for measuring ion channel activity. The success rate of sodium channel activity in BLMs was lower when formed over thinner and less hydrophobic filter supports (i.e., silanised silver) than on PTFE (Table 1). Materials with low contact angle and low bubble point showed low or no ion channel currents. Thicker supports also produced higher current responses. Polycarbonate was the thinnest filter tested and had the lowest bubble point, suggesting low hydrophobicity which would be consistent with a poor ability to retain proteoliposomes. We did find, however that proteoliposomes added to bath solution

after BLMs been formed on polycarbonate produced some sodium currents (data not shown), indicating that while they cannot retain preloaded proteoliposomes, these filters can provide a suitable BLM environment for ion channels. This is consistent with the use of polycarbonate filters to support mixed hybrid BLMs that provide a functional environment for glutamate-gated chloride ion channels [6].

4. Conclusions

The findings in this study showed that bilayer lipid membranes were most stable when supported by highly hydrophobic materials. Filter supports with greater tortuosity and thickness produced the most ion channel activity when preloaded with proteoliposomes. PTFE was the most versatile filter material of those tested in that it supported long-lived BLMs, and ion channel function when preloaded with ion channel protein. Understanding factors that contribute to BLM stability will help in selection of materials and improved design for customised biosensor systems using membrane proteins.

Acknowledgments

The authors thank Erwin Berthier for measurements of contact angles. This paper was funded by The New Economy Research Fund, from the Foundation for Research Science and Technology of New Zealand, an AgResearch Postdoctoral Fellowship, and AgResearch Research and Capability and PreSeed Funds.

References

[1] M. Mayer, J. K. Kriebel, M. T. Tosteson, and G. M. Whitesides, "Microfabricated Teflon membranes for low-noise recordings of ion channels in planar lipid bilayers," *Biophysical Journal*, vol. 85, no. 4, pp. 2684–2695, 2003.

[2] M. A. Dhoke, P. J. Ladha, F. J. Boerio et al., "Porous membranes for reconstitution of ion channels," *Biochimica et Biophysica Acta*, vol. 1716, no. 2, pp. 117–125, 2005.

[3] C. Hennesthal, J. Drexler, and C. Steinem, "Membrane-suspended nanocompartments based on ordered pores in Alumina," *ChemPhysChem*, vol. 3, no. 10, pp. 885–889, 2002.

[4] M. Thompson, R. B. Lennox, and R. A. McClelland, "Structure and electrochemical properties of microfiltration filter-lipid membrane systems," *Analytical Chemistry*, vol. 54, no. 1, pp. 76–81, 1982.

[5] G. Favero, L. Campanella, A. D'Annibale, R. Santucci, and T. Ferri, "Mixed hybrid bilayer lipid membrane incorporating valinomycin: improvements in preparation and functioning," *Microchemical Journal*, vol. 74, no. 2, pp. 141–148, 2003.

[6] G. Favero, L. Campanella, S. Cavallo et al., "Glutamate receptor incorporated in a mixed hybrid bilayer lipid membrane array, as a sensing element of a biosensor working under flowing conditions," *Journal of the American Chemical Society*, vol. 127, no. 22, pp. 8103–8111, 2005.

[7] B. Schuster, D. Pum, M. Sára, O. Braha, H. Bayley, and U. B. Sleytr, "S-layer ultrafiltration membranes: a new support for stabilizing functionalized lipid membranes," *Langmuir*, vol. 17, no. 2, pp. 499–503, 2001.

[8] J. Drexler and C. Steinem, "Pore-suspending lipid bilayers on porous alumina investigated by electrical impedance spectroscopy," *Journal of Physical Chemistry B*, vol. 107, no. 40, pp. 11245–11254, 2003.

[9] E. K. Schmitt, M. Vrouenraets, and C. Steinem, "Channel activity of OmpF monitored in nano-BLMs," *Biophysical Journal*, vol. 91, no. 6, pp. 2163–2171, 2006.

[10] X. Han, A. Studer, H. Sehr et al., "Nanopore arrays for stable and functional free-standing lipid bilayers," *Advanced Materials*, vol. 19, no. 24, pp. 4466–4470, 2007.

[11] T. Phung, Y. Zhang, J. Dunlop, and J. Dalziel, "Bilayer lipid membranes supported on Teflon filters: a functional environment for ion channels," *Biosensors and Bioelectronics*, vol. 26, pp. 3127–3135, 2011.

[12] R. Förch, H. Schönherr, and A. T. A. Jenkins, *Surface Design*, Wiley-VCH, Weinheim, Germany, 2009.

[13] F. Hofmann, "Integrity testing of microfiltration membranes," *Journal of Parenteral Science and Technology*, vol. 38, no. 4, pp. 148–158, 1984.

[14] W. S. Singleton, M. S. Gray, M. L. Brown, and J. L. White, "Chromatographically homogeneous lecithin from egg phospholipids," *Journal of the American Oil Chemists' Society*, vol. 42, no. 1, pp. 53–56, 1965.

[15] Y. L. Zhang, J. Dunlop, and J. E. Dalziel, "Recombinant human voltage-gated skeletal muscle sodium channels are pharmacologically functional in planar lipid bilayers," *Biosensors and Bioelectronics*, vol. 22, no. 6, pp. 1006–1012, 2007.

[16] J. Sabo, A. Ottova, G. Laputkova, M. Legin, L. Vojcikova, and H. T. Tien, "A combined AC-DC method for investigating supported bilayer lipid membranes," *Thin Solid Films*, vol. 306, no. 1, pp. 112–118, 1997.

[17] F. Bordi, C. Cametti, and A. Gliozzi, "Impedance measurements of self-assembled lipid bilayer membranes on the tip of an electrode," *Bioelectrochemistry*, vol. 57, no. 1, pp. 39–46, 2002.

[18] A. Janshoff, H.-J. Galla, and C. Steinem, in *Planar Lipid Bilayers (BLMs) and Their Applications*, H. T. Tien and A. Ottova-Leitmannova, Eds., Elsevier, Amsterdam, The Netherlands, 2003.

[19] W. Römer, Y. H. Lam, D. Fischer et al., "Channel activity of a viral transmembrane peptide in micro-BLMs: Vpu 1-32 from HIV-1," *Journal of the American Chemical Society*, vol. 126, no. 49, pp. 16267–16274, 2004.

[20] A. E. Vallejo and C. A. Gervasi, "Impedance analysis of ion transport through gramicidin channels in supported lipid bilayers," *Bioelectrochemistry*, vol. 57, no. 1, pp. 1–7, 2002.

[21] G. Wiegand, N. Arribas-Layton, H. Hillebrandt, E. Sackmann, and P. Wagner, "Electrical properties of supported lipid bilayer membranes," *Journal of Physical Chemistry B*, vol. 106, no. 16, pp. 4245–4254, 2002.

[22] S. Gritsch, P. Nollert, F. Jähnig, and E. Sackmann, "Impedance spectroscopy of porin and gramicidin pores reconstituted into supported lipid bilayers on indium-tin-oxide electrodes," *Langmuir*, vol. 14, no. 11, pp. 3118–3125, 1998.

[23] P. Mueller and D. O. Rudin, "Action potentials induced in biomolecular lipid membranes," *Nature*, vol. 217, no. 5130, pp. 713–719, 1968.

[24] W. Römer and C. Steinem, "Impedance analysis and single-channel recordings on nano-black lipid membranes based on porous alumina," *Biophysical Journal*, vol. 86, no. 2, pp. 955–965, 2004.

SAGE-Hindawi Access to Research
International Journal of Electrochemistry
Volume 2011, Article ID 934893, 5 pages
doi:10.4061/2011/934893

Research Article

Immobilization of HRP Enzyme on Layered Double Hydroxides for Biosensor Application

Zouhair M. Baccar[1] and Imène Hafaiedh[2]

[1] *Nanobioengineering Group, National Institute of Research and Physicochemical Analysis (INRAP), Biotechnopôle de Sidi Thabet, Sidi Thabet 2020, Tunisia*
[2] *Unity of Research of Physico-Chemistry of Polymers, IPEST, University of Carthage, BP 57, La Marsa 2075, Tunisia*

Correspondence should be addressed to Zouhair M. Baccar, zouhair_baccar@topnet.tn

Received 20 May 2011; Revised 9 June 2011; Accepted 11 June 2011

Academic Editor: Farnoush Faridbod

Copyright © 2011 Z. M. Baccar and I. Hafaiedh. This is an open access article distributed under the Creative Commons Attribution License, which permits unrestricted use, distribution, and reproduction in any medium, provided the original work is properly cited.

We present a new biosensor for hydrogen peroxide (H_2O_2) detection. The biosensor was based on the immobilization of horseradish peroxidase (HRP) enzyme on layered double hydroxides- (LDH-) modified gold surface. The hydrotalcite LDH (Mg_2Al) was prepared by coprecipitation in constant pH and in ambient temperature. The immobilization of the peroxidase on layered hybrid materials was realized via electrostatic adsorption autoassembly process. The detection of hydrogen peroxide was successfully observed in PBS buffer with cyclic voltammetry and the chronoamperometry techniques. A limit detection of 9 μM of H_2O_2 was obtained with a good reproducibility. We investigate the sensitivity of our developed biosensor for H_2O_2 detection in raw milk.

1. Introduction

Horseradish peroxidase (HRP) is a glycoprotein with four lysine residues for conjugation to a labeled molecule. It produces a colored, fluorimetric, or luminescent derivative of the labeled molecule when incubated with a proper substrate, allowing it to be detected and quantified. Horseradish peroxidase was often used in conjugates to determine the presence of a molecular target and was also commonly used in techniques such as ELISA and Immunohistochemistry. Horseradish peroxidase is ideal in many respects for these applications because it is smaller, more stable, and less expensive than other popular alternatives such as alkaline phosphatase. Conductor's polymers and magnetic nanoparticles were used in the fabrication of various types of HRP-based biosensors [1, 2]. To stabilize the immobilized enzyme in the matrix of film, glutaraldehyde (GA) is usually employed as a bifunctional agent to cross-link enzyme molecules [3–6], but the cross-linking efficiency under standard conditions is not always satisfactory [6, 7], which results in the lower sensitivity and poor stability of the resulting biosensor. It was established that cationic clays and especially anionic ones or layered double hydroxides were considered as a new class of materials with a high trapping potential of molecules of different sizes and that they form hybrid materials. Indeed, these materials present very attractive advantages such as a low cost of purification or synthesis and their biocompatibility. Furthermore, the bi-dimensional structure of LDHs with the general formula: $[M^{2+}_{1-X}\ M^{3+}_{X}\ (OH)_2]^{x+} \cdot [A_{x/q}]^{q-} \cdot nH_2O$ [8, 9] present additional advantages relatively to cationic clays. LDHs can be synthesized using the same protocol, and the obtained materials have a large range of physicochemical properties. A wide varieties of LDHs can be achieved by changing the anionic ion A ($CO_3{}^{2-}$, $SO_4{}^{2-}$, $HPO_4{}^{2-}$, $NO_3{}^{-}$, F^-, Cl^-, Br^-, and I^-) or the metallic divalent (M^{2+} : Mg, Zn, Ni, Co, Pd, etc.) or trivalent ions (M^{3+} : Al, Cr, Fe, V, etc.). This type of material presents high anionic-exchanging capacities by changing the divalent and trivalent ion ratio ($x = [M^{2+}]/[M^{3+}]$) and adjusting the interlayer anions $[A_{x/q}]^{q-}$ to intercalate different molecules [3–10]. Therefore, this kind of materials can be considered very attractive for new hybrid biomaterials development and for functionalized surfaces for ionic and biologic detection [10–12]. It has been previously shown that immobilization

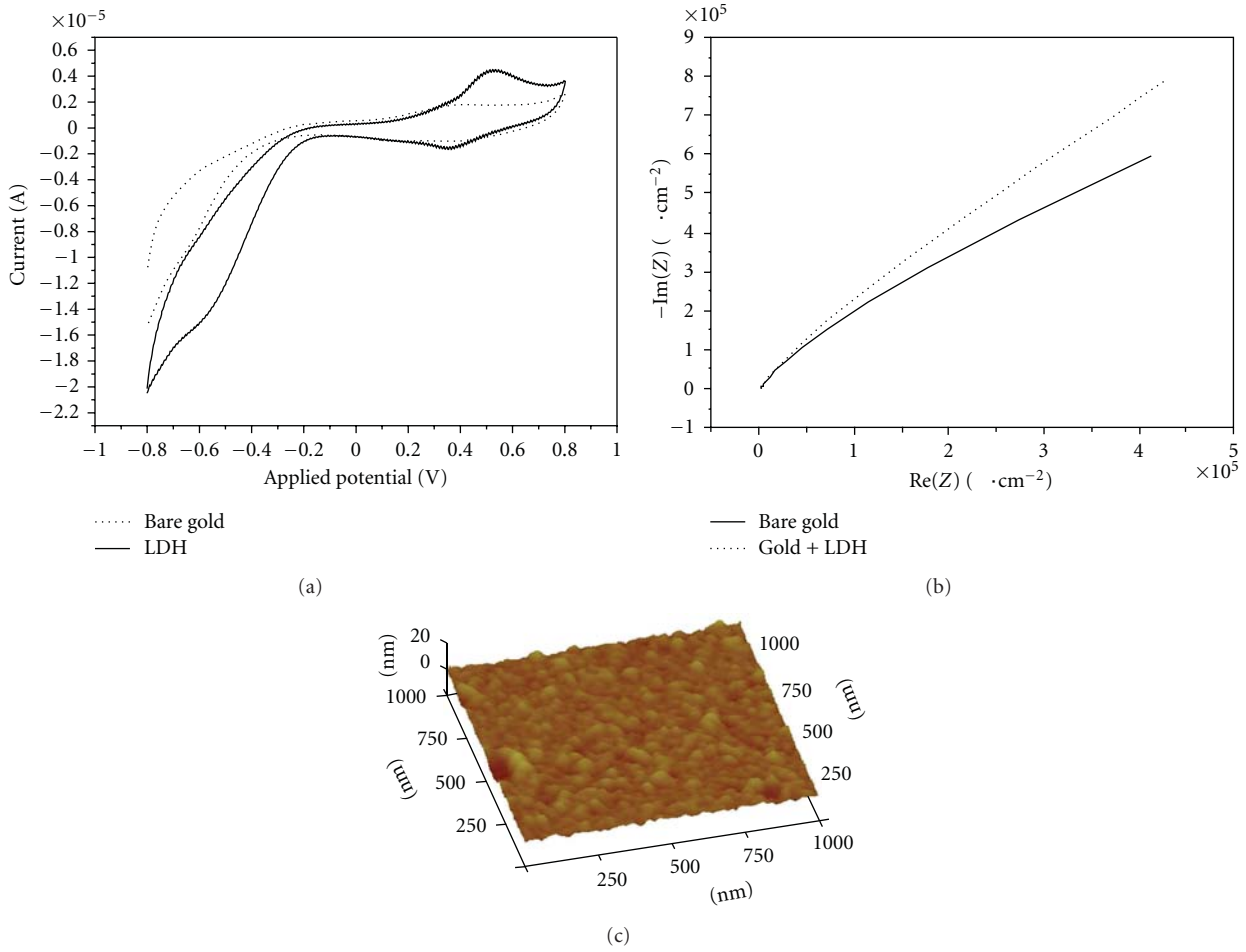

Figure 1: (a) Cyclic voltammetry measurement in PBS buffer of bare gold electrode and gold electrode with LDH, respectively. (b) Nyquist diagram (Z_i versus Z_r) of impedance measurement corresponding to the gold electrode without and with LDH layer. (c) Atomic force microscopy photo of gold surface treated with LDH. It shows a homogenous surface with roughness below 1 nm.

of urease in LDH is of high interest for the fabrication of biosensors [12]. The panel of applications of these materials is very large; they can be used for monitoring food process, diagnosis and medical monitoring, or for therapeutic and pharmaceutical applications such as the encapsulation of active molecules for drugs [13–15] or radioactive substances.

In this work, we present a new biosensor for hydrogen peroxide (H_2O_2) detection based on layered double hydroxides (LDH) layer. The biosensor was based on the immobilization of horseradish peroxidase (HRP) enzyme on LDH-modified gold surface. The hydrotalcite LDH (Mg_2Al) was prepared by coprecipitation in constant pH and in ambient temperature. The immobilization of the peroxidase in layered hybrid materials was realized via electrostatic adsorption autoassembly process. The detection of hydrogen peroxide was successfully observed in PBS buffer with cyclic voltammetry and the chronoamperometry techniques.

2. Experimental Setup

2.1. Reagents and Apparatus. The hybrid biomembranes Enzyme/LDH were prepared in two steps: the LDH synthesis, followed by the peroxidase immobilization. We synthesized hydrotalcite LDH by coprecipitation method at constant pH and temperature. The ratio volume of solutions of $MgCl_3$ and $AlCl_3$ 0.1 M was fixed at 2 in order to obtain a final LDH of Mg_2AlCO_3. Mg_2AlCO_3 LDH was prepared according to the process described by Baccar et al. [16]. We added drop to drop and under vortex agitation the solution of $AlCl_3$ and the $MgCl_2$. The pH reaction of coprecipitation was fixed at pH 8 by adding a basic solution of NaOH (NaOH 2 M + Na_2CO_3 0.125 M). The final solution obtained was washed with milli-Q water and filtered to eliminate the ions chlorides, then dried at 100°C in dark during 12 hours, and finally crushed.

2.2. Gold Cleaning and Functionalization. The gold electrodes (1 cm × 1 cm) were fabricated at the National Center of Microelectronics of Barcelona (Spain). Evaporated gold (~300 nm thickness) was deposited on silicon, using a titanium under layer (~30 nm thickness) as substrate. Before modification, the gold electrodes were cleaned in acetone solution for 20 min with ultrasonic bath. After that, they were dried under a nitrogen flow and then dipped for 10 min into "piranha solution" 7 : 3 (v/v) 96%H_2SO_4/30%H_2O_2.

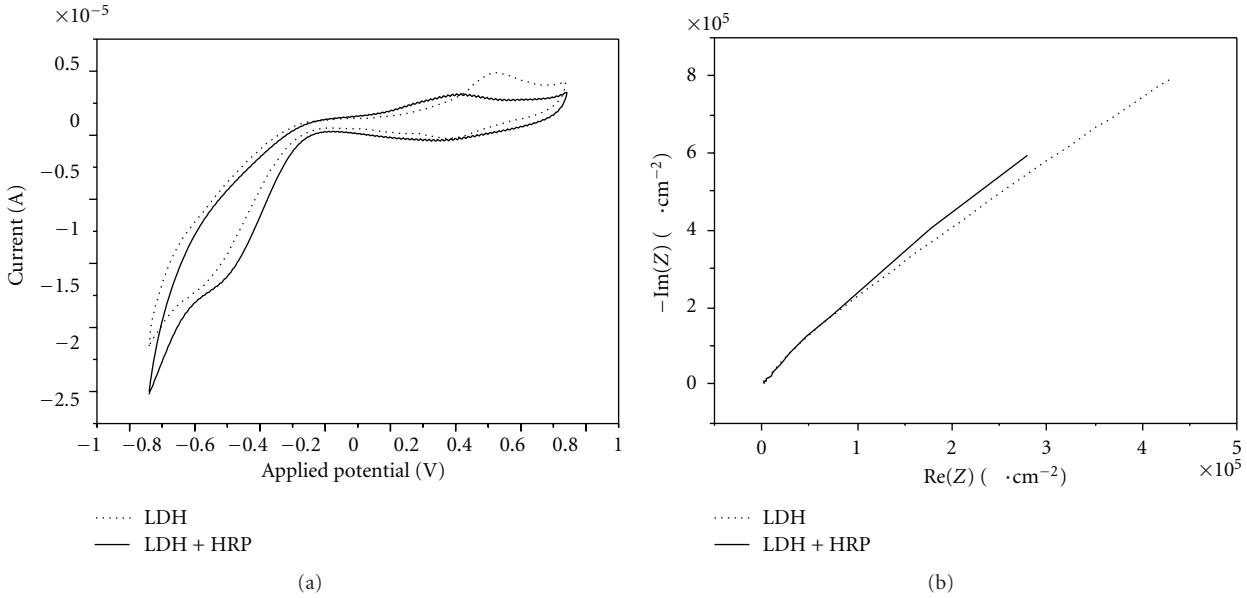

Figure 2: (a) Cyclic voltammogram of gold electrode functionalized with LDH before and after HRP immobilization. (b) Nyquist diagram (Z_i versus Z_r) of impedance measurement corresponding to the gold-electrode with LDH before and after HRP immobilization.

Finally, the gold substrates were rinsed 2 to 3 times with ultrapure water and immediately immersed in an ethanol solution. After cleaning, the gold electrodes were immediately placed on an electrochemical cell. For DHL deposition on gold electrodes, a drop (approximately 10 μL by cm^2) of dispersed LDH (Mg_2Al 2.5 mg/mL) in deionised water (milli-Q) was deposited and coated by spin coating at less than 1000 rms/min during 10 s and about 4000 rms/min during 30 s. After that, a drop (approximately 10 μL by 1 cm^2) of HRP (equal to 0.250–0.330 Units) dispersed in milli-Q water was deposited in surface and dried at 4°C overnight. Finally, the nonbounded enzymes were eliminated by washing samples with a solution of 20 mM PBS. After testing, the samples were stored in a solution of 20 mM PBS, pH 7.4 at 4°C.

2.3. Cyclic Voltammetry and Chronoamperometry. Cyclic voltammetry and chronoamperometry measurement were performed at room temperature in a conventional voltammetric cell with a three-electrode configuration using Autolab impedance analyzer (Eco Chemie, The Netherland). The gold electrode (0.16 cm^2) was used as working electrode and platinum (1 cm^2) and Ag/AgCl electrodes were used as counter and reference electrodes, respectively. All cyclic voltammetry measurements were carried out with scan rate of 75 mV/s in PBS at pH 7 and in Faraday cage. More details can be found in [17].

2.4. Atomic Force Microscopy and Impedance Spectroscopy. Atomic Force microscopy was performed using a Dimension 3100 (Veeco) Atomic Force Microscope operating in tapping mode. The impedance analysis was performed with the Autolab 302 N impedance analyzer (Eco Chemie, The Netherland) in the frequency range 0.05 Hz–100 kHz, using a modulation voltage of 10 mV. More details on electrochemical impedance spectroscopy can be found in [18–20].

3. Results and Discussions

3.1. Gold Electrode Functionalization. Cyclic voltammetry is an electrochemical technique which can be used to study the kinetic of redox reactions of materials, their insulating and conducting properties. Cyclic voltammograms of the gold electrode (Figure 1(a)) show a reversible wave which is the typical behavior of gold surface in PBS buffer. After modification of the gold surface with the LDH membrane, the current increases due to the high conductivity properties of the LDH layer and anion exchange (Figure 1(a)). Typical Nyquist plots for gold electrode and gold electrode with LDH layer from 50 mHz to 100 KHz at 0.2 V potential (versus Calomel electrode) in PBS were shown in Figure 1(b). Impedance spectra were interpreted through equivalent circuits representing the different processes involved in the description of the system with discrete electric elements [20, 21]. The semicircle diameter of impedance spectra represents the charge transfer resistance, R_{ct}. This resistance controls the electron transfer kinetics of the ions at the electrode interface. Figure 1(c) shows the atomic force microscopy image of gold surface treated with LDH in tapping mode. It shows a homogenous surface with roughness less than 1 nm. The same observation was observed with scanning electron microscopy (SEM) in [22].

3.2. HRP Immobilization. Figure 2(a) shows the cyclic voltammogram of gold electrode functionalized with LDH layer before and after HRP immobilization. We observe a decrease of the current for positive potential after HRP immobilization. The peak at 350 mV corresponds to the oxidation

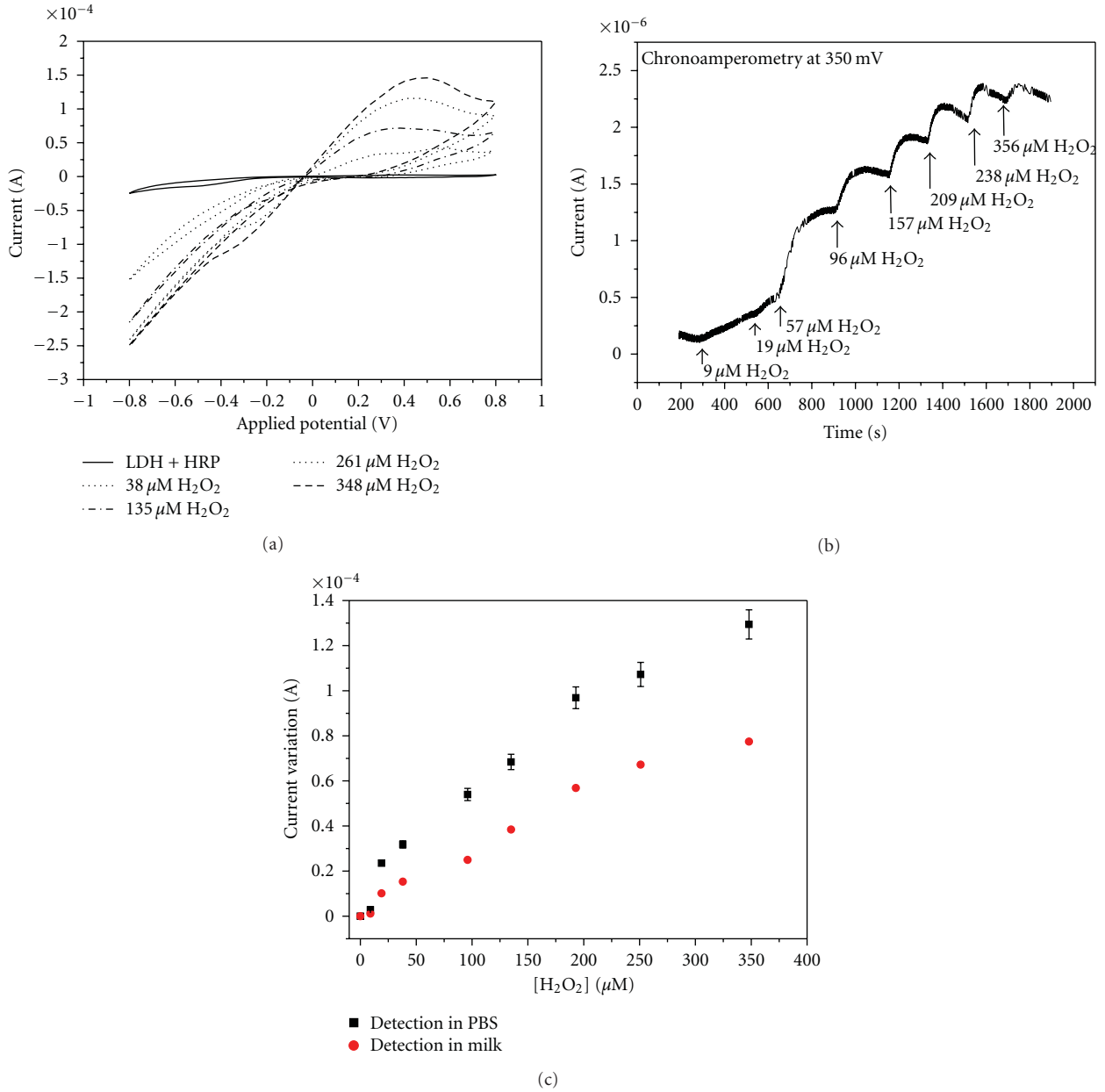

Figure 3: (a) Cyclic voltammogram of gold electrode functionalized with HRP before and after the injection of different H_2O_2 concentration. (b) The chronoamperometry curve of functionalized gold electrode with HRP at a fixed potential of 350 mV after H_2O_2 injections. (c) Current variation (current after H_2O_2 injection) of the developed biosensor after different injection of H_2O_2 concentration at 350 mV obtained from Figure 3(a) in PBS buffer and raw milk. Linear regression was observed between 0 and 200 μM.

potential of HRP. Figure 2(b) shows the Nyquist diagram of impedance measurement at fixed potential (0.2 V) for gold electrode with LDH and with HRP enzyme. The increase of the charge transfer resistance is due to the success immobilization of the HRP enzyme. This result confirms the result obtained with cyclic voltammetry.

3.3. Biosensors Applications. Figure 3(a) shows the cyclic voltammogram of the gold electrode functionalized with HRP enzyme before and after injection of H_2O_2. Upon the addition of the hydrogen peroxide to the electrochemical cell, the oxidation peak (at 350 mV) appears, showing a typical electron transfer between the H_2O_2 and the HRP molecule:

$$\begin{aligned} H_2O_2 + HRP_{red} &\longrightarrow HRP_{ox} + H_2O, \\ HRP_{ox} + 2e^- &\longrightarrow HRP_{red}. \end{aligned} \quad (1)$$

The chronoamperometry can be used to explore the current response of the biosensor in presence of the hydrogen peroxide. Figure 3(b) shows the chronoamperometry curve of functionalized electrode with HRP at a fixed potential of 350 mV after H_2O_2 injections. The current increases with

increasing H_2O_2 concentration which agrees with result shown in Figure 3(a). The addition of the hydrogen peroxide to the buffer solution increases the steady state current. Figure 3(c) shows the calibration curves of the biosensor exposed to different concentration of hydrogen peroxide obtained from Figure 3(a) (at a potential of 350 mV). The curves were represented by a linear regression (between 0 to 200 μM), and a best sensitivity was obtained. A limit detection of 9 μM of H_2O_2 was obtained with a good reproducibility for the developed biosensor. Moreover, we investigate the sensitivity of our developed biosensor for H_2O_2 detection in raw milk. Figure 3(c) shows the calibration curve obtained in raw milk after H_2O_2 injection. It shows a lower sensitivity due to coexisting electroactive species such as casein (and other proteins) in raw milk.

4. Conclusion

In this work, we present new biosensors for the detection of hydrogen peroxide (H_2O_2) with LDH functionalized layer. The biosensor was developed by the immobilization of horseradish peroxidase (HRP) enzyme on LDH-modified gold electrode. The deposition of LDH layer and HRP enzyme was verified with cyclic voltammetry and impedance spectroscopy. The detection of hydrogen peroxide was successfully observed in PBS using the cyclic voltammetry and the chronoamperometry techniques. A limit detection of 9 μM of H_2O_2 was obtained with a good reproducibility. We investigate the sensitivity of our developed biosensor for H_2O_2 detection in raw milk.

References

[1] S. Helali, H. Baccar, A. Abdelghani, and N. Jaffrezic-Renault, "Electrochemical study of horseradish peroxidase biosensor based on functionalised magnetic beads and polypyrrole film," *Sensor Letters*, vol. 7, no. 5, pp. 808–811, 2009.

[2] C. C. Chen, J. S. Do, and Y. Gu, "Immobilization of HRP in mesoporous silica and its application for the construction of polyaniline modified hydrogen peroxide biosensor," *Sensors*, vol. 9, no. 6, pp. 4635–4648, 2009.

[3] K. Arora, G. Sumana, V. Saxena et al., "Improved performance of polyaniline-uricase biosensor," *Analytica Chimica Acta*, vol. 594, no. 1, pp. 17–23, 2007.

[4] V. Luo and J. S. Do, "Urea biosensor based on PANi(urease)-Nafion/Au composite electrode," *Biosensors and Bioelectronics*, vol. 20, no. 1, pp. 15–23, 2004.

[5] A. H. Parente, E. T. A. Marques, W. M. Azevedo, F. B. Diniz, E. H. M. Melo, and J. L. L. Filho, "Glucose biosensor using glucose oxidase immobilized in polyaniline," *Applied Biochemistry and Biotechnology*, vol. 37, no. 3, pp. 267–273, 1992.

[6] I. Migneault, C. Dartiguenave, M. J. Bertrand, and K. C. Waldron, "Glutaraldehyde: behavior in aqueous solution, reaction with proteins, and application to enzyme crosslinking," *BioTechniques*, vol. 37, no. 5, pp. 790–802, 2004.

[7] K. F. Fernandes, C. S. Lima, H. Pinho, and C. H. Collins, "Immobilization of horseradish peroxidase onto polyaniline polymers," *Process Biochemistry*, vol. 38, no. 9, pp. 1379–1384, 2003.

[8] E. P. Giannelis, D. G. Nocera, and T. J. Pinnavaia, "Anionic photocatalysts supported in layered double hydroxides: intercalation and photophysical properties of a ruthenium complex anion in synthetic hydrotalcite," *Inorganic Chemistry*, vol. 26, no. 1, pp. 203–205, 1987.

[9] M. Meyn, K. Beneke, and G. Lagaly, "Anion-exchange reactions of layered double hydroxides," *Inorganic Chemistry*, vol. 29, no. 26, pp. 5201–5207, 1990.

[10] H. Barhoumi, A. Maaref, M. Rammah et al., "Urea biosensor based on Zn3Al-Urease layered double hydroxides nanohybrid coated on insulated silicon structures," *Materials Science and Engineering C*, vol. 26, no. 2-3, pp. 328–333, 2006.

[11] J. V. Melo, S. Cosnier, C. Mousty, C. Martelet, and N. Jaffrezic-Renaultt, "Urea biosensors based on immobilization of urease into two oppositely charged clays (Laponite and Zn-Al layered double hydroxides)," *Analytical Chemistry*, vol. 74, no. 16, pp. 4037–4043, 2002.

[12] Z. M. Baccar, S. Hidouri, A. Errachid, and O. Ruiz-Sanchez, vol. 11, *Journal of Nanoscience and Nanotechnology*. In press.

[13] B. Li, J. He, D. G. Evans, and X. Duan, "Inorganic layered double hydroxides as a drug delivery system—intercalation and in vitro release of fenbufen," *Applied Clay Science*, vol. 27, no. 3-4, pp. 199–207, 2004.

[14] M. Del Arco, S. Gutievreg, C. Martin, V. Rives, and J. Rocha, "Synthesis and characterization of layered double hydroxides (LDH) intercalated with non-steroidal anti-inflammatory drugs (NSAID)," *Journal of Solid State Chemistry*, vol. 177, no. 11, pp. 3954–3962, 2004.

[15] S. Y. Kwak, Y. J. Jeong, J. S. Park, and J. H. Choy, "Bio-LDH nanohybrid for gene therapy," *Solid State Ionics*, vol. 151, no. 1-4, pp. 229–234, 2002.

[16] Z. M. Baccar, S. Hidouri, N. El Bari, N. Jaffrezic-Renault, A. Errachid, and N. Zine, "Stable immobilization of anti-beta casein antibody onto layered double hydroxides materials for biosensor applications," *Sensor Letters*, vol. 7, no. 5, pp. 647–655, 2009.

[17] A. Tlili, A. Abdelghani, S. Ameur, and N. Jaffrezic-Renault, "Impedance spectroscopy and affinity measurement of specific antibody-antigen interaction," *Materials Science and Engineering C*, vol. 26, no. 2-3, pp. 546–550, 2006.

[18] M. Hnaien, S. Helali, M. F. Diouani et al., "Immobilization of specific antibody on SAM functionalized gold electrode for rabies virus detection by electrochemical impedance spectroscopy," *Biochemical Engineering Journal*, vol. 39, no. 3, pp. 443–449, 2008.

[19] H. B. Fredj, S. Helali, L. Vonna, L. Vidal, A. Abdelghani, and C. Esseghaier, "Labeled magnetic nanoparticles assembly on polypyrrole film for biosensor applications," *Talanta*, vol. 75, no. 3, pp. 740–747, 2008.

[20] M. F. Diouani, S. Helali, I. Hafaid et al., "Miniaturized biosensor for avian influenza virus detection," *Materials Science and Engineering C*, vol. 28, no. 5-6, pp. 580–583, 2008.

[21] S. Helali, A. Abdelghani, I. Hafaiedh, K. Cherifa, and G. Tournierb, "Characterization of tin dioxide film for chemical vapors sensor," *Materials Science and Engineering C*, vol. 28, no. 5-6, pp. 584–587, 2008.

[22] C. Mousty, O. Kaftan, V. Prevot, and C. Forano, "Alkaline phosphatase biosensors based on layered double hydroxides matrices: role of LDH composition," *Sensors and Actuators, B*, vol. 133, no. 2, pp. 442–448, 2008.

SAGE-Hindawi Access to Research
International Journal of Electrochemistry
Volume 2011, Article ID 863196, 17 pages
doi:10.4061/2011/863196

Review Article

Electrochemical Aptamer-Based Biosensors: Recent Advances and Perspectives

Abd-Elgawad Radi

Department of Chemistry, Faculty of Science, Mansoura University, Dumyat 34517, Egypt

Correspondence should be addressed to Abd-Elgawad Radi, abdradi@yahoo.com

Received 17 February 2011; Revised 12 May 2011; Accepted 16 May 2011

Academic Editor: Farnoush Faridbod

Copyright © 2011 Abd-Elgawad Radi. This is an open access article distributed under the Creative Commons Attribution License, which permits unrestricted use, distribution, and reproduction in any medium, provided the original work is properly cited.

This paper reviews the advancements of a wide range of electrochemical aptamer-based biosensors, electrochemical aptasensors, for target analytes monitoring. Methods for immobilizing aptamers onto an electrode surface are discussed. Aptasensors are presented according to their detection strategies. Many of these are simply electrochemical, aptamer-based equivalents of traditional immunochemical approaches, sandwich and competition assays employing electroactive signaling moieties. Others, exploiting the unusual physical properties of aptamers, are signal-on (positive readout signal) and signal-off (negative readout signal) aptasensors based on target binding-induced conformational change of aptamers. Aptamer label-free devices are also discussed.

1. Introduction

Biosensors are devices detecting the presence of a target by using a particular recognition element and then monitoring the mass, optical, electronic, or magnetic signal changes, which are induced by the interaction of the recognition element and the analyte of interest. Molecular recognition is consequently the key for the sensor performance. The recognition elements were initially isolated naturally from living systems; now, they are available by synthesis in the lab, including receptors, enzymes, antibodies, nucleic acids, molecular imprints and lectins. The mostly used recognition components for clinic diagnostics and genomics/proteomics studies are antibodies and nucleic acids based on affinity assays owing to their special high sensitivity and selectivity in the affinity to target molecules. Antibodies are produced by immune system when it responds to antigens (i.e., toxins, chemicals, drugs, and virus particles, spores, bacterial toxins, and other foreign substrates). Antibodies were generated by animal immunization, and now, cell clone technology can produce poly/monoclonal antibodies in large quantities. The antibodies still encounter the challenges of pH and temperature sensitivity, short shelf life, easily degradation, and consequently, its repeatable usage is also a problem.

Aptamers, first reported in 1990, are attracting interest in the areas of therapeutics and diagnostics [1–3]. Aptamers are specific oligonucleic acid sequences (ca. 30 to 100 nucleotides), which recognize specific ligands and bind to various target molecules ranging from small ions to large proteins with high affinity and specificity. The term aptamer derives from aptus that means to fit. The RNA or DNA aptamers molecules are selected in vitro (selection evolution of ligands by exponential enrichment, SELEX process) from vast populations of random sequences. Aptamers are often called synthetic antibodies and can mimic antibodies in a number of applications. The selected aptamers bind their targets with affinities and specificities that can be comparable to those of antibodies. Aptamers present some advantages compared to antibodies, especially accurate and reproducible chemical production. Moreover, Aptamer offering chemical stability under a wide range of buffer conditions, resistant to harsh treatments without losing its bioactivity, and the thermal denaturation is reversible for aptamer. While it is important to remain proteins in a moisturized environment to maintain their bioactivity, and the physical or chemical denaturation is irreversible for antibodies. Aptamer has a wide range of molecular and therapeutic targets, including amino acids, any class of proteins (enzymes, membrane

proteins, viral proteins, cytokines and growth factors, and immunoglobulins), drugs, metal ions, other small bio-/organic/inorganic small molecules, and even whole cells. However, antibody is only employed for immunogenic compounds. Aptamers are small in size, cost effective, offering remarkable flexibility and convenience in designing their special structure. Moreover, combinatorial chemical synthesis offers a wide variety of methods for aptamer sequence modifications such as the terminal tagging chemical groups.

Biosensors based on aptamers as biorecognition elements have been coined aptasensors. The aptamers were initially used as therapeutic agents. For example, aptamer that selectively binds thrombin, a multifunctional serine protease that plays an important role in procoagulant and anticoagulant functions, was developed with the purpose of application as an anticoagulant [4]. Only recently, the aptamers have been used as recognition elements in biosensing. The first aptasensor was reported in 1996, with an optical biosensor based on fluorescently labeled aptamers [5]. To date, the best investigated aptamers are those for thrombin. The first electrochemical aptasensor with an amperometric sandwich-based biosensor based on glucose dehydrogenase-labeled signaling aptamers was described in 2004 [6]. The field of research is progressing so rapidly that new achievements have appeared, especially those focused on electrochemical methods of detection. Electrochemical devices have received considerable recent attention in connection to the transduction of aptamer interactions. Electrochemical transduction presents considerable advantages over optical, piezoelectric or thermal detection. The electrochemical detection offer high sensitivity and selectivity, compatibility with novel microfabrication technologies, inherent miniaturization, low cost, disposability, minimal simple-to-operate, robust, power requirements, and independence of sample turbidity. This paper examines electrochemical aptasensor discussing surface immobilization techniques and different detection schemes used to detect target analytes.

2. Immobilization of Aptamers

The crucial step in electrochemical aptasensors development is the immobilization of aptamers to an electrode surface, and it is important to develop strategies for reliable immobilization of aptamers so that they retain their biophysical characteristics and binding abilities, as well as for minimizing nonspecific binding/adsorption events. In principle these strategies are similar to those applied previously for the immobilization of single- or double-stranded DNA in genosensors or DNA biosensors for detection of DNA damage [7].

The methods of immobilization based on physical adsorption of DNA by means of electrostatic interactions are in general not suitable due to low stability caused by aptamers desorption from the surface. The common pathways for immobilizing a stable, flexible and repeatable aptamer layer surface are chemical covalent attachment, via avidin-to-biotin conjugation [8], and self-assembling the thiolated aptamer onto gold substrate using a thiol-alkane linked to the aptamer sequence [7]. streptavidin-polymer-coated indium-tin oxide electrode for immobilizing a DNA aptamer against lysozyme have been also designed.

Mixed two-component alkanethiol self assembly monolayers of recognition and shielding components, similar to those used in DNA hybridization sensors, are extremely attractive for achieving the desired balance between high loading, minimal nonspecific interactions, and preferred/accessible orientation. Such mixed coassembly monolayers have been widely used in DNA hybridization sensors and are being employed for the design of electrochemical aptasensors [9, 10]. Aptamers can be attached to the solid support at either the 5′-end or the 3′ end; both positions have been reported as being used for aptasensor development. However, there are very few studies looking at the effect of the two types of end attachment. Recent work suggests that it depends on the particular aptamer [11] although for biological targeting, it may be that the 3′ end is more suitable, since the 3′ end is the primary target for exonucleases, and thus, its coupling to the solid support would simultaneously confer resistance to nucleases.

It is also highly advantageous to explore the possibility of immobilization of aptamers onto novel materials, especially through the covalent linking approaches onto gold films/particles, silicates and silicon oxide surfaces, quantum dots, carbon fabricated nanotubes, and carbohydrates or dendrimers [12]. The advantage of dendrimers is their high stability and relatively large surface in comparison with flat electrode [13, 14]. An aptasensor based on a polyamidoamine dendrimer modified gold electrode was developed for the determination of thrombin. Amino-terminated polyamidoamine dendrimer was firstly covalently attached to the cysteine functionalized gold electrode through glutaraldehyde coupling. Subsequently, the dendrimer was activated with glutaraldehyde, and amino-modified thrombin aptamer probe was immobilized onto the activated dendrimer monolayer film. Poly(amidoamine) dendrimers were also used for aptamer immobilization [14], using glutaraldehyde for crosslinking of avidin to a dendrimer surface then immobilization of biotinylated aptamers.

Multiwalled carbon nanotubes (MWCNTs) were used as modifiers of screen-printed carbon electrotransducers (SPCEs) to immobilize 5′ amino linked aptamer sequence showed improved characteristics compared to the bare SPCEs [15].

The nanotubes were pretreated with carbodiimidazole-activated Tween 20 and 3-end of thrombin aptamer was modified by groups, which allowed covalent binding of thrombin aptamer [16] for detection of thrombin. single-walled carbon nanotubes SWCNTs allowed covalent attachment of the amino aptamers at the surface of field effect transistor [17] for effective detection of IgE. A Nafion-multiwalled carbon nanotubes coated electrode modified with electrochemical probe of methylene blue was designed [18], and gold-platinum alloy nanoparticles Au-PtNPs were electrodeposited onto the electrode surface for the immobilization of aptamer. For pathogen detection, an aptamer attached to an electrode coated with SWCNTs interacts selectively with bacteria [19] resulting highly accurate and

reproducible electrochemical response at ultralow bacteria concentrations.

The effect of aptamer structure and immobilization platform on the efficiency of thrombin characteristics was investigated with aptasensors based on glassy carbon electrodes covered with multiwalled carbon nanotubes (MWNTs) [20]. Aptamers with one or two binding sequences GGTTGGTGTGGTTGG specific for thrombin and poly(dA) and poly(dT) tags able to form dimeric products (aptabodies) were used to establish significance of steric and electrostatic factors in aptasensor performance. The electropolymerization of methylene blue onto MWNTs significantly improved electrochemical characteristics and sensitivity of thrombin detection against bare MWNTs. Amine-modified capture thrombin-binding aptamer probe (12-mer) was covalently conjugated to the MWCNTs-modified glassy carbon electrode (GCE) [21]. The target aptamer probe (21-mer) contains TBA (15-mer) labeled with ferrocene (Fc), which is designed to hybridize with capture probe and specifically recognize thrombin, is immobilized on the electrode surface by hybridization reaction.

Aptasensing layer-by-layer (LBL) strategy was developed for protein detection using self-assembled multilayers with ferrocene-appended poly(ethyleneimine) (Fc-PEI), carbon nanotubes (CNTs), and aptamer [22]. The Fc-PEI, CNTs, and DNA aptamer are LBL assembled on the electrode surface via electrostatic interaction. The single-walled carbon nanotube (SWNT) network-based biosensor using aptamers as a protein recognition site have been successfully demonstrated [23]. Aluminum was first patterned on the substrate with CVD-grown oxide. Then, gold was electrolessly plated on the Al electrodes and SWNTs were dip-coated on the substrate. Finally, aptamers were attached on the surface of SWNTs and were used as a recognition site for human serum albumin.

The biocatalytic growth of high-density gold agglomerates on a gold electrode surface to form a carrier for aptamer probe immobilization was described [24]. The approach provides a simple strategy to promote the seed-mediated deposition of Au from $AuCl_4$ onto surface-attached Au nanoparticles (AuNPs) in the presence of reductive coenzyme and surfactant. This nanostructured platform is effective and prospective toward the aptamer probe immobilization.

3. Electrochemical Aptasensors Detection Schemes

The electrochemical aptasensors can be divided into three broad classes depending on the assay format and the method of detection. These detection schemes will be reviewed. The first class of electrochemical aptasensors is sandwich- and competition-type assays. The electrochemical sandwich assays are reminiscent of the exceedingly well-established ELISA (enzyme-linked immunosorbent assay) approach, in which an electrode-bound aptamer is used to bring a complex composed of the target and some redox-active species to the electrode. Another commonly employed immunochemical approach is the competition or displacement assay in which unlabeled target molecules compete with exogenously added, redox-labeled target molecules for a limited number of binding sites on the sensing electrode. The second class of electrochemical aptasensors are based on detecting targets adsorbed to an aptamer-modified electrode surface using electrochemical impedance spectroscopy. The third class of electrochemical aptasensor involves the use of electrochemistry to monitor binding-specific conformational changes in an electrode-bound aptamer. This class of electrochemical aptasensors, for which no antibody-based analogue has been reported, appears to offer particular promise with regard to rapid, reagentless detection under realistically complex, real-time conditions. The approach is relatively insensitive to nonspecific binding of interferants and allows using them in complex sample matrices. Nevertheless, these systems present a limited application, whereas target binding-induced strand displacement appears as a more generalizable procedure. Sandwich structure strategy offers the advantages of high sensitivity and simple operation for biosensor fabrication when compared to the strategy by using only one recognition element to capture and label the target molecules. In a sandwich structured aptasensor, the target should have two or more recognition elements including aptamer, one is utilized as capturing element to be immobilized on electrode surface and catch target molecules, and the other one serves as probing element to marker the target with electroactive molecules or nanoparticles.

3.1. Sandwich or Competition (Displacement-) Type Electrochemical Detection. Sandwich or competition (displacement-) type electrochemical detection approaches have adapted by several groups. An electrochemical assay based on the aptamer and the signal of amplification of nanoparticles (NPs) was constructed for the determination of thrombin [25]. Aptamers immobilized on the electrode and AuNPs could be assembled with the target protein to form a sandwich structure. Differential pulse voltammetry was employed to detect the CdS NPs loaded on the surface of the Au NPs through the linker DNA, which was related to the concentration of the target protein. The assay took advantage of the amplification ability of Au nanoparticles carrying multiplex CdS NPs and the specific affinity of aptamers. Thrombin was detected in real samples with high sensitivity and good selectivity.

A sandwich structure detection model by using antibody as the capturing element, aptamer as the detecting element, and methylene blue as the electroactive marker intercalating into the aptamer bases was introduced [26]. An immobilization interface consisting of nanogold-chitosan composite film was used to improve the conductivity and performance characteristics of the electrode. The capturing antibody was linked to the glassy carbon electrodes modified with composite film via a linker of glutaraldehyde. Au nanoparticles as the electroactive labels tagged at probing aptamer was used to measure thrombin on a screen-printed carbon electrode using differential pulse voltammetry signal. The signal was further amplified by hybridizing the aptamer with its

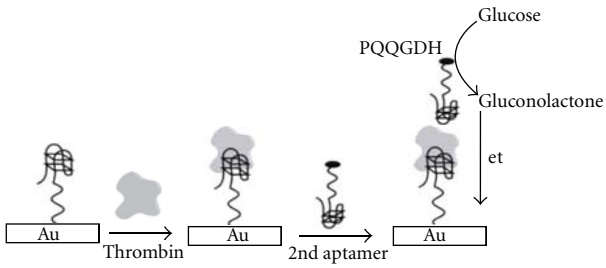

Figure 1: Sandwich assay: the immobilized aptamer captures thrombin and aptamer labeled with pyrroquinoline quinone glucose dehydrogenase ((PQQ)GDH) generates electrical current upon glucose addition.

complementary DNA, which was also labeled with gold nanoparticles [21]. Consequently, more gold nanoparticles were attached to each target protein, and thus, the signal was significantly enhanced.

A sandwich-type aptasensing system was constructed of two different aptamers which recognize different positions of thrombin (Figure 1) [6, 27]. One aptamer was immobilized onto the gold electrode for capturing thrombin onto the electrode and the other was used for detection. The aptamer for detection was labeled with pyrroquinoline quinone glucose dehydrogenase ((PQQ)GDH), and the electrical current, generated from glucose addition after the formation of the complex of thrombin, gold immobilized aptamer, and the (PQQ)GDH-labeled aptamer on the electrode, was measured. The increase of the electric current generated by (PQQ)GDH was observed in dependent manner of the concentration of thrombin.

A method utilized antibodies immobilized on the electrode surface to capture the protein target, the platelet-derived growth factor B-chain (PDGF-BB) as a model target, and the surface-captured protein was then sandwiched by an aptamer-primer complex was adapted for the detection of the amplified copies via enzymatic silver deposition then allowed enormous sensitivity enhancement in the assay of target protein [28].

A sensitive electrochemical aptasensor was successfully fabricated for the detection of adenosine triphosphate (ATP) by combining three-dimensionally ordered macroporous (3DOM) gold film and quantum dots (QDs) [29]. 5′-Thiolated ATP-binding aptamer (ABA) was first assembled onto the 3DOM gold film. Then, 5′-biotinated complementary strand (BCS) was immobilized via hybridization reaction to form the DNA/DNA duplex. The tertiary structure of the aptamer was stabilized in the presence of target ATP, the duplex can be denatured to liberate BCS. The reaction was monitored by electrochemical stripping analysis of dissolved QDs which were bound to the residual BCS through biotin-streptavidin system. The unique interconnected structure in 3DOM gold film along with the built-in preconcentration remarkably improved the sensitivity.

An ultrasensitive and highly specific electrochemical aptasensor for thrombin based on amplification of aptamer-gold nanoparticles-horseradish peroxidase (aptamer-AuNPs-HRP) conjugates was successfully developed [30]. In this electrochemical protocol, aptamer1 (Apt1) was immobilized on core/shell Fe_3O_4/Au magnetic nanoparticles (AuMNPs) and served as capture probe. Aptamer2 (Apt2) was dual labeled with AuNPs and HRP and used as detection probe. Remarkable signal amplification was realized by taking the advantage of AuNPs and catalytic reactions of HRP. The presence of proteins, such as human serum albumin, lysozyme, fibrinogen, and IgG did not show significant interference with the assay for thrombin.

An ultrasensitive aptasensor for the electronic monitoring of proteins through a dual amplified strategy was presented [31]. The target protein thrombin is sandwiched between an electrode surface confined aptamer and an aptamer-enzyme-carbon nanotube bioconjugate. The analytical signal amplification is achieved by coupling the signal amplification nature of multiple enzymes with the biocatalytic signal enhancement of redox recycling. This approach could be an attractive alternative to other common PCR-based signal amplification in ultralow level of protein detection.

A sandwich format of magnetic nanoparticle/thrombin/gold nanoparticle and thiocyanuric acid was presented for detection of thrombin [32]. An aptamer I was immobilized on the magnetic nanoparticles, aptamer II was labeled with gold nanoparticles. The magnetic nanoparticle was used for separation and collection, and gold nanoparticle offered excellent electrochemical signal transduction. The significant signal amplification was further implemented by forming network-like thiocyanuric acid/gold nanoparticles. The presence of other proteins such as BSA and lysozyme did not affect the detection of thrombin.

Electrochemical aptasensing of three configurations for thrombin detection was reported [33]. In the most straightforward configuration, the thrombin interaction with an aptamer selective for thrombin was detected electrochemically by the quantification of p-nitroaniline produced by the thrombin's enzymatic reaction [33]. Thrombin was also detected using an enzyme labeled sandwich format. Peroxidase-labeled thrombin was incubated with the aptamer and the interaction was measured electrochemically by detection of a diffusional mediator generated in a peroxidase catalyzed reaction (Figure 2). In a third strategy also employing an enzyme label, thrombin was immobilized on the sensor surface and incubated with a biotin labeled aptamer. The sensor was subsequently incubated with streptavidin-HRP (horseradish peroxidase), which bound to the biotin on the aptamer. The aptamer was again quantified by the electrochemical detection of a peroxidase catalyzed reaction. This strategy was applicable to competitive assays for detection of unlabeled thrombin.

Polsky and coworkers used platinum nanocrystals on the secondary aptamer as electrocatalysts to reduce hydrogen peroxide and transfer electrons directly from the electrode [34]. Using this approach, they report thrombin detection at 1 nM, which is more than 25-fold below the aptamer solution-phase dissociation constant.

A nanoporous gold- (NPG-) based electrochemical aptasensor for thrombin detection was developed [35]. The substrate electrode NPG was in situ fabricated by a facile

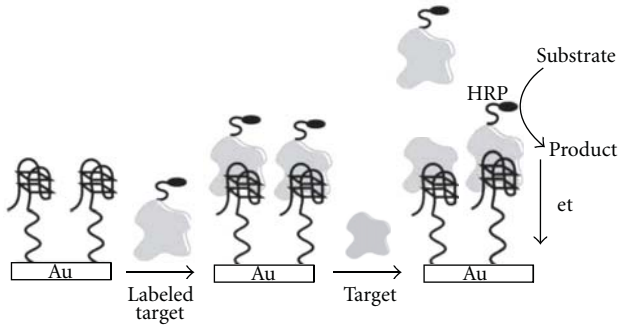

Figure 2: Competition (or displacement) assays: target molecules in a sample displace labeled-target molecules previously bound to the sensor surface.

one-step square wave potential pulse treatment. The electrochemical aptasensor was fabricated using a layer-by-layer assembling strategy. The sandwich structure was formed via thrombin connecting the aptamer-modified NPG and the aptamer-modified Au nanoparticles (AuNPs). The AuNPs was modified with two kinds of single-strand DNA (ssDNA). One was aptamer of thrombin, but the other was not, reducing the cross-reaction between thrombin and its aptamer on the same AuNP. The electrochemical signal produced by the $[Ru(NH_3)_6]^{+3}$ bound to ssDNA via electrostatic interaction was measured by chronocoulometry [36]. This NPG-based aptasensor also exhibited excellent sensitivity, due to the amplification effects of both NPG and AuNPs.

The advantages of aptamer, nanomaterial, and antibody to design an electrochemical sandwich immunoassay for the ultrasensitive detection of human immunoglobulin E (IgE) was combined by using methylene blue (MB) as electrochemical indicator [36]. The sandwich structure was fabricated by using goat antihuman IgE as capturing probe. Aptamer-Au nanoparticles (NPs) conjugates were used both as a sandwich amplification element as well as an accumulation reagent of MB. Once the aptamer-Au NPs conjugates specifically bind to electrode surface, MB molecules were accumulated on its surface by the specific interaction of MB with G base of aptamer-Au NPs conjugates. Therefore, with the increase of human IgE concentration, more aptamer-AuNPs conjugates were bound, and thus, more MB molecules were accumulated. This sensing system showed excellent specificity for the detection of human IgE against other proteins: BSA, human IgA, and human IgM.

An electrochemical detection based on enzymatic silver deposition has been proposed to detect thrombin [37]. The target protein, thrombin, was first captured by thrombin-binding thiolated aptamer self-assembled monolayers (SAMs) on the gold electrode surface and then sandwiched with another biotinylated thrombin-binding aptamer for the association of alkaline phosphatase (Av-ALP). The attached Av-ALP enzymatically converted the nonelectroactive substrate p-aminophenyl phosphate (p-APP) to p-aminophenol (p-AP) which could reduce silver ions in solution leading to deposition of the metal onto the electrode surface. Linear sweep voltammetry was used to detect the amount of deposited silver which reflected the amount of the target protein captured into the sandwich configuration.

A multifunctional electrochemical strategy based on a dual-aptamer for the detection of adenosine and thrombin in one-pot was developed, based on biobarcode amplification assay [38, 39]. The capture DNA aptamer I was immobilized on the Au electrode. The functional Au nanoparticles (DNA-AuNPs) were loaded with barcode-binding DNA and aptamer II. Through the specific recognition for thrombin, a sandwich format of Au/aptamerI/thrombin/DNA-AuNPs was fabricated. After hybridization with the PbSNPs-labeled barcode DNA, the assembled sensor was obtained. The concentration of thrombin was monitored based on the concentration of lead ions dissolved through differential pulse anodic stripping voltammetry.

A disposable electrochemical assay involving magnetic particles and carbon-based screen-printed electrodes (SPCEs) was developed for the detection of C-reactive protein (CRP) [40]. The assay was based on a sandwich format in which a RNA aptamer was coupled to a monoclonal antibody and alkaline phosphatase (AP) was used as enzymatic label. After the sandwich assay, the modified magnetic beads were captured by a magnet on the surface of a graphite working electrode and the electrochemical detection was thus achieved through the addition of the AP substrate (α-naphthyl-phosphate) and α-naphthol produced during the enzymatic reaction was detected using differential pulse voltammetry. The assay was applied to the analysis of CRP free serum and serum samples.

A sensitively amplified electrochemical aptasensor was designed for adenosine triphosphate (ATP) detection [41]. In the sensing process, duplexes consisting of partly complementary strand (PCS1), ATP aptamer (ABA), and another partly complementary strand (PCS2) were immobilized onto Au electrode through the 5′-HS on the PCS1. Meanwhile, PCS2 was grafted with the Au nanoparticles (AuNPs) to amplify the detection signals. In the absence of ATP, probe methylene blue (MB) bound to the DNA duplexes and also bound to guanine bases specifically to produce a strong differential pulse voltammetry signal. In the presence of ATP, the ABA-PCS2 or ABA-PCS1 part duplexes might be destroyed, which decreased the amount of MB on the electrode and led to obviously decreased DPV signal. Therefore, such PCS1-ABA-PCS2/AuNPs sensing system could provide a promising signal-amplified model for aptamer-based small-molecules detection.

The self-assembly of labeled aptamer subunits in the presence of their substrates provides a method for the fluorescence or electrochemical detection of the substrate [42]. For electrochemical detection of cocaine, the thiolated aptamer subunit is assembled on an Au electrode. The methylene blue-labeled subunit binds to the surface-confined fragment in the presence of cocaine. The amperometric response of the system allows the detection of cocaine.

An aptamer-based sandwich assay with electrochemical detection for thrombin analysis was proposed using Au nanoparticles [43]. The primary aptamer was immobilized on the surface of a screen-printed carbon electrode (SPCE) and

the secondary aptamer was immobilized on Au nanoparticles. The electrochemical reduction current response of Au nanoparticles was monitored for the quantitative detection of thrombin. The effect of interfering proteins such as bovine serum albumin (BSA) was investigated. Control experiments also involved the use of an aptamer that has a binding affinity to immunoglobulin E (IgE).

An electrochemical method for the detection of thrombin based on a gold-nanoparticles sensing platform and usage of stripping voltammetry technique was developed [44]. The aptamer was immobilized on a screen-printed electrode modified with gold-nanoparticles by avidin-biotin technology. The oxidation of gold surface resulted in gold oxide formation upon polarization served as a basis for analytical response. The cathodic peak area was found proportional to thrombin quantity specifically adsorbed onto electrode surface. Binding of thrombin to an aptamer has also been detected using the ferricyanide/ferrocyanide redox couple as electrochemical indicator.

The Au nanoparticles-doped conducting polymer nanorods electrodes (AuNPs/CPNEs) were prepared by coating Au nanorods (AuNRs) with a conducting polymer layer [45]. The AuNRs were prepared through an electroless deposition method using the polycarbonate membrane as a template. The AuNPs/CPNEs combining catalytic activity of ferrocene to ascorbic acid were used for the fabrication of an ultrasensitive aptamer sensor for thrombin detection. Sandwiched immunoassay for r-human thrombin with NH_2-functionalized-thrombin-binding aptamer (Apt) immobilized on AuNPs/3D-CPNEs was studied through the electrocatalytic oxidation of ascorbic acid by the ferrocene moiety that was bound with an antithrombin antibody and attached with the Apt/3D-CPNEs probe through target binding. The selectivity and the stability of the proposed thrombin aptamer sensor were excellent, and it was tested in a real human serum sample for the detection of spiked concentrations of thrombin.

A simple electrochemical approach for the detection of thrombin, using aptamer-gold nanoparticles-modified electrodes was presented [46]. 1,6-Hexanedithiol was used as the medium to link Au nanoparticles to a bare gold electrode. Anti-thrombin aptamers were immobilized on the gold nanoparticles surfaces by self-assembly. The use of gold nanoparticles results in significant signal enhancement for subsequent detection. The total amount of aptamer probes immobilized on the gold nanoparticle surface is six-fold higher than that on the bare electrode, leading to increased sensitivity of the aptasensor.

The electrochemical thrombin detection system was developed using two different aptamers recognizing different parts of the protein in sandwich manner [47]. Aptamer 1-thrombin-ap2 glucose dehydrogenase complex was formed in the presence of thrombin, and a response current of the enzyme label was obtained.

An ultrasensitive label-free bioelectrochemical method for rapid determination of thrombin has been developed by directly detecting the redox activity of adenine (A) nucleobases of anti-thrombin aptamer using a pyrolytic graphite electrode [48]. The bioelectrochemical protocol involves a sandwich format Thrombin, captured by immobilized anti-thrombin antibody on microtiter plates, and was detected by anti-thrombin aptamer-Au nanoparticle biobarcodes. The adenine nucleobases were released by acid or nuclease from Au nanoparticles bound on microtiter plates. Differential pulse voltammetry was employed to investigate the electrochemical behaviors of the purine nucleobases based on the well-defined adenine signal. There was substantial amplification and thrombin can be detected at a very low level of detection as the nanoparticle carries a large number of aptamers per thrombin binding event. This method has been used to detect thrombin in complex matrix such as fetal calf serum with minimum background interference.

A method for the determination of platelet-derived growth factor BB (PDGF-BB) was developed using an electrochemical immunosensor with an aptamer-primed, long-strand circular detection probe [49]. Rabbit antihuman PDGF-B polyclonal antibody was immobilized on the electrode to serve as the capture antibody. The detection probe was synthesized via polymerase extension along a single-stranded circular plasmid DNA template with a primer headed by the anti-PDGF-B aptamer. In the presence of the analyte, the aptamer-primed circular probe was captured on the electrode via the formation of an antibody/PDGF-BB/aptamer sandwiched complex. The electroactivity indicator methylene blue was adsorbed on the electrode surface via the analyte-sandwiched complex with long-strand circular DNA, thus yielding a strong oxidation peak current of methylene blue in square wave voltammetric signal for the quantification of PDGF-BB. This strategy allowed electrochemical detection with enormous signal amplification arising from the long-strand localized circular probe.

Immense effort has been placed on the realization of immunoassays exploiting displacement of redox-labeled target molecules, due to the ease of use and applicability to immunochromatographic strips and immunosensors. Most of the efforts reported to date focus on the use of a redox-labeled target molecules target that is displaceable by the unlabeled target molecules toward which the antibody has higher affinity. Limited success has been achieved due to difficulty in obtaining redox-labeled target molecules targets to which the antibody has enough affinity to bind while at the same time having lower levels of affinity in comparison to the unlabeled target molecules to facilitate displacement. Aptamers, in contrast to antibodies, require the formation of a three-dimensional structure for target binding and can, thus, be anticipated to have a much higher affinity for binding its target rather than a modified form of the target (e.g., redox-labeled target). This phenomenon can be exploited for the development of a displacement assay, using enzyme-labeled target as a displaceable molecule.

In the first, Baldrich et al. measured thrombin at concentrations down to 5 nM via competition between horseradish peroxidase (HRP) modified thrombin and unlabeled target molecules in the sample [50].

The coupling of aptamers with the coding and amplification features of inorganic nanocrystals offer a highly sensitive and selective simultaneous bioelectronic detection of several

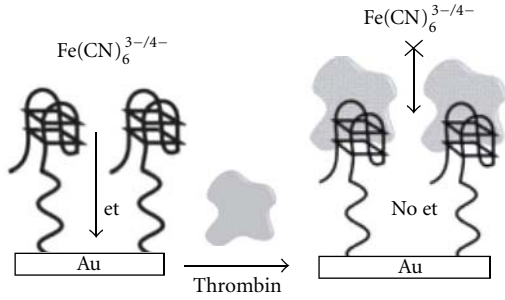

Figure 3: Impedimetric aptasensor: the binding of a target to the aptamer reduces the electron transfer (et) of a small redox mediator diffusing to the electrode surface and the increase the interfacial resistance, which provides a means of measuring the concentration of bound target via impedance spectroscopy.

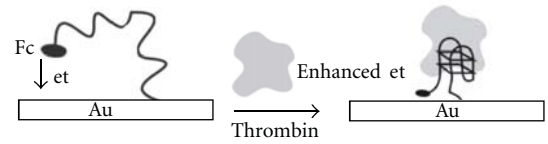

Figure 4: Electrochemical aptasensor based on the binding-induced folding of aptamers. In the absence of thrombin, the aptamer is largely unfolded, allowing for frequent collisions between the terminal redox moiety and the electrode. Upon target binding, the aptamer folds, enhancing electron transfer and producing a signal-on aptasensor.

protein targets [51]. This is accomplished in a single-step displacement assay in connection to a self-assembled monolayer of several thiolated aptamers conjugated to proteins carrying different inorganic nanocrystals. Electrochemical stripping detection of the nondisplaced nanocrystal tracers results in a remarkably low detection limit, that is, significantly lower than those of existing aptamer biosensors. The new device offers great promise for measuring a large panel of disease markers present at ultralow levels during early stages of the disease progress.

A modified RNA-aptasensor for the detection of small molecules in biological samples was presented [52]. A competitive displacement assay was applied to the detection of aminoglycoside neomycin B in whole milk using a fully 2′-O-methylated RNA aptamer with faradaic impedance spectroscopic detection. Neomycin B in solution displaces the aptamer from its complex with the SAM-immobilized neomycin B. The reusable aptasensor is capable of discriminating neomycin B from paromomycin, which differs from it in the substitution of a single amine group with a hydroxyl one. The modified endonuclease-resistant RNA aptamer maintains the exquisite selectivity of the natural aptamer and allows the examination of biological samples of high protein content.

3.2. Label-Free Impedance Spectroscopy Detection. The advantages and the limitations of using label-free detection strategies have been highlighted [53]. An impedimetric aptasensor using a mixed self-assembled monolayer composed of thiol-modified thrombin binding aptamer and 2-mercaptoethanol on a gold electrode is reported for thrombin detection [54]. The changes of interfacial features of the electrode were probed in the presence of the reversible redox couple, Fe(CN)$_6^{3-/4-}$, using impedance measurements. The electrode surface was partially blocked due to the self-assembly of aptamer or the formation of the aptamer-thrombin complex, resulting in an increase of the interfacial electron-transfer resistance detected by electrochemical impedance spectroscopy or cyclic voltammetry (Figure 3).

An electrochemical impedance spectroscopy method aptamer-based array consisting of single-stranded DNA containing a hairpin loop, was reported for detection of Human IgE. [55]. The binding of aptamers immobilized on gold electrodes leads to impedance changes associated with target protein binding events. A hybrid modified layer containing aptamers and cysteamine was fabricated on the photolithographic gold surface through molecular self-assembly, to increase the binding efficiency for proteins. Human IgE could be specifically captured by the aptamer and stand well above the self-assembled monolayer (SlAM) surface. The impedance spectroscopy detection provided higher sensitivity and better selectivity for aptamer-modified electrodes.

An aptamer-based biosensing assay for label-free thrombin detection and quantification by measuring the change in electrochemical impedance upon thrombin-aptamer complex formation was demonstrated [56]. A self-assembly of the DNA aptamer on a microfabricated thin film gold electrode, followed by the recognition of the protein binding event via monitoring the interfacial electron transfer resistance with electrochemical impedance spectroscopy.

A bifunctional derivative of the thrombin-binding aptamer with a redox-active ferrocene (Fc) moiety and a thiol group at the termini of the aptamer strand was synthesized [57]. The ferrocene-labeled aptamer thiol was self-assembled through S-Au bonding on a polycrystalline gold electrode surface. The aptamer-modified electrode was characterized electrochemically by cyclic voltammetry, differential pulse voltammetry, and electrochemical impedance spectroscopy. The modified electrode showed a voltammetric signal due to a one-step redox reaction of the surface-confined ferrocenyl moiety of the aptamer immobilized on the electrode surface. The impedance measurement, in agreement with the differential pulse voltammetry, showed decreased faradaic resistances in the same sequence. The "signal-on" upon thrombin association could be attributed to a change in conformation from random coil-like configuration on the probe-modified film to the quadruplex structure. The Fc oxidation signal increased in the thrombin concentration (Figure 4). The molecular beacon aptasensor was amenable to full regeneration and could be regenerated 25 times with no loss in electrochemical signal upon subsequent thrombin binding.

Different model systems, such as thrombin-antithrombin antibody, and Rev-peptide—anti-Rev aptamer were presented. In order to improve the signal-to-noise ratio, the use of reference sensors has been explored. The interaction of prostate specific antigen (PSA) to an anti-PSA antibody was shown to demonstrate the detection at concentrations as low as 10 nM.

An aptamer immobilization method based on electrically addressed fabrication has been developed for the preparation of aptamer-modified arrayed electrodes, by which the human IgE aptamer was oriented and immobilized on the gold electrode surface [58]. The optimization of the experimental conditions including the applied potential, time, and scan rate of potential was investigated. The method was successfully used to immobilize the aptamer onto the desired electrodes, pixel by pixel, based on the electrically addressed approach. Compared to the control electrodes, the resulting aptamer-modified electrodes showed their specific recognition for human IgE. The method owns several advantages such as rapid and simple immobilization as well as its automatic addressed capability by the electric approach.

A label-free electrochemical impedance aptasensing protocol utilizes the affinity interaction between the thrombin and the self-assembled DNA aptamer on gold electrode [59]. The specific interaction increases the electrode interfacial electronic transfer resistance. The resistance signal is then amplified by using guanidine hydrochloride to denature the captured thrombin for increasing the hydrated radius of the thrombin, consequently blocking the electron transfer from solution to electrode.

A label free, reagentless aptasensor for adenosine was developed on an ISFET device. The separation of an aptamer/nucleic acid duplex by adenosine led to the aptamer/adenosine complex that altered the gate potential of the ISFET [60]. The immobilization of the aptamer/nucleic acid duplex on an Au-electrode and the separation of the duplex by adenosine monophosphate (AMP) enabled the electrochemical detection of adenosine by faradaic impedance spectroscopy. The separation of the aptamer/nucleic acid duplex by adenosine and the formation of the aptamer/adenosine complex resulted in a decrease in the interfacial electron-transfer resistance in the presence of $[Fe(CN)_6]^{3-/4-}$ as redox active substrate.

An electrochemical biosensor utilizing pyrolyzed carbon as a working electrode for the aptamer-based thrombin detection was presented [61]. Electron transfer resistance changes due to thrombin binding onto the carbon surface modified with thrombin aptamer were measured using electrochemical impedance spectroscopy techniques.

A biosensor applying aptamer as probe and nonfaradic electrochemical impedance spectroscopy as the detection method for neuroinflammatory cytokines has been developed [62]. Platelet-derived growth factor BB (PDGF-BB), one of the important cytokines involved in neural inflammation has been selected as a detection target. Binding of PDGF to its aptamer immobilized on the silicon electrode surface leads to a decrease in capacitance measured by nonfaradic electrochemical impedance spectroscopy. The online measurement result exhibited negligible response for nonspecific adsorption but significant signal changes for the specific target. The biosensor design was promising for in vivo monitoring, as the nonfaradic strategy did not require any reagent to be loaded when performing the test, together with the ability of online measurements.

An impedance-sensor with two different geometries have been compared for the detection of Rev peptides with a molecular weight of 2.4 kDa [63]. Planar, two-dimensional interdigitated capacitor (IDC) sensors as well as three-dimensional nanogap sensors have been used. The specific interaction of the Rev peptide to an immobilized RNA anti-Rev aptamer (9.2 kDa) was detected for peptide concentrations in the range of $100\,nM^{-2}\,\mu M$. For the IDC sensor, only peptide concentrations above 500 nM gave detectable signals. For the nanogap sensor, the binding process was clearly visible for all concentrations applied. The higher sensitivity of the nanogap compared to the IDC is ascribed to the improved surface-to-volume ratio. [64]

A label-free aptasensor of mixed self-assembled monolayers (SAMs) composed of a thiol-modified PDGF binding aptamer and 6-mercaptohexanol (MCH) on a gold electrode [65] for platelet-derived growth factor (PDGF) protein was reported [65]. The SAMs were characterized by cyclic voltammetry (CV), electrochemical impedance spectroscopy (EIS), and differential pulse voltammetry (DPV) before and after binding of the protein using $[Fe(CN)_6]^{3-/4-}$, a redox marker ion as an indicator for the formation of a protein-aptamer complex. The electron transfer resistance). R_{et} was used to monitor the binding of the target protein. The results showed that without any modification to the aptamer, the target protein can be recognized effectively at the PDGF-binding aptamer SAMs at the electrode surface. Control experiments using nonbinding oligonucleotides assembled at the electrode surfaces showed that there was no formation of an aptamer-protein complex. The DPV signal at the aptamer functionalized electrode showed a linearly decreased marker ion peak current in presence of target protein. Thus, label-free detection of PDGF protein at an aptamer modified electrode has been demonstrated.

A bifunctional aptamer that includes two aptamer units for cocaine and adenosine 5′-monophosphate (AMP) was blocked by a nucleic acid to form a hybrid structure with two duplex regions [66]. The displacement of the aptamer by any of the substrates alters the interfacial electron transfer resistance at the electrode surface, thus providing an electronic signal for the sensing process.

Label-free electrical detection of a panel of peptide aptamers that recognise specific protein partners of the cyclin-dependent kinase (CDK) family interactions has been achieved by direct measurement of variations at open circuit potential (OCP) using an accurate differential voltage measurement [67]. Different peptide aptamers immobilized on gold electrodes were used for the detection of human CDK2 and CDK4. The interaction of the peptide aptamers with CDK proteins was successfully detected by direct OCP measurements. Variations in charge transfer resistance and in protein/double-layer capacitance were investigated by means of electrochemical impedance spectroscopy with charged redox markers in solution. The electrical detection of protein interactions could be achieved by direct measurement of OCP variations using suitable differential voltage instrumentation.

An electrochemical impedance biosensor utilizing pyrolyzed carbon film for aptamer-based thrombin detection was presented [68]. Thrombin aptamer was grafted onto the pyrolyzed carbon surface using carbodiimide-mediated

chemistry, followed by Triton-X 100 and BSA treatment to reduce nonspecific binding of thrombin. Electron-transfer resistance changes due to thrombin binding onto the carbon surface were measured, using electrochemical impedance spectroscopy. Pyrolyzed carbon can provide a new approach for miniaturization, integration, and low-cost fabrication in electrochemical biosensors.

GNPs electrodeposited on GCE used as a platform for the immobilization of the thiolated aptamer can improve the sensitivity of an EIS biosensor for the determination of thrombin [69]. In the measurement of thrombin, the change in interfacial electron transfer resistance of the biosensor using a redox couple of $[Fe(CN)_6]^{3-/4-}$ as the probe was monitored. The association and dissociation constants of three different immobilized aptamers binding with thrombin were measured and the difference of the dissociation constants obtained was discussed.

Electrochemical protein biosensors using aptamers probe doped in polypyrrole and subsequent electrochemical impedance spectroscopy have been successfully developed [70, 71]. Two targets, platelet-derived growth factor and immunoglobulin E, have been also tested [70]. A sensitive and real-time biosensor for inflammatory cytokine detection has been successfully measured in both offline ElS characterization and real-time impedance monitoring [71].

An aptamer-based sensor development, utilizing a model system of human alpha thrombin interacting with a thiolated DNA aptamer, immobilized on gold electrodes [72]. EIS measurements took place in the presence of iron ferrocyanides.

A simple and highly sensitive electrochemical impedance spectroscopy (EIS) biosensor based on nano-MnO_2 as a platform for the immobilization of the aptamer was developed for the determination of adenosine [73]. In the measurement of adenosine, the change in interfacial electron transfer resistance (R_{et}) of the biosensor using a redox couple of $[Fe(CN)_6]^{3/4}$ as the probe was monitored. The sensor was shown to exhibit high sensitivity, desirable selectivity and good stability.

An impedimetric electrochemical biosensor was developed for the label-free and selective detection of leukemia cells based on aptamer-modified gold electrode using electrochemical impedance spectroscopy (EIS) technique [74]. The thiol-terminated aptamer selected for acute leukemia cells was self-assembled onto the gold electrode surface as recognition probe, which was characterized by cyclic voltammetry (CV) and EIS using $Fe(CN)_6^{3-/4-}$ as a redox probe. The electron-transfer resistance R_{et} of $[Fe(CN)_6]^{3-/4-}$ on the sensor surface increased substantially upon incubation of aptamer-modified electrode in cell solution. The work provided a simple, convenient, low-cost, and label-free method for early leukemia diagnosis.

A label-free and sensitive faradic impedance spectroscopy (FIS) aptasensor based on target-induced aptamer displacement was developed for the determination of lysozyme [75]. The aptasensor was fabricated by self-assembling the partial complementary single-strand DNA (pcDNA)-lysozyme binding aptamer (LBA) duplex on the surface of a gold electrode. The introduction of target lysozyme induced the displacement of the LBA from the pcDNA-LBA duplex on the electrode into the solution, decreasing the electron transfer resistance of the aptasensor. The fabricated aptasensor shows a high sensitivity, good selectivity, and satisfactory regeneration. This work demonstrates that a high sensitivity of the fabricated aptasensor can be obtained using a relatively short pcDNA.

Faradaic impedance spectroscopy and ion-sensitive field-effect transistor (ISFET) were applied to sense aptamer-substrate complexes [76]. The methods utilized anticocaine aptamer fragments that self-assembled, in the presence of cocaine, to a supramolecular aptamer fragments/cocaine complex on the electrode surface or ISFET gate. One of the aptamer fragments is assembled on a Au electrode or the ISFET gate. The second thiolated aptamer fragment is used to modify Au NPs that are used as amplifying labels for the two detection schemes. The impedimetric and ISFET methods enabled the analysis of cocaine.

A protein assay method based on a DNA array was developed in which human immunoglobulin E (hIgE) and its DNA aptamer were used as an analytical model [77]. The target protein hIgE was captured by the aptamer in homogeneous solution and then the resulting hIgE-aptamer complex was hybridized onto probes self-assembled on the DNA array. The charge transfer resistance (R_{ct}) of electrodes before and after hybridization were measured by electrochemical impedance spectroscopy (EIS). To test the selectivity of the method, four different probes with one-to-three mismatched bases were immobilized on respective electrodes. The results showed that the complex could be hybridized and detected out on the electrodes modified with the fully complementary sequences. In addition, the DNA array could be employed to analyze multiple samples selectively with the matched aptamer.

A reusable label-free electrochemical nucleic acid aptasensor for the determination of cocaine by the immobilization of thiolated self-assembled DNA sequences on a gold nanoparticles-modified electrode was constructed [78]. When cocaine was complexed specifically to the aptamer, the configuration of the nucleic acid aptamer switched to a locked structure and the interface of the biosensor changed, resulting in a variation of the corresponding peak current of an electrochemical probe ($[Fe(CN)_6]^{3-/4}$ as monitored by cyclic voltammetry and electrochemical impedance spectroscopy (EIS).

A sensitive aptamer-based electrochemical biosensor to detect human immunoglobulin E (IgE) was designed [79]. 5′ Biotin labeled 45 mer DNA aptamer sequence was immobilized onto streptavidin coated graphite surfaces. Interaction between human IgE and DNA aptamer was monitored by electrochemical impedance spectrometry.

A multispecific electrochemical array with eight individually addressable gold working electrodes for rapid biosensing of 2.7 kb-long target Yersinia pestis DNA and for protein sensing of ricin toxin chain A (RTA) in the presence of redox agent were designed [80]. The array allowed to incorporate multiple negative controls in the course of a single binding experiment as well as to perform parallel identical

experiments to improve reliability of detection. Eight individual EIS measurements were completed in 15 min. The array is disposable, economical, and easy to use.

A dual RNA/peptide aptamer probe for simultaneous detection of PSMA (+) and PSMA (−) prostate cancer cells using electrochemical impedance spectroscopy was reported [81]. This approach can be applied as a general tool for early diagnosis of prostate cancer.

Aptamer-based capacitive label-free biosensors for monitoring aptamer-protein recognition events, based on charge distribution under the applied frequency by nonfaradaic impedance spectroscopy (NFIS) was reported [82, 83]. The biosensors based on gold interdigitated (GID) capacitor arrays functionalized with synthetic RNA aptamers. The RNA aptamers served as biorecognition elements for C-reactive protein (CRP). The signal is generated as a result of the change in relative capacitance occurring as a result of the formation of an RNA-CRP complex on GID capacitors. The RNA-protein complex on GID capacitors could be extended to the development of electrical biosensor systems for the early diagnosis.

Two modified aptamers, a partially (ATA) and a fully O-methylated aptamer (FATA), were proposed as recognition elements for the detection of tobramycin at therapeutic range in human serum [84]. A displacement assay was developed using faradaic electrochemical impedance spectroscopy (F-EIS) as a detection technique. The affinity constant, KDb, for both aptamers was estimated, and the selectivity towards other aminoglycosides was also tested.

Lysozyme has been detected selectively in a mixture containing a large excess of six proteins and amino acids (both electroactive and nonelectroactive) by combining aptamer-coated magnetic beads and chronopotentiometric stripping measurements of the captured protein (in connection to the intrinsic electroactivity of the protein) [85]. The protein measurement by adsorptive chronopotentiometric based on scanning the guanine bases of the guanine-rich secondary aptamer. When involving PCR reaction to amplify these guanine bases, fM level of detection limit has been obtained. The approach has also been employed for electrochemically investigating amino acid amides by using guanine-rich DNA aptamer as the electroactive marker.

The effect of aptamer structure and immobilization platform on the efficiency of thrombin binding and its detection using electrochemical impedance spectroscopy (EIS) characteristics was investigated with aptasensors based on glassy carbon electrodes covered with multiwalled carbon nanotubes (MWNTs) [86]. Aptamers with one or two binding sequences GGTTGGTGTGGTTGG specific for thrombin and poly(dA) and poly(dT) tags able to form dimeric products (aptabodies) were used to establish significance of steric and electrostatic factors in aptasensor performance. The electropolymerization of methylene blue onto MWNTs significantly improved electrochemical characteristics and sensitivity of thrombin detection against bare MWNTs.

The biosensors based on DNA aptamers immobilized by electrostatic adsorption onto electropolymerized methylene Green imprinted with DNA have been developed and examined for thrombin detection using electrochemical impedance spectroscopy and potentiometry [87]. The addition of DNA at the electropolymerization stage followed by acidic treatment of the coating significantly improved the efficiency of electrostatic adsorption of the DNA aptamer and provided sensitive detection of thrombin.

An amperometric aptasensor based on DNA aptamers immobilized by avidin-biotin method or by electrostatic adsorption onto multiwalled carbon nanotube layer contained methylene blue have been developed and examined for thrombin detection in buffer and in spiked blood serum [88]. The presence of MB increases the binding capacity of the surface layer and enhances the range of thrombin concentrations to be determined.

An artificial receptor formed by hybridization of two DNA aptamers for human thrombin (aptabody) was reported [89]. The aptasensor based on multiwalled carbon nanotubes allowed to detect thrombin with detection limit, 3 times better in comparison with conventional aptamer.

A potentiometric detection of DNA-protein interactions has been proposed [90]. The polymeric phenothiazine dyes, methylene blue and methylene green, were electrochemically deposited onto the glassy carbon electrode and covered with double stranded DNA (dsDNA) as a target for antibodies (DNA sensor) or DNA aptamer specific to human α-thrombin. The developed potentiometric biosensors can be used for preliminary diagnostics of autoimmune diseases and thrombin detection with sensitivity comparable to traditional methods.

Electrochemical indicator methylene blue and differential pulse voltammetry allowed to determine charge transfer from electrode surface to the thrombin bounded on a DNA aptamer with high selectivity in comparison with nonspecific binding caused by human IgG or human serum albumin [91]. The method of detection thrombin-aptamer interaction based on measurement the charge consumption from the electrode covered by DNA aptamers to an electrochemical indicator methylene blue (MB), which is bounded to a thrombin.

An electrochemical sensor to detect interferon (IFN)-γ, a selective marker for tuberculosis pleurisy, using its RNA or DNA 5′-thiol-modified aptamer probe immobilized on the gold electrode [92]. Interaction between IFN-γ and the aptamer was recorded using electrochemical impedance spectroscopy. IFN-γ was detected in fetal bovine serum, a mimicked biological system, which has similar components to pleural fluid.

A multifunctional reusable label-free electrochemical biosensor based on an integrated aptamer for parallel detection of adenosine triphosphate (ATP) and α-thrombin, by using electrochemical impedance spectroscopy (EIS) and cyclic voltammetry (CV), was reported [93]. Au electrode as the sensing surface was modified with a part DNA duplex which contained a 5′-thiolated partly complementary strand (PCS) and a mixed aptamer (MBA). The unimolecular MBA contained small-molecule ATP-binding aptamer (ABA) and also protein α-thrombin binding aptamer (TBA). Thus, the aptasensor could be used for detection of ATP and α-thrombin. The aptasensor held several advantages such

as label-free detection, high sensitivity, regeneration, multifunctional recognition, and sensing ability such as the simultaneous detection for multianalysis.

A sandwich system of aptamer/thrombin/aptamer-functionalized Au nanoparticles (Apt-AuNPs) was fabricated as the sensing platform [94]. The change of the interfacial feature of the electrode was characterized by electrochemical impedance analysis with the redox probe $[Fe(CN)_6]^{3-/4-}$. The three-level cascaded impedimetric signal amplification was developed: Apt-AuNPs as the first-level signal enhancer, the steric-hindrance between the enlarged Apt-AuNPs as the second-level signal amplification, the electrostatic-repulsion between sodium dodecylsulfate (SDS) stabilized Apt-AuNPs, and the redox probe $[Fe(CN)_6]^{3-/4-}$ as the third-level signal amplification. The aptasensor based on the enlargement of negatively charged Apt-AuNPs showed an increased response of the electron-transfer resistance to the increase of thrombin concentration.

A sandwich sensing platform was fabricated, in which the thiolated aptamers are firstly immobilized on a gold substrate to capture the thrombin molecules, and then, the aptamer functionalized Au nanoparticles (AuNPs) are used to amplify the impedimetric signals [95]. Such designed aptamer/thrombin/AuNPs sensing system could not only improve the detection sensitivity compared to the reported impedimetric aptasensors but also provide a promising signal amplified model for aptamer-based protein detection.

A label-free electrochemical aptasensor based on direct immobilization of the redox probes on an electrode surface was reported [96]. The gold electrode coated Nafion was firstly modified with redox probe-thionine (Thi) through ion exchange adsorption. Then, negatively charged nano-Au and positively charged Thi were layer-by-layer (LBL) self-assembled onto the modified electrode surface, which formed multilayer films for improving the amount of redox probes and immobilizing thiolated thrombin aptamers (TBA). In the presence of target thrombin (TB), the TBA on the multilayer film could catch the TB onto the electrode surface, which resulted in a barrier for electrontransfer, leading to decrease of the current. The method avoided the cubosome redox probe labeling process, increased the amount of redox probe, and reduced the distance between the redox probe and electrode surface.

A label-free electrochemical impedimetric aptasensor based on an anti-lysozyme-aptamer as a molecular recognition element, was developed for the detection of lysozyme [97]. Improvement in sensitivity was achieved by utilizing gold nanoparticles (AuNPs), which were electrodeposited onto the surface of a gold electrode, as a platform for immobilization of the aptamer. To quantify the amount of lysozyme, changes in the interfacial electron transfer resistance (R_{et}) of the aptasensor were monitored using the redox couple of an $[Fe(CN)_6]^{3-/4-}$ probe. The aptasensor also showed good selectivity for lysozyme without being affected by the presence of other proteins.

A reusable aptamer-based impedimetric biosensor using Amino-terminated IgE aptamers were covalently attached to carboxyl-modified a a nanocrystalline diamond (NCD) film using carbodiimide chemistry for detection of human immunoglobulin E (IgE) [98]. The formation of aptamer-IgE complexes caused a significant change in the capacitance of the double-layer, in good correspondence with the IgE concentration. The NCD-based aptasensor was demonstrated to be highly selective even in the presence of a large excess of IgG.

3.3. Aptasensors Exploiting Conformational Changes in Aptamers. A classic biosensor directly transduces ligand-target binding events into a measurable physical readout. More recently, researchers have proposed novel biosensing strategies that couple ligand-induced structural switching of biomolecules with advanced electronic transducers [99]. This approach has proven to be a highly general platform for the development of new biosensors. In this account, a series of electrochemical nucleic acid sensors that use target-responsive DNA structures, employing surface-confined DNA structures with appropriate redox labels, which can monitor target-induced structural switching of DNA or aptamer-specific small molecule probes by measuring electrochemical currents that are directly associated with the distance between the redox label and the electrode surface.

An electrochemical biosensor for single-step detection of a homodimer protein PDGF-BB based on proximity-dependent surface hybridization assay was built up [99]. The strategy relied on simultaneous recognition of a target molecule by a pair of affinity probes, which was a prerequisite for efficiently promoting the ferrocene-labeled tail sequences of the proximate affinity probe pair to hybridize together with surface-tethered oligonucleotide, thus triggering the redox current of ferrocene at the electrode. The strategy, as a universal methodology for developing high-performance biosensors, was demonstrated using an aptamer probe to a homodimer protein PDGF-BB, and the aptasensor showed intrinsic high sensitivity, excellent resistance to nonspecific interferences, and ready reusability.

An ultrasensitive, reagentless, target label-free electrochemical aptasensor for thrombin detection was constructed [100]. The aptasensor was based on a chronoamperometric beacon system for biomolecular recognition. The ferrocene-labeled aptamer adopts a 3D conformational change when interacted with thrombin. Thus, the ferrocene label was approached to the microperoxise-11 (MP-11) attached on the electrode surface. The thrombin-aptamer interaction was detected via a microperoxidase mediated electron transfer between the ferrocene and the surface.

An electrochemical DNA aptamer-based biosensor for detection of interferon (IFN)-γ was described [101]. A DNA hairpin containing IFN-γ-binding aptamer was thiolated, conjugated with methylene blue (MB) redox tag, and immobilized on a gold electrode by self-assembly. Binding of IFN-γ caused the aptamer hairpin to unfold, pushing MB redox molecules away from the electrode and decreasing electron-transfer efficiency. The change in redox current was quantified using square wave voltammetry (SWV) and was found to be highly sensitive to IFN-γ concentration. The

aptasensor was specific to IFN-γ in the presence of overabundant serum proteins. The aptasensor could be regenerated by disrupting aptamer-IFN-γ complex in urea buffer and reused multiple times.

A signal on electrochemical sensing strategy for the simultaneous detection of adenosine and thrombin is developed based on switching structures of aptamers [102]. An Au electrode as the sensing surface is modified with two kinds of thiolated capture probes complementary to the linker DNA that contains either an adenosine aptamer or thrombin aptamer. The capture probes hybridize with their corresponding linker DNA, which has prehybridized with the reporter DNA loaded onto the gold nanoparticles (AuNPs). The AuNP contained two kinds of biobarcode DNA: one is complementary to the linker DNA (reporter), whereas the other is not (signal) and is tagged with different metal sulfide nanoparticles. The aptamer parts bind with their targets and fold to form the complex structures. As a result, the biobarcoded AuNPs are released into solution. The metal sulfide nanoparticles are measured by anodic stripping voltammetry.

A signal-on, reagentless target-responsive electrochemical aptamer switch (TREAS) for the development of aptamer-based biosensors for adenosine triphosphate ATP detection was designed [103]. The aptamer oligonucleotide dually labeled with thiol and ferrocene groups is hybridized with its complementary strand, and the thiolated duplex is self-assembled on a gold electrode. This duplex is responsive to the target ATP, which liberates the complementary strand and forms the aptamer-target complex. The electroactive ferrocene moiety, which is distal to the electrode surface in the absence of ATP, is moved to the proximal position during the binding-induced structural transition. This binding turns on the electron transfer and leads to measurable electrochemical signals for quantification of ATP.

A sensitive, label-free electrochemical aptasensor for adenosine triphosphate (ATP) has been developed based on gold nanoparticles (AuNPs) amplification [104]. The aptasensor was fabricated as a tertiary hybrid DNA-AuNPs system, which involved the anchored DNA (ADNA) immobilized on gold electrode, reporter DNA (RDNA) tethered with AuNPs and target-responsive DNA (TRDNA) linking ADNA and RDNA. Electrochemical signal is derived from chronocoulometric interrogation of $[Ru(NH_3)_6]^{3+}$ (RuHex) that quantitatively binds to surface-confined DNA via electrostatic interaction. The introduction of ATP triggers the structure switching of the TRDNA to form aptamer-ATP complex, which results in the dissociation of the RDNA capped AuNPs (RDNA-AuNPs) and release of abundant RuHex molecules trapped by RDNA-AuNPs. The incorporation of AuNPs in this strategy significantly enhances the sensitivity of ATP assay.

An electrochemical sensing strategy for highly sensitive detection of small molecules was developed based on switching structures of aptamers from DNA/DNA duplex to DNA/target complex [105]. A gold electrode was first modified with gold nanoparticles (AuNPs), and thiolated capture probe was immobilized onto the electrode via sulfur-gold affinity. Then, a sandwich-type strategy was employed, which involved a linker DNA containing antiadenosine aptamer sequence and reporter DNA loaded on AuNPs. In the presence of adenosine, the aptamer part bound with adenosine and folded to the complex structure. As a result, the reporter probes together with AuNPs were released into solution and reduced a decrease in peak current. The sensor exhibited excellent selectivity against other nucleosides and could be used to detect adenosine from real human serum samples.

A label-free electrochemical aptasensor introducing a probe immobilization technique by the use of a layer-by-layer (LBL) self-assembled multilayer with ferrocene-appended poly(ethyleneimine) (Fc-PEI) on an indium tin oxide (ITO) array electrode for detection of cocaine was first constructed [106]. The Fc-PEI and gold nanoparticles (AuNPs) were LBL assembled on the electrode surface via electrostatic interaction. Then, cocaine aptamer fragments, SH-C2, were covalently labeled onto the outermost AuNP layer. When the target cocaine and cocaine aptamer C1 were present simultaneously, the SH-C2 layer hybridized partly with C1 to bind the cocaine, which led to a decreased differential pulse voltammetry (DPV) signal of Fc-PEI. The sensor was specific to cocaine in complex biologic fluids such as human plasma and human saliva.

A strategy based on the utilization of the aptamer-complementary DNA (cDNA) oligonucleotides as the probes for electrochemical sensing was described [107]. The sequences at both ends of the cDNA are tailor-made to be complementary, and both the ferrocene redox moiety and thiol group are labeled onto the cDNA. The labeled cDNA are hybridized with their respective aptamers (i.e., ATP- and thrombin-binding aptamers) to form double-stranded DNA (ds-DNA) and the electrochemical aptasensors are prepared by self-assembling the labeled ds-DNA onto Au electrodes. Upon target binding, the aptamers confined onto electrode surface dissociate from their respective cDNA oligonucleotides into the solution and the single-stranded cDNA could, thus, tend to form a hairpin structure through the hybridization of the complementary sequences at both its ends. Such a conformational change of the cDNA resulting from the target binding-induced dissociation of the aptamers essentially leads to the change in the voltammetric signal of the redox moiety labeled onto the cDNA and thus constitutes the mechanism for the electrochemical aptasensors for specific target sensing.

A reusable electrochemical aptasensor for highly sensitive detection of adenosine had been developed using sensing interface of self-assembling the part DNA duplex hybridized by 5′-thiolated part complementary strand (TPCS) and 3′-ferrocene(Fc)-labeled adenosine-binding aptamer strand (FABA) through S-Au bonding on a gold electrode surface [108]. When the modified electrode was incubated in the adenosine solutions, the aptamer made structure switching to bind adenosine. As a result, Fc-labeled adenosine-binding aptamer strand was taken off from the sensing interface, resulting in a decrease of the redox current. The aptasensor was characterized electrochemically by cyclic voltammetry and electrochemical impedance spectroscopy.

4. Conclusion

Aptasensors appear as promising devices based on aptamers that are very small in size compared to other biorecognition molecules like antibodies or enzymes. Nonspecific adsorption phenomena are usually less pronounced on nucleic acid-derivatized surfaces as compared to protein derivatized ones. Generally, regeneration of aptamer derivatized surfaces is quite easy to perform. Aptamers can undergo multiple denaturation/regeneration cycles, whereas antibodies suffer from permanent degradation. DNA aptamers are suitable for designing reusable aptasensors, whereas RNA aptamers allow single shot measurements. The major limitation is due to RNA aptamer degradation by ribonucleases. This can be overcome by chemical modification of RNA aptamers or use of enantiomeric aptamers known as spiegelmers.

Currently, the SELEX is a highly automated procedure and only few days are necessary for development of aptamers for certain ligands. This is much shorter in comparison with the selection of antibodies, where usually several months are required. Due to effectivity of the SELEX, the library of aptamers against various ligands has become wider. On the other hand, the primary procedure does not result in all cases in aptamers with desired affinity. Therefore, optimization of aptamer structure is required. This optimization is performed through biased library generation. As a result, it is possible to select aptamers with sensitivity to small modification of the ligand. Aptamers can even distinguish the chirality of molecules and their secondary structure. In principle, there is no restriction in the type of target for which the aptamer can be selected.

Several problems related to the practical application of aptamers are still under study, for example, how the immobilization of aptamers to the supported films and their microenvironment will affect the aptamer structure and aptamer-ligand interactions. The aptamers configuration is sensitive to the salt composition; therefore, liquid composition may affect the aptasensor properties [109]. Problems are connected with the application of aptamers in the complex biological systems. Several proteins may interact with DNA aptamers nonspecifically. They could bind to the sugar-phosphate backbone of DNA, and thus mask the specific binding of analyte. The presence of nucleic acid in the biological liquids may cause hybridization with aptamers, and thus affect the aptamers conformation and maintaining the proper binding site. It should be also mentioned that currently only approx. 250 aptamers are available, while the number of various antibodies is much larger. The continuous growth of immune test is also due to lack of aptamer-based kits at the market. Thus, despite the advantages of aptamers over antibodies, further effort is required for wide spreading aptamers-based technology in practical applications. Given the rapid pace of advances in this field, the development of miniaturized, easy-to-use electrochemical aptasensor diagnostic systems for large-scale clinical testing seems a realistic goal.

Future direction will probably see growth of electrochemical microchips and nanochips. The development of microarrays based on DNA aptamers used as receptors can be seen as a logical continuation of the DNA-chip technology development although the principle of target recognition is not based on hybridization but is analogous to the immunochemical assay. In the near future, aptamer microarrays are expected to play a dominant role in proteomics, thus extending the use of aptamer-based microarrays.

References

[1] D. L. Robertson and G. F. Joyce, "Selection in vitro of an RNA enzyme that specifically cleaves single-stranded DNA," *Nature*, vol. 344, no. 6265, pp. 467–468, 1990.

[2] A. D. Ellington and J. W. Szostak, "In vitro selection of RNA molecules that bind specific ligands," *Nature*, vol. 346, no. 6287, pp. 818–822, 1990.

[3] C. Tuerk and L. Gold, "Systemic evolution of ligands by exponential enrichment: RNA ligands to bacteriophage T4 DNA polymerase," *Science*, vol. 249, no. 4968, pp. 505–510, 1990.

[4] W. Kuliczkowski, J. Floyd, A. Malinin, and V. Serebruany, "Aptamers: the emerging class of future anticoagulation for vascular disease," *Expert Review of Cardiovascular Therapy*, vol. 8, no. 4, pp. 503–507, 2010.

[5] K. A. Davis, B. Abrams, Y. Lin, and S. D. Jayasena, "Use of a high affinity DNA ligand in flow cytometry," *Nucleic Acids Research*, vol. 24, no. 4, pp. 702–706, 1996.

[6] K. Ikebukuro, C. Kiyohara, and K. Sode, "Electrochemical detection of protein using a double aptamer sandwich," *Analytical Letters*, vol. 37, no. 14, pp. 2901–2909, 2004.

[7] M. I. Pividori, A. Merkoçi, and S. Alegret, "Electrochemical genosensor design: Immobilisation of oligonucleotides onto transducer surfaces and detection methods," *Biosensors and Bioelectronics*, vol. 15, no. 5-6, pp. 291–303, 2000.

[8] M. C. Rodriguez, A. N. Kawde, and J. Wang, "Aptamer biosensor for label-free impedance spectroscopy detection of proteins based on recognition-induced switching of the surface charge," *Chemical Communications*, no. 34, pp. 4267–4269, 2005.

[9] A. E. Radi and C. K. O'Sullivan, "Aptamer conformational switch as sensitive electrochemical biosensor for potassium ion recognition," *Chemical Communications*, no. 32, pp. 3432–3434, 2006.

[10] R. J. White, N. Phares, A. A. Lubin, Y. Xiao, and K. W. Plaxco, "Optimization of electrochemical aptamer-based sensors via optimization of probe packing density and surface chemistry," *Langmuir*, vol. 24, no. 18, pp. 10513–10518, 2008.

[11] E. J. Cho, J. R. Collett, A. E. Szafranska, and A. D. Ellington, "Optimization of aptamer microarray technology for multiple protein targets," *Analytica Chimica Acta*, vol. 564, no. 1, pp. 82–90, 2006.

[12] K. Maehashi and K. Matsumoto, "Label-free electrical detection using carbon nanotube-based biosensors," *Sensors*, vol. 9, no. 7, pp. 5368–5378, 2009.

[13] T. Hianik, V. Ostatná, M. Sonlajtnerova, and I. Grman, "Influence of ionic strength, pH and aptamer configuration for binding affinity to thrombin," *Bioelectrochemistry*, vol. 70, no. 1, pp. 127–133, 2007.

[14] Z. Zhang, W. Yang, J. Wang, C. Yang, F. Yang, and X. Yang, "A sensitive impedimetric thrombin aptasensor based on polyamidoamine dendrimer," *Talanta*, vol. 78, no. 4-5, pp. 1240–1245, 2009.

[15] P. Kara, A. de la Escosura-Muñiz, M. Maltez-da Costa, M. Guix, M. Ozsoz, and A. Merkoçi, "Aptamers based electrochemical biosensor for protein detection using carbon nanotubes platforms," *Biosensors and Bioelectronics*, vol. 26, no. 4, pp. 1715–1718, 2010.

[16] H. M. So, D. W. Park, H. Chang, and J. O. Lee, "Carbon nanotube biosensors with aptamers as molecular recognition elements," *Methods in Molecular Biology*, vol. 625, pp. 239–249, 2010.

[17] P. Hu, J. Zhang, L. Li, Z. Wang, W. O'Neill, and P. Estrela, "Carbon nanostructure-based field-effect transistors for label-free chemical/biological sensors," *Sensors*, vol. 10, no. 5, pp. 5133–5159, 2010.

[18] Y. Yuan, R. Yuan, Y. Chai, Y. Zhuo, L. Bai, and Y. Liao, "A signal-on electrochemical probe-label-free aptasensor using gold-platinum alloy and stearic acid as enhancers," *Biosensors and Bioelectronics*, vol. 26, no. 2, pp. 881–885, 2010.

[19] G. A. Zelada-Guillen, J. Riu, A. Düzgün, and F. X. Rius, "Immediate detection of living bacteria at ultralow concentrations using a carbon nanotube based potentiometrie aptasensor," *Angewandte Chemie—International Edition*, vol. 48, no. 40, pp. 7334–7337, 2009.

[20] A. V. Porfireva, G. A. Evtugyn, A. N. Ivanov, and T. Hianik, "Impedimetric aptasensors based on carbon nanotubes—poly(methylene blue) composite," *Electroanalysis*, vol. 22, no. 19, pp. 2187–2195, 2010.

[21] X. Liu, Y. Li, J. Zheng, J. Zhang, and Q. Sheng, "Carbon nanotube-enhanced electrochemical aptasensor for the detection of thrombin," *Talanta*, vol. 81, no. 4-5, pp. 1619–1624, 2010.

[22] Y. Du, C. Chen, B. Li, M. Zhou, E. Wang, and S. Dong, "Layer-by-layer electrochemical biosensor with aptamer-appended active polyelectrolyte multilayer for sensitive protein determination," *Biosensors and Bioelectronics*, vol. 25, no. 8, pp. 1902–1907, 2010.

[23] D. W. Kim, S. M. Seo, and Y. J. Park, "Single-walled carbon nanotube network based biosensors using aptamers and its characteristics," in *Proceedings of the Nanotechnology Conference and Trade Show*, pp. 94–96, June 2008.

[24] J. L. He, Z. S. Wu, P. Hu, S. P. Wang, G. L. Shen, and R. Q. Yu, "Biocatalytic growth of gold agglomerates on an electrode for aptamer-based electrochemical detection," *Analyst*, vol. 135, no. 3, pp. 570–576, 2010.

[25] C. Ding, Y. Ge, and J. M. Lin, "Aptamer based electrochemical assay for the determination of thrombin by using the amplification of the nanoparticles," *Biosensors and Bioelectronics*, vol. 25, no. 6, pp. 1290–1294, 2010.

[26] Y. Kang, K. J. Feng, J. W. Chen, J. H. Jiang, G. L. Shen, and R. Q. Yu, "Electrochemical detection of thrombin by sandwich approach using antibody and aptamer," *Bioelectrochemistry*, vol. 73, no. 1, pp. 76–81, 2008.

[27] Y. Osawa, M. Takase, K. Sode, and K. Ikebukuro, "DNA aptamers that bind to PQQGDH as an electrochemical labeling tool," *Electroanalysis*, vol. 21, no. 11, pp. 1303–1308, 2009.

[28] L. Zhou, L. J. Ou, X. Chu, G. L. Shen, and R. Q. Yu, "Aptamer-based rolling circle amplification: a platform for electrochemical detection of protein," *Analytical Chemistry*, vol. 79, no. 19, pp. 7492–7500, 2007.

[29] J. Zhou, H. Huang, J. Xuan, J. Zhang, and J. J. Zhu, "Quantum dots electrochemical aptasensor based on three-dimensionally ordered macroporous gold film for the detection of ATP," *Biosensors and Bioelectronics*, vol. 26, no. 2, pp. 834–840, 2010.

[30] Y. Xiang, Y. Zhang, X. Qian, Y. Chai, J. Wang, and R. Yuan, "Ultrasensitive aptamer-based protein detection via a dual amplified biocatalytic strategy," *Biosensors and Bioelectronics*, vol. 25, no. 11, pp. 2539–2542, 2010.

[31] J. Zhao, Y. Zhang, H. Li et al., "Ultrasensitive electrochemical aptasensor for thrombin based on the amplification of aptamer-AuNPs-HRP conjugates," *Biosensors and Bioelectronics*, vol. 26, no. 5, pp. 2297–2303, 2011.

[32] J. Zheng, W. Feng, L. Lin et al., "A new amplification strategy for ultrasensitive electrochemical aptasensor with network-like thiocyanuric acid/gold nanoparticles," *Biosensors and Bioelectronics*, vol. 23, no. 3, pp. 341–347, 2007.

[33] M. Mir, A. T. A. Jenkins, and I. Katakis, "Ultrasensitive detection based on an aptamer beacon electron transfer chain," *Electrochemistry Communications*, vol. 10, no. 10, pp. 1533–1536, 2008.

[34] R. Polsky, R. Gill, L. Kaganovsky, and I. Willner, "Nucleic acid-functionalized Pt nanoparticles: Catalytic labels for the amplified electrochemical detection of biomolecules," *Analytical Chemistry*, vol. 78, no. 7, pp. 2268–2271, 2006.

[35] H. Qiu, Y. Sun, X. Huang, and Y. Qu, "A sensitive nanoporous gold-based electrochemical aptasensor for thrombin detection," *Colloids and Surfaces B*, vol. 79, no. 1, pp. 304–308, 2010.

[36] J. Wang, A. Munir, Z. Li, and H. S. Zhou, "Aptamer-Au NPs conjugates-accumulated methylene blue for the sensitive electrochemical immunoassay of protein," *Talanta*, vol. 81, no. 1-2, pp. 63–67, 2010.

[37] T. H. Degefa, S. Hwang, D. Kwon, J. H. Park, and J. Kwak, "Aptamer-based electrochemical detection of protein using enzymatic silver deposition," *Electrochimica Acta*, vol. 54, no. 27, pp. 6788–6791, 2009.

[38] X. Li, J. Liu, and S. Zhang, "Electrochemical analysis of two analytes based on a dual-functional aptamer DNA sequence," *Chemical Communications*, vol. 46, no. 4, pp. 595–597, 2010.

[39] X. Zhang, B. Qi, Y. Li, and S. Zhang, "Amplified electrochemical aptasensor for thrombin based on bio-barcode method," *Biosensors and Bioelectronics*, vol. 25, no. 1, pp. 259–262, 2009.

[40] S. Centi, L. B. Sanmartin, S. Tombelli, I. Palchetti, and M. Mascini, "Detection of C reactive protein (CRP) in serum by an electrochemical aptamer-based sandwich assay," *Electroanalysis*, vol. 21, no. 11, pp. 1309–1315, 2009.

[41] Y. Du, B. Li, F. Wang, and S. Dong, "Au nanoparticles grafted sandwich platform used amplified small molecule electrochemical aptasensor," *Biosensors and Bioelectronics*, vol. 24, no. 7, pp. 1979–1983, 2009.

[42] R. Freeman, Y. Li, R. Tel-Vered, E. Sharon, J. Elbaz, and I. Willner, "Self-assembly of supramolecular aptamer structures for optical or electrochemical sensing," *Analyst*, vol. 134, no. 4, pp. 653–656, 2009.

[43] K. Kerman and E. Tamiya, "Aptamer-functionalized Au nanoparticles for the electrochemical detection of thrombin," *Journal of Biomedical Nanotechnology*, vol. 4, no. 2, pp. 159–164, 2008.

[44] E. Suprun, V. Shumyantseva, T. Bulko et al., "Au-nanoparticles as an electrochemical sensing platform for aptamer-thrombin interaction," *Biosensors and Bioelectronics*, vol. 24, no. 4, pp. 825–830, 2008.

[45] M. A. Rahman, I. S. Jung, M. S. Won, and Y. B. Shim, "Gold nanoparticles doped conducting polymer nanorod electrodes: ferrocene catalyzed aptamer-based thrombin immunosensor," *Analytical Chemistry*, vol. 81, no. 16, pp. 6604–6611, 2009.

[46] L. Li, H. Zhao, Z. Chen, X. Mu, and L. Guo, "Aptamer-based electrochemical approach to the detection of thrombin by modification of gold nanoparticles," *Analytical and Bioanalytical Chemistry*, vol. 398, no. 1, pp. 563–570, 2010.

[47] K. Ikebukuro, C. Kiyohara, and K. Sode, *Electrochemical Sensing of Protein Using Two Aptamers in Sandwich Manner*, 2004.

[48] P. He, L. Shen, Y. Cao, and D. Li, "Ultrasensitive electrochemical detection of proteins by amplification of aptamer-nanoparticle bio bar codes," *Analytical Chemistry*, vol. 79, no. 21, pp. 8024–8029, 2007.

[49] Y. Huang, X. M. Nie, S. L. Gan, J. H. Jiang, G. L. Shen, and R. Q. Yu, "Electrochemical immunosensor of platelet-derived growth factor with aptamer-primed polymerase amplification," *Analytical Biochemistry*, vol. 382, no. 1, pp. 16–22, 2008.

[50] E. Baldrich, J. L. Acero, G. Reekmans, W. Laureyn, and C. K. O'Sullivan, "Displacement enzyme linked aptamer assay," *Analytical Chemistry*, vol. 77, no. 15, pp. 4774–4784, 2005.

[51] J. A. Hansen, J. Wang, A. N. Kawde, Y. Xiang, K. V. Gothelf, and G. Collins, "Quantum-dot/aptamer-based ultrasensitive multi-analyte electrochemical biosensor," *Journal of the American Chemical Society*, vol. 128, no. 7, pp. 2228–2229, 2006.

[52] N. De-los-Santos-Álvarez, M. J. Lobo-Castañón, A. J. Miranda-Ordieres, and P. Tuñón-Blanco, "Modified-RNA aptamer-based sensor for competitive impedimetric assay of neomycin B," *Journal of the American Chemical Society*, vol. 129, no. 13, pp. 3808–3809, 2007.

[53] N. de-los-Santos-Álvarez, M. J. Lobo-Castañón, A. J. Miranda-Ordieres, and P. Tuñón-Blanco, "Aptamers as recognition elements for label-free analytical devices," *TrAC—Trends in Analytical Chemistry*, vol. 27, no. 5, pp. 437–446, 2008.

[54] A. E. Radi, J. L. A. Sánchez, E. Baldrich, and C. K. O'Sullivan, "Reusable impedimetric aptasensor," *Analytical Chemistry*, vol. 77, no. 19, pp. 6320–6323, 2005.

[55] D. Xu, D. Xu, X. Yu, Z. Liu, W. He, and Z. Ma, "Label-free electrochemical detection for aptamer-based array electrodes," *Analytical Chemistry*, vol. 77, no. 16, pp. 5107–5113, 2005.

[56] H. Cai, T. M. H. Lee, and I. M. Hsing, "Label-free protein recognition using an aptamer-based impedance measurement assay," *Sensors and Actuators B*, vol. 114, no. 1, pp. 433–437, 2006.

[57] A. E. Radi, J. L. Acero Sánchez, E. Baldrich, and C. K. O'Sullivan, "Reagentless, reusable, ultrasensitive electrochemical molecular beacon aptasensor," *Journal of the American Chemical Society*, vol. 128, no. 1, pp. 117–124, 2006.

[58] D. Xu, H. Han, W. He, Z. Liu, D. Xu, and X. Liu, "Electrically addressed fabrication of aptamer-based array electrodes," *Electroanalysis*, vol. 18, no. 18, pp. 1815–1820, 2006.

[59] Y. Xu, L. Yang, X. Ye, P. He, and Y. Fang, "An aptamer-based protein biosensor by detecting the amplified impedance signal," *Electroanalysis*, vol. 18, no. 15, pp. 1449–1456, 2006.

[60] M. Zayats, Y. Huang, R. Gill, C. A. Ma, and I. Willner, "Label-free and reagentless aptamer-based sensors for small molecules," *Journal of the American Chemical Society*, vol. 128, no. 42, pp. 13666–13667, 2006.

[61] J. A. Lee, S. Hwang, K.-C. Lee et al., *Pyrolyzed Carbon Biosenosor for Aptamer-Protein Interactions Using Electrochemical Impedance Spectroscopy*, 2007.

[62] W. Liao and X. T. Cui, "Reagentless aptamer based impedance biosensor for monitoring a neuro-inflammatory cytokine PDGF," *Biosensors and Bioelectronics*, vol. 23, no. 2, pp. 218–224, 2007.

[63] U. Schlecht, A. Malavé, T. M. A. Gronewold, M. Tewes, and M. Löhndorf, "Detection of Rev peptides with impedance-sensors—comparison of device-geometries," *Biosensors and Bioelectronics*, vol. 22, no. 9-10, pp. 2337–2340, 2007.

[64] J. Bai, H. Wei, B. Li et al., "[$Ru(bpy)_2$(dcbpy)NHS] labeling/aptamer-based biosensor for the detection of lysozyme by increasing sensitivity with gold nanoparticle amplification," *Chemistry—An Asian Journal*, vol. 3, no. 11, pp. 1935–1941, 2008.

[65] T. H. Degefa and J. Kwak, "Label-free aptasensor for platelet-derived growth factor (PDGF) protein," *Analytica Chimica Acta*, vol. 613, no. 2, pp. 163–168, 2008.

[66] J. Elbaz, B. Shlyahovsky, D. Li, and I. Willner, "Parallel analysis of two analytes in solutions or on surfaces by using a bifunctional aptamer: applications for biosensing and logic gate operations," *ChemBioChem*, vol. 9, no. 2, pp. 232–239, 2008.

[67] P. Estrela, D. Paul, P. Li et al., "Label-free detection of protein interactions with peptide aptamers by open circuit potential measurement," *Electrochimica Acta*, vol. 53, no. 22, pp. 6489–6496, 2008.

[68] J. A. Lee, S. Hwang, J. Kwak, S. I. Park, S. S. Lee, and K. C. Lee, "An electrochemical impedance biosensor with aptamer-modified pyrolyzed carbon electrode for label-free protein detection," *Sensors and Actuators B*, vol. 129, no. 1, pp. 372–379, 2008.

[69] X. Li, L. Shen, D. Zhang et al., "Electrochemical impedance spectroscopy for study of aptamer-thrombin interfacial interactions," *Biosensors and Bioelectronics*, vol. 23, no. 11, pp. 1624–1630, 2008.

[70] W. Liao, B. A. Randall, N. A. Alba, and X. T. Cui, "Conducting polymer-based impedimetric aptamer biosensor for in situ detection," *Analytical and Bioanalytical Chemistry*, vol. 392, no. 5, pp. 861–864, 2008.

[71] W. Liao, B. Randall, N. Alba, and X. T. Cui, *Conducting Polymer-Based Aptamer Biosensor for in Situ Monitoring of Cytokine*, 2008.

[72] A. Bogomolova, E. Komarova, K. Reber et al., "Challenges of electrochemical impedance spectroscopy in protein biosensing," *Analytical Chemistry*, vol. 81, no. 10, pp. 3944–3949, 2009.

[73] Z. Liu, Z. Li, G. Shen, and R. Yu, "Reagentless aptamer based impedance biosensor for monitoring adenosine," *Electroanalysis*, vol. 21, no. 16, pp. 1781–1785, 2009.

[74] C. Pan, M. Guo, Z. Nie, X. Xiao, and S. Yao, "Aptamer-based electrochemical sensor for label-free recognition and detection of cancer cells," *Electroanalysis*, vol. 21, no. 11, pp. 1321–1326, 2009.

[75] Y. Peng, D. Zhang, Y. Li, H. Qi, Q. Gao, and C. Zhang, "Label-free and sensitive faradic impedance aptasensor for the determination of lysozyme based on target-induced aptamer displacement," *Biosensors and Bioelectronics*, vol. 25, no. 1, pp. 94–99, 2009.

[76] E. Sharon, R. Freeman, T. V. Ran, and I. Willner, "Impedimetric or ion-sensitive field-effect transistor (ISFET) aptasensors based on the self-assembly of au nanoparticle-functionalized supramolecular aptamer nanostructures," *Electroanalysis*, vol. 21, no. 11, pp. 1291–1296, 2009.

[77] J. Wang, D. Xu, and H. Y. Chen, "A novel protein analytical method based on hybrid-aptamer and DNA-arrayed electrodes," *Electrochemistry Communications*, vol. 11, no. 8, pp. 1627–1630, 2009.

[78] M. Hua, M. Tao, P. Wang et al., "Label-free electrochemical cocaine aptasensor based on a target-inducing aptamer switching conformation," *Analytical Sciences*, vol. 26, no. 12, pp. 1265–1270, 2010.

[79] P. Kara, B. Meric, and M. Ozsoz, "Development of a label free IgE sensitive aptasensor based on electrochemical Impedance Spectrometry," *Combinatorial Chemistry and High Throughput Screening*, vol. 13, no. 7, pp. 578–581, 2010.

[80] E. Komarova, K. Reber, M. Aldissi, and A. Bogomolova, "New multispecific array as a tool for electrochemical impedance spectroscopy-based biosensing," *Biosensors and Bioelectronics*, vol. 25, no. 6, pp. 1389–1394, 2010.

[81] K. Min, K. M. Song, M. Cho et al., "Simultaneous electrochemical detection of both PSMA (+) and PSMA (-) prostate cancer cells using an RNA/peptide dual-aptamer probe," *Chemical Communications*, vol. 46, no. 30, pp. 5566–5568, 2010.

[82] M. S. Mannoor, T. James, D. V. Ivanov, L. Beadling, and W. Braunlin, "Nanogap dielectric spectroscopy for aptamer-based protein detection," *Biophysical Journal*, vol. 98, no. 4, pp. 724–732, 2010.

[83] A. Qureshi, Y. Gurbuz, S. Kallempudi, and J. H. Niazi, "Label-free RNA aptamer-based capacitive biosensor for the detection of C-reactive protein," *Physical Chemistry Chemical Physics*, vol. 12, no. 32, pp. 9176–9182, 2010.

[84] E. González-Fernández, N. de-los-Santos-Álvarez, M. J. Lobo-Castañón, A. J. Miranda-Ordieres, and P. Tuñón-Blanco, "Impedimetric aptasensor for tobramycin detection in human serum," *Biosensors and Bioelectronics*, vol. 26, no. 5, pp. 2354–2360, 2011.

[85] A. N. Kawde, M. C. Rodriguez, T. M. H. Lee, and J. Wang, "Label-free bioelectronic detection of aptamer-protein interactions," *Electrochemistry Communications*, vol. 7, no. 5, pp. 537–540, 2005.

[86] G. Evtugyn, A. Porfireva, A. Ivanov, O. Konovalov, and T. Hianik, "Molecularly imprinted polymerized methylene green as a platform for electrochemical sensing of aptamer-thrombin interactions," *Electroanalysis*, vol. 21, no. 11, pp. 1272–1277, 2009.

[87] G. Evtugyn, A. Porfireva, M. Ryabova, and T. Hianik, "Aptasensor for thrombin based on carbon nanotubes-methylene blue composites," *Electroanalysis*, vol. 20, no. 21, pp. 2310–2316, 2008.

[88] G. A. Evtugyn, A. V. Porfireva, T. Hianik, M. S. Cheburova, and H. C. Budnikov, "Potentiometric DNA sensor based on electropolymerized phenothiazines for protein detection," *Electroanalysis*, vol. 20, no. 12, pp. 1300–1308, 2008.

[89] T. Hianik, V. Ostatná, Z. Zajacová, E. Stoikova, and G. Evtugyn, "Detection of aptamer-protein interactions using QCM and electrochemical indicator methods," *Bioorganic and Medicinal Chemistry Letters*, vol. 15, no. 2, pp. 291–295, 2005.

[90] T. Hianik, A. Porfireva, I. Grman, and G. Evtugyn, "Aptabodies—new type of artificial receptors for detection proteins," *Protein and Peptide Letters*, vol. 15, no. 8, pp. 799–805, 2008.

[91] A. Porfirieva, G. Evtugyn, and T. Hianik, "Polyphenothiazine modified electrochemical aptasensor for detection of human α-thrombin," *Electroanalysis*, vol. 19, no. 18, pp. 1915–1920, 2007.

[92] K. Min, M. Cho, S. Y. Han, Y. B. Shim, J. Ku, and C. Ban, "A simple and direct electrochemical detection of interferon-γ using its RNA and DNA aptamers," *Biosensors and Bioelectronics*, vol. 23, no. 12, pp. 1819–1824, 2008.

[93] Y. Du, B. Li, H. Wei, Y. Wang, and E. Wang, "Multifunctional label-free electrochemical biosensor based on an integrated aptamer," *Analytical Chemistry*, vol. 80, no. 13, pp. 5110–5117, 2008.

[94] C. Deng, J. Chen, Z. Nie et al., "Impedimetric aptasensor with femtomolar sensitivity based on the enlargement of surface-charged gold nanoparticles," *Analytical Chemistry*, vol. 81, no. 2, pp. 739–745, 2009.

[95] B. Li, Y. Wang, H. Wei, and S. Dong, "Amplified electrochemical aptasensor taking AuNPs based sandwich sensing platform as a model," *Biosensors and Bioelectronics*, vol. 23, no. 7, pp. 965–970, 2008.

[96] Y. Yuan, R. Yuan Ruo, Y. Chai et al., "A novel label-free electrochemical aptasensor for thrombin based on the nano-Au/thioninen multilayer films as redox probes," *Analytica Chimica Acta*, vol. 668, no. 2, pp. 171–176, 2010.

[97] Z. Chen, L. Li, H. Zhao, L. Guo, and X. Mu, "Electrochemical impedance spectroscopy detection of lysozyme based on electrodeposited gold nanoparticles," *Talanta*, vol. 83, no. 5, pp. 1501–1506, 2011.

[98] D. T. Tran, V. Vermeeren, L. Grieten et al., "Nanocrystalline diamond impedimetric aptasensor for the label-free detection of human IgE," *Biosensors and Bioelectronics*, vol. 26, no. 6, pp. 2987–2993, 2011.

[99] Y. L. Zhang, Y. Huang, J. H. Jiang, G. L. Shen, and R. Q. Yu, "Electrochemical aptasensor based on proximity-dependent surface hybridization assay for single-step, reusable, sensitive protein detection," *Journal of the American Chemical Society*, vol. 129, no. 50, pp. 15448–15449, 2007.

[100] M. Mir, M. Vreeke, and I. Katakis, "Different strategies to develop an electrochemical thrombin aptasensor," *Electrochemistry Communications*, vol. 8, no. 3, pp. 505–511, 2006.

[101] Y. Liu, N. Tuleouva, E. Ramanculov, and A. Revzin, "Aptamer-based electrochemical biosensor for interferon gamma detection," *Analytical Chemistry*, vol. 82, no. 19, pp. 8131–8136, 2010.

[102] X. Li, J. Xia, W. Li, and S. Zhang, "Multianalyte electrochemical biosensor based on aptamer- and nanoparticle-integrated bio-barcode amplification," *Chemistry—An Asian Journal*, vol. 5, no. 2, pp. 294–300, 2010.

[103] X. Zuo, S. Song, J. Zhang, D. Pan, L. Wang, and C. Fan, "A target-responsive electrochemical aptamer switch (TREAS) for reagentless detection of nanomolar ATP," *Journal of the American Chemical Society*, vol. 129, no. 5, pp. 1042–1043, 2007.

[104] W. Li, Z. Nie, X. Xu et al., "A sensitive, label free electrochemical aptasensor for ATP detection," *Talanta*, vol. 78, no. 3, pp. 954–958, 2009.

[105] S. Zhang, J. Xia, and X. Li, "Electrochemical biosensor for detection of adenosine based on structure-switching aptamer and amplification with reporter probe DNA modified Au nanoparticles," *Analytical Chemistry*, vol. 80, no. 22, pp. 8382–8388, 2008.

[106] Y. Du, C. Chen, J. Yin et al., "Solid-state probe based electrochemical aptasensor for cocaine: a potentially convenient, sensitive, repeatable, and integrated sensing platform for drugs," *Analytical Chemistry*, vol. 82, no. 4, pp. 1556–1563, 2010.

[107] Y. Lu, X. Li, L. Zhang, P. Yu, L. Su, and L. Mao, "Aptamer-based electrochemical sensors with aptamer-complementary DNA oligonucleotides as probe," *Analytical Chemistry*, vol. 80, no. 6, pp. 1883–1890, 2008.

[108] Z. Liu, R. Yuan, Y. Chai et al., "Highly sensitive, reusable electrochemical aptasensor for adenosine," *Electrochimica Acta*, vol. 54, no. 26, pp. 6207–6211, 2009.

[109] M. Cho, Y. Kim, S. Y. Han et al., "Detection for folding of the thrombin binding aptamer using label-free electrochemical methods," *Journal of Biochemistry and Molecular Biology*, vol. 41, no. 2, pp. 126–131, 2008.

SAGE-Hindawi Access to Research
International Journal of Electrochemistry
Volume 2011, Article ID 643683, 10 pages
doi:10.4061/2011/643683

Research Article

A Solid Binding Matrix/Mimic Receptor-Based Sensor System for Trace Level Determination of Iron Using Potential Measurements

Ayman H. Kamel, Felismina T. C. Moreira, Tamara I. Silva, and M. Goreti F. Sales

REQUIMTE, Instituto Superior de Engenharia do Porto, Rua Benardino de Almeida 431, 4200-072 Porto, Portugal

Correspondence should be addressed to M. Goreti F. Sales, goreti.sales@gmail.com

Received 14 March 2011; Accepted 2 May 2011

Academic Editor: Vinod Kumar Gupta

Copyright © 2011 Ayman H. Kamel et al. This is an open access article distributed under the Creative Commons Attribution License, which permits unrestricted use, distribution, and reproduction in any medium, provided the original work is properly cited.

Iron(II)-(1,10-phenanthroline) complex imprinted membrane was prepared by ionic imprinting technology. In the first step, Fe(II) established a coordination linkage with 1,10-phenanthroline and functional monomer 2-vinylpyridine (2-VP). Next, the complex was copolymerized with ethylene glycol dimethacrylate (EGDMA) as a crosslinker in the presence of benzoyl peroxide (BPO) as an initiator. Potentiometric chemical sensors were designed by dispersing the iron(II)-imprinted polymer particles in 2-nitrophenyloctyl ether (*o*-NPOE) plasticizer and then embedded in poly vinyl chloride (PVC) matrix. The sensors showed a Nernstian response for $[Fe(phen)_3]^{2+}$ with limit of detection 3.15 ng mL^{-1} and a Nernstian slope of 35.7 mV per decade.

1. Introduction

Heavy metals constitute an important class of pollutants that degrade the environment due to their persistent nature and their industrial importance. Among these, iron is one of the most common metals in nature. Infiltration from rainwater in soils and underlying geologic formations dissolves iron, transporting it into groundwater. Large quantities of iron are also disposed in the environment as a result of anthropogenic activities. Iron and its compounds have widespread industrial applications, from constructional material for drinking-water pipes, to food colours, coagulants in water treatment, pigments in paints and plastics. In tap water, dissolved ferrous iron gives a disagreeable taste. An appropriate knowledge of iron levels in both environmental waters and water for human consumption is very desirable. The relevancy of this subject has conducted to numerous reported methods using UV/Vis spectrophotometry [1–12], chemiluminescence [13–17], atomic absorption spectroscopy [18–22], and voltammetry [23, 24]. The design and development of portable devices such as sensors rather than laboratory-based instruments in monitoring iron at trace levels in real samples is still of considerable interest.

Imprinted materials in sensors have attracted considerable attention during the past few years [25–27]. Molecular imprinting mimics natural receptors with regard to their molecular/ionic recognition. Most investigations of molecular imprinting polymers have been carried out using polymerization in the presence of the template in order to incorporate specific template sites into the polymer. The development of synthetic membranes with molecular imprinting functionality is an important approach for future functional separation or purification materials [28].

Ionic imprinting is a process, in which a functional monomer is allowed to self-assemble around templated ions and subsequently is crosslinked as required. The selectivity of a specific target ion is obtained by providing the polymers with cavities, in which complexing ligands are arranged to match charge, coordination number, coordination geometry and size of that target ion. This process creates the ionic recognition site, which is a specific location for the target ion chemical functionality and spatial arrangement. Recent developments in molecular imprinting have been reviewed [29]. The high selectivity of ion-imprinted polymers (IIPs) arises from the memory effect of the polymer to the imprinted ions for example, from the specificity of interaction

of ligand with the metal ions, the coordination geometry and coordination number of metal ions; the charge of the metal ions and to a large extent on the size of them [30]. In recent years, a lot of IIPs have been prepared for Pd^{2+} [31], Ni^{2+} [32, 33], Fe^{3+} [34], Cd^{2+} [35, 36], Zn^{2+} [37], Cu^{2+} [38], Dy [39], UO_2^{2+} [40–42], Ca^{2+} [43], Er^{3+} [44], Th^{4+} [45], Hg^{2+}[46], and Gd^{3+} [47, 48].

The integration of IIP materials in electrochemical sensors yields selective, sensitive, simple, and rapid analytical methods. Electrochemical transducers monitor the activity of a chemical species in a given matrix and rely on interactions between analyte and receptor. Host-guest interactions are coupled to a signal transduction mechanism that yields the useful information about the species involved. The binding between the analyte and receptor can be effectively monitored and measured by such electrochemical techniques.

In this study, an ion-imprinting polymer was introduced for selective extraction of iron complex from aqueous solution. In synthesis processes, 1,10-phenanthroline, 2-vinylpyridine (2-VP), ethyleneglycol dimethacrylate (EGDMA), and benzoyl peroxide (BPO) were used as Fe(II) complexing agent, monomer, crosslinker and initiator, respectively. The synthesized polymer was dispersed in 2-nitrophenyloctyl ether (NPOE) and embedded in polyvinylchloride (PVC) matrix, for the monitoring of traces of iron.

2. Experimental

2.1. Apparatus. All potential measurements between reference and indicator electrodes were measured by means of a Crison μpH 2002 decimilivoltammeter ($\pm$0.1 mV sensitivity). An Orion, 90-00-29, double-junction electrode was used as reference. The analytical output signal was transferred to a commutation point reconnected to one of six ways out, each with an electrical antenna connector for adaptation to electrode device. The selective electrodes had no internal reference solution and an epoxy-graphite matrix as conductive solid contact. All measurements were carried out with the electrochemical cell graphite contact |Fe selective membrane| test solution || Na_2SO_4 salt bridge || Ag/AgCl (3M KCl). The pH values were measured by a Crison CWL/S7 combined glass electrode connected to a decimilivoltammeter Crison, pH meter, GLP 22. All potential measurements were carried out under constant stirring, by a Crison micro ST 2038. Infrared spectra were collected in a Nicolet 6700 FTIR spectrometer. Atomic absorption spectrometric measurements of Fe(II) were made with Perkin-Elmer spectrometer (AAnalyst 200) using the recommended optimum conditions [49].

2.2. Reagents and Solutions. All chemicals were of analytical grade and deionized water (conductivity $<0.1\,\mu S\,cm^{-1}$) was employed throughout. 1,10 phenanthroline (phen), *o*-nitrophenyloctyl ether (*o*-NPOE), *Bis*(2-ethylhexyl)sebacate (BEHS) dibutyl phthalate (DBP), cyclodextrin (Fe°Cyc), tetrakis(4-chlorophenyl) borate, sodium tetraphenyl borate (TPB^-), PVC of high molecular weight, 4-vinyl pyridine (4-VP), and ethyleneglycoldimethacrylate (EGDMA) were purchased from Fluka. Tetrahydrofuran (THF), acetic acid, citric acid, benzoyl peroxide (BPO), and ammonium iron sulfate were obtained from Riedel-deHaën. The evaluation of the effect of pH and other interfering species required sodium hydroxide, hydrochloride acid, cadmium sulphate, potassium sulphate, sodium chloride (all purchased from Merck), nickel chloride, manganese sulfate, magnesium chloride (all from Chemika), barium chloride (Sigma), silver nitrate, and copper sulfate (from Riedel-deHaën).

A solution of 0.1 mol L^{-1} of 1,10-phenanthroline was prepared in 10% ethanol. A 0.1 mol L^{-1} stock solution of Fe^{2+} was prepared by dissolving 4.0 g of iron(II) ammonium sulfate in 3 mL of 0.5 mol L^{-1} H_2SO_4, diluted with water in 100 mL calibration flask. A 10^{-2} mol L^{-1} stock solution of tris-(1,10-phenanthroline) iron(I1) (ferroin) was prepared by mixing 10 mL of standard 10^{-1} mol L^{-1} iron(II) ammonium sulphate, 30 mL of 10^{-1} mol L^{-1} l,l0-phenanthroline and 10 mL acetate buffer (pH 4.7). The mixture was transferred into an l00 mL volumetric flask and made up to the mark with water. Standard ferroin solutions (10^{-3}–10^{-8}, mol L^{-1}) were prepared by accurate dilution.

Solutions of the diverse ions used in the interference study were 0.01 mol L^{-1} in buffer. Hydroxylamine hydrochloride solution (10% w/v) was prepared by dissolving the reagent in water. Acetate buffer solutions of pH 3.5–6.6 were freshly prepared by mixing the appropriate amounts of 1 mol L^{-1} acetic acid and 1 mol L^{-1} sodium acetate solutions. All these solutions were stored in polyethylene containers.

2.3. Preparation of Ion Exchanger Sensor. It was carried out by mixing 50 mL of a 1.0×10^{-2} mol L^{-1} Fe(II) solution with 50 mL of a 1.0×10^{-2} mol L^{-1} sodium TPB solution or tetrakis(4-chlorophenyl)borate. Resulting solid was isolated by filtration, thoroughly washing with water, and kept in a dark flask inside a desiccator in order to prevent alterations caused by light and humidity.

2.4. Preparation of Metal Complex Imprinted Polymers. In a typical preparation of Fe^{2+} imprinted polymer (IIP), 1.0 mmo1 1,10-phenanthroline, and 1.0 mmo1 $(NH_4)_2FeSO_4 \cdot 6H_2O$ were weighed, placed into a 18 mm glass test tube and dissolved in 3 mL ethanol. To it 2.0 mmol 4-VP, 20 mmol EGDMA, and 70 mg BPO were added. The polymerization mixture were purged with nitrogen gas for 10 min, sealed, and then heated in a water bath at 60°C for 1 h. The resultant bulk polymer was ground and sieved, collected, and washed with ethanol/acetic acid (5 : 1) (V/V) overnight to remove the template. The reference polymer (NIP) was similarly prepared but without $(NH_4)_2FeSO_4 \cdot 6H_2O$ and 1,10-phenanthroline during the polymerization.

2.5. Constructions and Calibrations of Iron Membrane with Imprinted Material. The sensing membranes were prepared by mixing 200 mg of PVC powder and 7.0 mg of MIP and 2.0 mg of potassium tetrakis[2-chlorophenyl]borate [ISE I], 6.7 mg of MIP only [ISE II], 7.0 mg of NIP, and 2.0 mg of potassium tetrakis[2-chlorophenyl]borate [ISE

III], 7.0 mg of NIP and 2.0 mg of potassium tetrakis[2-chlorophenyl]borate [ISE IV], and 2.0 mg of potassium tetrakis[2-chlorophenyl]borate [ISE V], with 400 mg of plasticizer *o*, NPOE and 200 mg of PVC. The mixture was stirred until the PVC was well moistened and dispersed in 3.0 mL THF. These membranes were placed in conductive supports of conventional or tubular shapes. Membranes were allowed to dry for 24 h and placed in a 1×10^{-3} mol L^{-1} $[Fe(phen)_3]^{2+}$ solution. The electrodes were stored in these conditions when not in use.

All potentiometric measurements were carried out at room temperature. The emf of each electrode was measured in buffer. Different concentrations were obtained by transferring different aliquots of 1.0×10^{-3} mol L^{-1} of $[Fe(phen)_3]^{2+}$ ions aqueous solutions to 100 mL beaker containing 50.0 mL of 10^{-2} mol L^{-1} acetate buffer of pH 4.7. Potential readings were recorded after stabilization to ±0.2 mV, and emf was plotted as a function of logarithm iron(II) concentration. Calibration graphs were used for subsequent determination of unknown iron(II) concentrations (see Table 1).

2.6. Constructions and Calibrations of Iron Membrane with Ion Exchange Material. Sensor solutions were prepared by dissolving an appropriate amount of sensor in about 62% BEHS or DBP. These were added of 32% of PVC formerly dissolved in 2 mL of THF. Composition of the resulting membranes is presented in Table 1. After application in the conventional support, each membrane was let dry for 24 h.

All electrodes were placed in a convenient support over a magnetic stirrer and immersed in 50.00 mL of IS or buffer solution. Suitable increments of a 2.00×10^{-2} mol L^{-1} Fe(II) standard solution were added to provide a series of Fe(II) concentrations ranging 4.10×10^{-6} mol L^{-1} to 3.33×10^{-3} mol L^{-1}. The potential readings of the stirred Fe(II) solutions were measured at room temperature and recorded after stabilization to ±0.1 mV. A calibration plot was constructed connecting logarithm concentration with electromotive force.

3. Results and Discussion

Positioning of metal ions to match the arrangement of ligands on a substrate molecule through preorganization of the substrate with a metal-complexing monomer and its subsequent crosslinking polymerisation is an attractive means to prepare synthetic receptor materials. Furthermore, the strength and specificity of metal-ligand coordination may be enhanced by choosing the suitable functional groups for the IIP.

Despite the potential advantages offered by metal-coordination interaction, relatively few efforts have been taken to use this binding mode to design molecularly imprinted polymers. In this work, a noncovalent molecular imprinting method [50, 51] was used to synthesize a synthetic host for ferroin.

3.1. FTIR Spectra. Figure 1 presents the FTIR spectra of (a) IIP, (b) NIP, (c) $FeSO_4$, and (d) 1,10-phenanthroline. It can be seen that the shape and position of most peaks in (a) and (b) spectra are similar. This was as expected, because both polymers have the same chemical functions. The slight difference between these was related to some ferroin complex sequestered within the imprinted matrix. This is confirmed by (d) spectra; the peak at 853.5 cm^{-1} should correspond to absorption band of C–H stretching vibration for H atoms adjacent in the pyridine ring in 1,10-phenanthroline compound. The characteristic ring frequencies in 1,10-phenanthrene were shown at approximately 1502 cm^{-1} the second appearing as a triplet with the centre component at 1585 cm^{-1} and the third band shifting to 1423 cm^{-1}. The 1423 cm^{-1} band was most sensitive in this respect, but the other two showed a slightly discernable shift of the order of 10 to 25 cm^{-1}.

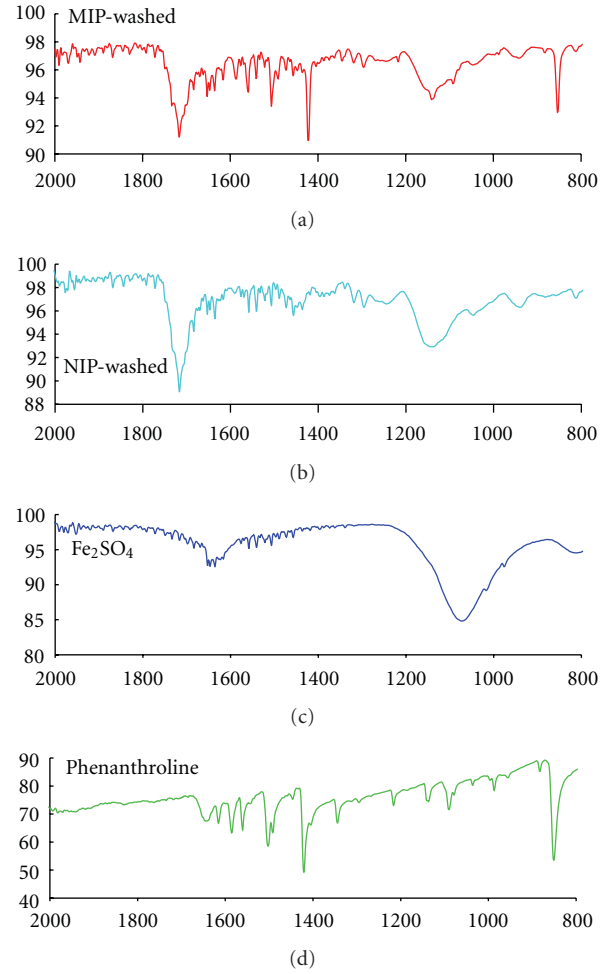

Figure 1: FTIR spectra of IIP (a), NIP (b), FeSO4, and 1,10-phenanthroline (d). (Scan from 2000 to 800 cm^{-1}, with background correction, and room temperature/humidity control).

3.2. Binding Studies. Adsorption isotherms yield important information concerning binding energies, modes of binding, and site distributions in the interaction of small molecules with adsorbent surfaces. In the liquid phase applications of imprinted materials, a molecule in solution interacts with binding sites in a solid adsorbent. The adsorption isotherms

Table 1: Response characteristics of ferroin-IIP PVC membrane sensors.

Membrane composition/ parameter	ISE I	ISE II	ISE III	ISE IV	ISE V	ISE VI	ISE VII	ISE VIII	ISE IX	ISE X	ISE XI
Ionophore	IIP	IIP	NIP	NIP	—	Fe°Phe	Fe°Cyc	Fe°P_{Cl}PB	Fe°Phe	Fe°Cyc	Fe°P_{Cl}PB
Additive	Tk_4ClPB	—	Tk_4ClPB	—	Tk_4ClPB	Tk_4ClPB	Tk_4ClPB	Tk_4ClPB	Tk_4ClPB	Tk_4ClPB	Tk_4ClPB
Plasticizer	*o-NPOE*	*o-NPOE*	*o-NPOE*	*o-NPOE*	*o-NPOE*	DBP	DBP	DBP	*b*EHS	*b*EHS	*b*EHS
Slope (mV decade^{-1})*	35.7 ± 1.2	29.6 ± 0.9	27.6 ± 1.5	26.3 ± 0.7	24.0 ± 1.4	33.3	35.8	37.9	33.6	36.1	38.6
Correlation coefficient (r)*	0.9970	0.9979	0.9998	0.9986	0.9991	0.991	0.990	0.993	0.994	0.991	0.991
Lower limit of linear range (mol L^{-1})	1.78×10^{-7}	1.81×10^{-6}	1.78×10^{-7}	2.31×10^{-6}	1.78×10^{-7}	8.99×10^{-5}	3.00×10^{-5}	5.00×10^{-5}	5.00×10^{-5}	5.00×10^{-5}	3.00×10^{-5}
Detection limit (ng mL^{-1})	0.05	0.50	0.05	0.64	0.05	3.91	4.39	4.39	10.56	6.22	5.56
Response time for 10^{-5} M (sec)	20	30	20	30	20	20	30	20	30	20	20
Recovery time (sec)	30	50	30	50	30	30	50	30	50	30	30
Working pH range	3–6	3–6	3–6	3–6	3–6	4–12.5	4–12.5	4–12.5	2.5–6	4–12.5	2.5–6

* Average of three measurements.

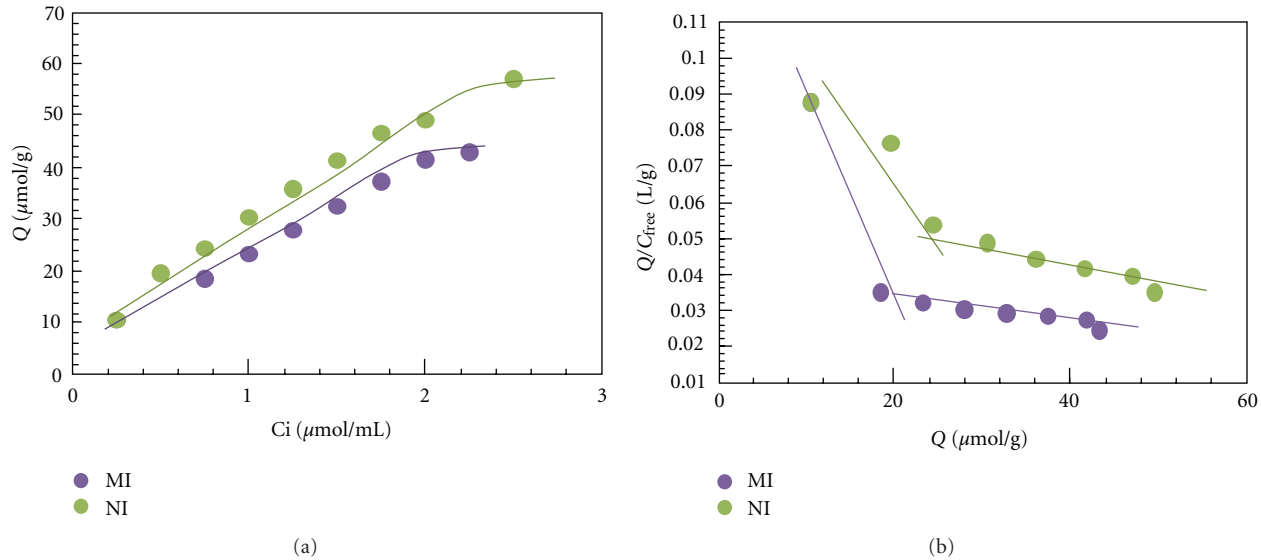

FIGURE 2: Binding isotherm (a) and Scatchard plot (b) for the Ferroin-imprinted (MI) or nonimprinted (NI) polymer. Q = Ferroin bound to 50.0 mg of the corresponding polymer; temperature = 25°C; volume = 4.00 mL; binding time: 12 h.

are then simply plots of the equilibrium concentrations of bound ligand (adsorbate) versus the concentration of free ligand. The isotherms can be fitted using various models. The most simple is the Langmuir type adsorption isotherm, where the adsorbent is assumed to contain only one type of site; adsorbate-adsorbate interactions are assumed not to occur, and the system is assumed ideal.

In order to investigate the binding performance of IIP, the equilibrium binding experiments were carried out by varying the concentrations $[Fe(phen)_3]^{2+}$ complex from 0.2 mmol L^{-1} to 2 mmol L^{-1} in the presence of a fixed amount (50 mg) of IIP and the obtained data were plotted with the Scatchard analysis [52] to estimate the binding parameters of IIP

$$\frac{Q}{C} = \frac{(Q_{\max} - Q)}{K_d}, \quad (1)$$

where $Q_{\max}$ is the maximum apparent binding capacity and K_d the equilibrium dissociation constant. As shown in Figure 2(a), the Scatchard plot is not linear, indicating that the binding sites in either IIP or NIP are heterogeneous in respect to the affinity for $[Fe(phen)_3]^{2+}$. Clearly, within the plot, there are two distinct sections and two straight lines can be obtained from the linear regression. This indicates that the binding sites in the IIP and NIP could be classified into two distinct groups with specific binding properties $(K_d)l$ and $(Q_{\max})l$ of higher affinity binding sites can be calculated to be 152.4 μmol L^{-1} and 24.5 μmol g^{-1} dry polymer for IIP and NIP, respectively, from the slope and the intercept of the Scatchard plot (Figure 2(b)). Similarly, $(K_d)2$ and $(Q_{\max})2$ of lower affinity binding sites were 3251.2 μmol L^{-1} and 129.1 μmol g^{-1}, respectively.

3.3. ISEs Analytical Features

3.3.1. Imprinting Polymer. The dissolution of MIP within the selective membrane may conduct to alterations at the configuration of the imprinted shape. When the template is not extracted from the imprinted polymer, this change in configuration may be attenuated. Results obtained pointed out that template extraction was important, providing decreased limit of detection and higher sensitivity. These results suggest that configuration changes from MIP dissolution were not significant, even for NIP sensors. The synthesized IIP were incorporated into the PVC membrane and were tested as sensing materials in the proposed potentiometric sensor. The potential response obtained with the sensors prepared with $[Fe(phen)_3]^{2+}$ IIP membrane and blank membrane is given in Figure 3. As seen from the figure, the sensors exhibit linear potentiometric response to $[Fe(phen)_3]^{2+}$ ions with lower limit of linear range 1.81×10^{-6} and 2.31×10^{-6}, 1.78×10^{-7} mol L^{-1}, and detection limits of 4.45, 6.89, and 17.7 ng mL^{-1}, for ISE's [II], [IV], and [V], respectively. All sensors exhibit near-Nernstian slopes of 29.6±0.9 (r^2 = 0.9979), 26.3±0.7 and 24.0±1.4 mV $decade^{-1}$, respectively. Addition of anionic additive potassium tetrakis[2-chlorophenyl]borate to either MIP [ISE I] or NIP [ISE III]-based membrane resulted in a Nernestian pattern with a slope 35.7 ± 1.2 (r^2 = 0.9979) and 27.6 ± 1.5 (r^2 = 0.9998) mV $decade^{-1}$, lower limit of linear range of 1.78×10^{-7} and 2.0×10^{-7} mol L^{-1}, and lower detection limit of 3.15 and 5.12 ng mL^{-1}, respectively. The composition and potentiometric response characteristics of the membrane sensors incorporating MIP and NIP as selective ion recognitions and with/without tetrakis[2-chlorophenyl]borate as anionic additive are shown in Table 1.

3.3.2. Ion Exchanger Sensor. Six membrane compositions were prepared by varying electroactive materials and solvent plasticizers (Table 1). Complexes of iron with phenanthroline, cyclodextrin, or tetrakis(4-chlorophenyl)borate served as ionophores and BEHS or DPB were used as plasticizers. All membranes were of plasticized PVC with 31-32 wt%

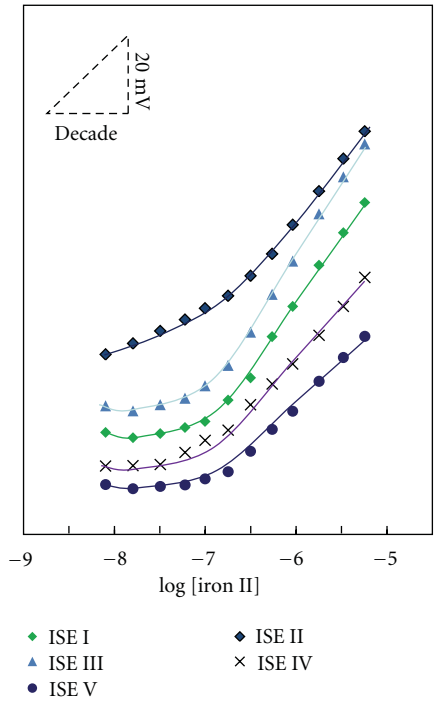

Figure 3: Calibration curve in acetate buffer at pH 4.7 for different sensors.

PVC, 61–63 wt% plasticizing solvent and 3%-4% of anionic additive and 3 wt% of electroactive material.

Electrodes showed supra-Nernstian responses in buffer (Table 1). Slopes ranged 33.3 to 38.6 mV decade^{-1} and linear behavior was mainly observed from 3.0×10^{-5} up to 3.3×10^{-3} mol L^{-1}. Sensors of Fe°Cyc or Fe°PClPB were greatly dependent on the plasticizing solvent, showing better responses for DBP.

3.4. Effect of PH. The influence of pH on the potentiometric response of the proposed sensors was examined over a pH range of 3–10 for $[Fe(phen)_3]^{2+}$ standard solutions of 1.0×10^{-5} mol L^{-1}. The pH of the solution was adjusted with either hydrochloric acid and/or sodium hydroxide solutions. The pH plot shows that the variation of solution pH over the range 3–6 has no significant effect on the potentiometric response for all membrane based sensors.

For the ion exchange membranes the potential versus pH profiles show that the electrodes do not respond to pH changes in the ranges 2.5–6 for sensors IX and XI and pH 4–12.5 for sensors VI, VII, VIII, and X. Only sensors IX and XI showed the effect of the severe precipitation of metals taking place in the alkaline range. All other sensors showed no effect from pH within this range. This is most evidently an abnormal behaviour for which no logical explanation may be found.

Because the solubility and ionisation of Fe(II) were both promoted by acidic solutions, studies under constant pH were carried out in the acidic range.

Evaluation of main operating features for all electrodes under constant pH was carried out in several buffer solutions prepared with different pHs within 2 and 6. Results showed that electrodes provided slopes ranging 67.0 to 202.2 mV decade-1 in citric acid pH 2.5, 33.3 to 40.6 mV decade-1 in citric acid pH 4, and 29.4 to 137.7 mV decade-1 in citric acid pH 6, over a wide concentration range. Best general analytical features for all electrodes were achieved with citrate buffer of pH 4.

3.5. Response Time. The dynamic response times of the sensors were examined by recording the potential readings at time intervals of 10 s over 2 min. The time required to reach 95% of equilibrium was ~20 s for electrodes [I, III, and V] with a recovery time ~30 and ~30 s for electrodes [II and IV] with a recovery time ~50 s. These results indicate that both sensors are amenable for use with automated systems.

3.6. Selectivity Studies. The selectivity of the chemical sensor is one of the most important potentiometric features. One component of the selective membrane exerting great influence upon this property is the electroactive material, as the mechanism of selectivity is mainly based on stereospecificity and electrostatic environment. It is dependent on how much fitting is present between locations of the lipophilicity sites in the two competing species in the bathing solution side and those present in the sensor [53]. The performance of the ferroin sensor in the presence of some cations was assessed by measuring the selectivity coefficient values log $K^{POT}_{Fe^{2+},J^{z+}}$ using the separate solutions method [54]. The results obtained showed no effect for high concentrations (>1000-fold excess) of many common cations such as NH_4^+, Na^+, K^+, Ba^{2+}, Ca^{2+}, and Mg^{2+}. These cations do not form complexes with 1,l0-phenanthroline reagent. Metal ions known to form insoluble metal phenanthroline chelates or metal halides (e.g., Pb^{2+}, Hg^{2+}, and Ag^+) did not interfere. Metals which form water soluble charged complexes with phenanthroline such as Zn^{2+}, Cu^{2+}, Ni^{2+}, and Cd^{2+} interfered seriously but interferences caused by these cations were completely circumvented by using suitable masking agents. The response behavior of the MIP and NIP membrane-based sensors towards these complexed cations were presented in Figure 4.

3.7. Analytical Application. In order to access the applicability of the iron selective electrodes, the potentiometric method was applied for the determination of iron in different materials of various natures by formation of ferroin followed by monitoring with the IIP-ferroin sensor. Iron contents (0.05–0.30 mg L^{-1}) of different tap water collected from the laboratory taps and were added of buffer prior to analysis in order to ensure similar background as that of standard solutions were determined. The samples spiked with various standard iron concentrations display results agreed fairly well within ±1.5% with those obtained with the standard spectrophotometric method. Determination of Fe^{2+} in the presence of large quantities of Fe^{3+} has received considerable attention in corrosion and environmental studies. Several reports confirmed that the spectrophotometric ferroin method for determining Fe^{2+} in the presence of excess Fe^{3+} is not reliable and the recovery of Fe^{2+} is always high [55].

Table 2: Potentiometric determination of iron in some pharmaceutical formulation samples using the proposed ferroin sensors.

Trade name	Nominal iron (mg/tablet)	Iron recovery (%)*		
		IIP sensor		Standard method
		Static	Hydrodynamic	
Centrum	14	95 ± 0.5	93 ± 1.1	98 ± 0.1
(Wyeth, Portugal)	90	98 ± 0.1	96 ± 0.4	99 ± 0.3

Table 3: Analytical features of the present method reported in the literature.

Technique/method	Principle of the method	Detection limit (mg/L)	Linear range (mg/L)	Repeatability (%)	Application	Sample preparation	Ref.
UV/Vis	Iron complex with 1-nitroso-2-naphhtol (446 nm)	1.7×10^{-3}	1.7×10^{-3}–0.12	2.57	Industrial waste water	(SPE)	[2]
	Catalytic spectrophotometric flow injection (514 nm)	20×10^{-3}	Up to 2×10^{-6}		Real water samples	Filtered water samples were acidified to 0.1 M hydrochloric acid)	[3]
	Adaptation of the ferrozine method (560 nm)	5850	1755 to 23400	2	In situ analysis	No	[7]
	Reaction betwen hydroquinone and chromate in acidic media (350 nm)	0.05	—	—	—	No	[8]
Chemiluminescence	Neutralisation reaction	0.56	2.8–560	—	Fresh water samples	Reduction of iron(III) with	[13]
	—	5.85×10^{-5}	14625 to 87750	—	Fresh water samples	Hydroxylammonium chloride	[14]
HPLC	Photometric detection (550 nm)	0.2×10^{-3}	10×10^{-3} to 10	—	Spiked tap water	No	[55]
Potentiometry/ISE	Chiral 2,6-bis-(carboxamide methyl ester)pyridine derivative sensor, PVC membrane		0.25–56.0	—	Drug formulations	—	[56]
	IIP sensor in a PVC selective membrane	4.45	0.014	2.4	Pharmaceutical formulation samples	No	This method

In the present work, mixtures of Fe^{2+} and Fe^{3+} covering the concentration ratios of 1 : 1 to 1 : 50 (Fe^{2+} : Fe^{3+}) were prepared and treated with l, l0-phenanthroline at pH 4.7. After a reaction time of 1 min, EDTA was added to mask Fe^{3+}, and $[Fe(phen)_3]^{2+}$ was potentiometrically measured with the ferroin sensor. In a second run, the total iron [Fe^{2+} and Fe^{3+}] was assessed by a prior reduction with hydroxylamine and formation and measurement of ferroin. Results with average recoveries of 98.4% (S.D. = 1.5%) and 95.7% (S.D. = 1.4%) were obtained ($n = 4$) for iron(II) and iron(III), respectively.

The proposed sensor was also used to determine iron in pharmaceutical preparations both in batch and in flow conditions. The results obtained with some polyvitamin/mineral tablets and capsules showed an average recovery of 95.5% of the nominal value and a mean standard deviation of ±0.9% (Table 2). These results were checked and confirmed by an independent method from the pharmacopoeia. The results obtained showed a close agreement between the data of the spectrophotometry and ferroin sensor, thus confirming the accuracy of the proposed method.

4. Conclusions

Proposed Fe potentiometric detectors are simple, of low cost, and easy to manipulate. The electrodes based on dispersion of mimic receptor for ferroin in PVC matrix and plasticized in *o*-NPOE might be useful detectors for analysis of environmental waters. They display high selectivity and wide dynamic response range. In general, the overall procedure is precise, accurate, and inexpensive regarding

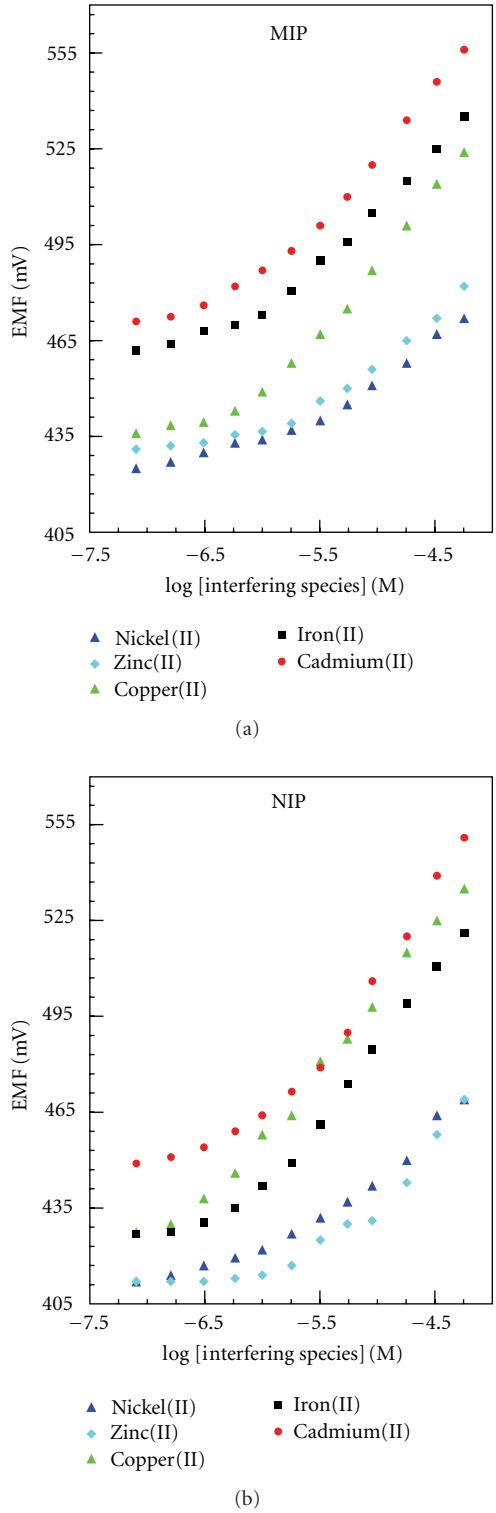

Figure 4: The response behavior of the proposed sensors towards different metal ion complexes.

reagent consumption and equipment involved, especially compared to other methods previously reported (Table 3). Considering its routine application, a main advantage arises from composition and quantity of emitted effluents, with small concern in terms of environmental issues. Aside from dilution with buffer, no sample pretreatment or separation steps are required.

References

[1] L. S. G. Teixeira and F. R. P. Rocha, "A green analytical procedure for sensitive and selective determination of iron in water samples by flow-injection solid-phase spectrophotometry," *Talanta*, vol. 71, no. 4, pp. 1507–1511, 2007.

[2] G. A. Shar and G. A. Soomro, "Derivative spectrophotometric determination of nickel (II) with 1-nitroso-2-naphthol in aqueous phase," *Journal of the Chemical Society of Pakistan*, vol. 28, p. 39, 2006.

[3] S. Lunvongsa, M. Oshima, and S. Motomizu, "Determination of total and dissolved amount of iron in water samples using catalytic spectrophotometric flow injection analysis," *Talanta*, vol. 68, no. 3, pp. 969–973, 2006.

[4] S. Lunvongsa, T. Tsuboi, and S. Motomizu, "Sequential determination of trace amounts of iron and copper in water samples by flow injection analysis with catalytic spectrophotometric detection," *Analytical Sciences*, vol. 22, no. 1, pp. 169–172, 2006.

[5] M. A. Feres and B. F. Reis, "A downsized flow set up based on multicommutation for the sequential photometric determination of iron(II)/iron(III) and nitrite/nitrate in surface water," *Talanta*, vol. 68, no. 2, pp. 422–428, 2005.

[6] N. Devanna, K. P. Satheesh, and K. B. C. Sekhar, "Derivative spectrophotometric determination of iron(II) using diacetylmonoxime benzoyl hydrazone," *Asian Journal of Chemistry*, vol. 17, no. 3, pp. 1767–1772, 2005.

[7] P. M. Sarradin, N. Le Bris, C. Le Gall, and P. Rodier, "Fe analysis by the ferrozine method: adaptation to FIA towards in situ analysis in hydrothermal environment," *Talanta*, vol. 66, no. 5, pp. 1131–1138, 2005.

[8] D. Mihai, A. Rustoiu-Csavdari, and I. Baldea, "Potential application of the reaction between hydroquinone and chromate with respect to the kinetic determination of iron," *Analytical and Bioanalytical Chemistry*, vol. 381, no. 7, pp. 1362–1366, 2005.

[9] P. K. Tarafder and R. Thakur, "Surfactant-mediated extraction of iron and its spectrophotometric determination in rocks, minerals, soils, stream sediments and water samples," *Microchemical Journal*, vol. 80, no. 1, pp. 39–43, 2005.

[10] V. M. Ostrovskaya, N. V. Davidovskii, O. A. Prokopenko, and D. A. Man'Shev, "Rapid test determination of iron(II) in aqueous media by reagent indicator paper," *Journal of Analytical Chemistry*, vol. 59, no. 9, pp. 882–884, 2004.

[11] J. H. Chen, Q. F. Hu, G. Y. Yang, and J. Y. Yin, "Solid phase extraction and spectrophotometric determination of iron in water with 8-hydroxyquinadine," *Chinese Journal oF Analytica l Chemistry*, vol. 31, p. 853, 2003.

[12] A. Asan, M. Andac, and I. Isildak, "Flow-injection spectrophotometric determination of nanogram levels of iron(III) with N,N-dimethylformamide," *Analytical Sciences*, vol. 19, no. 7, pp. 1033–1036, 2003.

[13] B. R. M. Al-Gailani, G. M. Greenway, and T. McCreedy, "A miniaturized flow-injection analysis (μFIA) system with on-line chemiluminescence detection for the determination of iron in estuarine water," *International Journal of Environmental Analytical Chemistry*, vol. 87, no. 9, pp. 637–646, 2007.

[14] M. Yaqoob, A. Waseem, and A. Nabi, "Determination of total iron in fresh waters using flow injection with potassium permanganate chemiluminescence detection," *Journal of Analytical Chemistry*, vol. 61, no. 9, pp. 917–921, 2006.

[15] J. G. Lv and Z. J. Zhang, "A microchip with air sampling and chemiluminescence detection for analyzing iron in nature water and in whole blood," *Analytical Letters*, vol. 37, no. 7, pp. 1401–1408, 2004.

[16] G. H. Zhu, H. X. Ju, and B. F. Ye, "A sensitive fluorescence quenching method for the determination of iron(II) with 1,10-phenanthroline," *Chinese Journal of Chemistry*, vol. 21, no. 2, pp. 301–320, 2003.

[17] W. Qin, Z. J. Zhang, and F. C. Wang, "Chemiluminescence flow system for the determination of Fe(II) and Fe(III) in water," *Fresenius Journal of Analytical Chemistry*, vol. 360, no. 1, pp. 130–132, 1998.

[18] S. Saracoglu, M. Soylak, D. S. K. Peker et al., "A preconcentration procedure using coprecipitation for determination of lead and iron in several samples using flame atomic absorption spectrometry," *Analytica Chimica Acta*, vol. 575, no. 1, pp. 133–137, 2006.

[19] Y. Bakircioglu, D. Bakircioglu, and N. Tokman, "A novel preconcentration method for determination of iron and lead using Chromosorb-103 and flame atomic absorption spectrometry," *Analytica Chimica Acta*, vol. 547, no. 1, pp. 26–30, 2005.

[20] S. Tautkus, L. Steponeniene, and R. Kazlauskas, "Determination of iron in natural and mineral waters by flame atomic absorption spectrometry," *Journal of the Serbian Chemical Society*, vol. 69, no. 5, pp. 393–402, 2004.

[21] P. C. Aleixo and J. A. Nobrega, "Direct determination of iron and selenium in bovine milk by graphite furnace atomic absorption spectrometry," *Food Chemistry*, vol. 83, no. 3, pp. 457–462, 2003.

[22] A. Ohashi, H. Ito, C. Kanai, H. Imura, and K. Ohashi, "Cloud point extraction of iron(III) and vanadium(V) using 8-quinolinol derivatives and Triton X-100 and determination of 10-7 mol dm -3 level iron(III) in riverine water reference by a graphite furnace atomic absorption spectroscopy," *Talanta*, vol. 65, no. 2, pp. 525–530, 2005.

[23] N. Y. Stozhko, O. V. Inzhevatova, and L. I. Kolyadina, "Determination of iron in natural and drinking Waters by stripping voltammetry," *Journal of Analytical Chemistry*, vol. 60, no. 7, pp. 668–672, 2005.

[24] A. Bobrowski, K. Nowak, and J. Zarebski, "Application of a bismuth film electrode to the voltammetric determination of trace iron using a Fe(III)-TEA-BrO3- Catalytic system," *Analytical and Bioanalytical Chemistry*, vol. 382, no. 7, pp. 1691–1697, 2005.

[25] H. Yan and K. H. Row, "Characteristic and synthetic approach of molecularly imprinted polymer," *International Journal of Molecular Science*, vol. 7, no. 5, pp. 155–178, 2006.

[26] A. Katz and M. E. Davis, "Molecular imprinting of bulk, microporous silica," *Nature*, vol. 403, no. 6767, pp. 286–289, 2000.

[27] S.L. Gong, Z.J. Yu, L.Z. Meng, L. Hu, and Y.B. He, "E-molecular-imprinted polysiloxanes. II. Preparation, characterization, and recognition behavior," *Journal of Applied Polymer Science*, vol. 93, p. 637, 2004.

[28] T. Kobayashi, H. Y. Wang, and N. Fujii, "Molecular imprint membranes of polyacrylonitrile copolymers with different acrylic acid segments," *Analytica Chimica Acta*, vol. 365, no. 1-3, pp. 81–88, 1998.

[29] T. Takeuchi and J. Haginaka, "Separation and sensing based on molecular recognition using molecularly imprinted polymers," *Journal of Chromatography B*, vol. 728, no. 1, pp. 1–20, 1999.

[30] G. Wulff, "Molecular imprinting in cross-linked materials with the aid of molecular templates—a way towards artificial antibodies," *Angewandte Chemie*, vol. 34, no. 17, pp. 1812–1832, 1995.

[31] H. Zheng, D. Zhang, W. Y. Wang, Y. Q. Fan, J. Li, and H. P. Han, "Highly selective determination of palladium(II) after preconcentration using Pd(II)-imprinted functionalized silica gel sorbent prepared by a surface imprinting technique," *Microchimica Acta*, vol. 157, p. 7, 2007.

[32] A. Ersöz, R. Say, and A. Denizli, "Ni(II) ion-imprinted solid-phase extraction and preconcentration in aqueous solutions by packed-bed columns," *Analytica Chimica Acta*, vol. 502, no. 1, pp. 91–97, 2004.

[33] N. Jiang, X. J. Chang, H. Zheng, Q. He, and Z. Hu, "Selective solid-phase extraction of nickel(II) using a surface-imprinted silica gel sorbent," *Analytica Chimica Acta*, vol. 577, no. 2, pp. 225–231, 2006.

[34] X. J. Chang, N. Jiang, H. Zheng et al., "Solid-phase extraction of iron(III) with an ion-imprinted functionalized silica gel sorbent prepared by a surface imprinting technique," *Talanta*, vol. 71, no. 1, pp. 38–43, 2007.

[35] G. Z. Fang, J. Tan, and X. P. Yan, "An ion-imprinted functionalized silica gel sorbent prepared by a surface imprinting technique combined with a sol-gel process for selective solid-phase extraction of cadmium(II)," *Analytical Chemistry*, vol. 77, p. 1734, 2005.

[36] F. Li, H. Q. Jiang, and S. S. Zhang, "An ion-imprinted silica-supported organic-inorganic hybrid sorbent prepared by a surface imprinting technique combined with a polysaccharide incorporated sol-gel process for selective separation of cadmium(II) from aqueous solution," *Talanta*, vol. 71, no. 4, pp. 1487–1493, 2007.

[37] Q. He, X. J. Chang, H. Zheng, N. Jiang, Z. Hu, and Y. Zhai, "Preconcentration and separation of Zn2+ using surface zinc(II) imprinted functionalized silica gel sorbent," *Chemia Analityczna*, vol. 51, no. 5, pp. 715–725, 2006.

[38] I. Fujiwara, A. Uchiyama, Y. Sasaki, M. Maeda, and M. Takagi, "Preparation of CuII-imprinted microspheres with imidazole groups at the surfaces by surface imprinting polymerization," *Bunseki Kagaku*, vol. 52, no. 2, pp. 147–150, 2003.

[39] N. Zhang, B. Hu, and C. Z. Huang, "A new ion-imprinted silica gel sorbent for on-line selective solid-phase extraction of dysprosium(III) with detection by inductively coupled plasma-atomic emission spectrometry," *Analytica Chimica Acta*, vol. 597, no. 1, pp. 12–18, 2007.

[40] S. Y. Bae, G. L. Southard, and G. M. Murray, "Molecularly imprinted ion exchange resin for purification, preconcentration and determination of UO22+by spectrophotometry and plasma spectrometry," *Analytica Chimica Acta*, vol. 397, no. 1–3, pp. 173–181, 1999.

[41] G. D. Saunders, S. P. Foxon, P. H. Walton, M. J. Joyce, and S. N. Port, "A selective uranium extraction agent prepared by polymer imprinting," *Chemical Communications*, no. 4, pp. 273–274, 2000.

[42] J. M. Gladis and T. P. Rao, "Synthesis and analytical applications of uranyl ion imprinted polymer particles," *Analytical Letters*, vol. 36, no. 10, pp. 2107–2121, 2003.

[43] T. Rosatzin, L. I. Andersson, W. Simon, and K. Mosbach, "Preparation of Ca2+ selective sorbents by molecular imprinting using polymerisable ionophores," *Journal of the Chemical Society*, vol. 2, no. 8, pp. 1261–1265, 1991.

[44] R. Kala, J. M. Gladis, and T. P. Rao, "Preconcentrative separation of erbium from Y, Dy, Ho, Tb and Tm by using ion imprinted polymer particles via solid phase extraction," *Analytica Chimica Acta*, vol. 518, no. 1-2, pp. 143–150, 2004.

[45] S. Büyüktiryaki, R. Say, A. Ersöz, E. Birlik, and A. Denizli, "Selective preconcentration of thorium in the presence of UO 22+, Ce3+ and La3+ using Th(IV)-imprinted polymer," *Talanta*, vol. 67, no. 3, pp. 640–645, 2005.

[46] Y. Liu, X. Chang, D. Yang, Y. Guo, and S. Meng, "Highly selective determination of inorganic mercury(II) after preconcentration with Hg(II)-imprinted diazoaminobenzene–vinylpyridine copolymers," *Analytica Chimica Acta*, vol. 538, p. 85, 2005.

[47] O. Vigneau, C. Pinel, and M. Lemaire, "Ionic imprinted resins based on EDTA and DTPA derivatives for lanthanides(III) separation," *Analytica Chimica Acta*, vol. 435, no. 1, pp. 75–82, 2001.

[48] O. Vigneau, C. Pinel, and M. Lemaire, "Solid-liquid separation of lanthanide/lanthanide and lanthanide/actinide using ionic imprinted polymer based on a DTPA derivative," *Chemistry Letters*, no. 2, pp. 202–203, 2002.

[49] S. S. M. Hassan, *Organic Analysis Using Atomic Absorption Spectrometry*, Ellis Horwood, Chichester, UK, 1984.

[50] R. Arshady and K. Mosbach, "Synthesis of substrate-selective polymers by host-guest polymerization," *Makromolekulare Chemie*, vol. 182, pp. 687–692, 1981.

[51] A. H. Kamel, F. T. C. Moreira, S. A. A. Almeida, and M. G. F. Sales, "Novel potentiometric sensors of molecular imprinted polymers for specific binding of chlormequat," *Electroanalysis*, vol. 20, no. 2, pp. 149–202, 2008.

[52] N. T. A. Ghani, M. S. Rizk, and R. M. El-Nashar, "Salbutamol plastic membrane electrodes based on individual and mixed ion-exchangers of salbutamolium phosphotungstate and phosphomolybdate," *Analyst*, vol. 125, no. 6, pp. 1129–1133, 2000.

[53] IUPAC, "Analytical Chemistry Division Commission on Analytical Nomenclature," *Pure and Applied Chemistry*, vol. 72, p. 1851, 2000.

[54] H. Fadrus and J. Maly, "Suppression of iron(III) interference in the determination of iron(II) in water by the 1,10-phenanthroline method," *The Analyst*, vol. 100, no. 1193, pp. 549–554, 1979.

[55] P. G. Rigas and D. J. Pietrzyk, "Indirect photometric detection in liquid chromatography using iron(II)-1,10-phenanthroline complex as a mobile phase additive: origin, calibration and parameters," *Analytical Chemistry*, vol. 60, pp. 454–459, 1988.

[56] M. A. Abounassif, M. A. Al-Omar, A.-G. E. Amr, and G. A. E. Mostafa, "PVC membrane sensor for potentiometric determination of iron (II) in some pharmaceutical formulations based on a new neutral ionophore," *Drug Testing and Analysis*, vol. 3, pp. 373–379, 2011.

SAGE-Hindawi Access to Research
International Journal of Electrochemistry
Volume 2011, Article ID 764294, 10 pages
doi:10.4061/2011/764294

Research Article

Voltammetric Determination of Acetaminophen in the Presence of Codeine and Ascorbic Acid at Layer-by-Layer MWCNT/Hydroquinone Sulfonic Acid-Overoxidized Polypyrrole Modified Glassy Carbon Electrode

Saeed Shahrokhian[1, 2] and Reyhaneh-Sadat Saberi[1]

[1] *Department of Chemistry, Sharif University of Technology, Tehran 11155-9516, Iran*
[2] *Institute for Nanoscience and Technology, Sharif University of Technology, Tehran 11155-9516, Iran*

Correspondence should be addressed to Saeed Shahrokhian, shahrokhian@sharif.edu

Received 26 March 2011; Revised 19 May 2011; Accepted 21 May 2011

Academic Editor: Farnoush Faridbod

Copyright © 2011 S. Shahrokhian and R.-S. Saberi. This is an open access article distributed under the Creative Commons Attribution License, which permits unrestricted use, distribution, and reproduction in any medium, provided the original work is properly cited.

A very sensitive electrochemical sensor constructed of a glassy carbon electrode modified with a layer-by-layer MWCNT/doped-overoxidized polypyrrole (oppy/MWCNT /GCE) was used for the determination of acetaminophen (AC) in the presence of codeine and ascorbic acid (AA). In comparison to the bare glassy carbon electrode, a considerable shift in the peak potential together with an increase in the peak current was observed for AC on the surface of oppy/MWCNT/GCE, which can be related to the enlarged microscopic surface area of the electrode. The effect of the experimental conditions on the electrode response, such as types of counter ion, pyrrole and counter ion concentration, potential and number of cycles in the polymerization procedure, amount of MWCNT, and the pH, were investigated. Under the optimized conditions, the calibration curve was obtained over two concentration ranges of 2×10^{-7}–6×10^{-6} M and 4×10^{-5}–1×10^{-4} M of AC with a linear correlation coefficient (R^2) of 0.9959 and 0.9947, respectively. The estimated detection limit (3σ) for AC was obtained as 5×10^{-8} M. The developed method was successfully applied to analyze the pharmaceutical preparations of AC, and a recovery of 95% with a relative standard deviation of 0.98% was obtained for AC.

1. Introduction

The remarkable application potential of conducting polymers (CP) in chemical and biological sensors is one of the main reasons for the intensive investigation and development of the studies on these materials [1]. In the case of polypyrrole (ppy), useful features considered include its capacity to form adhesive coatings at different substrates, the possibility of growing it in aqueous media, easiness for chemical substitution to modify its properties, high porosity that enables fast kinetics of ion exchange with the surrounding medium, high electronic conductivity, high chemical stability, thickness controllability, ease of electrochemical polymerization, and good reversibility between its conducting and insulating states. These characteristics make ppy suitable in various electrochemical determinations including voltammetric and potentiometric [2], amperometric [3], and impedimetric [4, 5] techniques for the determination of various molecular species.

Polypyrrole in its oxidized form is a positively charged conducting polymer. Upon the overoxidation process, it loses its conductivity and charge and instead, its porosity would be improved. Characterization of these films revealed that overoxidation results in addition of carbonyl and carboxyle groups to the structure of the conducting polymer. These groups attract cationic species and reciprocally reject negatively charged ones, for example, ascorbate anions [6].

Carbon nanotubes (CNT) are considered as a novel form of carbon materials in two past decades [7]. In the recent years, carbon nanotubes (CNTs) have also been incorporated into the electrochemical sensors. While they have many properties of the other types of carbon, they offer unique

advantages including enhanced electronic properties, a large edge/basal plane ratio, and facile kinetics of the electrode processes. Therefore, in comparison to the traditional carbon electrodes, CNT-based sensors generally have higher sensitivities, lower limits of detection, and faster electron transfer kinetics [8].

Composites of intrinsically conducting polymer (ICP) are materials that utilize conjugated polymers with at least one secondary component that can be inorganic/organic materials or biologically active species. The goal is to produce a new composite material with distinct properties that were not observed in the individual components. This may include either new or improved chemical properties that can be exploited for chemical or biological sensing. Addition of carbon nanotubes as secondary component drastically influences the electrical and thermal conductivity of ICPs [9]. Sensor modification by this method is performed in two ways: layer by layer [10] and electropolymerization in a mixture of monomer and CNT [11, 12]. These modifications have concentrated on improving the electrical conductivity, mechanical strength, or electrochemical capacitance of the polymer. These polymer/CNT modified electrodes have been used successfully in electrochemical sensing applications [13, 14].

Acetaminophen (paracetamol, N-acetyl-p-aminophenol, AC) is an extensively used antipyretic analgesic drug and a suitable alternative for patients who are sensitive to aspirin [15]. Generally, AC does not exhibit any harmful side effects, but hypersensitivity or overdoses are known to cause severe liver and kidney damages, and adverse effects include rashes, blood dyscrasias, and pancreatitis [16, 17]. Therefore, acetaminophen quantity control in pharmaceutical formulation is vital since, as mentioned above, overdosage could be dangerous.

AC as an analgesics drug is often used in the presence of other drugs like; aspirin, cetirizine, tramadol, and codeine. So acetaminophen determination could be affected by the second ingredient in pharmaceutical formulation. Development of a method that could determine acetaminophen in pharmaceutical and clinical preparations without any interference from the other ingredient is of great importance. Since the electrochemical detection of AC has advantages including low cost, fast response, simple instrumentations, high sensitivity, and facile miniaturization, this kind of method has attracted a lot of attentions. Various electrodes such as poly(taurine)/MWCNT/GCE [18], nano-TiO_2/polymer/GCE [19], polypyrrole modified glassy carbon electrode [20], multiwall carbon nanotube (MWCNT) modified basal plane pyrolytic graphite electrode [21], single-walled carbon nanotube-film coated electrodes [22], polyaniline/MWCNT composite modified electrodes [23], carbon film resistor electrodes [24], gold nanoparticle modified carbon paste electrode [25], and thionine-immobilized multiwalled carbon nanotube modified carbon paste electrode [26] have been used for the voltammetric detection of AC.

In the present work, an oppy-MWCNT modified electrode has been fabricated by a new counter ion, hydroquinone sulfonic acid (HQSA). Cyclic voltammetry was used to investigate the electrocatalytic oxidation of AC at oppy-MWCNT modified electrode. The results show a considerable increase in the corresponding peak current (up to 6-times) together with a decrease in the peak potential (~110 mV). Differential pulse voltammetry (DPV) was successfully used for the AC determinations in the presence of AA and codeine. Effects of pyrrole and counter ion concentration, potential, and number of cycles for polymerization, volume of the casted MWCNT suspension, and pH value of the test solution on the current response of the modified electrode toward AC were investigated and optimized. The prepared electrochemical sensor showed some remarkable advantages, for example, low detection limit, excellent reproducibility, and relatively wide linear dynamic range.

2. Experimental

2.1. Chemicals. Multi-wall carbon nanotubes (MWCNT, purity > 95%) with outer diameter less than 10 nm and tubes length of 5–15 μm were prepared from Nanostructured & Amorphous Materials (USA). Acetaminophen (AC) and ascorbic acid (AA) were from Merck. Codeine was taken kindly from Kharazmi drug Company. Hydroquinone sulfonic acid (HQSA) was purchased from Fluka and used as counter ion, in the electropolymerization procedure. Pyrrole and dimethylformamide (DMF) were purchased from Merck. Stock solutions of AC were freshly prepared as required in 0.1 M of appropriate buffer solutions. In these experiments, 0.1 M acetate was used for preparation of pHs 4 and 5, and 0.1 M phosphate for pHs 3, 6, and 7. Aqueous solutions were prepared using doubled distilled water, which is prepared over the alkaline dilute permanganate solution. All solutions were deaerated by purging with nitrogen gas (99.999%) prior to each experiment. During the experiments, nitrogen gas was passed over the surface of the test solutions in order to avoid entrance of oxygen into the solution.

2.2. Apparatus. All electrochemical measurements were performed with a Metrohm Computrace Voltammetric Analyzer (model 757 VA) instrument. An electrochemical cell with a three-electrode configuration was used with a glassy carbon electrode (3 mm diameter, Princeton Applied Research, unmodified and/or modified) as working electrode. Counter and reference electrodes were a pt wire and saturated Ag/AgCl electrode, respectively.

A digital pH/mV/Ion meter (Metrohm, 827 pH lab) was utilized for preparation of the buffer solutions, which were used as supporting electrolyte in the voltammetric experiments.

2.3. Preparation of the Modified Electrode. Besides the fact that conducting polymers exhibit interesting properties, the rate of their interconversion is usually slow, because of the slow transport of counter ions into the polymer layer to maintain the charge balance. It is found that nanotubular structures are good candidates for realizing rapid switching between redox states. For this purpose, the appropriate

amount of pure MWCNT was functionalized under concentrated nitric acid treatment process for 24 hours in order to obtain more edge sites and better dispersion of nanotubes [27, 28]. After functionalization procedure, 1 mg of the functionalized MWCNT (CNT-COOH) was dispersed in 1 mL of DMF solvent under ultrasonic agitation for 1 h prior to use. Then a 15 μL of the dispersed CNTs was taken with a microsyringe, and after casting on the electrode surface, the electrode was heated in oven at 50°c for 15 min. The electrode was then kept in room temperature for 1 hour (named MWCNT/GC electrode). The electrodeposition of the ppy film on the surface of GC electrode precoated with CNT was carried out from an aqueous solution containing 0.02 M HQSA and 0.02 M pyrrole by potential cycling between 0.0 V and +0.75 V (*versus* Ag/AgCl) at scan rates of 50 mVs^{-1} for a total of five scans (Figure 1). Since the counter ion (HQSA) appears as an electroactive species, as seen in Figure 1, the corresponding redox peak currents are increased by progressing the electropolymerization procedure. The increase in the redox peak current via polymerization reveals more surface active area for the polymer-modified electrode. These advantages for HQSA make it as an interesting counter ion that affects various properties of the prepared conducting polymer in its applications as an electrochemical sensor. After the electropolymerization procedure, the electrode was overoxidized by potential cycling between −0.2 V to 1.3 V (*versus* Ag/AgCl) at scan rate of 100 mVs^{-1} for a total of thirty scans in buffer solution of pH 7.0. This electrode recognized as oppy/MWCNT/GCE in the following parts. On the other hand, in comparison to ppy films on the bare GC electrode formed under similar conditions, the polymer films on CNT were notably less brittle and more adhesive to the electrode surface.

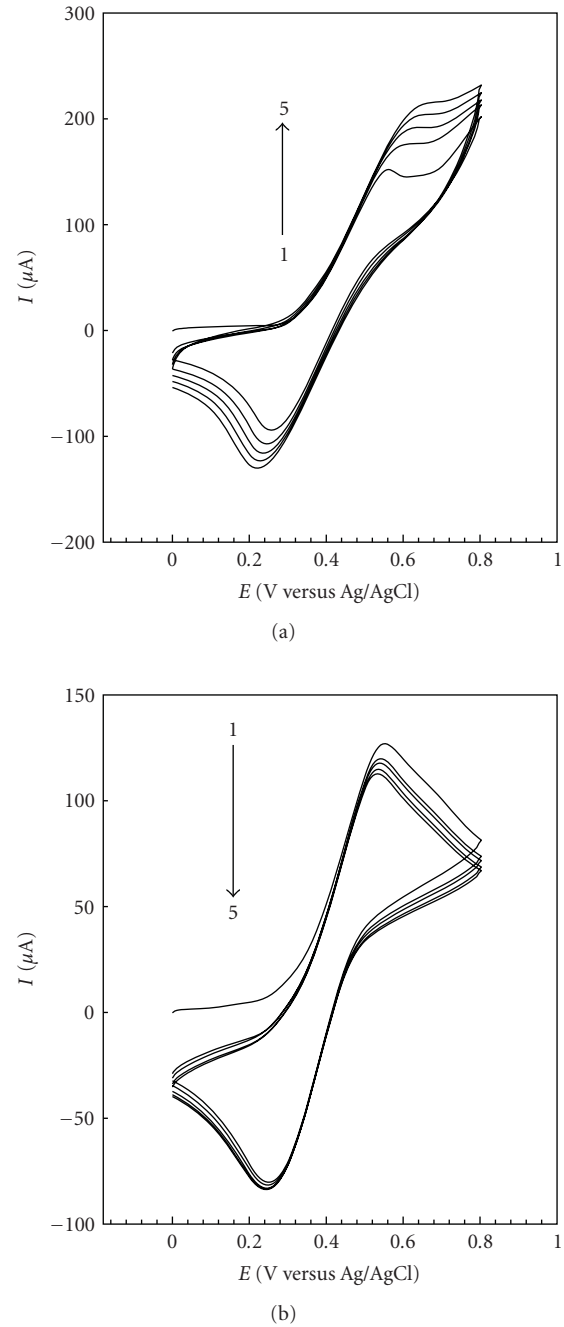

Figure 1: Consecutive cyclic voltammograms of (a) 0.02 M pyrrole and 0.02 M HQSA during electropolymerization process and (b) 0.02 M HQSA.

3. Results and Discussion

3.1. AFM Studies on the Electrode Surface. It has been reported that the overoxidation process on ppy films caused the increase of the porosity of the polymer film and created negative sites via carboxylate groups formed in its structure [6]. In order to prove the effect of the overoxidation on the porosity of the ppy film, the AFM images were obtained for MWCNT/GCEs, coated with ppy and over oxidized ppy. As can be seen in Figure 2, the overoxidation creates some grooves and pores in polymer film, leading to increase of the microscopic area of the electrode and facilitating the interlayer diffusion of the analyte species. Therefore, it can be predicted that by using this modified electrode, higher sensitivities in the electrochemical responses can be obtained.

3.2. Cyclic Voltammetric Studies. The electrochemical behavior of AC was investigated by the means of cyclic voltammetry (CV) technique on the surface of different electrodes including bare glassy carbon electrode (GC), glassy carbon electrode coated with CNT (MWCNT/GC), and layer-by-layer modified electrode (oppy/MWCNT/GCE), respectively. As can be seen in Figure 3, the electrooxidation of AC is very weak and totally irreversible on the surface of bare GC. On the other hand, on the surface of the nanotube-modified electrode (MWCNT/GCE), the peak current is remarkably increased from about 11 μA to 68 μA (up to 6-times) associated with a significant negative shift in the anodic peak potential (~110 mV). The investigations showed that the anodic peak current for AC oxidation on the surface of the oppy/MWCNT/GCE is about 1.5-times greater than that at glassy carbon electrode coated with only a film of nanotube (MWCNT/GCE). It means that the electropolymerization,

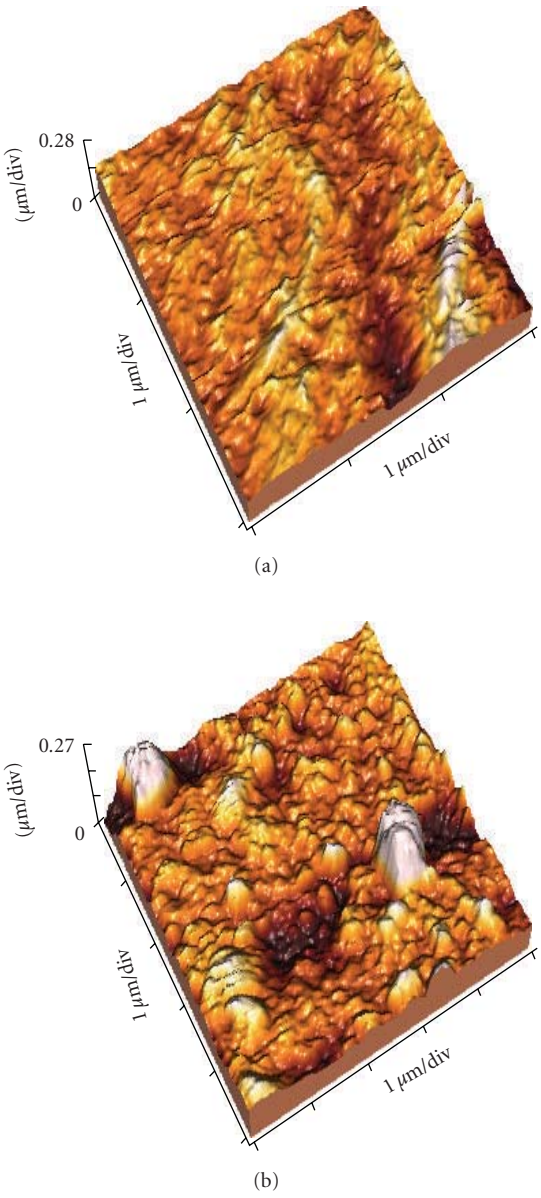

Figure 2: AFM image of (a) ppy/MWCNT/GCE and (b) oppy/MWCNT/GCE.

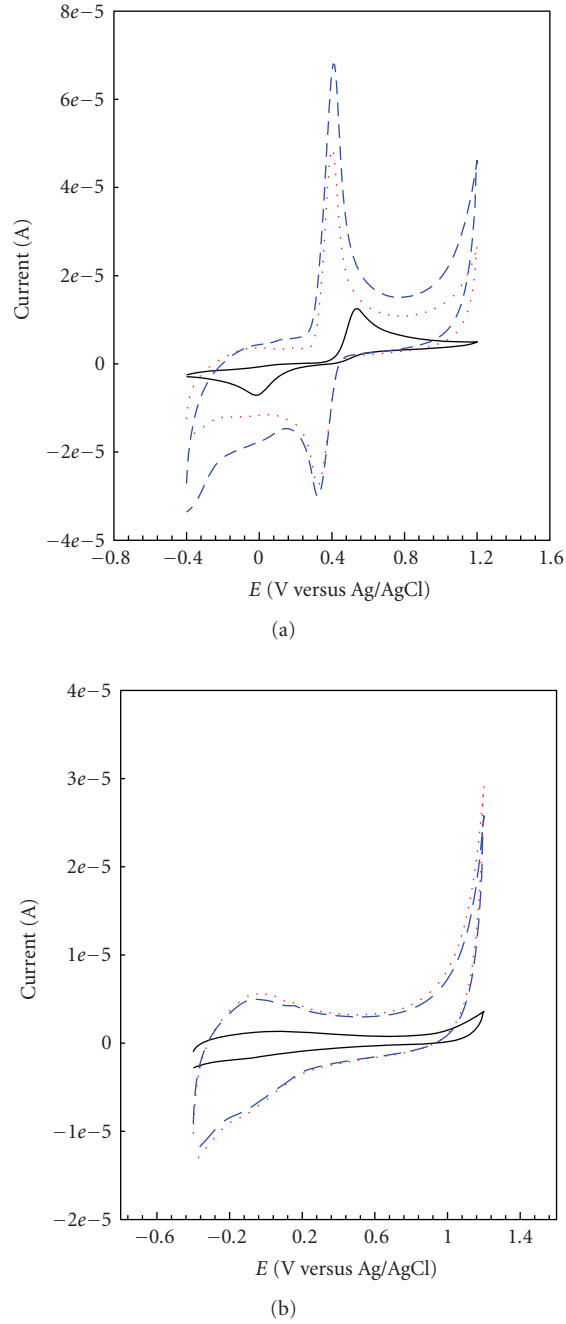

Figure 3: Cyclic voltammograms of various electrodes; bare GCE (—), CNT-GCE (· · ·), and oppy/MWCNT/GCE (- - -). (a) 0.1 mM AC and (b) buffer solution. Potential sweep rate was 100 mV s^{-1} and supporting electrolyte was 0.1 M phosphate buffer solution of pH 7.0.

and consequently overoxidation process, increased the active surface area of the electrode. On the other hand, by application of the oppy/MWCNT modified electrode the kinetics of the electron transfer for the electro-oxidation of AC is considerably improved (Figure 3). The catalytic activity of the modifier film caused a considerable decrease in the activation overpotential, increasing the sharpness of the waves and reversibility of the electrode process. It is obvious that the roughness characteristic of the electrode surface has a significant effect on the diffusion mechanism into the porous modifier film. The results of investigations showed that the overoxidized polymer on MWCNT/GCE has a more porous structure in relation to ordinary polymer on the surface of the MWCNT coated electrode. This improved porosity enhances the diffusion of the analyte species via interlayer diffusion through the modifier thin film [6, 29–32]. A synergetic effect of the porosity of the overoxidized polymer/nanotube and great edge sites in the structure of functionalized MWCNT, which enhanced the catalytic effect of nanotube [29–32], resulted in very sharp and reversible voltammetric responses of AC.

3.3. Effects of pH and Potential Sweep Rate. In order to achieve the optimum pH for the anodic oxidation of AC on the surface of oppy/MWCNT/GCE, the electrochemical behavior was investigated in various pHs of the buffered solutions (pH = 3.0–7.0). From the results of cyclic voltammetric investigations (data not shown) the modified electrode shows electrochemical responses with very good sensitivity and repeatability in physiological conditions of pH 7.0. Since the more appropriate condition for analysis in biological samples is pH 7.0, all experiments were performed in phosphate buffer solutions of this pH as supporting electrolyte. On the other hand, the negative shift in anodic peak potential ($E_{p,a}$) with pH can be described by the following equation:

$$E_{p,a} = +0.8164 - 0.057\text{pH} \quad \left(\text{V versus } \frac{\text{Ag}}{\text{AgCl}}\right). \quad (1)$$

An experimental slope of −57 mV/pH was obtained in these experiments that is close to the theoretical slope (−59 mV/pH) for a classical Nernstian two-electron, two-proton process. The difference between theoretical and experimental slopes can be related to the quasireversible mechanism.

The effect of potential sweep rate was also investigated in a solution containing AC with pH 7.0. Obviously, the oxidation process is controlled by adsorption as deduced from the linear dependence of the anodic peak current ($I_{p,a}$) on the potential scan rate (υ) over a wide range of potential scan rates (from 5 to 400 mV s^{-1}, data not shown).

3.4. Effect of the Thickness of Film Modifier. In order to investigate the effect of film thickness on the electrochemical responses toward AC, the parameters influencing the film thickness including monomer and counter ion concentration, number of cycles during the electropolymerization, and the volume of CNT suspension were investigated. The optimum results (maximum peak currents for AC) were obtained using following conditions: 15 μL of CNT suspension, polymerization solution containing 0.02 M of pyrrole and 0.02 M HSQA, and 7 consecutive cycles of potential in the range of 0.00 to 0.75 V. The results showed that the type of counter ion has a very important role in the stability and conductivity of the polymer. In this regard, the electrochemical responses of the modified electrode incorporating HSQA were compared with the electrode containing Cl^- as an inorganic counter ion (Figure 4). The response for polymer doped with HQSA is 2.5-times larger than polymer doped with KCl. High stability of HQSA on the surface of the electrode can be related to its aromatic structure and effective π-π interactions with polymer. It can be predicted that HQSA as an aromatic anion with 1 negative charge produced a polymer with better conductivity. It was found that the electrochemical responses of AC on the surface of oppy/MWCNT/GCE are decreased as the thickness of the film increased. On the other hand, by increasing the thickness of the polymer film, the capacitive background current is increased, which caused higher detection limit in voltammetric measurements. From these observations, it can be concluded that the polymer layer with high thickness, which was formed on the surface of the CNT-coated GC electrode, makes the electrode surface passive and caused to some extent weakening the voltammetric responses. Our investigations with GCE coated with various amounts of CNT (μL of suspension casted on the electrode surface) showed that the maximum sensitivity for the response toward AC can be obtained with 15 μL of CNT suspension. A higher volume of suspension is caused to some inappropriate mechanical properties and decreased the adherence of the CNT film on the GCE surface. Therefore, a polymer-coated electrode with the above-mentioned optimum condition for the electropolymerization was chosen as the modified electrode in all voltammetric studies.

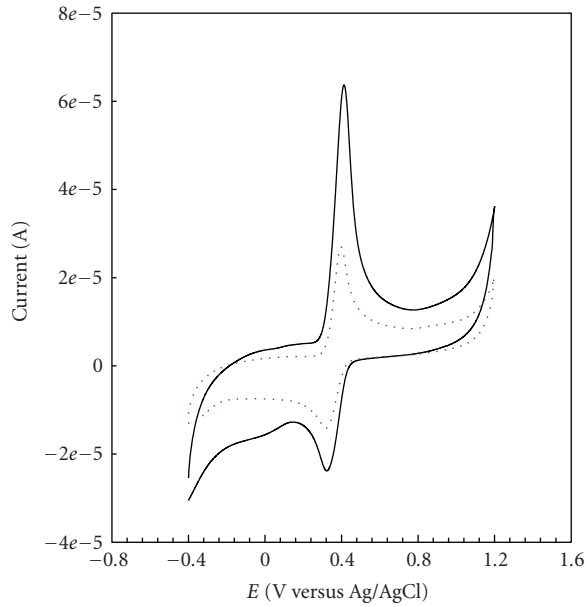

Figure 4: Cyclic voltammograms of 0.1 mM AC on the surface of oppy/MWCNT/GCE in pH = 7 various polymerization counter ion; KCl (dotted line), and HQSA (solid line).

3.5. Voltammetric Response toward Ascorbic Acid. In the electrochemical investigations of AC in clinical preparations, presence of some potentially interfering compounds, especially ascorbic acid (AA), is considered as a significant problem in the accuracy of the determinations. This compound generally shows overlapping signals on the surface of most chemically modified electrodes, which limit the analytical applicability of the sensors.

In order to investigate the effect of AA on the response of the modified electrode, the cyclic voltammograms were recorded at various electrodes in buffer solutions of pH 7.0. As can be seen in Figure 5, a totally irreversible voltammetric response is resulted on the surface of bare GCE with a peak potential of 312 mV. On the surface of GCE coated with MWCNT, this peak is shifted to slightly less anodic potentials and the corresponding peak current is considerably increased. Based on this evident, AA must be considered as a serious interference in the determination

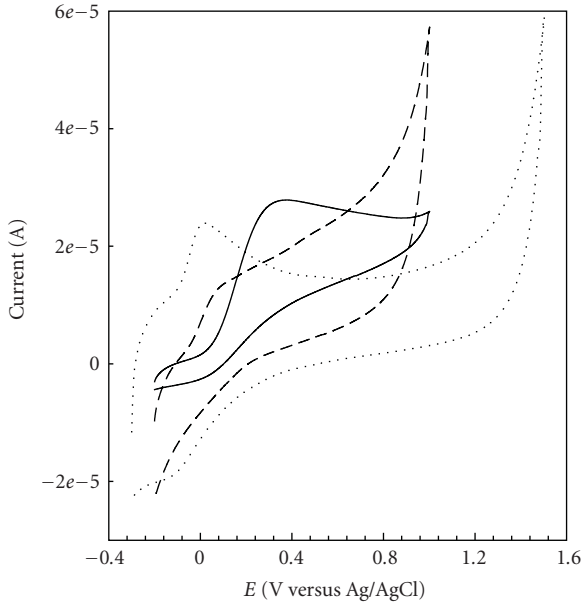

Figure 5: Cyclic voltammograms of 1 mM AA in phosphate buffer solution of pH 7.0 on the surface of various electrodes; bare GCE (solid line), CNT-GCE (dotted line), and oppy/MWCNT/GCE (dashed line). Potential sweep rate was 100 mV s^{-1}.

of AC using these electrodes. On the other hand, on the surface of the oppy/MWCNT/GCE the voltammetric response of AA completely disappeared. Such a behavior was previously reported on the surface of the GCE coated with ppy doped with multivalent organic anions such as congo-red in determination of dopamine [33] and tiron in determination of uric acid [9] in solutions with pH ≥ 5.0. It is clear that AA with a pK_a of 4.17 can exist mainly as anionic form in the experimental conditions (pH 7.0) and therefore, has repulsive interaction with the anionic sites of the film-modified electrode. On the other hand, the presence of the carboxyl groups in the structure of the overoxidized polymer film, in addition to the presence of the HQSA anion, creates highly negative charge density that exclude anionic analyte species, like AA [6]. The induced charge discrimination by the modifier film makes the electrode suitable for simultaneous determination of AC in the presence of high concentrations of AA.

3.6. Analytical Characterization. Under the optimized conditions, the DPV of various concentrations of AC were recorded in buffered solutions of pH 7.0 using an optimized accumulation time of 120 s (Figure 6). The calibration curve of the anodic peak current for solutions containing different amounts of AC is constructed and two linear ranges of 2×10^{-7}–6×10^{-6} M and 4×10^{-5}–1×10^{-4} M are obtained with correlation coefficients (R^2) of 0.9959 and 0.9947 and slopes of 22.01 μA/μM and 0.7257 μA/μM, respectively. The reason for changing the slope is creation of a monolayer of accumulated AC at the surface of modified electrode, so for more accumulation on the surface of this new surface the slope of electrode will change. In these measurements, based upon linear extrapolation of the first range of the calibration curve [34], a theoretical detection limit (S/N = 3) of 5×10^{-8} M is resulted for the voltammetric determination of AC.

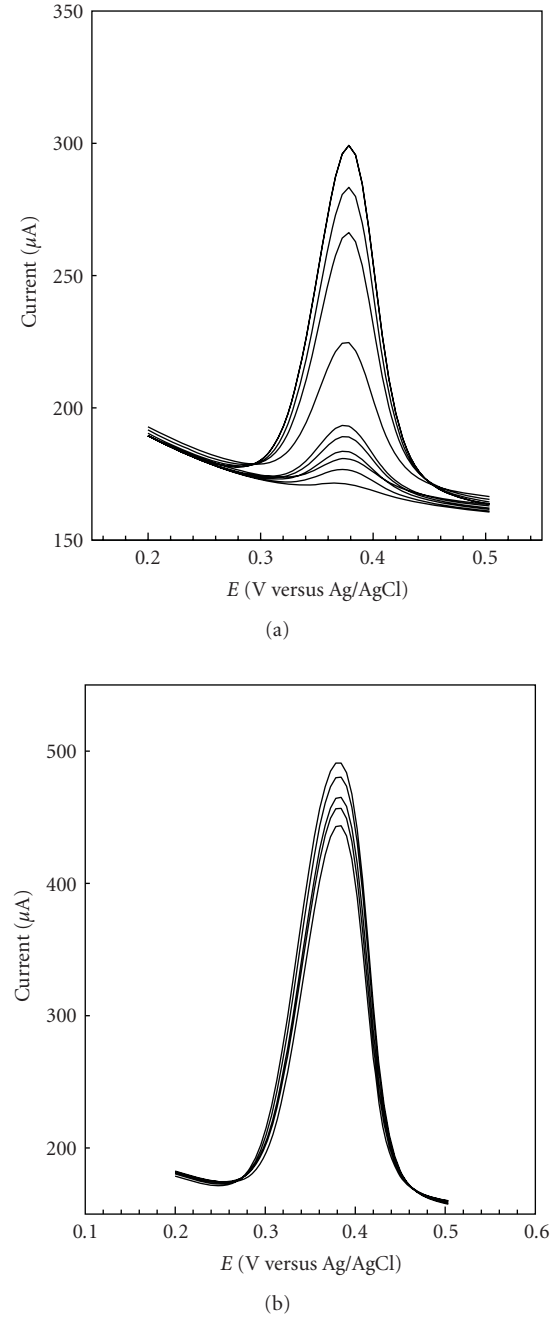

Figure 6: Differential pulse voltammograms of 0.1 M phosphate buffer solution containing various concentrations of AC (down to up); (a) 0.2, 0.4, 0.5, 0.6, 0.8, 1, 2, 4, 5, and 6 and (b) 40, 50, 60, 80, and 100 μM AC. Pulse amplitude was 50 mV. Accumulation time was 120 s.

AC, as an analgesics drug, often used in the presence of other drugs like, aspirin, cetirzine, tramadol, and codeine. Results of the present work showed that none of these pharmaceuticals interfere with AC signal on the surface of the prepared modified electrode (Figure 7). In this work cyclic

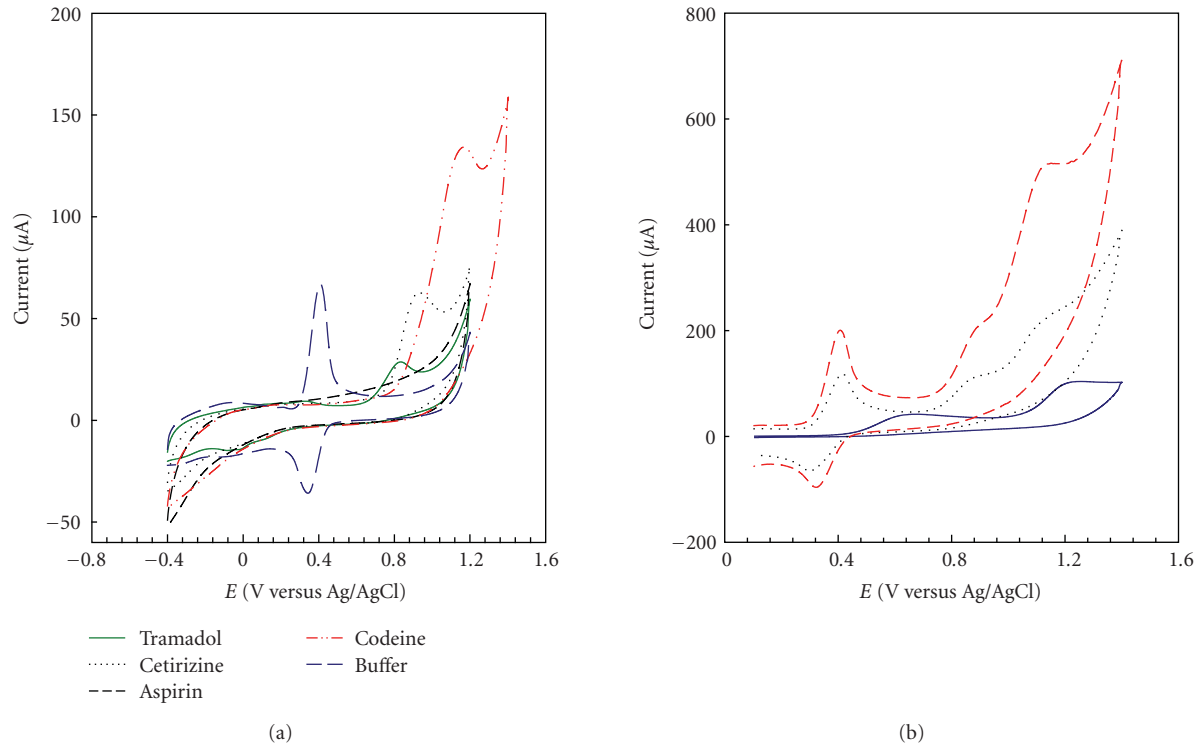

Figure 7: Cyclic voltammograms of (a) 0.1 mM of several drugs: tramadol, cetirzine, aspirin, codeine, and AC on the surface of oppy/MWCNT/GCE, (b) mixture solution containing 1 mM of AA, AC, and codeine on the surface of bare GCE (solid line), CNT-GCE (dotted line), and oppy/MWCNT/GCE (dashed line). Supporting electrolyte was phosphate buffer solution of pH 7.0 and potential sweep rate was 100 mV s^{-1}.

voltammograms of AC in the presence of codeine and AA are compared on the surface of three different electrodes: bare GCE, CNT-GCE, and oppy/MWCNT/GCE. As can be seen in Figure 7(b), remarkable enhancements in the peak current and reversibility of AC is resulted on the surface of the modified electrode. Also, a complete resolution of its peak from codeine signal and masking the effect of AA response is obtained by applying the oppy/MWCNT modified electrode. The results represent the applicability of the prepared modified electrode for AC determinations with good accuracy in the presence of other common pharmaceuticals.

The DPV of various concentrations of AC in the presence of a constant amount of codeine (1×10^{-4} M) are recorded in buffered solutions of pH 7.0 in the optimized accumulation time (120 s, Figure 8(a)). The calibration curve of the anodic peak current versus the concentration of AC (in the presence of a constant amount of codeine) showed a linear behavior in the range of $2 \times 10^{-7}$to 5×10^{-6} M with a correlation coefficient (R^2) of 0.994 and a slope of 5.1458 μA/μM. Since AC and codeine both adsorb on the surface of the electrode, the competition for the adsorption caused to decrease the response sensitivity toward AC. The investigations showed that the sensitivity of electrode response toward AC decreased with a factor of 5 in the presence of codeine. However, the determination method still has a good detection limit about 6×10^{-8} M that makes the modified electrode a very good sensor for AC determinations in the pharmaceutical preparations.

Standard addition is performed by spiking various concentrations of AC in the range of 0.2 to 3 μM to a fixed amount tablet sample. The calibration curve is obtained by plotting the peak current versus the spiked concentrations of AC. The resulted plot is compared with the plot obtained by addition of same concentrations of AC and constant amount of codeine to the buffer solution (Figure 8(b)). The results represent a very good accuracy for the determination of AC using the modified electrode. It means that the tablet matrix would not interfere in the voltammetric determination of AC. The results of the determinations in the presence of codeine (in the concentration range used in medical applications) represent a good recovery more than 95% for AC.

One of the remarkable advantages of the presented method is its low detection limit, which is obtained as 0.05 μM for AC. The prepared electrode showed highly sensitive responses toward AC in solutions with a pH near to physiological conditions (pH 7). Moreover, the prepared modified electrode showed very stable responses leading to a very good reproducibility that makes it a very sensitive and selective tool in determination of trace amounts of AC in pharmaceutical preparations. In this regard, Figure 9 shows the replicates DPVs during a day (a) and repetitive DPV measurements during 4 days (b) for 0.5 μM AC.

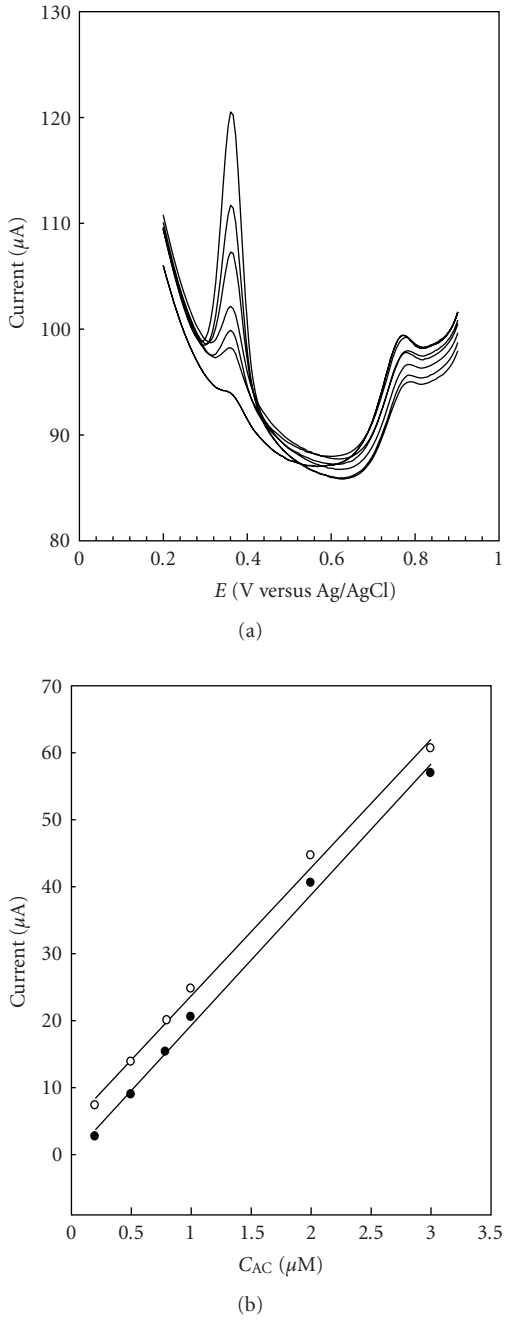

Figure 8: (a) Differential pulse voltammograms of 0.1 M phosphate buffer solution containing various concentrations of AC (down to up); 0.2, 0.5, 0.8, 1, 2, 3, 5 μM AC in the presence of 1×10^{-4} M codeine. (b) Linear calibration curve of the anodic peak current versus AC concentration added to (•) 0.1 M phosphate buffer solution of pH 7.0 and constant amount of codeine, (◦) AC tablet solution buffered in same pH.

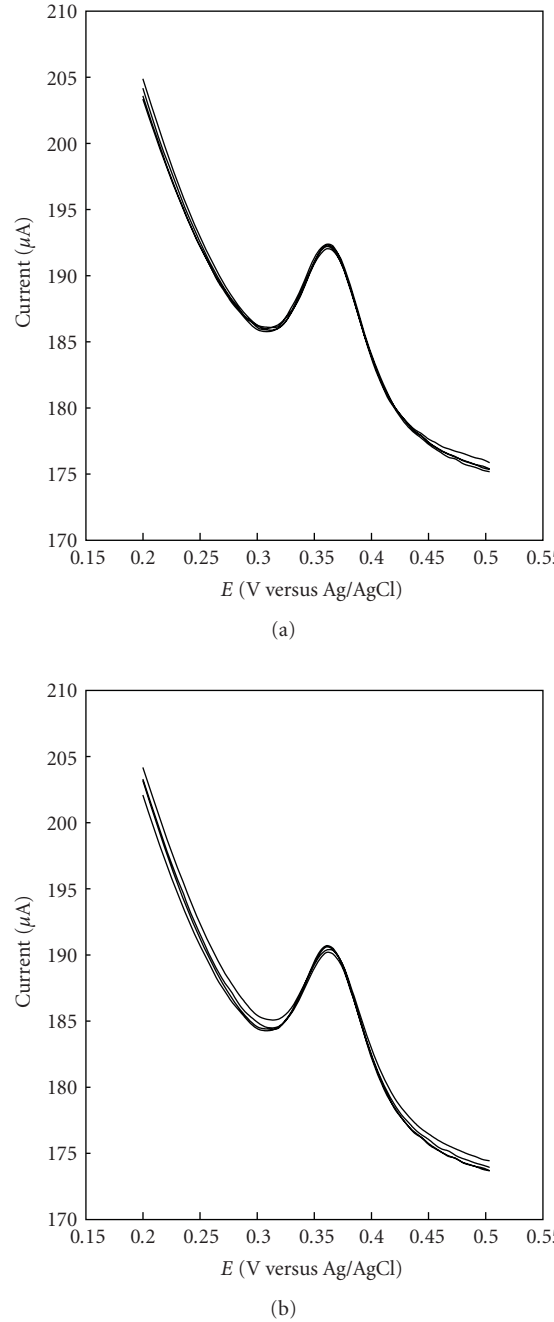

Figure 9: Four repetitive DPVs of 0.5 μM AC on the surface of oppy/MWCNT/GCE during (a) one day and (b) four days. Potential sweep rate was 100 mV s^{-1} and supporting electrolyte was 0.1 M phosphate buffer solution of pH 7.0.

Comparison with the analytical characteristics of the previous reports for AC determinations showed that the prepared modified electrode in the present work has a good detection limit with a relatively wide linear dynamic range. In the other hand, most of the sensors have been used for the determination of AC alone. However, the prepared modified electrode in this work can be successfully applied for the determination of AC in the presence of codeine with a low detection limit. Also, our investigations showed that other analgesics such as cetirizine, tramadol, and aspirin did not interfere in the voltammetric determinations of AC using the prepared modified electrode (Table 1).

Table 1: Voltammetric response characteristics of the oppy/MWCNT/GCE toward AC in comparison to other reported electrodes.

Electrode	Linear range (μM)	Detection limit (μM)	In the presence of other analytes	reference
Gold nanoparticle modified CPE	0.6–500	0.3	Alone	[25]
Nanopolypyrrole modified GCE	0.3–1.6	0.25	Alone	[20]
Poly(taurine)/MWCNT/GCE	1–100	0.5	Alone	[18]
Nano-TiO_2/polymer/GCE	12–120	2	Dopamine	[19]
MWCNT/basal plane PGE	0.01–2 and 2–20	0.01	Alone	[21]
Carbon film resistor	0.8–500	0.1	Alone	[24]
SWCNT/dicetyl phosphate film /GCE	0.1–20	0.04	Alone	[22]
PANI-MWCNT composite/GCE	1–100 and 250–2000	0.25	Alone	[23]
Hematoxylin biosensor	12–59 and 59–262	NR	Noradrenaline	[26]
Thionine MWCNT	0.1–100	0.05	AA and Izoniazid	[27]
oppy/MWCNT/GCE	0.1–100	0.05	AA and codeine	This work

4. Conclusions

In this study, we have first introduced a new kind of counter ion for pyrrole polymerization that its redox behavior can show the surface enhancement during polymerization process. In the other hand, we present a good sensor with high sensitivity and quality for AC determination in the presence of codeine and ascorbic acid. This sensor shows an electrocatalytic behavior which leads to a significant increase in the peak current (11 to 68 μA) and a great decrease in the peak potential ($\sim$110 mV). All these observations, as well as other properties, such as excellent reproducibility, low detection limit, and charge repulsion toward AA on overoxidized polypyrrole film, make the modified electrode very useful in construction of a simple device for the determination of AC in pharmaceutical preparations.

Acknowledgment

The authors gratefully acknowledge the support to this paper by the Research Council and the Center of Excellence for Nanostructures of the Sharif University of Technology, Tehran, Iran.

References

[1] U. Lange, N. V. Roznyatovskaya, and V. M. Mirsky, "Conducting polymers in chemical sensors and arrays," *Analytica Chimica Acta*, vol. 614, no. 1, pp. 1–26, 2008.

[2] A. R. Zanganeh and M. K. Amini, "Polypyrrole-modified electrodes with induced recognition sites for potentiometric and voltammetric detection of copper(II) ion," *Sensors and Actuators, B*, vol. 135, no. 1, pp. 358–365, 2008.

[3] H. Peng, L. Zhang, C. Soeller, and J. Travas-Sejdic, "Conducting polymers for electrochemical DNA sensing," *Biomaterials*, vol. 30, no. 11, pp. 2132–2148, 2009.

[4] M. Singh, P. K. Kathuroju, and N. Jampana, "Polypyrrole based amperometric glucose biosensors," *Sensors and Actuators, B*, vol. 143, no. 1, pp. 430–443, 2009.

[5] A. Ramanavičius, A. Ramanavičienė, and A. Malinauskas, "Electrochemical sensors based on conducting polymer—polypyrrole," *Electrochimica Acta*, vol. 51, pp. 6025–6037, 2006.

[6] S. Iijima, "Helical microtubules of graphitic carbon," *Nature*, vol. 354, no. 6348, pp. 56–58, 1991.

[7] C. B. Jacobs, M. J. Peairs, and B. J. Venton, "Review: carbon nanotube based electrochemical sensors for biomolecules," *Analytica Chimica Acta*, vol. 662, no. 2, pp. 105–127, 2010.

[8] D. W. Hatchett and M. Josowicz, "Composites of intrinsically conducting polymers as sensing nanomaterials," *Chemical Reviews*, vol. 108, no. 2, pp. 746–769, 2008.

[9] S. Shahrokhian and E. Asadian, "Electrochemical determination of l-dopa in the presence of ascorbic acid on the surface of the glassy carbon electrode modified by a bilayer of multiwalled carbon nanotube and poly-pyrrole doped with tiron," *Journal of Electroanalytical Chemistry*, vol. 636, no. 1-2, pp. 40–46, 2009.

[10] Y. Li, P. Wang, L. Wang, and X. Lin, "Overoxidized polypyrrole film directed single-walled carbon nanotubes immobilization on glassy carbon electrode and its sensing applications," *Biosensors and Bioelectronics*, vol. 22, no. 12, pp. 3120–3125, 2007.

[11] S. Korkut, B. Keskinler, and E. Erhan, "An amperometric biosensor based on multiwalled carbon nanotube-poly(pyrrole)-horseradish peroxidase nanobiocomposite film for determination of phenol derivatives," *Talanta*, vol. 76, no. 5, pp. 1147–1152, 2008.

[12] G. Cheng, J. Zhao, Y. Tu, P. He, and Y. Fang, "A sensitive DNA electrochemical biosensor based on magnetite with a glassy carbon electrode modified by muti-walled carbon nanotubes in polypyrrole," *Analytica Chimica Acta*, vol. 533, no. 1, pp. 11–16, 2005.

[13] A. Zhang, J. Chen, D. Niu, G. G. Wallace, and J. Lu, "Electrochemical polymerization of pyrrole in $BMIMPF_6$ ionic liquid and its electrochemical response to dopamine in the presence of ascorbic acid," *Synthetic Metals*, vol. 159, no. 15-16, pp. 1542–1545, 2009.

[14] W. Martindale and A. Wade, *The Extra Pharmacopoeia*, The Pharmaceutical Press, London, UK, 27th edition, 1979.

[15] B. D. Clayton and Y. N. Stock, *Basic Pharmacology for Nurses*, Mosby Inc, Harcourt Health Sciences Company, St. Louis, Mo, USA, 2001.

[16] J. E. F. Reynolds and W. Martindale, *The Extra Pharmacopoeia*, The Pharmaceutical Press, London, UK, 30th edition, 1993.

[17] Q. Wan, X. Wang, F. Yu, X. Wang, and N. Yang, "Poly(taurine)/MWNT-modified glassy carbon electrodes for the detection of

acetaminophen," *Journal of Applied Electrochemistry*, vol. 39, no. 6, pp. 785–790, 2009.

[18] S. A. Kumar, C. F. Tang, and S. M. Chen, "Electroanalytical determination of acetaminophen using nano-TiO_2/polymer coated electrode in the presence of dopamine," *Talanta*, vol. 76, no. 5, pp. 997–1005, 2008.

[19] B. Muralidharan, G. Gopu, C. Vedhi, and P. Manisankar, "Determination of analgesics in pharmaceutical formulations and urine samples using nano polypyrrole modified glassy carbon electrode," *Journal of Applied Electrochemistry*, vol. 39, no. 8, pp. 1177–1184, 2009.

[20] R. T. Kachoosangi, G. G. Wildgoose, and R. G. Compton, "Sensitive adsorptive stripping voltammetric determination of paracetamol at multiwalled carbon nanotube modified basal plane pyrolytic graphite electrode," *Analytica Chimica Acta*, vol. 618, no. 1, pp. 54–60, 2008.

[21] D. Sun and H. Zhang, "Electrochemical determination of acetaminophen using a glassy carbon electrode coated with a single-wall carbon nanotube-dicetyl phosphate film," *Microchimica Acta*, vol. 158, no. 1-2, pp. 131–136, 2007.

[22] M. Li and L. Jing, "Electrochemical behavior of acetaminophen and its detection on the PANI-MWCNTs composite modified electrode," *Electrochimica Acta*, vol. 52, no. 9, pp. 3250–3257, 2007.

[23] F. S. Felix, C. M. A. Brett, and L. Angnes, "Carbon film resistor electrode for amperometric determination of acetaminophen in pharmaceutical formulations," *Journal of Pharmaceutical and Biomedical Analysis*, vol. 43, no. 5, pp. 1622–1627, 2007.

[24] Z. Xu, Q. Yue, Z. Zhuang, and D. Xiao, "Flow injection amperometric determination of acetaminophen at a gold nanoparticle modified carbon paste electrode," *Microchimica Acta*, vol. 164, no. 3-4, pp. 387–393, 2009.

[25] N. Nasirizadeh and H. R. Zare, "Differential pulse voltammetric simultaneous determination of noradrenalin and acetaminophen using a hematoxylin biosensor," *Talanta*, vol. 80, no. 2, pp. 656–663, 2009.

[26] S. Shahrokhian and E. Asadian, "Simultaneous voltammetric determination of ascorbic acid, acetaminophen and isoniazid using thionine immobilized multi-walled carbon nanotube modified carbon paste electrode," *Electrochimica Acta*, vol. 55, no. 3, pp. 666–672, 2010.

[27] K. Esumi, M. Ishigami, A. Nakajima, K. Sawada, and H. Honda, "Chemical treatment of carbon nanotubes," *Carbon*, vol. 34, no. 2, pp. 279–281, 1996.

[28] A. Witkowski and A. Brajter-Toth, "Overoxidized polypyrrole films: a model for the design of permselective electrodes," *Analytical Chemistry*, vol. 64, no. 6, pp. 635–641, 1992.

[29] I. Streeter, G. G. Wildgoose, L. Shao, and R. G. Compton, "Cyclic voltammetry on electrode surfaces covered with porous layers: an analysis of electron transfer kinetics at single-walled carbon nanotube modified electrodes," *Sensors and Actuators, B*, vol. 133, no. 2, pp. 462–466, 2008.

[30] G. P. Keeley and M. E. G. Lyons, "The effects of thin layer diffusion at glassy carbon electrodes modified with porous films of single-walled carbon nanotubes," *International Journal of Electrochemical Science*, vol. 4, no. 6, pp. 794–809, 2009.

[31] L. Xiao, G. G. Wildgoose, and R. G. Compton, "Exploring the origins of the apparent "electrocatalysis" observed at C60 film-modified electrodes," *Sensors and Actuators, B*, vol. 138, no. 2, pp. 524–531, 2009.

[32] M. Ghalkhani and S. Shahrokhian, "Application of carbon nanoparticle/chitosan modified electrode for the square-wave adsorptive anodic striping voltammetric determination of Niclosamide," *Electrochemistry Communications*, vol. 12, no. 1, pp. 66–69, 2010.

[33] S. Shahrokhian and H. R. Zare-Mehrjardi, "Electrochemical synthesis of polypyrrole in the presence of congo red; application to selective voltammetric determination of dopamine in the presence of ascorbic acid," *Electroanalysis*, vol. 21, no. 2, pp. 157–164, 2009.

[34] M. C. Granger, J. Xu, J. W. Strojek, and G. M. Swain, "Polycrystalline diamond electrodes: basic properties and applications as amperometric detectors in flow injection analysis and liquid chromatography," *Analytica Chimica Acta*, vol. 397, no. 1–3, pp. 145–161, 1999.

SAGE-Hindawi Access to Research
International Journal of Electrochemistry
Volume 2011, Article ID 421387, 5 pages
doi:10.4061/2011/421387

Research Article

Magnetic Nanoparticles Immobilization and Functionalization for Biosensor Applications

M. B. Mejri,[1,2] A. Tlili,[1] and A. Abdelghani[1]

[1] *Nanotechnology Laboratory, Centre Urbain Nord, University of Carthage, INSAT, BP 676, Charguia Cedex 1080, Tunisia*
[2] *Laboratoire des Maladies Transmissibles et Substances Biologiquement Actives, Université de Monastir, Monastir 5000, Tunisia*

Correspondence should be addressed to A. Abdelghani, aabdelghan@yahoo.fr

Received 10 April 2011; Revised 5 May 2011; Accepted 5 May 2011

Academic Editor: Vinod Kumar Gupta

Copyright © 2011 M. B. Mejri et al. This is an open access article distributed under the Creative Commons Attribution License, which permits unrestricted use, distribution, and reproduction in any medium, provided the original work is properly cited.

We describe an approach for *E. coli* bacteria detection using an electrochemical immunosensor. The immunosensor was based on functionalized magnetic nanoparticles immobilized onto bare gold electrode. Cyclic voltammetry and impedance spectroscopy was performed before and after magnetic nanoparticles deposition. The magnetic nanoparticles functionalized with anti-*E. coli* polyclonal antibody were used for bacteria detection. Lytic T4-phage was used to confirm the success recognition of bacteria with the developed immunosensor. The specificity of the immunosensor was tested against *Enterococcus faecium* bacteria. A limit detection of 10^3 CFU/mL *E. coli* bacteria was obtained with a good reproducibility.

1. Introduction

One of the principal characteristics of *E. coli* bacteria was *their* genotypes diversity responsible for diseases. These *E. coli* genotypes called pathotypes lead too much dangerous pathology which affects human and animal species. Currently, we can identify six intestinal pathotypes and two extraintestinal pathotypes agreed by the scientific community [1–3]. Among them, we can cite enterotoxigenic *E. coli* (ETEc) which is frequently an agent of human and animal diarrhea; 600 million cases of human diarrhea and 800.000 worldwide deaths principally in children under the age of five years [4] were attributed to (ETEC) infections. The EPEC infection leads to aqueous diarrhea with some associated pathologic manifestation as vomiting, fever, and dehydration [5–7]. The enteroaggregative *E. coli* (EAEc) pathology was described as watery diarrhea with the presence of abdominal spasms but no fever. It shows no invasion of blood vessels, but it is marked by persistent rashes and chronic watery diarrhea. Small outbreaks have been recorded both in industrialized countries than in developing countries [8–12].

Toward these inflectional menaces, food contamination is controlled by rigorous legislations [13], and foodborne safety was presented as preventive solution allowing avoiding *E. coli* diseases. This is why bacterial detection and recognition are principal aims of the health strategies. Conventional methods for *E. coli* detection were based on bacterial culture and colony counting [14], this way requires 24 h to yield results and can require up to 7 days for other bacterial strains [15, 16]. However, biosensors are currently imposed as powerful analytical tools which yield together sensitivity, specificity, and real-time detection. Several successful biosensors for microbial agent were developed [17–22], among them are impedimetric biosensors [23, 24]. Magnetic nanoparticles were widely used in the biosensors conceptions [25]. They carry the advantage of increasing the ratio surface/volume, and also it is easy to immobilize to any electrode surface by applying a magnetic field. In previous works, authors were interested in exploiting the high specific interaction between bacteriophages and their target bacteria using various transducers [26]. Lytic phage can be used as a specific bioreceptor allowing bacterial recognition, where the phage-bacteria detection generates dual impedimetric behavior. The first one is corresponding to bacteria immobilization and shows impedance increase, and the second behavior is awarded to bacterial lysis which shows impedance decrease [27]. In this work, we used

T4 phages as free bioreceptor allowing *E. coli* bacteria detection as a second tool for our biosensing strategy. Functionalized magnetic nanoparticles immobilized onto a bare gold electrode were used as an immunosensor. Cyclic voltammetry and impedance spectroscopy was performed before and after magnetic nanoparticles deposition. T4-phage was used to confirm the success recognition of bacteria with the developed immunosensor. The specificity of the immunosensor was tested against nonspecific *Enterococcus faecium* bacteria.

2. Experimental Setup

2.1. Reagents and Apparatus. The used antibody is goat polyclonal IgG anti-*E. coli* (ab13627) purchased from Abcam (UK). A phosphate buffer solution (PBS) of $5\,\mu g\,mL^{-1}$ of antibody with pH = 7.2 was prepared. The magnetic beads used are supplied by Sigma Aldrich (France). They are composed of iron oxide particles coated with a polymer and grafted by COOH groups, and their diameter is about 200 nm. All other materials, including 1-ethyl-3-(3-(dimethylamino)-propyl) carbodiimide (EDC) (Aldrich) and N-hydroxy succinimide (NHS) (Aldrich), were used as supplied.

The buffer solution used was phosphate-buffered saline (PBS) containing 140 mM NaCl, 2.7 mM KCl, 0.1 Mm Na_2HPO_4, and 1.8 mM KH_2PO_4, at pH 7.2. This solution was added by a redox couple $[Fe(CN)_6]^{-4/-3}$ (5 mM) (ox/red) and used for cyclic voltammetry and impedance spectroscopy. All reagents were of analytical grade, and ultrapure water (resistance $\geq 18.2\,M\Omega\cdot cm^{-1}$) produced by a Millipore Milli-Q system was used.

2.2. Bacterial Culture. *E. coli* cells were grown in LB broth or on LB agar plates, and *Enterococcus faecium* cells were grown in BHI broth or on BHI agar plates. High titer of bacteria suspension was prepared as follows: liquid culture mediums were inoculated by 100 μL of preculture solution and cultivated at 37°C for 8–10 h. Centrifuge the cells at 6200 rpm for 5 min, wash the cells twice, and resuspend the cells in sterile PBS. Determine the viable cells and bacterial concentration with spread-plate technique. The optical density OD of the bacterial culture has been measured for the determination of bacterial growth stationary phase.

2.3. Phage Culture. The *E. coli* K12 liquid culture mediums were inoculated at exponential phase with 500 μL of phage-T4 solution and were incubated at 37°C in a rotary shaker (200 rpm) for three hours. Chloroform was added to final concentration of 10% and kept at 4°C for 20 min before centrifugation at 4°C (19000 g). Double-layer plates of each phage dilutions were prepared to give confluent lysis of the indicator strain *E. coli* K12. This allows us to determine the phage concentration in PFU.

2.4. Gold Cleaning. Gold substrates were provided by the Neuchatel Institute (Switzerland). They were fabricated using standard silicon technologies. (100)-oriented, P-type (3–5 $\Omega\cdot$cm) silicon wafers were thermally oxidized to grow an 800 nm-thick field oxide. Then, a 30 nm thick titanium layer and a 300 nm-thick gold top layer were deposited by evaporation under vacuum. Before modification, the gold electrodes were cleaned in acetone solution for 20 min with ultrasonic bath. After that, they were dried under a nitrogen flow and then dipped for 10 min into "piranha solution" 7 : 3 (v/v) 96% H_2SO_4/30% H_2O_2. Finally, the gold substrates were rinsed 2 to 3 times with ultrapure water and immediately immersed in an ethanol solution and finally dried under nitrogen flow.

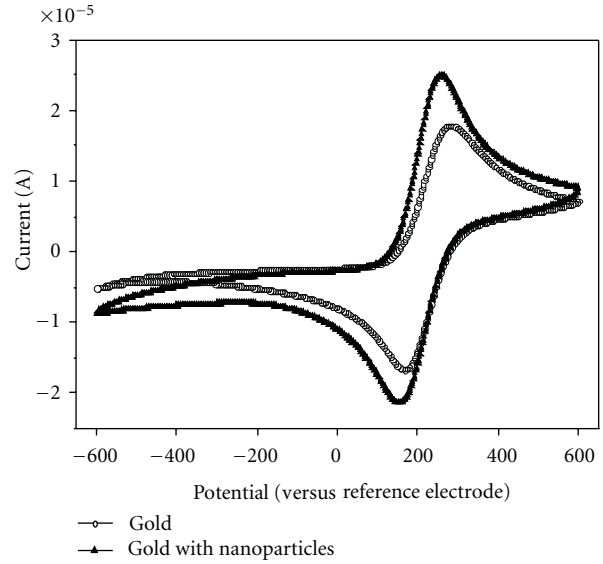

Figure 1: Cyclic voltammograms of (a) bare gold electrode; (b) bare gold electrode/magnetic beads. In presence of a 5 mM redox, probe $K_3[Fe(CN)_6]/K_4[Fe(CN)_6]$ versus SCE.

2.5. Magnetic Nanoparticles Functionalization. The stock solution of carboxylic magnetic nanoparticles was diluted in ultrapure water. A volume of 40 μL of the diluted solution of nanoparticles was injected onto a cleaned gold electrode already positioned in an electrochemical cell. A magnetic field of 300 mT was applied during all the measurements using a cylindrical magnet. The magnetic nanoparticles layer was formed on the gold surface. The immobilized nanoparticles were treated with 0.4 Mm EDC-0.1 mM NHS for 1 h to convert the terminal carboxylic groups to an active NHS ester. The polyclonal antibodies solution ($5\,\mu g\,mL^{-1}$) was dropped on the gold surface for 1 h at room temperature. Modified electrode was finally treated by BSA solution (1%) to block the nonspecific sites.

2.6. Cyclic Voltammetry. The deposition of magnetic nanoparticles onto gold electrode was checked with cyclic voltammetry. Measurements were recorded in PBS solution with redox couple ($[Fe(CN)_6]^{-4/-3}$), using a scanning potential sweep from −700 mV to 700 mV with a scan rate of 100 mV/s.

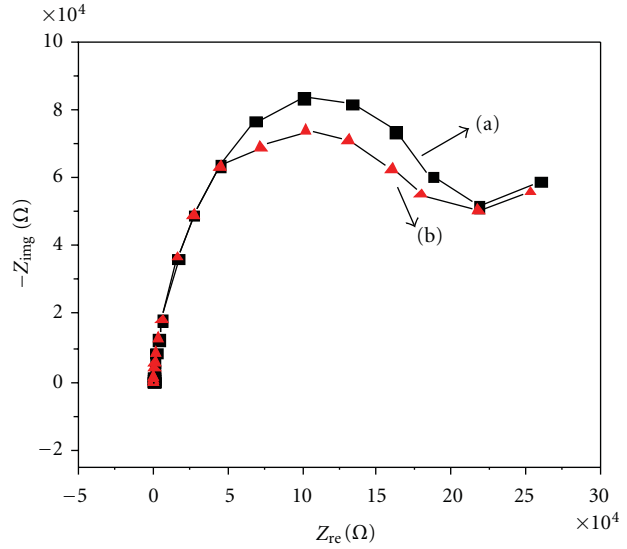

Figure 2: Impedance spectra of (a) bare gold electrode; (b) bare gold electrode functionalized with magnetic nanoparticles.

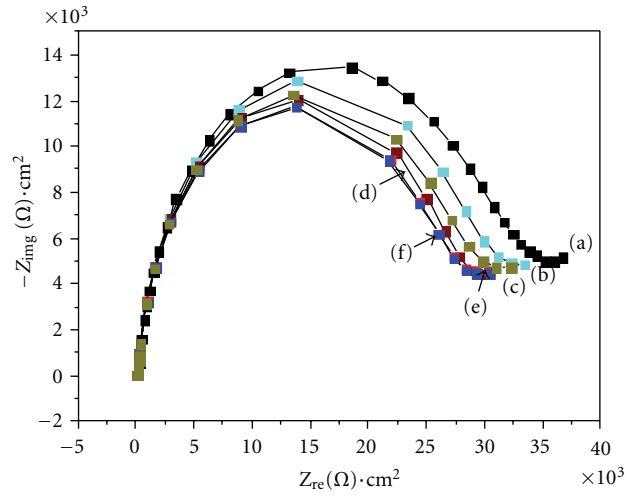

Figure 3: Impedance spectra of (a) bare gold electrode/magnetic beads/polyclonal Ab anti-*E. coli*; (b) 10^3 CFU/mL; (c) 10^4 CFU/mL; (d) 10^5 CFU/mL; (e) 10^6 CFU/mL; (f) 10^7 CFU/mL; (f=g) 10^8 CFU/mL.

2.7. Electrochemical Impedance Spectroscopy. Conventional electrochemical cell with a three-electrode configuration was used to measure impedance spectroscopy. Modified gold electrode was considered as working electrode (0.11 cm^2), a platinum electrode (0.54 cm^2) as the counterelectrode, and a saturated calomel electrode (SCE) as the reference electrode. The impedance spectra were recorded in a frequency range from 50 mHz to 100 kHz, and apparatus used in all electrochemical measurements is an Autolab 302N impedance analyser (Ecochemie, The Netherlands) equipped with the NOVA1.4 acquisition software.

3. Results and Discussions

3.1. Characterization of Magnetic Nanoparticles Layer

3.1.1. Cyclic Voltammetry. Figure 1 shows the cyclic voltammetry measurement of bare gold surface before and after magnetic nanoparticles immobilization. A reversible voltammogram corresponding to a bare cleaned gold electrode can be observed. The two observed peaks correspond to the oxydoreduction potential of the used redox couple $[Fe(CN)_6]^{-4/-3}$. The success immobilization of magnetic nanoparticles was confirmed with the increase of the current. This indicates that the resistance decreases due to the presence of the magnetic beads covering the electrode.

3.1.2. Electrochemical Impedance Spectroscopy. Figure 2 shows the electrochemical impedance spectra of gold bare electrode before and after the deposition of magnetic nanoparticles layer at 0 V. The obtained spectra can be modelized with an electric model shown in a previous work [19]. The diameter of semicircle corresponds to the charge transfer resistance of the electrode/electrolyte interface. The decrease of the charge transfer resistance is due to the conductivity increase at the gold-electrolyte interface after magnetic nano-particles immobilization.

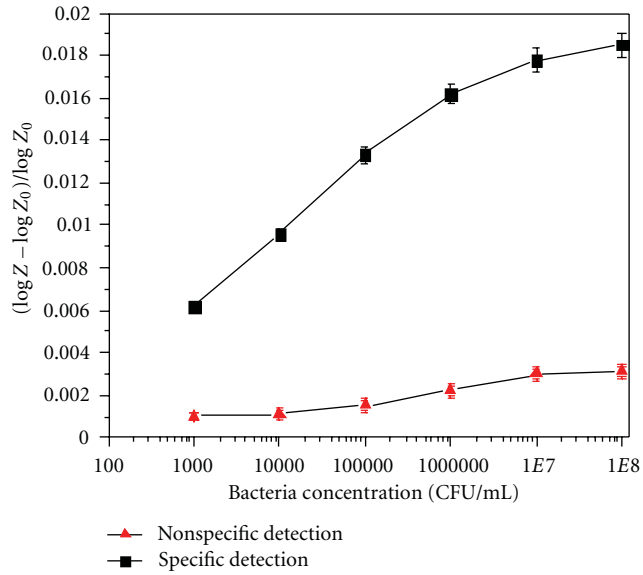

Figure 4: Calibration curve: the variation of the absolute value of $|(\text{Log } Z - \text{Log } Z_0)/\text{Log } Z_0|$ versus bacteria concentration (CFU/mL) at 233 mHz. The specific detection was with *E. coli* and nonspecific detection with *Enterococcus faecium* bacteria.

3.2. Bacteria Immunodetection. The immunodetection of *E. coli* bacteria was performed in an electrochemical cell containing sterile PBS. Different volumes corresponding to different bacterial concentrations in CFU/mL were injected. Figure 3 shows the impedance spectra obtained after different bacteria concentrations injection (between 10^3 and 10^8 CFU/mL). The decrease of the charge transfer resistance

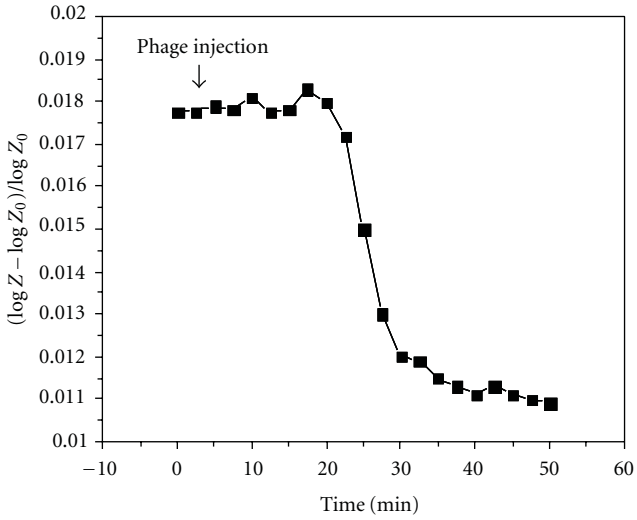

Figure 5: Variation of the absolute value of $|(\mathrm{Log}\,Z - \mathrm{Log}\,Z_0)/\mathrm{Log}\,Z_0|$ after phage injection versus time at a fixed frequency of 233 mHz. *E. coli* bacteria concentration is 10^7 CFU/mL.

is due to the specific bacteria recognition. The resistance decreases gradually as the bacteria concentration increases. This decrease is different from the previous results obtained without magnetic nanoparticles [27] where we have an impedance increase. A saturation behavior was reached at a concentration of 10^7 CFU/mL.

A calibration curve was obtained by calculating the absolute value of $(\mathrm{Log}\,Z - \mathrm{Log}\,Z_0)/\mathrm{Log}\,Z_0$ at a fixed frequency (233 mHz), where Z is the value of the impedance after bacteria binding to antibody, Z_0 is the value of impedance only with the antibody. Figure 4 shows a linear increase of the absolute value of the impedance and a beginning of saturation for higher bacteria concentrations. The detection limit of 10^3 CFU/mL was obtained with a good reproducibility. The negative test was performed by injecting several concentrations of *Enterococcus faecium* bacteria. The absence of any significant change confirms the specificity of the developed immunosensor.

3.3. T4-Phage Injection. We used lytic phage (T4-phage) as second recognition to confirm the previous signal generated by the immunosensor. For this purpose, we inject a concentration (10^7 CFU/mL) of T4 phage onto the functionalized gold electrode after *E. coli* recognition. A 50 μL of T4 phage solution was introduced into electrochemical cell where immunosensor was already saturated with the bacteria (10^7 CFU/mL). As it is shown in Figure 5, a stable impedimetric behavior was recorded, while after 15 min, a strong decrease of the absolute value of the impedance was observed. This kinetic behavior is typical for phage-bacteria interaction [27] and confirms the immunosensing results.

4. Conclusion

In this work, we describe an approach for *E. coli* bacteria detection using immunosensor based on functionalized magnetic nanoparticles immobilized onto a bare gold electrode. Cyclic voltammetry and impedance spectroscopy was performed before and after magnetic nanoparticles deposition. The magnetic nanoparticles functionalized with polyclonal antibody were used for *E. coli* detection. T4-phage was used to confirm the success recognition of bacteria by the developed immunosensor. The specificity of the immunosensor was tested against *Enterococcus faecium* bacteria. A limit detection of 10^{+03} CFU/mL was obtained with a good reproducibility. For future work, interdigitated microelectrodes arrays integrated in microfluidic cell will be used to perform limit detection and sensitivity.

Acknowledgments

Dr. A. Abdelghani thanks the Alexander Von Humboldt Stiftung (Germany) for the material donation. The authors thank Biophage Pharma (Canada) for providing them T4-phage, Dr. Mohamed Zourob (Canada), Professor A. Simonian (USA), Dr. Eva Baldrich (CNM Barcelona, Spain), F. J. Del Campo (CNM Barcelona, Spain), and Professor N. Jaffrezic-Renault (France) for their collaboration.

References

[1] J. P. Nataro and J. B. Kaper, "Diarrheagenic *Escherichia coli*," *Clinical Microbiology Reviews*, vol. 11, no. 1, pp. 142–201, 1998.

[2] J. P. Nataro, T. Steiner, and R. L. Guerrant, "Enteroaggregative *Escherichia coli*," *Emerging Infectious Diseases*, vol. 4, no. 2, pp. 251–261, 1998.

[3] J. B. Kaper, J. P. Nataro, and H. L. T. Mobley, "Pathogenic *Escherichia coli*," *Nature Reviews Microbiology*, vol. 2, no. 2, pp. 123–140, 2004.

[4] World Health Organization, *The World Health Report 1999: Making a Difference*, World Health Organization, Geneva, Switzerland, 1999.

[5] A. E. Jerse, J. Yu, B. D. Tall, and J. B. Kaper, "A genetic locus of enteropathogenic *Escherichia coli* necessary for the production of attaching and effacing lesions on tissue culture cells," *Proceedings of the National Academy of Sciences of the United States*, vol. 87, no. 20, pp. 7839–7843, 1990.

[6] B. Kenny, R. DeVinney, M. Stein, D. J. Reinscheid, E. A. Frey, and B. B. Finlay, "Enteropathogenic E. coli (EPEC) transfers its receptor for intimate adherence into mammalian cells," *Cell*, vol. 91, no. 4, pp. 511–520, 1997.

[7] C. S. Tailor, A. Nour, C. G. Lee, C. Kozak, and D. Kabat, "Cloning and characterization of a cell surface receptor for xenotropic and polytropic murine leukemia viruses," *Proceedings of the National Academy of Sciences of the United States* , vol. 96, no. 3, pp. 927–932, 1999.

[8] J. P. Nataro, J. B. Kaper, R. Robins-Browne, V. Prado, P. Vial, and M. M. Levine, "Patterns of adherence of diarrheagenic *Escherichia coli* to HEp-2 cells," *Pediatric Infectious Disease Journal*, vol. 6, no. 9, pp. 829–831, 1987.

[9] J. P. Nataro, Y. Deng, S. Cookson et al., "Heterogeneity of enteroaggregative *Escherichia coil* virulence demonstrated in volunteers," *Journal of Infectious Diseases*, vol. 171, no. 2, pp. 465–468, 1995.

[10] I. C. A. Scaletsky, S. H. Fabbricotti, R. L. B. Carvalho et al., "Diffusely adherent *Escherichia coli* as a cause of acute diarrhea

in young children in northeast Brazil: a case-control study," *Journal of Clinical Microbiology*, vol. 40, no. 2, pp. 645–648, 2002.

[11] J. R. Johnson, T. T. O'Bryan, P. Delavari et al., "Clonal relationships and extended virulence genotypes among *Escherichia coli* isolates from women with a first or recurrent episode of cystitis," *Journal of Infectious Diseases*, vol. 183, no. 10, pp. 1508–1517, 2001.

[12] J. R. Johnson, S. J. Weissman, A. L. Stell, E. Trintchina, D. E. Dykhuizen, and E. V. Sokurenko, "Clonal and pathotypic analysis of archetypal *Escherichia coli* cystitis isolate NU14," *Journal of Infectious Diseases*, vol. 184, no. 12, pp. 1556–1565, 2001.

[13] WHO, *International Health Regulations. The Fifty-Eighth World Health Assembly*, World Health Organization, Geneva, Switzerland, 2005.

[14] H. Ayçiçek, H. Aydogan, A. Küçükkaraaslan, M. Baysallar, and A. C. Basustaoglu, "Assessment of the bacterial contamination on hands of hospital food handlers," *Food Control*, vol. 15, pp. 253–254, 2004.

[15] S. Artault, J. L. Blind, J. Delaval, Y. Dureuil, and N. Gaillard, "Detecting Listeria monocytogenes in food," *International Food Hygiene*, vol. 12, p. 23, 2001.

[16] E. Deboer and R. R. Beumer, "Methodology for detection and typing of foodborne micro-organisms," *The International Journal of Food Microbiology*, vol. 50, pp. 119–130, 1999.

[17] W.M. Hassen, C. Chaix, A. Abdelghani, F. Bessueille, D. Leonard, and N. Jaffrezic, "An impedimetric DNA sensor based on functionalized magnetic nanoparticles for HIV and HBV detection," *Sensors &Actuators B*, vol. 134, no. 2, pp. 755–760, 2008.

[18] M. Hnaien, M. F. Diouani, S. Helali et al., "Immobilization of specific antibody on SAM functionalized gold electrode for rabies virus detection by electrochemical impedance spectroscopy," *Biochemical Engineering Journal*, vol. 39, no. 3, pp. 443–449, 2008.

[19] M. F. Diouani, S. Helali, I. Hafaid et al., "Miniaturized biosensor for avian influenza virus detection," *Materials Science and Engineering C*, vol. 28, no. 5-6, pp. 580–583, 2008.

[20] M. G. Silva, S. Helali, C. Esseghaier, C. E. Suarez, A. Oliva, and A. Abdelghani, "An impedance spectroscopy method for the detection and evaluation of Babesia bovis antibodies in cattle," *Sensors & Actuators B*, vol. 135, no. 1, pp. 206–213, 2008.

[21] M. B. Mejri, M. Marrakchi, H. Baccar et al., "Electrochemical impedance spectroscopy for specific detection of enterovirus," *Sensor Letters*, vol. 7, no. 5, pp. 896–899, 2009.

[22] H. Baccar, M. B. Mejri, I. Hafaiedh, T. Ktari, M. Aouni, and A. Abdelghani, "Surface plasmon resonance immunosensor for bacteria detection," *Talanta*, vol. 82, pp. 810–814, 2010.

[23] L. I. Yang, Y. B. Li, C. L. Griffis, and M. G. Johnson, "Interdigitated microelectrode (IME) impedance sensor for the detection of viable Salmonella typhimurium," *Biosensors & Bioelectronics*, vol. 19, no. 10, pp. 1139–1147, 2004.

[24] L. Yang and R. Bashir, "Electrical/electrochemical impedance for rapid detection of foodborne pathogenic bacteria," *Biotechnology Advances*, vol. 26, no. 2, pp. 135–150, 2008.

[25] M. Varshney and Y. Li, "Interdigitated array microelectrode based impedance biosensor coupled with magnetic nanoparticle-antibody conjugates for detection of *Escherichia coli* O157:H7 in food samples," *Biosensors & Bioelectronics*, vol. 22, no. 11, pp. 2408–2414, 2007.

[26] S. Balasubramanian, I. B. Sorokulova, V. J. Vodyanoy, and A. L. Simonian, "Lytic phage as a specific and selective probe for detection of *Staphylococcus aureus*—a surface plasmon resonance spectroscopic study," *Biosensors & Bioelectronics*, vol. 22, no. 6, pp. 948–955, 2006.

[27] M. B. Mejri, H. Baccar, E. Baldrich et al., "Impedance biosensing using phages for bacteria detection: generation of dual signals as the clue for in-chip assay confirmation," *Biosensors & Bioelectronics*, vol. 26, no. 4, pp. 1261–1267, 2010.

SAGE-Hindawi Access to Research
International Journal of Electrochemistry
Volume 2011, Article ID 603257, 4 pages
doi:10.4061/2011/603257

Research Article

Functionalized Palladium Nanoparticles for Hydrogen Peroxide Biosensor

H. Baccar,[1,2] T. Ktari,[1,2] and A. Abdelghani[1,2]

[1] *University of Carthage, Nanotechnology Laboratory, National Institute of Applied Science and Technology, Centre Urbain Nord, BP 676, 1080 Charguia Cedex, Tunisia*
[2] *Unité de Recherche de Physico-Chimie des Matériaux Polymères, IPEST, Université de Carthage, La Marsa 2070, Tunisia*

Correspondence should be addressed to A. Abdelghani, aabdelghan@yahoo.fr

Received 30 March 2011; Accepted 30 April 2011

Academic Editor: Farnoush Faridbod

Copyright © 2011 H. Baccar et al. This is an open access article distributed under the Creative Commons Attribution License, which permits unrestricted use, distribution, and reproduction in any medium, provided the original work is properly cited.

We present a comparison between two biosensors for hydrogen peroxide (H_2O_2) detection. The first biosensor was developed by the immobilization of Horseradish Peroxidase (HRP) enzyme on thiol-modified gold electrode. The second biosensor was developed by the immobilization of cysteamine functionalizing palladium nanoparticles on modified gold surface. The amino groups can be activated with glutaraldehyde for horseradish peroxidase immobilization. The detection of hydrogen peroxide was successfully observed in PBS for both biosensors using the cyclic voltammetry and the chronoamperometry techniques. The results show that the limit detection depends on the large surface-to-volume ratio attained with palladium nanoparticles. The second biosensor presents a better detection limit of 7.5 μM in comparison with the first one which is equal to 75 μM.

1. Introduction

The scope of H_2O_2 is very broad in our days, it affects many areas like chemistry [1], food industries [2], clinical applications, and environmental chemistry [3]. Many determinations methods of hydrogen peroxide have been developed using titrimetry [4, 5], spectrophotometry [4, 6], chemiluminescence [4, 7], and electrochemical [2, 4, 8–10]. The first three techniques reveal inaccuracy and are complex and expensive [10]. Besides, the electrochemical methods are very selective, sensitive, and illustrate low detection limits for hydrogen peroxide [2, 8, 11].

Between numerous enzymes, horseradish peroxidase (HRP) has commonly been chosen to detect H_2O_2 due to the easy availability in high purity and low cost [12–14]. Nanoparticles have received considerable attention in these last years. Nanoparticles can bring many advantages when they are immobilized on an electrode surface. They have a large surface-to-volume ratio which contributes to the probability of electrocatalytic activity [9, 15, 16]. Palladium nanoparticles with small size (1 nm) were used due to their higher electron conductivity. In this present work, two biosensors were developed for hydrogen peroxide detection. The first biosensor was developed by the immobilization of Horseradish Peroxidase (HRP) enzyme on thiol modified gold electrode. The second biosensor was developed by the immobilization of cysteamine functionalizing palladium nanoparticles on modified gold surface. The detection of hydrogen peroxide was successfully observed in PBS for both biosensors using the cyclic voltammetry and the chronoamperometry techniques. The results show that the limit detection depends on the large surface-to-volume ratio attained with small palladium nanoparticles.

2. Experimental Setup

2.1. Reagents. All chemicals were commercially available and used as received. The Palladium acetate was purchased from Strem Chemicals (USA). Horseradish peroxidase, n-dodecyl sulfide, 16-mercaptohexadecanoic acid (MHDA) 90%, cystaminedihydrochloride, 1-ethyl-3-(3-(dimethylamino)-propyl) carbodiimide (EDC), and N-hydroxy succinimide (NHS) were purchased from Sigma Aldrich (USA). The buffer solution used for all experiments was phosphate buffered saline (PBS) containing 140 mM NaCl, 2.7 mM

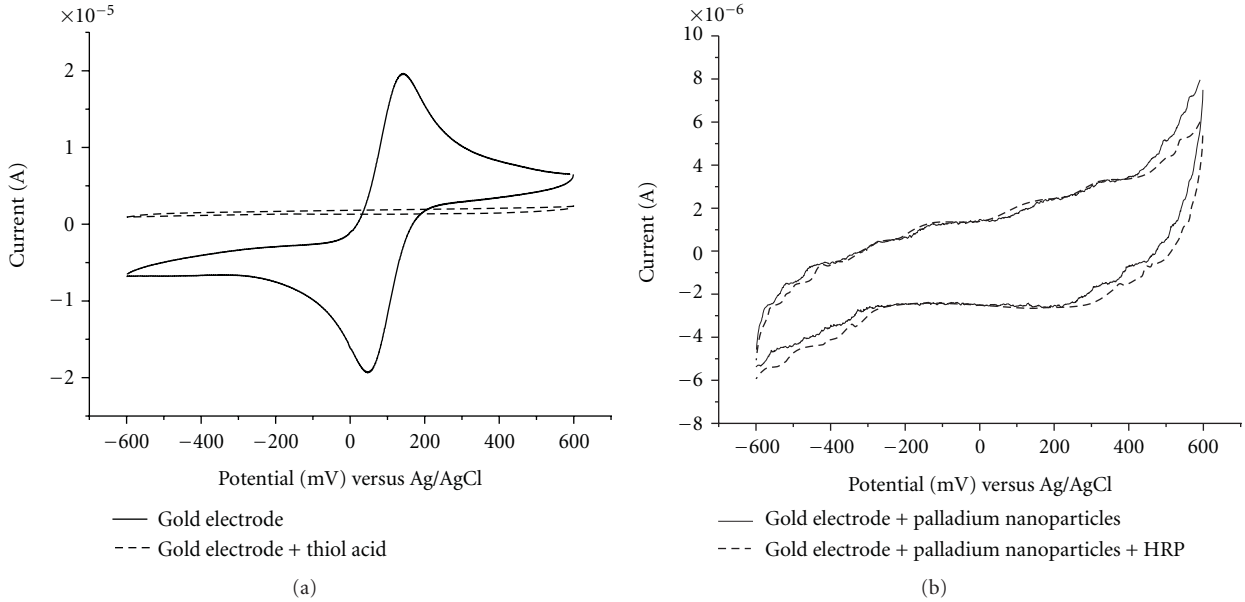

Figure 1: (a) Cyclic voltammogram of gold electrode and gold electrode with thiol acid. (b) Cyclic voltammogram of gold electrode with palladium nanoparticles and gold electrode with palladium nanoparticles with HRP.

KCl, 0.1 mM Na_2HPO_4, 1.8 mM KH_2PO_4, pH 7.0, and the redox couple $Fe(CN)_6^{3-}/Fe(CN)_6^{4-}$ at 5 mM concentration. All reagents were of analytical grade and ultrapure water (resistance, 18.2 MΩ·cm^{-1}) produced by a Millipore Milli-Q system was used throughout.

2.2. Instrumentation. Cyclic voltammetry and chronoamperometry measurement were performed at room temperature in a conventional voltammetric cell with a three electrode configuration using Autolab impedance analyzer (Ecochemie, The Netherlands). The gold electrode (0.16 cm^2) was used as working electrode, platinum (1 cm^2) and Ag/AgCl electrodes were used as counter and reference electrodes, respectively. All the electrochemical measurement were carried out in PBS at pH 7.0 with 5 mM $Fe(CN)_6^{3-}/Fe(CN)_6^{4-}$ and in Faraday cage.

2.3. Sensors Development. For the first biosensor, the gold electrode was immersed in an ethanol solution containing 1 mM of MHDA for 12 hours at room temperature. The treated electrode was then immersed in a solution of EDC (0.4 mM) and NHS (0.1 mM) for 1 h. A drop of HRP solution with a concentration of 100 μg/mL was deposited on the treated electrode for 1 hour. Then, a drop of a 1% BSA solution was added on the substrate for 30 min to block the free spaces between the enzyme and the SAM.

For the second biosensor, gold electrode was immersed in 1 mM of MHDA solution for 12 h, then activated with EDC and NHS for 1 h. After that, the electrode was immersed in a solution of Pd nanoparticles (1 nm size) functionalized previously with cysteamine dihydrochloride for 12 hours. The amine-thiol groups can be activated by immersing the substrate in PBS solution containing 5% (v/v) glutaraldehyde (GA) for 2 h. After rinsing with PBS, a solution of HRP (100 μg/mL) was added onto the surface for 1 hour to achieve the base reaction between the aldehyde group and the amino group of the enzyme. Then, a drop of a 1% BSA solution was added on the substrate for 1 hour to block the unspecific sites.

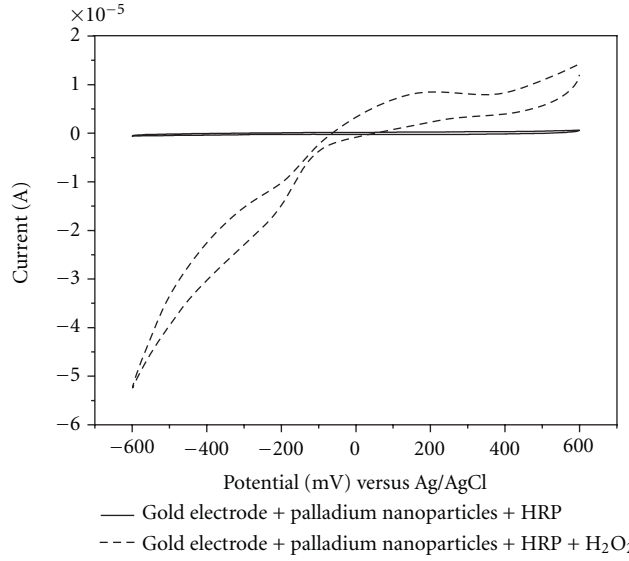

Figure 2: Cyclic voltammogram of gold electrode with palladium nanoparticles functionalized with HRP with 1,5 mM H_2O_2.

3. Results and Discussions

The synthesis and morphological characterization of Pd nanoparticles have been discussed elsewhere [17]. Cyclic voltammetry is a convenient methodology for studying

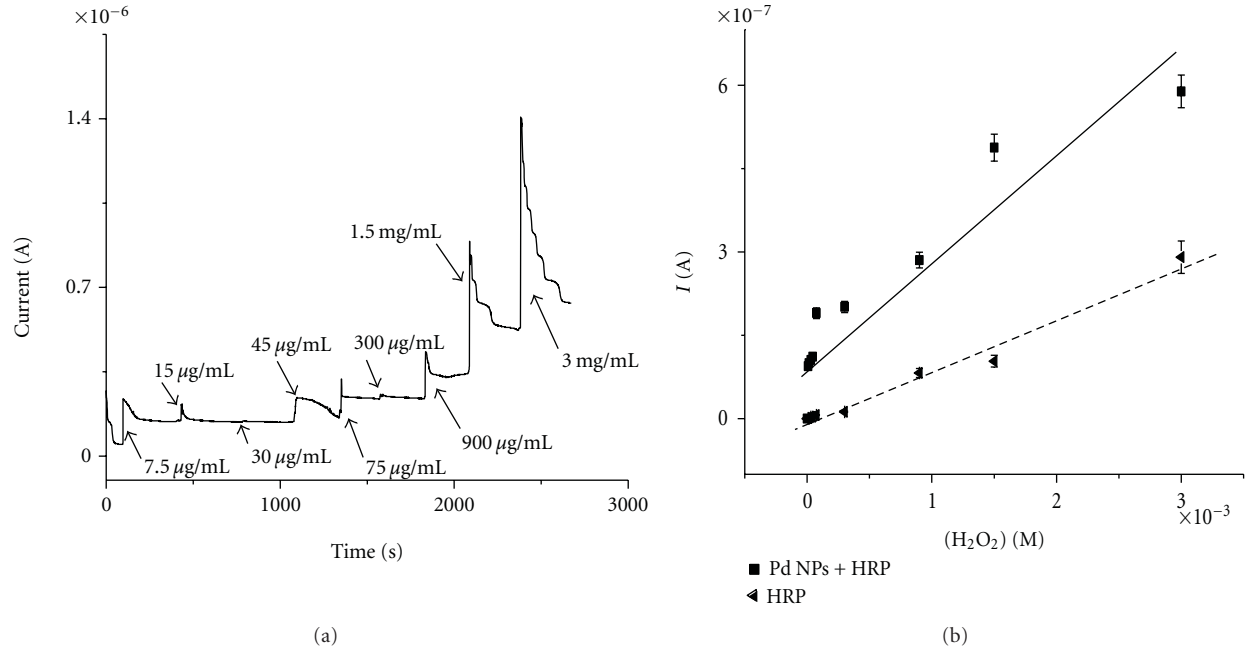

Figure 3: (a) Chronoamperometry curve of gold electrode with thiol acid and with Pd NPs and with HRP. (b) Calibration curve of gold electrode with thiol acid and Pd NPs and HRP (squares) and gold electrode with thiol acid and HRP and BSA (triangles) with different concentrations of H_2O_2.

the kinetics of an oxidation reduction reaction and the electrical properties of material in electrolyte interface. Figure 1(a) shows a typical cyclic voltammogram of the bare gold electrode, where a two peaks correspond to the ferrocyanide redox couples. After thiol deposition, the two current peaks disappeared showing the high insulating properties of the thiol monolayer. After the palladium nanoparticles deposition, the current decreases gradually due to the insulating properties of cysteamine covering the nanoparticles. The same behavior was obtained after HRP immobilization (Figure 1(b)). Figure 2 shows a cyclic voltammogram of the gold electrode functionalized with palladium nanoparticles and with HRP molecule before and after injection of H_2O_2 (1.5 mM). Upon the addition of the hydrogen peroxide to the electrochemical cell, the reduction peak (at −200 mV) appears, showing a typical electron transfer between the H_2O_2 and the HRP molecule [14]:

$$\begin{aligned} H_2O_2 + HRP_{red} &\longrightarrow HRP_{ox} + H_2O \\ HRP_{ox} + 2e^- &\longrightarrow HRP_{red} \end{aligned} \quad (1)$$

The chronoamperometry can be used to explore the current response of the biosensor in presence of the hydrogen peroxide. Figure 3(a) shows the chronoamperometry curve of functionalized electrode with palladium nanoparticles with HRP at a fixed potential −200 mV after H_2O_2 injections. The current increases with increasing H_2O_2 concentration. Figure 3(b) shows the current time curves of the two biosensors exposed to different concentration of hydrogen peroxide. The addition of the hydrogen peroxide to the buffer solution increases the steady state current. The curves were represented by a linear regression and a best sensitivity was obtained with palladium nanoparticles. A limit detection of 75 μM and 7.5 μM H_2O_2 was obtained with a good reproductibility for the first and the second biosensors, respectively. This difference in sensitivity and limit detection were due to the large surface to volume ratio given by the palladium nanoparticles. Moreover, the small size of nanoparticles (1 nm) increases the electron confinement in palladium which induces a higher electric conductivity, thus, an easier electron exchange.

4. Conclusion

In this paper, we present a comparison between two new biosensors for the detection of hydrogen peroxide (H_2O_2). The first biosensor was developed by the immobilization of Horseradish Peroxidase (HRP) enzyme on thiol modified gold electrode. The second biosensor was developed by the immobilization of cysteamine functionalizing palladium nanoparticles on modified gold surface. The amino-groups can be activated with glutaraldehyde for horseradish peroxidase immobilization. The detection of hydrogen peroxide was successfully observed in PBS for both biosensors using the cyclic voltammetry and the chronoamperometry techniques. The results show that the biosensor response depends on the conductivity and the large surface-to-volume ratio attained with palladium nanoparticles.

Acknowledgments

The authors thank Pr. Sherine Obare (University of Michigan, USA) and Pr. N. Jaffrezic-Renault (UCB-Lyon1, France) for their collaboration.

References

[1] X. Bo, J. Bai, J. Bju, and L. Guo, "A sensitive amperometric sensor for hydrazine and hydrogen peroxide based on palladium nanoparticles/onion-like mesoporous carbon vesicle," *Analytica Chimica Acta*, vol. 675, no. 1, pp. 29–35, 2010.

[2] T. Dodevska, E. Horozova, and N. Dimcheva, "Electrocatalytic reduction of hydrogen peroxide on modified graphite electrodes: application to the development of glucose biosensors," *Analytical and Bioanalytical Chemistry*, vol. 386, no. 5, pp. 1413–1418, 2006.

[3] A. Senol, A. Sibel Kilinc, D. Zekerya, and T. Azmi, "Development of a new biosensor for mediatorless voltammetric determination of hydrogen peroxide and its application in milk samples," *Journal of Applied Electrochemistry*, vol. 39, no. 7, pp. 971–977, 2009.

[4] C.-X. Lei, S.-Q. Hu, G.-L. Shen, and R.-Q. Yu, "Immobilization of horseradish peroxidase to a nano-Au monolayer modified chitosan-entrapped carbon paste electrode for the detection of hydrogen peroxide," *Talanta*, vol. 59, no. 5, pp. 981–988, 2003.

[5] E. C. Hurdis and H. Romeyn, "Accuracy of determination of hydrogen peroxide by cerate oxidimetry," *Analytical Chemistry*, vol. 26, no. 2, pp. 320–325, 1954.

[6] M. S. Bloomfield, "A rapid and precise assay for peroxide as "active oxygen" in products, by flow injection analysis in a high pressure system with spectrophotometric detection," *Talanta*, vol. 64, no. 5, pp. 1175–1182, 2004.

[7] K. Nakashima, K. Maki, S. Kawaguchi et al., " Peroxyoxalate chemiluminescence assay of hydrogen peroxide and glucose using 2,4,6,8-tetrathiomorpholinopyrimido[5,4-d]pyrimidine as a fluorescent component," *Analytical Sciences*, vol. 7, pp. 709–713, 1991.

[8] Z. Liu, Y. Yang, H. Wang, Y. Liu, G. Shen, and R. Yu, "A hydrogen peroxide biosensor based on nano-Au/PAMAM dendrimer/cystamine modified gold electrode," *Sensors and Actuators B*, vol. 106, no. 1, pp. 394–400, 2005.

[9] J. D. Qiu, H. Z. Peng, R. P. Liang, J. Li, and X. H. Xia, "Synthesis, characterization, and immobilization of Prussian blue-modified au nanoparticles: application to electrocatalytic reduction of H_2O_2," *Langmuir*, vol. 23, no. 4, pp. 2133–2137, 2007.

[10] L. Wang and E. Wang, "A novel hydrogen peroxide sensor based on horseradish peroxidase immobilized on colloidal au modified ITO electrode," *Electrochemistry Communications* , vol. 6, pp. 225–229, 2004.

[11] D. Ravi Shankaran, K. I. Iimura, and T. Kato, "A novel metal immobilized self-assembled surface for electrochemical sensing," *Sensors and Actuators B*, vol. 96, no. 3, pp. 523–526, 2003.

[12] C. Esseghaier, Y. Bergaoui, H. ben Fredj et al., "Impedance spectroscopy on immobilized streptavidin horseradish peroxidase layer for biosensing," *Sensors and Actuators B*, vol. 134, no. 1, pp. 112–116, 2008.

[13] X. L. Luo, J. J. Xu, Q. Zhang, G. J. Yang, and H. Y. Chen, "Electrochemically deposited chitosan hydrogel for horseradish peroxidase immobilization through gold nanoparticles self-assembly," *Biosensors and Bioelectronics*, vol. 21, no. 1, pp. 190–196, 2005.

[14] S. Helali, H. Baccar, A. Abdelghani, and N. Jaffrezic-Renault, "Electrochemical study of horseradish peroxidase biosensor based on functionalised magnetic beads and polypyrrole film," *Sensor Letters*, vol. 7, no. 5, pp. 808–811, 2009.

[15] Y. Tang, Y. Cao, S. Wang, G. Shen, and R. Yu, "Surface attached-poly(acrylic acid) network as nanoreactor to in-situ synthesize palladium nanoparticles for H_2O_2 sensing," *Sensors and Actuators B*, vol. 137, no. 2, pp. 736–740, 2009.

[16] C. Fang, Y. Fan, J. M. Kong, G. J. Zhang, L. Linn, and S. Rafeah, "DNA-templated preparation of palladium nanoparticles and their application," *Sensors and Actuators, B*, vol. 126, no. 2, pp. 684–690, 2007.

[17] M. Ganesan, R. G. Freemantle, and S. O. Obare, "Monodisperse thioether-stabilized palladium nanoparticles: synthesis, characterization, and reactivity," *Chemistry of Materials*, vol. 19, no. 14, pp. 3464–3471, 2007.

SAGE-Hindawi Access to Research
International Journal of Electrochemistry
Volume 2011, Article ID 619782, 7 pages
doi:10.4061/2011/619782

Research Article

Electrochemical Detection of Sequence-Specific DNA with the Amplification of Gold Nanoparticles

Yuzhong Zhang, Zhen Wang, Yuehong Wang, Lei Huang, Wei Jiang, and Mingzhu Wang

College of Chemistry and Materials Science, Anhui Key Laboratory of Chemo-Biosensing, Anhui Normal University, Wuhu 241000, China

Correspondence should be addressed to Yuzhong Zhang, zhyz65@mail.ahnu.edu.cn

Received 6 December 2010; Accepted 28 March 2011

Academic Editor: Farnoush Faridbod

Copyright © 2011 Yuzhong Zhang et al. This is an open access article distributed under the Creative Commons Attribution License, which permits unrestricted use, distribution, and reproduction in any medium, provided the original work is properly cited.

A sensitive electrochemical DNA biosensor was prepared based on mercaptoacetic acid (MAA)/gold nanoparticles (AuNPs) modified electrode. Probe DNA (NH_2-DNA) was covalently linked to the carboxyl group of MAA in the presence of 1-ethyl-3-(3-dimethylaminopropyl) carbodiimide hydrochloride (EDC) and N-hydroxyl-succinimide (NHS). Scanning electron microscopy (SEM) and electrochemical impedance spectra (EIS) were used to investigate the film assembly process. The DNA hybridization events were monitored by differential pulse voltammetry (DPV), and adriamycin was used as the electrochemical indicator. Also the factors influencing the performance of the DNA hybridization were investigated in detail. Under the optimal conditions, the signal was linearly changed with target DNA concentration increased from 5.0×10^{-13} to 1.0×10^{-9} M and had a detection limit of 1.7×10^{-13} M (signal/noise ratio of 3). In addition, the DNA biosensor showed good reproducibility and stability during DNA assay.

1. Introduction

Nowadays, specific sequences DNA detection has become a most important research field due to its application in disease diagnosis, drug screening, epidemic prevention, and environmental protection [1–3]. Many methods have been used for DNA detection including optics [4, 5], piezoelectricity [6], surface plasmon resonance spectroscopy [7], and electrochemistry [8–11]. Among them, it should be noted that electrochemical DNA sensor is a promising candidate because of its simple, rapid, inexpensive, high sensitivity and selectivity.

AuNPs are well-known low-dimensional functional materials with large surface-to-volume ratios and biocompatibility with biosystem. So it is often used for DNA biosensor material. Zhang et al. [12] and Zhang et al. [13, 14] have fabricated some AuNPs-based electrochemical DNA sensors. Wang and his coworkers have invented a DNA biosensor based on amplified voltammetric detection of DNA hybridization via oxidation of ferrocene caps on gold nanoparticle/streptavidin conjugates [15]. Abouzar and his coworkers have developed a label-free electrical detection of DNA hybridization functionalized with AuNPs [16]. Our groups have fabricated several DNA biosensor based on AuNPs amplification [17–19]. Castañeda et al. have a review on electrochemical sensing of DNA using AuNPs [20].

In the present paper, we fabricate an electrochemical DNA biosensor for detection of E. coli sequence with the amplification of gold nanoparticles. AuNPs were firstly electrodeposited on the surface of the gold electrode. And the modified AuNPs were used to increase the electrode surface area for more binding amount of MAA so as to enhance the immobilization amount of probe DNA. DPV was used to monitor DNA hybridization event by measurement of the intercalated adriamycin. This DNA biosensor shows a higher sensitivity and selectivity.

2. Experiment

2.1. Materials. Adriamycin, MAA, sodium dodecyl sulfate (SDS), EDC, and NHS were purchased from Alfa Aesar (Tianjing, China). $HAuCl_4 \cdot 4H_2O$ was obtained from Shanghai Chemical Reagent Co., Ltd. Sodium hydroxide and Phosphate were obtained from Nanjing Chemical Reagent (Nanjing, China). Various oligonucleotides were purchased from Shanghai Sangon Bioengineering Technology & Services Co., Ltd. (Shanghai, China). And their sequences are as follows.

Probe Sequence. 5′-NH_2-GAG CGG CGC AAC ATT TCA GGT CGA-3′.

Complementary Sequence. 5′-TCG ACC TGA AAT GTT GCG CCG CTC-3′.

Noncomplementary Sequence. 5′-AGC TGG ACT TTA CAA CGC GGC GAG-3′.

Single-Base Mismatched Sequence. 5′-TCG ACC TGA AAC GTT GCG CCG CTC-3′.

Stock solutions of oligonucleotides were prepared with 0.01 M phosphate buffer solution (PBS, pH 7.40) and stored in a freezer. The following buffer solutions were used: hybridization buffer solution (0.1 M NaCl + 0.01 M PBS, pH 7.40) and electrochemical test solution (0.01 M PBS, pH 7.40). All chemicals were of analytical grade and used without further purification. All solutions were prepared with twice-quartz-distilled water.

2.2. Apparatus. All electrochemical measurements such as electrochemical impedance spectroscopy (EIS), cyclic voltammetry (CV), and DPV were performed on a CHI 660A electrochemical workstation (Shanghai Chenhua Instruments Co., China). The three-electrode system was used in the experiment with bare gold electrode or modified electrode as working electrode, a saturated calomel electrode (SCE) as reference electrode and platinum wire as counter electrode. EIS was performed in 0.1 M KCl solution containing 5.0 mM $K_4Fe(CN)_6/K_3Fe(CN)_6$ (pH 7.40) with the frequency range between 0.1 and 100 kHz at the formal potential of 0.115 V. CV and DPV were carried out in a 10 mL electrochemical cell with 5 mL solutions, from which oxygen was removed by purging with high-purity nitrogen for 20 min, and a blanket of nitrogen was maintained over the solution during the measurements. The morphology of AuNPs was obtained by scanning electron microscopy (SEM) using a JEOLJSM-6700F microscope (Hitachi, Japan).

2.3. Preparation of ssDNA/MAA/AuNPs Modified Electrode. Prior to modification, the bare gold electrode was firstly polished to a mirror-like surface with gamma alumina suspensions (1.0 μm, 0.25 μm and 0.05 μm, resp.). Then it was rinsed with twice-quartz-distilled water and cleaned ultrasonically sequentially in water and 95% ethanol for 3 min. Finally, the electrode was electrochemically cleaned between −0.3 and +1.55 V in 0.5 M H_2SO_4 until a stable CV was obtained.

AuNPs electrochemical deposition was performed in 2.0×10^{-3} M $HAuCl_4$/0.2 M KNO_3 solution and electrodeposition time is 50 s at −250 mV (versus SCE). The electrode was denoted as AuNPs/Au. Then the AuNPs/Au electrode was immersed into a 10.0 mM MAA for 4 h to form MAA film through Au–S bond. The obtained electrode was denoted as MAA/AuNPs/Au.

After the MAA/AuNPs/Au modified electrode was immersed in a mixture of 5.0 mM EDC and 8.0 mM NHS (pH 7.40) for 45 min, 8 μL of 1.0×10^{-5} M probe DNA was dropped on the surface of MAA/AuNPs/Au and kept it for 12 h at the room temperature. Finally, the probe modified electrode was immersed into 0.1% SDS solution for 10 min to remove the unbound probe DNA. Thus the probe DNA modified electrode was prepared, and it was denoted ssDNA/MAA/AuNPs/Au.

2.4. Hybridization and Electrochemical Detection. The hybridization experiment was carried out by immersing the probe modified electrode into hybridization buffer solution containing different concentrations of target DNA for 25 min at 37°C. The hybridized electrode was then rinsed with PBS containing 0.1% SDS to remove the unhybridized target DNA. After that, it was incubated in 1.0×10^{-6} M adriamycin for 20 min, followed by rinsing with water and 0.01 M PBS for three times to remove physically absorbed adriamycin.

The DNA hybridization was assessed with the DPV peak current of intercalated adriamycin in pH 7.0 PBS, and the concentration of complementary DNA was quantified by peak current of adriamycin (ΔI), which was subtracted from the reduction peak current generated at the ssDNA/MAA/AuNPs modified electrode ($\Delta I = I_{\text{ds-DNA}} - I_{\text{ss-DNA}}$). DPV parameters were as follows: potential range: −0.45 ~ −0.80 V; amplitude: 0.05 V; pulse width: 0.05 s; sample width: 0.0167 s; pulse period: 0.2 s; quiet time: 2 s. The schematic diagram of the DNA biosensor fabrication and electrochemical detection is illustrated in Scheme 1.

3. Results and Discussion

3.1. Electrochemical Impedance Spectroscopy at Different Modified Electrode. Impedance spectroscopy is an effective method for probing the surface features of the modified electrode. In EIS, the semicircle part at higher frequencies corresponds to the electron transfer limited process or the electron transfer resistance (R_{et}). The linear sect at lower frequencies shows a controlled diffusion process. Figure 1 compares the Nyquist plots of 5.0 mM $K_4Fe(CN)_6/K_3Fe(CN)_6$ at the different modified electrodes. When AuNPs were electrodeposited on the surface of the gold electrode (curve b), the R_{et} was decreased in contrast to the bare gold electrode (curve a). The results could be rationalized by improved electron transfer kinetics of redox probe on AuNPs modified electrode. The assembly of MAA monolayer on electrode surface induced a larger R_{et} (curve c) as compared with that of AuNPs electrode due to the electrostatic repulsion between the negative MAA and $K_4Fe(CN)_6/K_3Fe(CN)_6$. When the MAA/AuNPs/Au surface was activated with EDC and NHS,

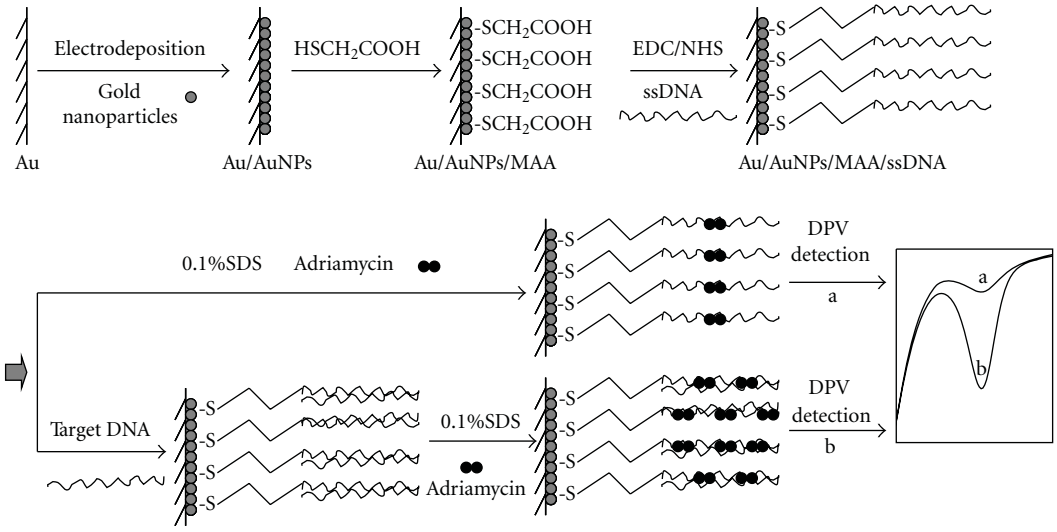

Scheme 1: The schematic diagram of the procedure available for DNA biosensor fabrication and electrochemical detection.

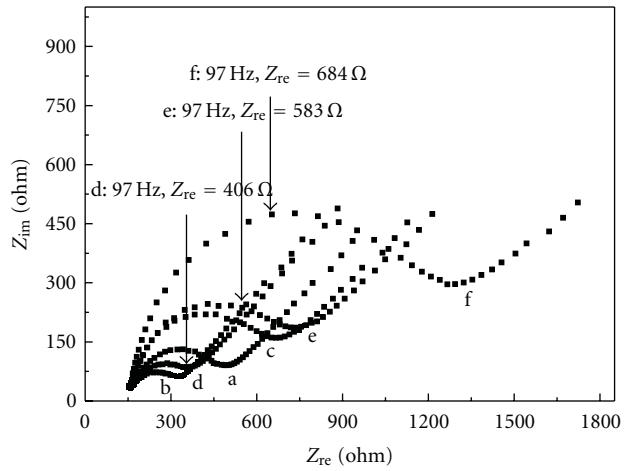

Figure 1: Nyquist plots obtained at different modified electrode. (a) Bare gold electrode, (b) AuNPs, (c) MAA/AuNPs, (d) activated MAA/AuNPs, (e) ss-DNA/MAA/AuNPs, and (f) ds-DNA/MAA/AuNPs modified electrodes. The supporting electrolyte was 0.1 M KCl solution containing 5.0 mM $K_4Fe(CN)_6/K_3Fe(CN)_6$.

the R_{et} was evidently decreased because the content of carboxyl group was decreased (curve d). When the probe DNA was covalently immobilized on the electrode surface, the R_{et} is obviously increased because of the strong electrostatic repulsion between the $K_4Fe(CN)_6/K_3Fe(CN)_6$ molecules and the negative-charged phosphate skeletons of DNA (curve e). After hybridization of the probe DNA with 1.0×10^{-10} M complementary ssDNA, R_{et} was obviously increased (curve f). Therefore, this impedance change indicated that modification and DNA hybridization successfully occurred on the electrode surface.

3.2. Optimization of DNA Assay Conditions. It is reported that the morphology, magnitude, and distribution of AuNPs could be controlled through controlling deposition time or $HAuCl_4$ concentrations [21]. In order to obtain an optimization for DNA immobilization and hybridization, in this work, magnitude and distribution of AuNPs was performed by changing deposition time and keeping $HAuCl_4$ concentrations a constant. Two different methods (SEM, DPV) were used to investigate the optimization of Au deposition time, respectively.

Figure 2(A) shows SEM images of AuNPs at different periods of deposition time. It can be observed that morphology and distribution of AuNPs was depended on deposition time. When deposition time was 50 s, AuNPs are about 10 nm and have the same size (b), when the deposition time reached 110 s, a large number of gold clusters were found and lead to a very rough surface (c). Therefore, 50 s was the suitable for AuNPs preparation from the views of uniform size, higher density, and good shape.

The characteristic of AuNPs at different deposition time was investigated by DPV using adriamycin as electroactive indicator. Figure 2(B) shows the plot of the peak currents of adriamycin dependence of deposition time. It could be observed that peak current increased as deposition time from 0 to 50 s, and the peak current decreased slightly when the deposition time exceeded 50 s. So 50 s was selected as the optimal deposition time.

The amount of probe DNA immobilization on the electrode surface is an important factor because the amount of probe DNA directly influences the sensitivity of a DNA biosensor [22]. Figure 3(a) shows the peak current of adriamycin before and after hybridization dependence of probe DNA amount. From Figure 3(a), we can observe the peak current of adriamycin gradually increased with the amount of probe DNA from 3 to 8 μL, and a slight decrease when the amount of probe DNA is over 8 μL. Thus, 8 μL probe DNA was selected in our experiments.

The accumulation time of electrochemical indicator is another factor for sensitivity of DNA biosensor. Figure 3(b)

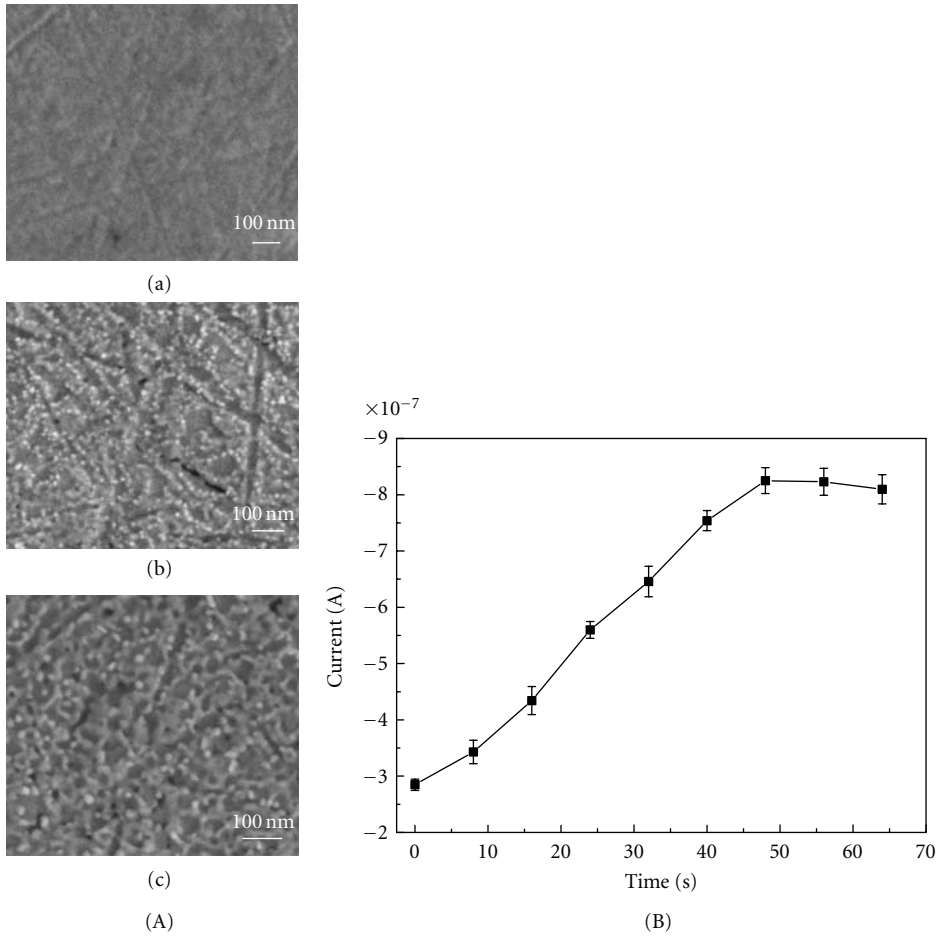

Figure 2: (A) SEM images of AuNPs at various deposition time. (a) 0, (b) 50 s, (c) 110 s, Deposition potential is −250 mV (versus SCE). (B) DPV responses of adriamycin dependence of deposition time. Electrochemical deposition was performed in 3.0 mM $HAuCl_4$ at various times ($t = 0, 8, 16, 24, 32, 40, 48, 56$, and 64 s). DPV measurement was performed in 0.01 M PBS (pH 7.40) containing 1.0×10^{-6} M adriamycin. DPV parameters were as follows: potential range: $-0.45 \sim -0.80$ V; amplitude: 0.05 V; pulse width: 0.05 s; sample width: 0.0167 s; pulse period: 0.2 s; quiet time: 2 s.

shows the reduction peak currents of adriamycin dependence of the accumulation time. It could be seen that the peak current increased significantly with the increasing accumulation time from 5 to 20 min. When the accumulation time is higher than 20 min, the peak current of adriamycin keeps constant relatively. Therefore, 20 min was selected as the optimum accumulation time.

Figure 3(c) shows the peak current of adriamycin dependence of the hybridization time. From Figure 3(c), it could be seen that the reduction peak currents of adriamycin increased significantly as the hybridization time increased from 5 to 25 min and keep constant after 25 min. This indicated that the hybridization reaction was completed after 25 min. From a view of the sensitivity and assay time, 25 min was generally used for hybridization time.

3.3. Amplification of AuNPs. Could the application of the gold nanoparticles enhance the immobilization capacity of probe DNA and amplify signal of DNA hybridization? In this paper, we fabricated two different sensors: one is a sensor containing AuNPs, and another containing no AuNPs. The electrochemical investigation was performed as experiment Section 2.4, and the results were shown in Figure 4. It could be observed that the sensor containing AuNPs has a large signal (Figure 4(A): 10.16×10^{-7} A) compared with the sensor containing no AuNPs (Figure 4(B): 2.29×10^{-7} A). These results suggested that the immobilization capacity of probe DNA and hybridization signal improved greatly in the presence of AuNPs.

3.4. Selectivity of the DNA Biosensor. Differentiation of single mismatches is of significant interest for a variety of important applications. In this paper, the selectivity of the DNA biosensor was also evaluated by using single-base mismatch, no complementary and complementary DNA sequences. As is shown in Figure 5, it could be observed that the response of single-base mismatch sequence has a significant difference with that of complementary sequence. These results indicated that this DNA biosensor can distinguish single-base mismatch DNA sequence.

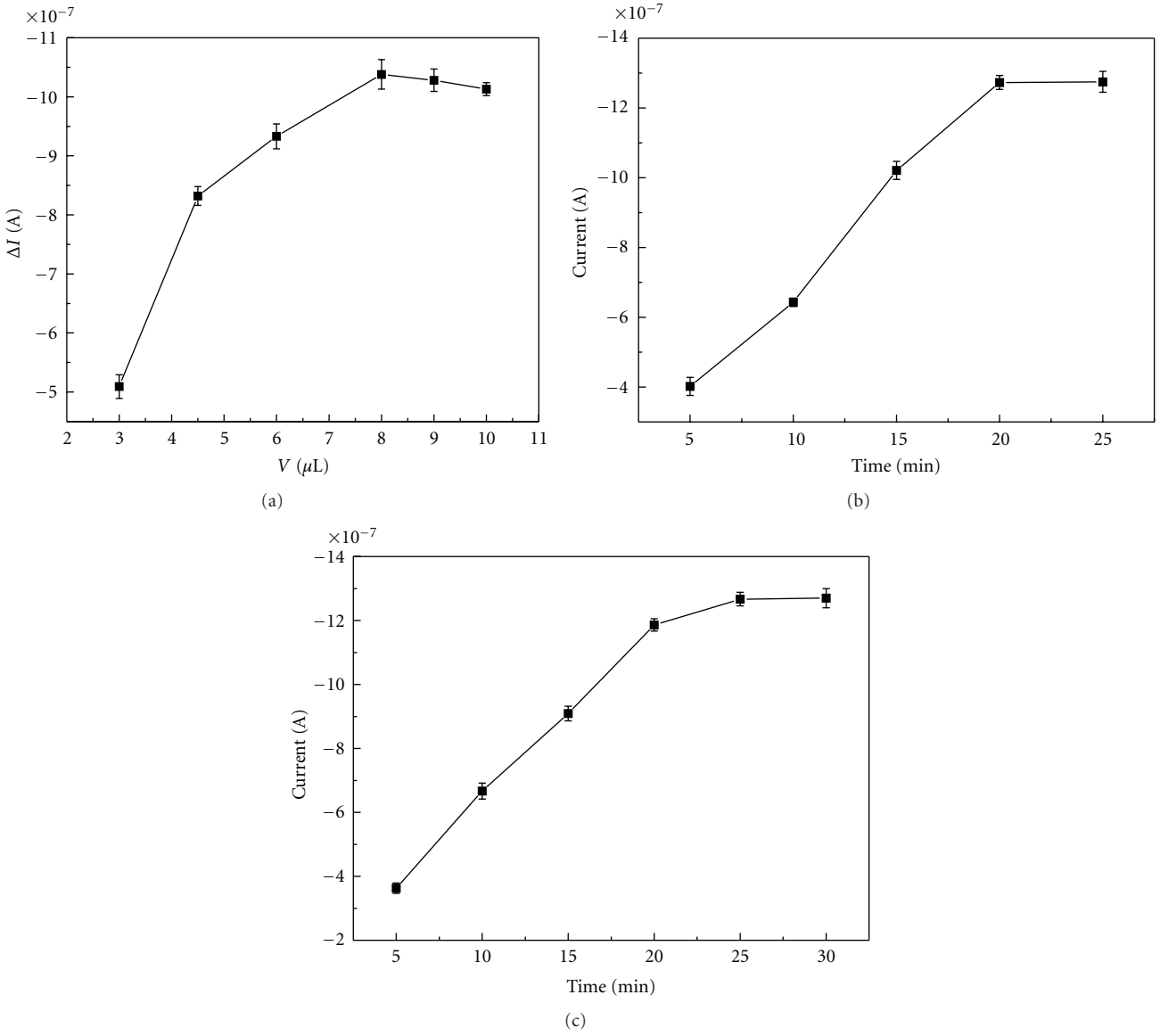

Figure 3: (a) Peak current of adriamycin (ΔI) dependence of amounts of probe DNA. The concentration of complementary target DNA is 1.0×10^{-10} M; DPV parameters were the same as in Figure 2(B). (b) Effect of accumulation time on the DPV signals of adriamycin. The concentration of adriamycin is 1.0×10^{-6} M; DPV parameters were the same as in Figure 2(B). (c) DPV signals of adriamycin dependence on DNA hybridization time. The concentration of adriamycin is 1.0×10^{-6} M; the concentration of complementary target DNA is 1.0×10^{-10} M. DPV parameters were the same as in Figure 2(B).

3.5. Analytical Performance. Under the optimal conditions, the analytical performance of the DNA biosensor was investigated using the immobilized probe DNA to hybridize with the different concentrations of the complementary sequence. Figure 6 shows the DPVs records of intercalated adriamycin at various complementary oligonucleotides concentrations. It could be observed that the peak currents of adriamycin increased with increasing the concentration of complementary DNA, and the peak currents difference (ΔI) was linear with the logarithmic value of the concentration of the complementary DNA in the range from 5.0×10^{-13} to 1.0×10^{-9} M. The regression equation was ΔI (10^{-7} A) = $3.5518 \log C_{\mathrm{DNA}} + 45.3301$ (unit of C is M), and the regression coefficient (R) of the linear curve was 0.9979. The detection limit is 1.7×10^{-13} M (S/N = 3). Compared with reported sensors [23–25], this DNA biosensor showed higher sensitivity.

3.6. Reproducibility, Reusability, and Stability of the DNA Biosensor. The reproducibility of biosensor is a very important factor for their application. Four DNA sensors were fabricated independently under the same conditions and used to detect 1.0×10^{-10} M complementary DNA. And the reduction peak currents of adriamycin were 1.217×10^{-6} A, 1.258×10^{-6} A, 1.259×10^{-6} A, and 1.227×10^{-6} A,

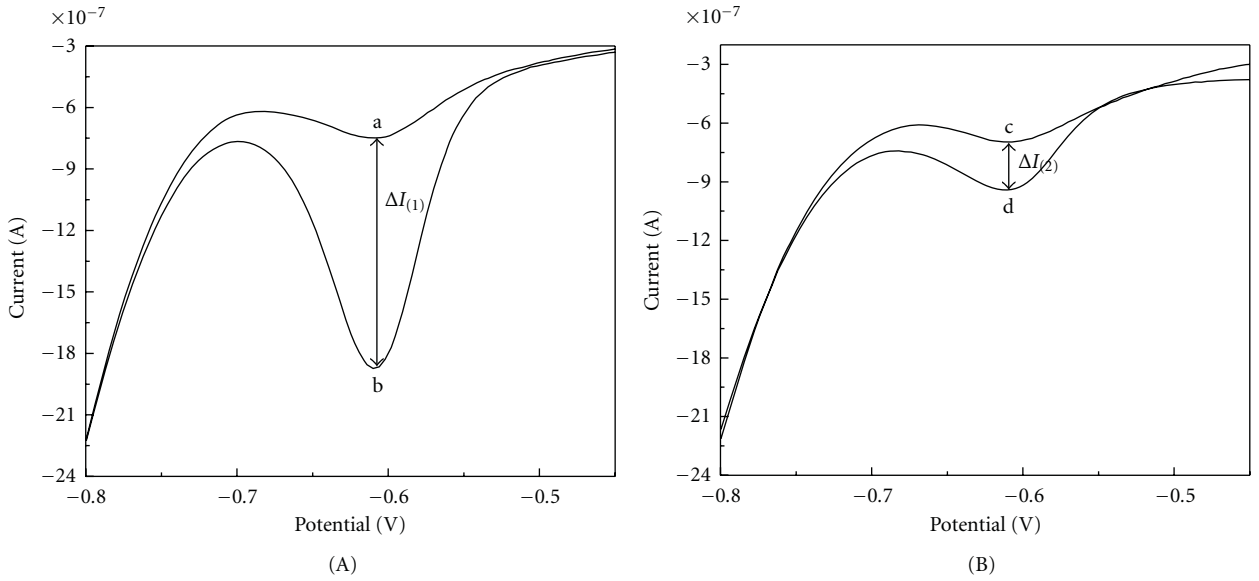

Figure 4: (A) DPV responses obtained for ss-DNA/MAA/AuNPs/Au (a), hybridized with 1.0×10^{-10} M complementary DNA (b). (B) DPV responses obtained for the ss-DNA/MAA/Au (c), hybridized with 1.0×10^{-10} M complementary DNA (d). Experiment condition: accumulation time of adriamycin: 20 min; hybridization time: 25 min. DPV parameters were the same as in Figure 2(B).

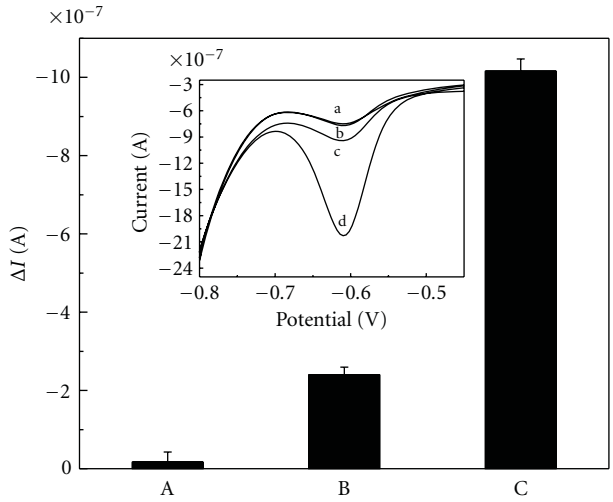

Figure 5: The histograms of the peak current difference (ΔI) of adriamycin versus different DNA sequences (1.0×10^{-10} M): (A) noncomplementary sequence, (B) single-base mismatch sequence, (C) complementary sequence. Inset: DPV responses of adriamycin recorded at probe modified electrode (a) and after hybridization with 1.0×10^{-10} M noncomplementary sequence (b); 1.0×10^{-10} M single-base mismatch sequence (c); 1.0×10^{-10} M complementary sequence (d). Accumulation time of adriamycin: 20 min; Hybridization time: 25 min. DPV parameters were the same as in Figure 2(B).

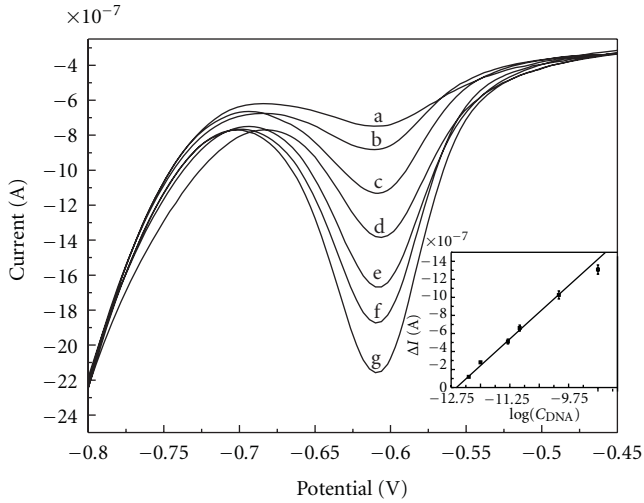

Figure 6: DPV response of the intercalated adriamycin recorded for the probe DNA modified electrode that hybridized with various concentrations of complementary DNA: (a) 0 M; (b) 5.0×10^{-13} M; (c) 1.0×10^{-12} M; (d) 5.0×10^{-12} M; (e) 1.0×10^{-11} M; (f) 1.0×10^{-10} M; (g) 1.0×10^{-9} M. Inset: Peak current (ΔI) of the intercalated adriamycin versus logarithm of concentration of complementary DNA. Error bars show the standard deviations of measurements taken from three independent experiments. Accumulation time of adriamycin: 20 min; hybridization time: 25 min. The DPV parameters were the same as in Figure 2(B).

respectively. The average value was 1.2402×10^{-6} A, and the relative standard deviation (RSD) was 2.15%.

The reusability of the DNA biosensor was investigated by immersing hybridized electrodes in hot water (80°C) for 5–10 min to make ds-DNA into ss-DNA via thermal denaturation. The renew sensor was used to test 1.0×10^{-10} M complementary DNA and found that the fifth regenerated sensor has 84.7% response of the initial sensor (initial: 1.24×10^{-6} A, final: 1.05×10^{-6} A). This result indicated the proposed DNA biosensor had a good reusability.

The stability of the biosensor was also examined. The DNA sensor was stored in a freezer at 4°C for two weeks, and no apparent change about the peak current of adriamycin was observed.

4. Conclusions

A simple and sensitive electrochemical DNA biosensor based on ss-DNA/MAA/AuNPs modified electrode was fabricated. AuNPs could enhance the immobilization capacity of probe DNA and amplify electrochemical signal. This DNA biosensor exhibited excellent selectivity and stability.

Acknowledgment

The authors gratefully acknowledge the National Nature Science Foundation of China (no. 20675002), which financially supported this work.

References

[1] F. Patolsky, G. Zheng, and C. M. Lieber, "Nanowire sensors for medicine and the life sciences," *Nanomedicine*, vol. 1, no. 1, pp. 51–65, 2006.

[2] D. Ivnitski, D. J. O'Neil, A. Gattuso, R. Schlicht, M. Calidonna, and R. Fisher, "Nucleic acid approaches for detection and identification of biological warfare and infectious disease agents," *BioTechniques*, vol. 35, no. 4, pp. 862–869, 2003.

[3] F. Lucarelli, I. Palchetti, G. Marrazza, and M. Mascini, "Electrochemical DNA biosensor as a screening tool for the detection of toxicants in water and wastewater samples," *Talanta*, vol. 56, no. 5, pp. 949–957, 2002.

[4] V. Benoit, A. Steel, M. Torres, Y. Y. Yu, H. Yang, and J. Cooper, "Evaluation of three-dimensional microchannel glass biochips for multiplexed nucleic acid fluorescence hybridization assays," *Analytical Chemistry*, vol. 73, no. 11, pp. 2412–2420, 2001.

[5] R. Y. Wang, M. N. Ji, R. Wang, and J. Shi, "Stopped-flow kinetic fluorimetric studies of the interaction of Ru(II) complex with DNA and its analytical application," *Spectrochimica Acta Part A*, vol. 71, no. 3, pp. 1042–1048, 2008.

[6] Q. Wang, X. Yang, and K. Wang, "Enhanced surface plasmon resonance for detection of DNA hybridization based on layer-by-layer assembly films," *Sensors and Actuators B*, vol. 123, no. 1, pp. 227–232, 2007.

[7] X. Yang, Q. Wang, K. Wang, W. Tan, and H. Li, "Enhanced surface plasmon resonance with the modified catalytic growth of Au nanoparticles," *Biosensors and Bioelectronics*, vol. 22, no. 6, pp. 1106–1110, 2007.

[8] J. Zhang, R. Lao, S. Song, Z. Yan, and C. Fan, "Design of an oligonucleotide-incorporated nonfouling surface and its application in electrochemical DNA sensors for highly sensitive and sequence-specific detection of target DNA," *Analytical Chemistry*, vol. 80, no. 23, pp. 9029–9033, 2008.

[9] C. Ding, F. Zhao, M. Zhang, and S. Zhang, "Hybridization biosensor using 2,9-dimethyl-1,10-phenantroline cobalt as electrochemical indicator for detection of hepatitis B virus DNA," *Bioelectrochemistry*, vol. 72, no. 1, pp. 28–33, 2008.

[10] M. Li, S. Huang, P. Zhu, L. Kong, B. Peng, and H. Gao, "A novel DNA biosensor based on ssDNA/Cyt c/l-Cys/GNPs/Chits/GCE," *Electrochimica Acta*, vol. 54, no. 8, pp. 2284–2289, 2009.

[11] T. G. Drummond, M. G. Hill, and J. K. Barton, "Electrochemical DNA sensors," *Nature Biotechnology*, vol. 21, no. 10, pp. 1192–1199, 2003.

[12] J. Zhang, S. Song, L. Zhang et al., "Sequence-specific detection of femtomolar DNA via a chronocoulometric DNA sensor (CDS): effects of nanoparticle-mediated amplification and nanoscale control of DNA assembly at electrodes," *Journal of the American Chemical Society*, vol. 128, no. 26, pp. 8575–8580, 2006.

[13] H. Zhong, X. Lei, X. Hun, and S. Zhang, "Design of one-to-one recognition triple Au nanoparticles DNA probe and its application in the electrochemical DNA biosensor," *Chemical Communications*, no. 45, pp. 6958–6960, 2009.

[14] S. Zhang, J. Xia, and X. Li, "Electrochemical biosensor for detection of adenosine based on structure-switching aptamer and amplification with reporter probe DNA modified Au nanoparticles," *Analytical Chemistry*, vol. 80, no. 22, pp. 8382–8388, 2008.

[15] J. Wang, J. Li, A. J. Baca et al., "Amplified voltammetric detection of DNA hybridization via oxidation of ferrocene caps on gold nanoparticle/streptavidin conjugates," *Analytical Chemistry*, vol. 75, no. 15, pp. 3941–3945, 2003.

[16] M. H. Abouzar, A. Poghossian, A. M. Pedraza et al., "An array of field-effect nanoplate SOI capacitors for (bio-)chemical sensing," *Biosensors and Bioelectronics*, vol. 26, no. 6, pp. 3023–3028, 2011.

[17] K. Zhang, H. Ma, L. Zhang, and Y. Zhang, "Fabrication of a sensitive impedance biosensor of DNA hybridization based on gold nanoparticles modified gold electrode," *Electroanalysis*, vol. 20, no. 19, pp. 2127–2133, 2008.

[18] H. Ma, L. Zhang, Y. Pan, K. Zhang, and Y. Zhang, "A novel electrochemical DNA biosensor fabricated with layer-by-layer covalent attachment of multiwalled carbon nanotubes and gold nanoparticles," *Electroanalysis*, vol. 20, no. 11, pp. 1220–1226, 2008.

[19] Y. Zhang, H. Ma, K. Zhang, S. Zhang, and J. Wang, "An improved DNA biosensor built by layer-by-layer covalent attachment of multi-walled carbon nanotubes and gold nanoparticles," *Electrochimica Acta*, vol. 54, no. 8, pp. 2385–2391, 2009.

[20] M. T. Castañeda, S. Alegret, and A. Merkoçi, "Electrochemical sensing of DNA using gold nanoparticles," *Electroanalysis*, vol. 19, no. 7-8, pp. 743–753, 2007.

[21] X. Zhang, F. Shi, X. Yu et al., "Polyelectrolyte multilayer as matrix for electrochemical deposition of gold clusters: toward super-hydrophobic surface," *Journal of the American Chemical Society*, vol. 126, no. 10, pp. 3064–3065, 2004.

[22] A. W. Peterson, R. J. Heaton, and R. M. Georgiadis, "The effect of surface probe density on DNA hybridization," *Nucleic Acids Research*, vol. 29, no. 24, pp. 5163–5168, 2001.

[23] S. F. Liu, Y. F. Li, J. R. Li, and L. Jiang, "Enhancement of DNA immobilization and hybridization on gold electrode modified by nanogold aggregates," *Biosensors and Bioelectronics*, vol. 21, no. 5, pp. 789–795, 2005.

[24] H. Cai, C. Xu, P. He, and Y. Fang, "Colloid Au-enhanced DNA immobilization for the electrochemical detection of sequence-specific DNA," *Journal of Electroanalytical Chemistry*, vol. 510, no. 1-2, pp. 78–85, 2001.

[25] J. Kang, X. Li, G. Wu, Z. Wang, and X. Lu, "A new scheme of hybridization based on the Au_{nano}-DNA modified glassy carbon electrode," *Analytical Biochemistry*, vol. 364, no. 2, pp. 165–170, 2007.

SAGE-Hindawi Access to Research
International Journal of Electrochemistry
Volume 2011, Article ID 529415, 6 pages
doi:10.4061/2011/529415

Research Article

Determination of Mercury (II) Ion on Aryl Amide-Type Podand-Modified Glassy Carbon Electrode

Sevgi Güney, Gülcemal Yıldız, and Gönül Yapar

Department of Chemistry, Faculty of Science and Letters, Istanbul Technical University, 34469, Maslak Istanbul, Turkey

Correspondence should be addressed to Sevgi Güney, kartal@itu.edu.tr

Received 30 December 2010; Revised 7 March 2011; Accepted 28 March 2011

Academic Editor: Farnoush Faridbod

Copyright © 2011 Sevgi Güney et al. This is an open access article distributed under the Creative Commons Attribution License, which permits unrestricted use, distribution, and reproduction in any medium, provided the original work is properly cited.

A new voltammetric sensor based on an aryl amide type podand, 1,8-bis(o-amidophenoxy)-3,6-dioxaoctane, (AAP) modified glassy carbon electrode, was described for the determination of trace level of mercury (II) ion by cyclic voltammetry (CV) and differential pulse voltammetry (DPV). A well-defined anodic peak corresponding to the oxidation of mercury on proposed electrode was obtained at 0.2 V versus Ag/AgCl reference electrode. The effect of experimental parameters on differential voltammetric peak currents was investigated in acetate buffer solution of pH 7.0 containing 1×10^{-1} mol L^{-1} NaCl. Mercury (II) ion was preconcentrated at the modified electrode by forming complex with AAP under proper conditions and then reduced on the surface of the electrode. Interferences of Cu^{2+}, Pb^{2+}, Fe^{3+}, Cd^{2+}, and Zn^{2+} ions were also studied at two different concentration ratios with respect to mercury (II) ions. The modified electrode was applied to the determination of mercury (II) ions in seawater sample.

1. Introduction

Podands, which are the member of the crown-ether family, have an importance in supramolecular chemistry because of their applications in ion sensing and also have high productivity and selectivity in forming complexes with alkali, alkaline earth metal, and transition metal ions [1–3]. Podands could allow conformational changing in structure for the binding of a guest molecule because they have more flexibility than their crown-ether analogues [4]. Since podand-type ligands have ability to form of spheroidal cavities and strong binding sites, they have attracted considerable interest in recent years. Amide-type podands have an importance for producing the complexes possessing high fluorescent properties [5].

Determination of mercury is an important issue because of high toxicity, reactivity, and excessive mobility of mercury in environment. In addition, mercury has crucial risk to human health [6]. Therefore, there is a necessity of improving fast, sensitive, and selective analytical techniques for analysis of mercury. Current instrumental analysis methods, such as UV spectrophotometry [7], X-ray fluorescence [8], atomic fluorescence spectrometry (AFS) [9], cold vapor atomic fluorescence spectrometry [10], atomic absorption spectrometry (AAS) [11], cold vapor atomic absorption spectrometry [12], and inductively coupled plasma mass spectrometry [13], have been extensively employed for trace determination of mercury (II) ion in the laboratory conditions. Since they are expensive, time-consuming and complicated for in situ measuring, they are not suitable for point-of-use applications. Alternatively, electrochemical techniques could be used for the mercury determination, because these techniques are easier and cheaper than the instrumental analysis methods mentioned above.

Chemically modified electrodes (CMEs) have attracted great attention in the past decades since they improve the sensitivity and selectivity of electrochemical analysis methods [14]. Description and fabrication of CMEs have been mentioned in an IUPAC report [15]. CMEs have various advantages, such as low cost, short analysis time, high sensitivity and selectivity in electroanalytical determinations of different compounds [16]. They are also used in different applications, for example, corrosion protection, selective electroorganic synthesis, solar energy conversion and

storage, molecular electronics, and electrochromic display devices [17]. Modification of the electrode surfaces with appropriate modifiers enhances the selectivity and sensitivity of electroanalytical methods. There are several ways to modify the working electrode surface, for example, electrochemical, chemical, or physical methods. Stripping electrochemical technique is an alternative method for mercury determination due to its versatility, sensitivity, and low cost [17]. A number of articles have been published for the analysis of mercury (II) ion by CMEs [18–23]. The limit of detection (LOD) was argued in the literature for the determination of mercury (II) ion by CMEs which were approximately in the range of 10^{-9} M as same as our current work. Furthermore, there has been no study in the literature for the determination of mercury (II) ion with AAP-modified electrode yet.

In the present study, the aryl amide type podand, AAP, was synthesized according to our previous work [24]. AAP modified glassy carbon electrode (AAP/GCE) was prepared, and differential pulse anodic stripping voltammetry was used for analytical response of mercury (II) ions. The effect of analytical parameters such as pH, deposition potential, deposition time, and the amount of AAP as modifying agent were investigated. Interference effects of other metallic ions that might also form complexes with Cl^- ion and the repeatability of the method were investigated, and also, detection mechanism was proposed. The accuracy of method was tested in the artificial seawater samples. AAP is a hopeful modifying agent in sensor application for determination of mercury (II) ion in mixture of aqueous solution compared with the other crown-ether molecules since it can be easily synthesized and also modified on electrode surface.

2. Experimental

2.1. Synthesis of AAP. Into a flask (50 mL) salicylamide (2.74 g, 20 mmoL), Na_2CO_3 (2.36 g, 22 mmoL), DMF (20 mL), and 1,8-dichloro-3,6-dioxaoctane (1.87 g, 10 mmoL) were added and heated at 80–85°C for 72 h. Then, the mixture of reaction was poured into water (200 mL). The filtered residue was washed with water and dried at 75°C. The crude product was dissolved in CH_2Cl_2 and chromatographed on silica gel (50 g) with CH_2Cl_2/acetone: 3/2 (v/v). 3.31 g, 85% yield, colorless leafs. Structure of synthesized AAP is shown in Scheme 1.

2.2. Reagents and Materials. All chemicals used in these experiments were of the highest purity (used without further purification) and were obtained from Merck, Fluka, and Riedel de Haen Chemical Companies. Salicylamide (Alfa Aesar), 1,8-dichloro-3,6-dioxaoctane and DMF (Fluka), silica gel 40–63 u 60 A (Fluorochem), Hg $(CH_3COO)_2$ (Merck). All solutions were prepared by using ultrapure water from Millipore MilliQ System (sensitivity equal to 18 MΩ). A stock solution of 1×10^{-2} M AAP was prepared in ethyl alcohol. Buffer solutions were prepared by adjustment of pH with HCl or KOH. All electrochemical experiments were carried out in a conventional three-electrode system under the room temperature (25 ± 1°C).

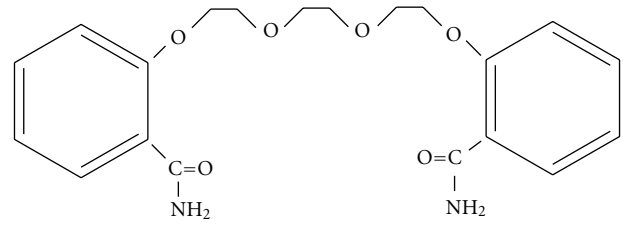

Scheme 1: The structure of the 1, 8-bis (o-amidophenoxy)-3, 6-dioxaoctane.

2.3. Instrumentation. All electrochemical measurements were carried out on Autolab PGSTAT 30 (Eco Chemie) potentiostat/galvanostat. A classical three-electrode cell consists of Ag/AgCl (3 M KCl) reference electrode, a platinum wire counter electrode (BAS MW 1032), and a glassy carbon working electrode (the diameter of working electrode is 3 mm, BAS MF-2012). Instrumental parameters were as follows: pulse amplitude 50 mV, pulse width 50 ms, potential step 4 mV pulse period 0.2 s, and scan rate 50 mV s^{-1}. Solutions were deoxygenated for 10 minutes with high-grade nitrogen, and an inert atmosphere was obtained over the solutions during analysis. The solutions were adjusted using a pH meter (WTW Inolab pH 720). An ultrasonic bath was used for preparing the homogeneous solutions (Bandelin Sonorex RK 100H). Spin coating of the glassy carbon electrode was performed by using IKEA RW 20 rotator.

2.4. Preparation of the AAP Modified Glassy Carbon Electrode (AAP/GCE). Before the modification, surface of the glassy carbon electrode (GCE) was polished to gain a mirror-like appearance with 1.0, 0.3, and 0.05 μm of aluminum oxide slurry, respectively. After the polishing, GCE was sonicated twice in ethyl alcohol and ultrapure water for 5 min each. After that, electrochemical pretreatment was performed by the potential step which was applied at +0.8 V for 5 minutes and −1.4 V for 1 minute in 1×10^{-1} moL L^{-1} H_2SO_4 solution, respectively. Then, modification of the surface of the electrode with AAP was performed by spin coating employing a rotator with a speed of 300 rpm. Two drops of 10 μL of 5.0×10^{-3} moL L^{-1} AAP dissolved in ethyl alcohol were dropped on the spinning electrode and then dried in room temperature.

2.5. Analytical Procedure. The procedure of preconcentration and voltammetric determination of mercury (II) ion on AAP modified electrode includes the following steps: (1) modifying the GC electrode with AAP, (2) dipping of the modified electrode in aqueous solution of mercury (II) at open circuit, (3) electrochemical reduction of mercury (II) ions to metallic mercury at −0.8 V for 12 min by stirring in an acetate buffer solution of pH 7.0 containing 0.1 moL L^{-1} NaCl, and (4) voltammetric determination of mercury (II) ions by DPV from −0.1 V to 0.4 V in the same solution. The modified electrode was reused by holding the potential +0.8 V for 3 min. to remove any previous

deposits for repeated determinations. AAP-modified glassy carbon electrode was tested in a new buffer solution without mercury (II) ions, before each experiment.

3. Results and Discussion

3.1. Voltammetric Behavior of Mercury (II) on AAP-Modified GCE. The capability of AAP/GCE for preconcentration and determination of mercury (II) was investigated. Figure 1 shows the CVs at AAP-modified GCE in the absence and presence of mercury (II) after preconcentration.

As can be seen in Figure 1, a well-defined anodic peak (I_p) was obtained at 0.2 V (solid line) due to the electrochemical oxidation of mercury (0) to mercury (II), and mercury (0) was produced by the electrochemical reduction of captured mercury (II) at the deposition step under negative potentials. Furthermore, no mercury peak was observed in the absence of mercury (II) as a control experiment (dashed line).

These experimental results showed that mercury (II) ions from the solution can form strong $HgCl_4^{2-}$ complex with Cl^- ions. Then $HgCl_4^{2-}$ complex is deposited on the modified electrode surface and reduced to Hg^0 following Hg^0 being oxidized to Hg^{2+} ion. Therefore, the possible electrochemical reaction mechanism can be illustrated as follows.

Deposition:

$$\left(HgCl_4{}^{2-}\right)_{\text{solution}} + \left(\frac{AAP}{GCE}\right)_{\text{surface}} \longrightarrow \left(HgCl_4{}^{2-} - \frac{AAP}{GCE}\right)_{\text{surface}}. \quad (1)$$

Reduction:

$$\left(HgCl_4{}^{2-} - \frac{AAP}{GCE}\right)_{\text{surface}} + 2e^- \longrightarrow \left(Hg^0 - \frac{AAP}{GCE}\right)_{\text{surface}} + 4Cl^-. \quad (2)$$

Oxidation:

$$\left(Hg^0 - \frac{AAP}{GCE}\right)_{\text{surface}} \longrightarrow (Hg^{2+})_{\text{solution}} + \left(\frac{AAP}{GCE}\right)_{\text{surface}} + 2e^-. \quad (3)$$

3.2. Optimization of Measurement Condition. In order to obtain optimum experimental conditions for mercury (II) determination, several parameters were investigated such as type and pH of the buffer solution, AAP concentration on electrode surface, deposition potential, and deposition time.

The effect of supporting electrolytes was investigated in acetate, phosphate, and B-R buffer solutions, respectively. The results indicated that voltammetric peaks were observed in all electrolyte solutions, but the electrochemical response of mercury (II) ion in 0.1 moL L^{-1} HAc + 0.1 moL L^{-1} NaCl solution gave the best shaped and largest peak current among these solutions. Therefore, this supporting electrolyte was used in following experiments. The effect of pH on the anodic stripping peak currents of mercury (II) ion on the modified electrode was studied by differential pulse voltammetry, and the graph of the peak currents against pH was plotted (data was not shown). AAP modified glassy carbon electrode showed the stable activity over the range of pH 3.0–12.0, and the best peak height and shape were obtained at pH 7.0. This pH-dependent behavior of mercury (II) ion can be explained by the fact that different protonation ability of AAP affects the formation constant of

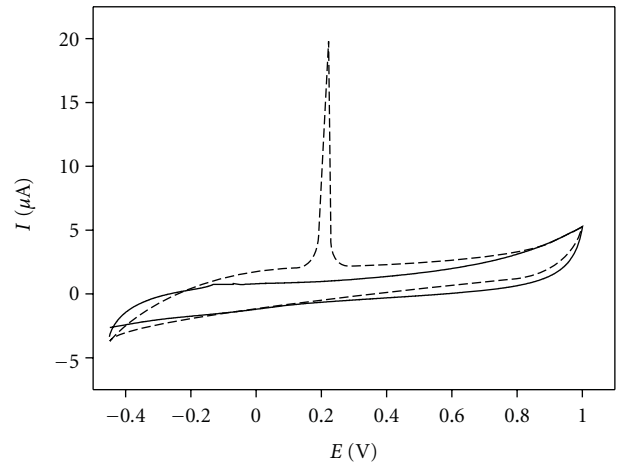

Figure 1: Cyclic voltammograms of blank solution (solid line) and 5×10^{-7} moL L^{-1} of Hg^{2+} at AAP modified GC electrode (dashed line). Electrolyte: 0.1 mol L^{-1} HAc + 0.1 mol L^{-1} NaCl (pH 7.0) solution. Deposition time (t_d): 12 min.; deposition potential (E_d): −0.8 V; scan rate (v): 50 mV/s. GC electrode modified with 0.125 μmoL AAP.

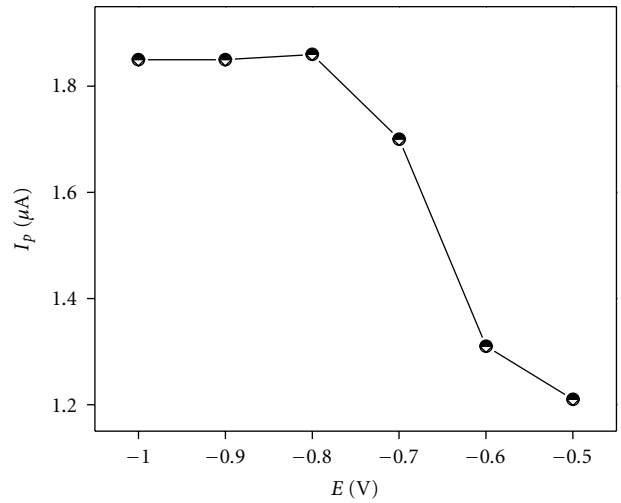

Figure 2: Effects of deposition potential on DPV peak currents for 5×10^{-7} moL of Hg^{2+} at AAP modified GC electrode. Electrolyte: 0.1 mol L^{-1}HAc + 0.1 mol L^{-1}NaCl (pH 7.0) solution. GC electrode modified with 0.063 μmol AAP, t_d: 10 min

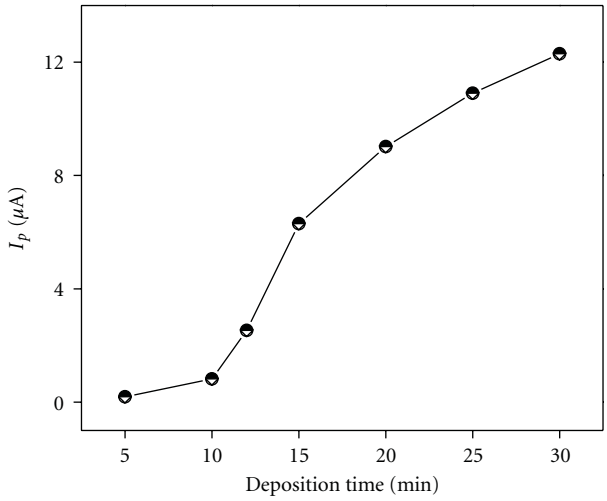

Figure 3: Effects of deposition time on DPV peak currents for 5×10^{-7} mol L^{-1} Hg^{2+} at AAP modified GCE. E_d: −0.8 V. The other conditions are the same as in Figure 2.

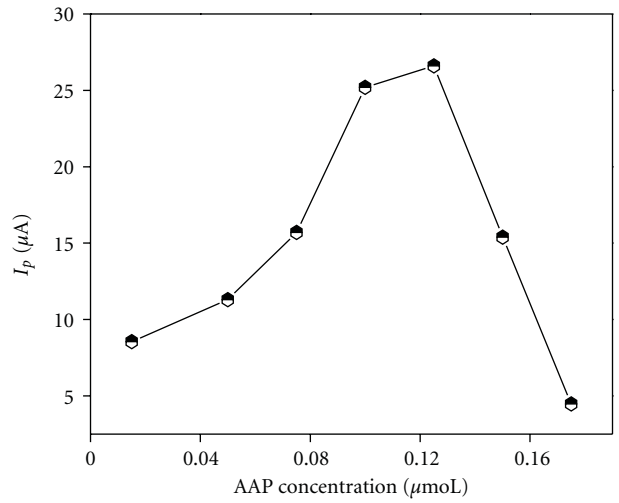

Figure 4: Effects of electrode surface concentration of AAP on DPV peak currents for 5×10^{-7} mol $L^{-1}Hg^{2+}$ at modified electrode. Electrolyte: 0.1 mol L^{-1}HAc + 0.1 mol L^{-1}NaCl (pH 7.0) solution. E_d: −0.8 V, t_d: 12 min.

the complex between mercury (II) ions and AAP at different pH.

Deposition potential (E_d) is an important parameter that affects the sensitivity of detection. AAP-modified GCE was kept at the potentials varying between −0.5 V and −1.0 V for 10 min. in a solution of 5×10^{-7} moL L^{-1} mercury (II), and DPV was performed. The change in DPV peak currents depending on the deposition potentials is shown in Figure 2. As can be seen in Figure 2, the peak current increases with the deposition potentials reaching a plateau at about −0.8 V, therefore, this potential was selected as optimal deposition potential.

The effect of deposition time (t_d) for mercury (II) determination is shown in Figure 3. The peak current increased with increasing deposition time. The longer the deposition time, the higher the sensitivity obtained in stripping voltammetry, but with narrow detection range results. In this detection system, deposition saturation was reached for 5×10^{-7} moL L^{-1} Hg^{2+} by the preconcentration of 30 minutes as shown in Figure 3. Considering the detection limit and linear range, deposition time of 12 minutes was chosen in this study.

The concentration of AAP on the electrode surface affects the deposition capacity of mercury (II) ion and changes the oxidation current (Figure 4). As can be seen in Figure 4, the initial peak current increased up to 0.125 μmoL of AAP since the reactive areas involved in the complexation reaction between mercury and AAP increase with AAP concentration. At the higher concentration of 0.125 μmoL of AAP, the electron transfer between the mercury and electrode was blocked resulting in decrease of current. Therefore, the concentration of 0.125 μmoL was selected as the optimum AAP concentration.

3.3. Interference of Foreign Metal Ions. Under optimized experimental conditions mentioned above, the possible interferences of other metal ions like Cd^{2+}, Pb^{2+}, Fe^{3+}, and Cu^{2+} for the determination of 1 μmoL L^{-1} μHg^{2+} were examined with AAP-modified electrode (Figure 5). The effect of the inference was tested in two compositions of the solution containing 1 and 10 μmoL L^{-1} of metal ions. The same experiment was also carried out with unmodified glassy carbon electrode (Figure 5, inset).

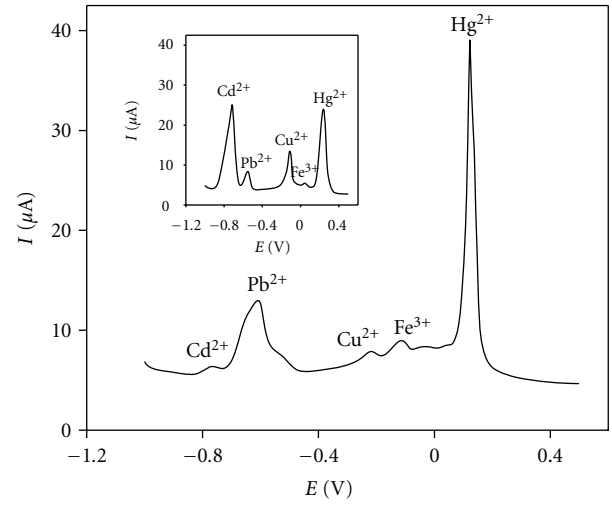

Figure 5: DPVs of 1 μmol L^{-1} Hg^{2+} in the presence of 10 μmol L^{-1} each of Cd^{2+}, Pb^{2+}, Cu^{2+}, Fe^{3+}, Zn^{2+} ions at AAP-modified GCE. The other conditions are those in Figure 4. Inset figure: DPVs of the same electrolyte on bare GCE.

As can be seen in Figure 5, the peak current belonging to Cd^{2+} decreased but the peak current of mercury (II) was twofold increased and shifted to more negative potential on modified electrode. On the other hand, Fe^{3+} and Cu^{2+} exhibit very small peak currents comparing to that of mercury (II). Pb^{2+} ion does not affect the mercury (II) peak current since the peak potential of Pb^{2+} is more negative than that of the

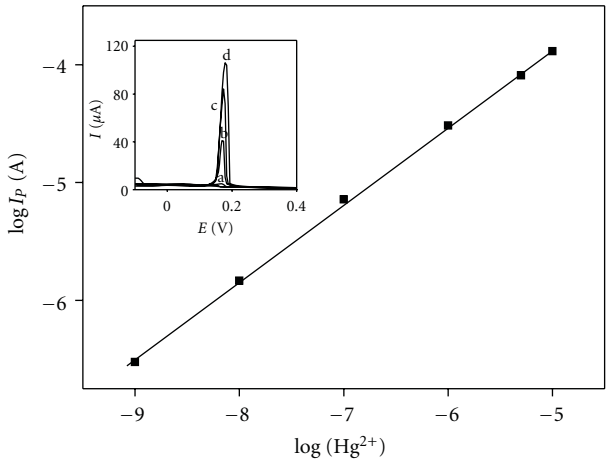

Figure 6: Calibration plot of logI_p versus log [Hg^{2+}]. Inset figure: DPVs of different concentrations of Hg^{2+} (a) 1.0×10^{-9}, (b) 1.0×10^{-8}, (c) 1.0×10^{-7}, (d) 1.0×10^{-6} mol L^{-1}. The other conditions are same as in Figure 4.

Table 1: The effect of interference of some metal ions on mercury determination under optimized experimental conditions at AAP/GCE. Solution contains 1 μmoL L-1 Hg2+ and interferences are (a) 1 μmoL L-1 and (b) 10 μmoL L-1.

cation	$I_p(Hg^{2+})$ μA	Recovery %	$I_p(Hg^{2+})$ μA	Recovery %
Hg^{2+}	49	100	49	100
Fe^{3+}	57[a]	116	66[b]	135
Zn^{2+}	47[a]	96	46[b]	94
Pb^{2+}	48[a]	99	48[b]	99
Cu^{2+}	54[a]	110	64[b]	130
Cd^{2+}	46[a]	94	45[b]	92

Table 2: Determination of Hg2+ in artificial seawater samples by DPV at AAP/GCE.

Added $Hg^{2+}(10^{-7}$ M)	Found $Hg^{2+}(10^{-7}$ M) ($n = 6$)	Recovery, %	RSD, % ($n = 6$)
5.0	4.93 ± 0.11	98.6	2.23
8.0	7.92 ± 0.15	99.0	1.89
10.0	9.91 ± 0.14	99.1	1.41

mercury (II). The interference effects of some metal ions are given in Table 1.

3.4. Calibration Plot, Limit of Detection, and Validation of Method. Under the optimum conditions described above, the reproducibility of the proposed method was evaluated with the solution of 1×10^{-7} mol L^{-1} mercury (II) for six repetitive measurements. The relative standard deviation (RSD) was 1.84% which presented the good reproducibility of the proposed modified electrode. Linearity of the calibration curve was also investigated in the mercury (II) concentration ranges from 1×10^{-9} mol L^{-1} to 1×10^{-5} mol L^{-1} (Figure 6, inset).

The calibration plot (Figure 6) shows a good linear behavior with correlation coefficient (R^2) of 0.9997, and the resulting equation is log $I(A) = 2 - 0.5954 + 0.6556$ log C (mol L^{-1}). The limit of detection is 4×10^{-9} mol L^{-1} ($S/N = 3$). These values verified the sensitivity of the proposed method for the determination of mercury (II). AAP/GCE can be stored about 4 weeks, and the decrease in response was 2.54%, indicating the good stability of electrode. When the proposed electrode was compared with the other macrocyclic kinds of modified electrodes for mercury (II) determination, it can be seen that the detection limits of them were in the range of 1.0×10^{-8} and 1.0×10^{-7} mol L^{-1} [22, 25–28]. Consequently, AAP modified electrode could be a promising voltammetric sensor for trace analysis of mercury (II) ion.

3.5. Analytical Applications. The accuracy of the proposed method was tested in artificial seawater sample by spiking known concentrations of mercury (II) ion. Artificial seawater was prepared according to the literature [29]. Determination of mercury (II) concentration was performed by the calibration curve method. The experimental parameters were the same as described above, and the results are summarized in Table 2.

4. Conclusion

A new kind of chemically modified electrode has been developed for highly selective and sensitive determination of mercury (II) by forming complex with AAP. It was shown that AAP-coated glassy carbon electrode could be used for determination of mercury (II) ion from aqueous solutions since the sensitivity is greatly improved. The immersion of electrode into the solution containing Cl^- ion increased the deposition of mercury (II) ion on the electrode surface due to formation of $HgCl_4^{2-}$ complex. The results also show that AAP-modified electrode has a good reproducibility, wide linear range, high selectivity, and low detection limit. It can be a very good alternative to expensive analytical techniques such as atomic absorption spectrometry and ICP-MS. The preparation and application of proposed modified electrode are simpler and also cheaper than those of the other electrodes modified with more complex and more expensive modifying agents.

Acknowledgments

The authors would like to thank Istanbul Technical University Research Foundation (ITU-BAP Project no. 32646) and Scientific and Technical Research Council of Turkey (TUBITAK Project no. 104T079) for their financial support.

References

[1] G. W. Gokel, "Comprehensive supramolecular chemistry," in *Molecular Recognition: Receptors for Cationic Guest*, J. L. Atwood, Ed., vol. 1, chapter 1, Pergamon, New York, NY, USA, 1996.

[2] G. Yidiz, G. Yapar, and C. Erk, "The association constants of Na with dibenzo[3n]crown-n in THF/water using ISE," *Talanta*, vol. 64, no. 4, pp. 865–868, 2004.

[3] H. J. Kim, D. S. Park, M. H. Hyun, and Y. B. Shim, "Determination of Hg ion with a 1,11-bis(8-quinoyloxy)-3,6,9-trioxaundecane-modified glassy carbon electrode using spin-coating technique," *Electroanalysis*, vol. 10, no. 5, pp. 303–306, 1998.

[4] J. W. Steed and J. L. Atwood, *Supramolecular Chemistry*, Wiley, New York, NY, USA, 2000.

[5] Y. Zhao, Y. Tang, W. S. Liu, N. Tang, and M. Y. Tan, "Synthesis and infrared and fluorescent properties of rare earth complexes with a new aryl amide podand," *Spectrochimica Acta—Part A*, vol. 65, no. 2, pp. 372–377, 2006.

[6] W. F. Fitzgerald, C. H. Lamborg, and C. R. Hammerschmidt, "Marine biogeochemical cycling of mercury," *Chemical Reviews*, vol. 107, no. 2, pp. 641–662, 2007.

[7] M. S. Jeoung and H. S. Choi, "Spectrophotometric determination of trace Hg(II) in cetyltrimethylammonium bromide media," *Bulletin of the Korean Chemical Society*, vol. 25, no. 12, pp. 1877–1880, 2004.

[8] E. K. Pavlos and G. K. K. Nikolaos, "Selective mercury determination after membrane complexation and total reflection X-ray fluorescence analysis," *Analytical Chemistry*, vol. 76, no. 15, pp. 4315–4319, 2004.

[9] L. Rahman, W. T. Corns, D. W. Bryce, and P. B. Stockwell, "Determination of mercury, selenium, bismuth, arsenic and antimony in human hair by microwave digestion atomic fluorescence spectrometry," *Talanta*, vol. 52, no. 5, pp. 833–843, 2000.

[10] M. Roulet, M. Lucotte, J. R. D. Guimarães, and I. Rheault, "Methylmercury in water, seston, and epiphyton of an Amazonian river and its floodplain, Tapajós River, Brazil," *Science of the Total Environment*, vol. 261, pp. 43–59, 2000.

[11] J. L. Capelo, I. Lavilla, and C. Bendicho, "Room temperature sonolysis-based advanced oxidation process for degradation of organomercurials: application to determination of inorganic and total mercury in waters by flow injection-cold vapor atomic absorption spectrometry," *Analytical Chemistry*, vol. 72, no. 20, pp. 4979–4984, 2000.

[12] S. C. Hight and J. Cheng, "Determination of total mercury in seafood by cold vapor-atomic absorption spectroscopy (CVAAS) after microwave decomposition," *Food Chemistry*, vol. 91, no. 3, pp. 557–570, 2005.

[13] J. C. A. Wuillouda, R. G. Wuillouda et al., "Gas chromatography/plasma spectrometry- an important analytical tool for elemental speciation studies," *Spectrochimica Acta—Part B*, vol. 59, no. 6, pp. 755–792, 2004.

[14] P. R. Moses and R. W. Murray, "Chemically modified electrodes. 3. SnO and TiO electrodes bearing an electroactive reagent [11]," *Journal of the American Chemical Society*, vol. 98, no. 23, pp. 7435–7436, 1976.

[15] R. A. Durst, A. J. Bäumner, R. W. Murray, R. P. Buck, and C. P. Andrieux, "Chemically modified electrodes: recommended terminology and definitions," *Pure and Applied Chemistry*, vol. 69, no. 6, pp. 1317–1323, 1997.

[16] C. Hu, K. Wu, X. Dai, and S. Hu, "Simultaneous determination of lead(II) and cadmium(II) at a diacetyldioxime modified carbon paste electrode by differential pulse stripping voltammetry," *Talanta*, vol. 60, no. 1, pp. 17–24, 2003.

[17] A. Giacomino, O. Abollino, M. Malandrino, and E. Mentasti, "Parameters affecting the determination of mercury by anodic stripping voltammetry using a gold electrode," *Talanta*, vol. 75, no. 1, pp. 266–273, 2008.

[18] N. L. Dias Filho and D. R. do Carmo, "Stripping voltammetry of mercury(II) with a chemically modified carbon paste electrode containing silica gel functionalized with 2,5-dimercapto-1,3,4- thiadiazole," *Electroanalysis*, vol. 17, no. 17, pp. 1540–1546, 2005.

[19] H. Zejli, P. Sharrock, J. L. H. H. De Cisneros, I. Naranjo-Rodriguez, and K. R. Temsamani, "Voltammetric determination of trace mercury at a sonogel-carbon electrode modified with poly-3-methylthiophene," *Talanta*, vol. 68, no. 1, pp. 79–85, 2005.

[20] M. Colilla, M. A. Mendiola, J. R. Procopio, and M. T. Sevilla, "Application of a carbon paste electrode modified with a schiff base ligand to mercury speciation in water," *Electroanalysis*, vol. 17, no. 11, pp. 933–940, 2005.

[21] A. Widmann and C. M. G. van den Berg, "Mercury detection in seawater using a mercaptoacetic acid modified gold microwire electrode," *Electroanalysis*, vol. 17, no. 10, pp. 825–831, 2005.

[22] H. M. Dong, L. Lin, H. Zheng, G. Zhao, and B. Ye, "Electrode modified with Langmuir-Blodgett (LB) film of calixarenes for preconcentration and stripping analysis of Hg(II)," *Electroanalysis*, vol. 18, no. 12, pp. 1202–1207, 2006.

[23] N. L. D. Filho, D. R. D. Carmo, and A. H. Rosa, "An electroanalytical application of 2-aminothiazole-modified silica gel after adsorption and separation of Hg(II) from heavy metals in aqueous solution," *Electrochimica Acta*, vol. 52, no. 3, pp. 965–972, 2006.

[24] S. Güney, G. Yapar, O. Güney, and G. Yildiz, "Elucidation of mercury ion binding property of a new aryl amide type podand by electrochemical and fluorescence measurements," *Analytical Letters*, vol. 42, no. 17, pp. 2879–2892, 2009.

[25] J. Q. Lu, X. W. He, X. S. Zeng, Q. J. Wan, and Z. Z. Zhang, "Voltammetric determination of mercury (II) in aqueous media using glassy carbon electrodes modified with novel calix[4]arene," *Talanta*, vol. 59, no. 3, pp. 553–560, 2003.

[26] A. A. Ensafi and M. Fouladgar, "A sensitive and selective bulk optode for determination of Hg(II) based on hexathiacyclooctadecane and chromoionophore V," *Sensors and Actuators, B*, vol. 136, no. 2, pp. 326–331, 2009.

[27] G. Roa-Morales, M. T. Ramírez-Silva, R. L. González, L. Galicia, and M. Romero-Romo, "Electrochemical characterization and determination of mercury using carbon paste electrodes modified with cyclodextrins," *Electroanalysis*, vol. 17, no. 8, pp. 694–700, 2005.

[28] C. Dridi, M. B. Ali, F. Vocanson et al., "Electrical and optical study on modified Thiacalix(4)arene sensing molecules: application to Hg ion detection," *Materials Science and Engineering C*, vol. 28, no. 5-6, pp. 765–770, 2008.

[29] D. R. Kester, I. W. Duedall, D. N. Connors, and R. M. Pytkowicz, "Preparation of artificial seawater," *Limnology & Oceanography*, vol. 12, pp. 176–179, 1967.

SAGE-Hindawi Access to Research
International Journal of Electrochemistry
Volume 2011, Article ID 482780, 6 pages
doi:10.4061/2011/482780

Research Article

Electrochemical Sensing of Nitric Oxide on Electrochemically Reduced Graphene-Modified Electrode

Yu-Li Wang and Guang-Chao Zhao

School of Chemistry and Materials Science, Anhui Normal University, Wuhu 241000, China

Correspondence should be addressed to Guang-Chao Zhao, gczhao@mail.ahnu.edu.cn

Received 31 January 2011; Revised 29 March 2011; Accepted 29 March 2011

Academic Editor: Vinod Kumar Gupta

Copyright © 2011 Y.-L. Wang and G.-C. Zhao. This is an open access article distributed under the Creative Commons Attribution License, which permits unrestricted use, distribution, and reproduction in any medium, provided the original work is properly cited.

Graphene-modified electrode was prepared through electrochemically reducing graphene oxide on the surface of a glassy carbon electrode in PBS solution. The as-prepared electrode owns higher stability and stronger catalytic activity towards the oxidation of nitric oxide (NO). At the electrode, an oxidation peak of NO can be observed at about 1.05 V (versus Ag/AgCl), and the electrode reaction of NO is controlled by diffusion process. Under the optimum conditions, the peak currents are dependent linearly on NO concentrations in the range from 7.2×10^{-7} to 7.84×10^{-5} M with a limit of detection of 2.0×10^{-7} M. The response time of the as-prepared electrode to NO is less than 3 s, and the sensitivity is about 299.1 μA/mM, revealing that the electrode can be used as an excellent sensor for the determination of NO. With further modification of Nafion, the determination is free from the interference of nitrite and some other biological substances. This investigation provides an alternate way for the determination of NO.

1. Introduction

Graphene, as a "rising star" of carbon material, has attracted a lot of interest from both the theoretical and experimental scientific communities since it was discovered and successfully isolated from bulk graphite just a few years ago. Graphene is a one-atom-thick planar sheet of sp^2-bonded carbon atoms arranged in a honey comb crystal lattice, the difference of whose structure from graphite's is shown in Figure 1 [1, 2]. Graphene can be wrapped up into zero-dimensional fullerenes, rolled into one-dimensional nanotubes, or stacked into three-dimensional graphite [3]. Hence, the two-dimensional carbon material, graphene, is considered as a building block for graphitic materials of all other dimensionalities [4]. Furthermore, owing to its extraordinary fast electron transportation, high surface area, unique graphitized basal plane structure, and low manufacturing cost, numerous novel applications of graphene nanosheets have been investigated, including graphene-based field-effect transistors [5, 6], batteries [7], and supercapacitors [8]. Particularly, because of its excellent conductivity (1.43×10^4 S·m^{-1}) [9] and high electrocatalytic activities, graphene-based electrochemical sensors and biosensors have recently received increasing attention in the field of electrochemistry [10, 11], such as direct electrochemistry of enzymes [12–14] and small biomolecules detection [15–17].

Nitric oxide as an important biological messenger and effective molecule [18] plays an important physiological role in the *in vivo* physiological and pathological process of broad participation [19]. NO is known to be one of the signaling functions existed in the central and peripheral nervous system and in vascular endothelium, while the result of the mussy level of NO will be devastating, wich may lead to inflammatory and degenerative diseases, immune response, septic shock, and Parkinson's and Alzheimer's diseases [20–22]. Due to the importance of NO in biology, it is important to develop the methods for detecting NO. One of the most promising methods of NO monitoring is electrochemical detection using different modified electrodes. A variety of modified electrodes have been developed in recent years [23–25].

In this paper, the graphene oxide (GO) on glassy carbon electrode surface was electrochemically reduced to form grapheme-modified electrode, noted as ERG electrode. The

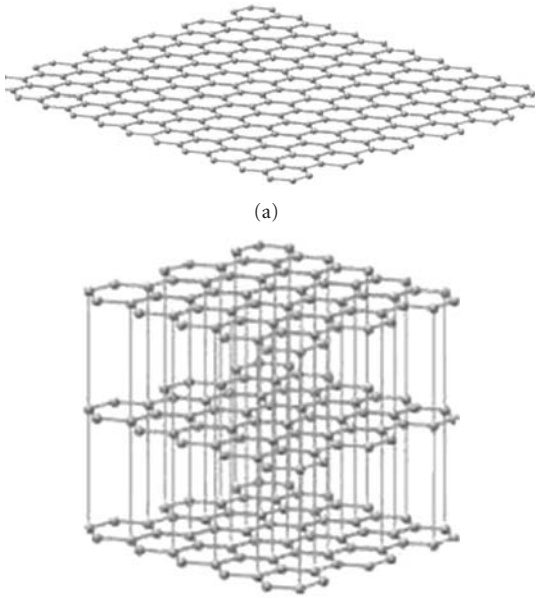

(a)

(b)

Figure 1: The structure of sp^2 carbon materials: graphene (a) and graphite (b).

properties of the modified electrode and its electrocatalytic oxidation of NO in aqueous solution were investigated in detail.

2. Experimental

2.1. Instruments and Reagents. Electrochemical experiments were performed with CHI 660A electrochemical analyzer (CHI, USA) with a conventional three-electrode system. The working electrode was an ERG electrode. A saturated calomel electrode (SCE) and a platinum electrode were used as the reference and the auxiliary electrode, respectively. Water used in all experiments was double distilled with a quartz apparatus. S-4800 scanning electron microscopy (Hitachi, Japan) was used for the characterization of graphene. High-purity nitrogen gas was used for deaeration in all electrochemical experiments.

Graphene oxide was synthesized from graphite according to Hummers' method [26]. Graphite was purchased from Shanghai Chemical Reagent Co. Nafion was purchased from Sigma. Saturated NO solutions were prepared as the previous literature. In detail, the double-distilled water was bubbled with high-purity nitrogen for 30 minutes to remove oxygen, and then the water was bubbled with pure NO gas for 30 minutes to prepare an NO-saturated solution. Aliquots of this saturated solution were used to prepare serial solutions of known NO concentration, using a value of 1.8×10^{-3} M as its saturation concentration at room temperature.

2.2. The Preparation of ERG Electrode. ERG electrode was prepared through electrochemically reducing graphene oxide on the surface of GC electrode. The detail process can

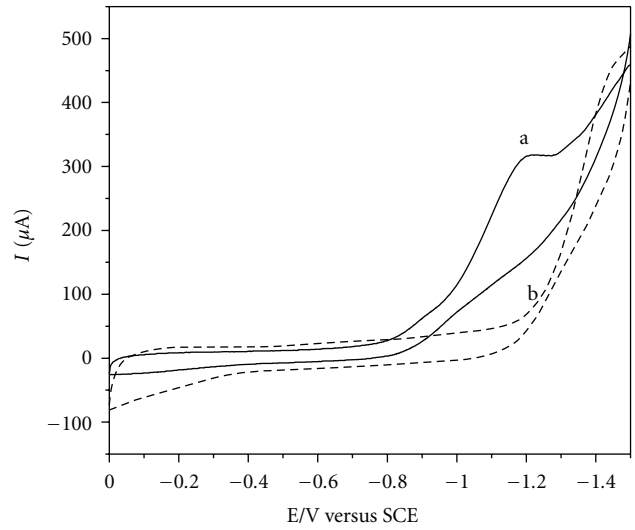

Figure 2: CVs of electrochemical reduction of graphene oxide on GC electrode in 10 mM PBS (pH 5.0) with a scan rate of 50 mV/s for (a) the first circle and (b) the fourth circle.

be described as follows. The synthesized graphene oxide was dispersed in water to create a 0.125 mg/mL aqueous solution. The bare glassy carbon electrode was polished with 0.3 μm alumina slurry, then thoroughly rinsed with double-distilled water, and sonicated in ethanol, acetone, and water (each for 5 minutes), respectively. A volume of 10 μL of graphene oxide aqueous solution was dropped on the GC electrode surface, and the electrode was dried in ambient air at room temperature to form a graphene oxide-modified electrode, noted as GO/GC electrode. The obtained electrode was dipped into 10 mM, pH 5.0 phosphate buffer solution, and five cyclic potential scans were performed in the potential range of $0.0 \sim -1.5$ V. In this process, the cyclic voltammograms (CVs) were recorded, and the typical CVs were shown in Figure 2. In the first cyclic, a broad cathodic current peak at -1.2 V with a starting potential of -0.8 V (Figure 2(a)) was observed, which corresponded to the reduction of C-O bond in graphene oxide [27]. After four cycles, the cathodic peak at -1.2 V disappeared (Figure 2(b)), suggesting that the electrochemical reduction was fulfilled and the graphene-modified electrode was obtained, noted as ERG/GC electrode.

3. Results and Discussion

3.1. Electrochemical Characterization of ERG Electrode. The redox couple of $[Fe(CN)_6]^{3-/4-}$ is close to an ideal quasireversible system and it was usually used to characterize the property of modified electrode. Figure 3 shows the CVs obtained by a bare GC electrode, GO/GC, electrode, and ERG electrode in 5 mM $[Fe(CN)_6]^{3-/4-}$ solution containing 0.1 M KCl. As shown in line a of Figure 3, a couple of well-defined redox peaks are observed for the bare GC electrode, which corresponds to the quasireversible one-electron redox behavior of ferricyanide ion. In contrast, for GO/GC electrode,

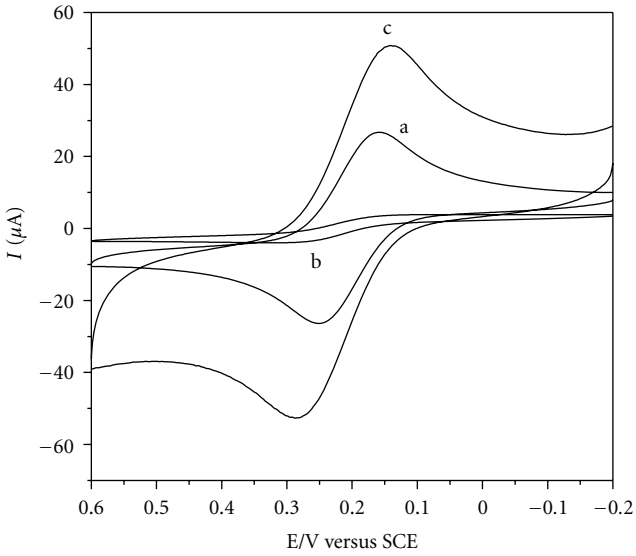

Figure 3: Typical CVs of different electrode in 1 mM $K_3Fe(CN)_6$ solution containing 0.1 M KCl. (a) Bare GC electrode, (b) GO/GC electrode, and (c) ERG/GC electrode.

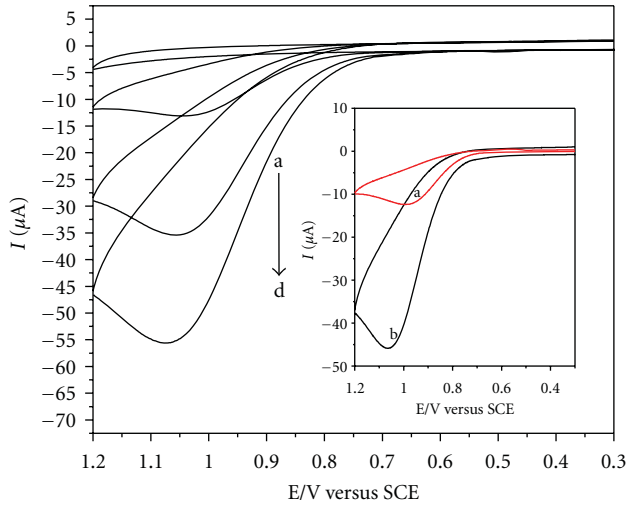

Figure 5: CVs of different NO concentrations at ERG/GC electrode in 0.1 M, pH 7.0 phosphate buffer solution. From a to d, the concentration of NO is 0, 7.2, 21.6, and 36.0 μM, respectively. Inset: CVs of 28.8 μM NO at bare GC electrode (a) and ERG/GC electrode (b) in the same condition.

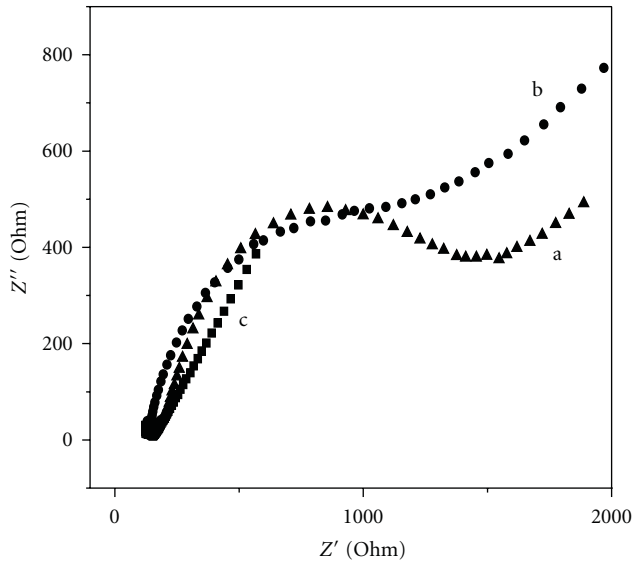

Figure 4: The Nyquist plots of different electrode recorded in the presence of 5 mM $Fe(CN)_6^{3-/4-}$ (1 : 1) by applying an AC impedance with 5 mV amplitude in a frequency range from 0.1 Hz to 100 kHz under open-circuit potential conditions. (a) GO/GC electrode, (b) ERG/GC electrode, and (c) bare GC electrode.

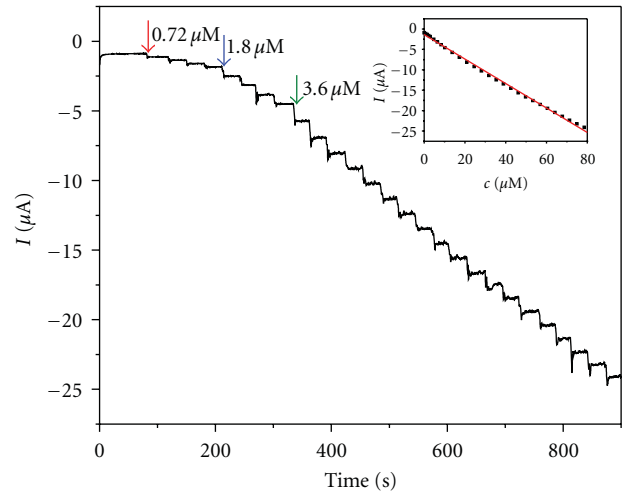

Figure 6: Amperometric response of ERG/GC electrode to NO. Conditions: a 1.05 V constant potential modulated with 50 mV pulse in the time intervals of 0.5 s, successive additions of NO to 0.1 M, pH 7.0 phosphate buffer solution.

cathodic and anodic peak currents dramatically decrease compared with that of bare GC electrode, as shown in line b of Figure 3. The reason may be that graphene oxide has low conductivity as a result of the existence of C–O bond, and the negative charge interface of graphene oxide largely blocked interfacial charge transfer between ferricyanide ion and electrode. Once the graphene oxide on the electrode surface was electrochemically reduced into graphene, thus formed an ERG/GC electrode, an obvious increase of both cathodic and anodic peak currents is observed as in line c of Figure 3, indicating that the high electroactive graphene interface was formed. Compared with the bare GCE, increased redox peak currents are observed on ERG/GCE mainly due to the high conductivity of graphene.

Electrochemical impedance spectroscopy (EIS) can provide the information on the impedance changes of the electrode surface during the modification progress. Figure 4 reveals the typical EIS of different electrodes. As can be seen, when graphene oxide is modified onto the GC electrode surface, the semicircle dramatically augments as compared to the bare GC electrode, suggesting that the graphene

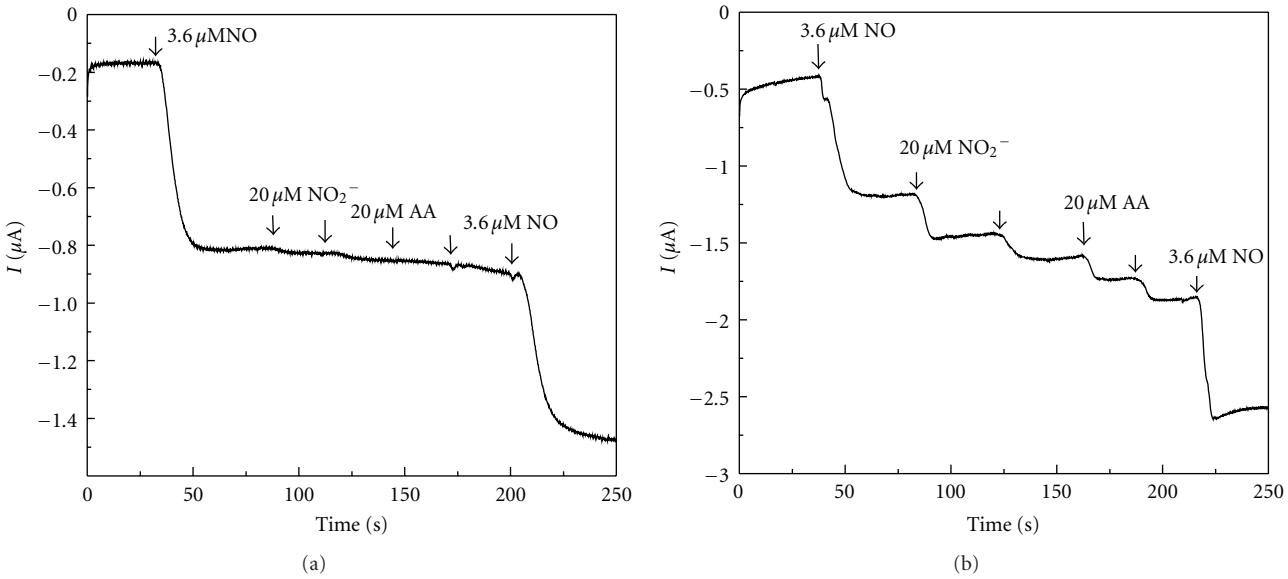

Figure 7: Amperometric response of the modified electrode after (a) and before (b) coated with Nafion to NO and interferences, NO_2^- and AA.

oxide acts as a low conductive layer which makes the interfacial charge transfer difficult and the surface negative charges of the graphene oxide repel the access of ferricyanide and ferrocyanide ions to the electrode surface for electron communication as well. After the graphene oxide is electrochemically reduced on the electrode, the semicircle decreases distinctively, indicating that graphene film has higher electrical conductivity, and it can obviously accelerate electron transfer between the probe $Fe(CN)_6^{3-/4-}$ and the electrode surface.

3.2. Electrooxidation Behavior and Amperometric Response of NO on the ERG/GC Electrode. The CVs of nitric oxide at the modified electrode in the oxygen-free 0.1 mol/L phosphate buffer solution (pH 7.0) was demonstrated in Figure 5. With the addition of NO into the solution, an obvious anodic peak was observed at about 1.05 V (versus Ag/AgCl), and the peak currents are dependent linearly on the NO concentration. Compared to bare GC electrode, the anodic peak current corresponding to the oxidation of NO increased significantly at modified electrode, as shown in the inset of Figure 5. These suggest that the ERG can act as a modifier to realize the electrochemical oxidation of NO. The anodic peak current is proportional linearly to the square root of scan rates in the range from 0.2 to 0.16 Vs^{-1} with a correlation coefficient of 0.9996, while the peak potential slightly shifted to positive direction. The results suggested that the oxidation of NO was undergoing a diffusion-controlled process in low scan rates.

Figure 6 demonstrates a typical current-time curve of ERG/GC electrode-applied potential of +1.0 V for successive additions of NO to pH 7.0 phosphate buffer solution. With the addition of NO, the steady-state currents can be reached less than 2 s and keep stable, suggesting a fast response time and high stability. The linear relationship between the catalytic current and the concentration is shown in the inset of Figure 6. As can be seen, the linear range is from 7.20×10^{-7} to 7.84×10^{-5} M with a correlation coefficient of 0.9986. The limit of detection is 2.0×10^{-7} M at a signal-to-noise ratio of 3 with a sensitivity of −299.1 μA/mM. We also summarized some other carbon-related materials NO sensors in Table 1 with respect to the linear range and the detection limit. It can be seen that the performance of the developed sensor is comparable to most of NO sensors in literature in one or more categories. Meanwhile, the proposed sensor is simpler in preparation.

In order to eliminate anion interferences like NO_2^-, Nafion was selected and modified on the surface of ERG/GC electrode. Nafion, a good cation exchanger, is widely used as a modifier to modify electrodes in electrochemistry. The negatively charged Nafion has a high degree of permeability for nitric oxide. But it prevents the diffusion of anions like NO_2^- to the modified electrode surface [30]. In this work, 10 μL of a 0.5% (w/v) Nafion solution in ethanol was cast on the prepared electrode surface to form a Nafion/ERG/GC electrode. The Nafion film can prevent anion interferences like NO_2^- and ascorbic acid from responding at the electrode. Five times relative to NO concentration of anion interferences did not disturb the detection of NO. As shown in Figure 7, amperometric response of the electrode after and before coated with Nafion to interferences, NO_2^- and AA, was compared. In the presence of Nafion, no response to NO_2^- and AA can be observed, as shown in Figure 7(a). Under the same conditions, in the absence of Nafion, the response of the electrode to NO_2^- and AA is obvious, as in Figure 7(b). So, Nafion obviously improves the selectivity of the electrode over other interfering anions. On the other hand, the electrode can be used for long time. Even after six weeks, the response signal of electrode can keep unchanged.

Table 1: Summary of some other carbon-related materials NO sensors.

No.	Electrode	Linear range	Detection limit	Reference
1	Hemoglobin adsorbed on the gold colloids-modified carbon paste electrode	9.0×10^{-7} to 3.0×10^{-4} M	1.0×10^{-7} M	[25]
2	Hemoglobin/montmorillonite/polyvinyl alcohol at a pyrolytic graphite electrode	1.0×10^{-6} to 2.5×10^{-4} M	5.0×10^{-7} M	[28]
3	Multiwall carbon nanotubes film-modified carbon fiber ultramicroelectrode	2.0×10^{-7} to 8.6×10^{-5} M	2×10^{-8} M	[29]
4	Electrochemically reduced grapheme-modified electrode	7.2×10^{-7} to 7.8×10^{-5} M	2.0×10^{-7} M	This work

4. Conclusion

In summary, we have prepared a grapheme-modified electrode through electrochemical reducing of graphene oxide on the glassy carbon electrode in this work. The graphene electrode gave a significant activity towards the electrochemical oxidation of nitric oxide. Interference effects of NO_2^- and some other biological substances are virtually eliminated because of the Nafion film. The prepared electrode shows fast response to NO and high sensitivity and stability and can be applied to the determination of nitric oxide. The preparation of graphene electrode through direct electrochemical reducing of graphene oxide on the substrate electrode surface can provide a new way to construct electrochemical sensing platform based on graphene.

Acknowledgment

This research was supported financially by the National Nature Science Foundation of China (20975001).

References

[1] C. N. R. Rao, A. K. Sood, K. S. Subrahmanyam, and A. Govindaraj, "Graphene: the new two-dimensional nanomaterial," *Angewandte Chemie—International Edition*, vol. 48, no. 42, pp. 7752–7777, 2009.

[2] S. Niyogi, E. Bekyarova, M. E. Itkis, J. L. McWilliams, M. A. Hamon, and R. C. Haddon, "Solution properties of graphite and graphene," *Journal of the American Chemical Society*, vol. 128, no. 24, pp. 7720–7721, 2006.

[3] A. K. Geim and K. S. Novoselov, "The rise of graphene," *Nature Materials*, vol. 6, no. 3, pp. 183–191, 2007.

[4] J. D. Fowler, M. J. Allen, V. C. Tung, Y. Yang, R. B. Kaner, and B. H. Weiller, "Practical chemical sensors from chemically derived graphene," *ACS Nano*, vol. 3, no. 2, pp. 301–306, 2009.

[5] C.-K. Tzahi, Q. Qing, Q. Li, Y. Fang, and C. M. Lieber, "Graphene and nanowire transistors for cellular interfaces and electrical recording," *Nano Letters*, vol. 10, no. 3, pp. 1098–1102, 2010.

[6] H. E. Romero, N. Shen, P. Joshi et al., "n-type behavior of graphene supported on Si/SiO_2 substrates," *ACS Nano*, vol. 2, no. 10, pp. 2037–2044, 2008.

[7] P. Guo, H. Song, and X. Chen, "Electrochemical performance of graphene nanosheets as anode material for lithium-ion batteries," *Electrochemistry Communications*, vol. 11, no. 6, pp. 1320–1324, 2009.

[8] F. Jiang, Y. Fang, Q. Xue, L. Chen, and Y. Lu, "Graphene-based carbon nano-fibers grown on thin-sheet sinter-locked Ni-fiber as self-supported electrodes for supercapacitors," *Materials Letters*, vol. 64, no. 2, pp. 199–202, 2010.

[9] S. J. An, Y. Zhu, S. H. Lee et al., "Thin film fabrication and simultaneous anodic reduction of deposited graphene oxide platelets by electrophoretic deposition," *Journal of Physical Chemistry Letters*, vol. 1, no. 8, pp. 1259–1263, 2010.

[10] Y. Shao, J. Wang, H. Wu, J. Liu, I. A. Aksay, and Y. Lin, "Graphene based electrochemical sensors and biosensors: a review," *Electroanalysis*, vol. 22, no. 10, pp. 1027–1036, 2010.

[11] M. Pumera, "Graphene-based nanomaterials and their electrochemistry," *Chemical Society Reviews*, vol. 39, no. 11, pp. 4146–4157, 2010.

[12] J. Lu, L. T. Drzal, R. M. Worden, and I. Lee, "Simple fabrication of a highly sensitive glucose biosensor using enzymes immobilized in exfoliated graphite nanoplatelets nafion membrane," *Chemistry of Materials*, vol. 19, no. 25, pp. 6240–6246, 2007.

[13] X. Kang, J. Wang, H. Wu, I. A. Aksay, J. Liu, and Y. Lin, "Glucose Oxidase-graphene-chitosan modified electrode for direct electrochemistry and glucose sensing," *Biosensors and Bioelectronics*, vol. 25, no. 4, pp. 901–905, 2009.

[14] K. Liu, J. Zhang, G. Yang, C. Wang, and J. J. Zhu, "Direct electrochemistry and electrocatalysis of hemoglobin based on poly(diallyldimethylammonium chloride) functionalized graphene sheets/room temperature ionic liquid composite film," *Electrochemistry Communications*, vol. 12, no. 3, pp. 402–405, 2010.

[15] M. Zhou, Y. Zhai, and S. Dong, "Electrochemical sensing and biosensing platform based on chemically reduced graphene oxide," *Analytical Chemistry*, vol. 81, no. 14, pp. 5603–5613, 2009.

[16] Y. Wang, Y. Li, L. Tang, J. Lu, and J. Li, "Application of graphene-modified electrode for selective detection of dopamine," *Electrochemistry Communications*, vol. 11, no. 4, pp. 889–892, 2009.

[17] S. Alwarappan, A. Erdem, C. Liu, and C. Z. Li, "Probing the electrochemical properties of graphene nanosheets for biosensing applications," *Journal of Physical Chemistry C*, vol. 113, no. 20, pp. 8853–8857, 2009.

[18] D. R. Richardson and H. C. Lok, "The nitric oxide-iron interplay in mammalian cells: transport and storage of dinitrosyl iron complexes," *Biochimica et Biophysica Acta*, vol. 1780, no. 4, pp. 638–651, 2008.

[19] H. Kosaka and A. Seiyama, "Physiological role of nitric oxide as an enhancer of oxygen transfer from erythrocytes to tissues," *Biochemical and Biophysical Research Communications*, vol. 218, no. 3, pp. 749–752, 1996.

[20] K. K. K. Chung and K. K. David, "Emerging roles of nitric oxide in neurodegeneration," *Nitric Oxide*, vol. 22, no. 4, pp. 290–295, 2010.

[21] E. Karpuzoglu and S. A. Ahmed, "Estrogen regulation of nitric oxide and inducible nitric oxide synthase (iNOS) in immune cells: implications for immunity, autoimmune diseases, and apoptosis," *Nitric Oxide*, vol. 15, no. 3, pp. 177–186, 2006.

[22] M. A. Titheradge, "Nitric oxide in septic shock," *Biochimica et Biophysica Acta*, vol. 1411, no. 2-3, pp. 437–455, 1999.

[23] L. Zhang, Y. Ni, X. Wang, and G. Zhao, "Direct electrocatalytic oxidation of nitric oxide and reduction of hydrogen peroxide based on α-Fe_2O_3 nanoparticles-chitosan composite," *Talanta*, vol. 82, no. 1, pp. 196–201, 2010.

[24] Y. C. Liu, S. Q. Cui, J. Zhao, and Z. S. Yang, "Direct electrochemistry behavior of cytochrome c/l-cysteine modified electrode and its electrocatalytic oxidation to nitric oxide," *Bioelectrochemistry*, vol. 70, no. 2, pp. 416–420, 2007.

[25] Y. Xu, C. Hu, and S. Hu, "A reagentless nitric oxide biosensor based on the direct electrochemistry of hemoglobin adsorbed on the gold colloids modified carbon paste electrode," *Sensors and Actuators, B*, vol. 148, no. 1, pp. 253–258, 2010.

[26] W. S. Hummers and R. E. Offeman, "Preparation of graphitic oxide," *Journal of the American Chemical Society*, vol. 80, no. 6, pp. 1339–1958, 1958.

[27] H. L. Guo, X. F. Wang, Q. Y. Qian, F. B. Wang, and X. H. Xia, "A green approach to the synthesis of graphene nanosheets," *ACS Nano*, vol. 3, no. 9, pp. 2653–2659, 2009.

[28] J. Pang, C. Fan, X. Liu, T. Chen, and G. Li, "A nitric oxide biosensor based on the multi-assembly of hemoglobin/montmorillonite/polyvinyl alcohol at a pyrolytic graphite electrode," *Biosensors and Bioelectronics*, vol. 19, no. 5, pp. 441–445, 2003.

[29] Y. Wang, Q. Li, and S. Hu, "A multiwall carbon nanotubes film-modified carbon fiber ultramicroelectrode for the determination of nitric oxide radical in liver mitochondria," *Bioelectrochemistry*, vol. 65, no. 2, pp. 135–142, 2005.

[30] G. A. Gerhardt, A. F. Oke, and G. Nagy, "Nafion-coated electrodes with high selectivity for CNS electrochemistry," *Brain Research*, vol. 290, no. 2, pp. 390–395, 1984.